An investigation of the role of two novel cancer targets, P-Rex1 and FAK, in genetically modified mouse models of melanoma

Colin Rowan Lindsay

This thesis is submitted to the University of Glasgow for the degree of Doctor of Philosophy

May 2012

The Beatson Institute for Cancer Research
Garscube Estate
Switchback Road
Glasgow
G61 1BD

Abstract

Background Metastases are the major cause of death from melanoma, a skin cancer which has the fastest rising incidence of any malignancy in the Western world. Molecular pathways that drive melanoblast migration in development are believed to underpin the movement and ultimately the metastasis of melanoma.

Aims In this thesis we use genetically modified mice models to characterise two novel anticancer targets, P-Rex1 and focal adhesion kinase (FAK). Embryonic melanoblast migration is compared with cancer outcomes for each genetic modification.

Results Mice lacking P-Rex1, a Rac-specific Rho GTPase guanine nucleotide exchange factor (GEF), have a melanoblast migration defect during development evidenced by a white belly. These *P-Rex1*$^{-/-}$ mice are resistant to metastasis when crossed to a murine model of melanoma, an effect specifically channeled through loss of P-Rex1 GEF activity. *FAK* disruption compromises melanoblast cell numbers and migration in development, but has no long-term effect on melanocyte homeostasis. FAK-deleted mice have a divergent role in melanomagenesis, delaying primary melanoma onset whilst promoting metastasis following disease onset.

Conclusions We conclude that P-Rex1 and FAK play important roles in melanoblast embryology and melanoma development and progression. Both P-Rex1 and FAK represent interesting therapeutic targets for the treatment of cancer.

Table of Contents

ABSTRACT **2**

TABLE OF CONTENTS **3**

LIST OF TABLES **6**

LIST OF FIGURES **7**

ACKNOWLEDGEMENTS **9**

DECLARATION **10**

DEFINITIONS/ABBREVIATIONS **11**

CHAPTER 1 ..... **13**

INTRODUCTION **13**

1.1 MELANOMA 14
1.1.1 A model of progression for melanoma *15*
1.1.2 Aetiology of melanoma and UVR *18*
1.1.3 Histological subtypes of melanoma *20*
1.1.4 Molecular pathways of melanoma and their animal models *21*
1.1.5 What melanoblasts tell us about melanoma *31*
1.2 METASTASIS 36
1.2.1 Metastatic theory *38*
1.2.2 Translational considerations in metastasis *41*
1.3 MELANOMA METASTASIS 44
1.3.1 Mouse models of melanoma metastasis *45*
1.4 CLINICAL TRANSLATION AND MELANOMA 54
1.4.1 Lessons from translational research *54*
1.4.2 Metastatic melanoma translation *56*
1.5 TWO NOVEL MELANOMA ANTICANCER TARGETS 59
1.5.1 PIP_3-dependent Rac-exchanger 1 (P-Rex1) *61*
1.5.2 Focal adhesion kinase (FAK) *70*

CHAPTER 2 ..... **76**

MATERIALS & METHODS **76**

2.1 EMBRYO ANALYSIS: ß-GALACTOSIDASE (*DCT-LACZ*) STAINING 77
2.1.1 Migration assays *77*
2.1.2 Melanoblast cell number assays *79*
2.2 EMBRYO ANALYSIS: *EX VIVO* MELANOBLAST LIVE IMAGING 81
2.2.1 GFP migration assays *83*
2.2.2 GFP cell number assays *83*
2.3 MOUSE TREATMENTS, AGEING AND SURVIVAL COHORTS 83
2.3.1 Tail vein (TV) treatments *84*
2.3.2 Tamoxifen *85*
2.4 STATISTICAL ANALYSES 85
2.5 SMALL ANIMAL REGULATIONS 85
2.6 TECHNIQUES USED IN MOUSE MODELLING 85
2.6.1 Transgenic expression or inactivation of genes *86*

2.6.2 Endogenous inactivation of tumour suppressors or oncogenes 86
2.6.3 Endogenous expression of oncogenes 87
2.6.4 Endogenous inducible oncogene expression 87
2.6.5 Reporter mouse strains 87
2.7 Mouse Alleles 88
2.8 Mouse Genotyping 91
2.8.1 LACZ PCR Protocol 93
2.8.2 NRAS^{Q61K} PCR Protocol 94
2.8.3 CDKN2A PCR Protocol 95
2.8.4 PREX1 PCR Protocol 96
2.8.5 BRAF^{V600E} PCR Protocol 97
2.8.6 FAK PCR Protocol 98
2.8.7 PTEN PCR Protocol 99
2.8.8 Z/EG PCR Protocol 100
2.8.9 RAC1 PCR Protocol 101
2.9 Immunohistochemistry 102
2.9.1 Ki67 102
2.9.2 P-Rex1 102
2.9.3 MelanA 103
2.9.4 S100 103
2.9.5 FAK 103
2.10 Melanocyte Isolation 103
2.11 Cell Culture 103
2.12 Immunoblotting 104
2.13 siRNA Treatments and RacGEF Constructs 104
2.14 Invasion Assays 106
2.15 RT-PCR 106
2.16 Microarray 107
2.17 Human Tissues 107
2.18 BRaf and NRas Mutation Status of Cell Lines 107

CHAPTER 3 110

THE ROLE OF P-REX1 IN NRAS^{Q61K}-DRIVEN MODELS OF MELANOMA 110

3.1 P-Rex1 deficiency does not alter primary melanoma in a *Tyr::Nras$^{Q61K/°}$; Ink4a$^{-/-}$* melanoma mouse model 112
3.2 P-Rex1 deficiency impairs metastasis in a *Tyr::Nras$^{Q61K/°}$; Ink4a$^{-/-}$* melanoma mouse model 115
3.2.1 P-Rex1 deficiency impairs frequency, growth, and organ spread of metastases 117
3.3 High P-Rex1 is sensitive for the development of metastases in immuno-deficient mice 121
3.4 P-Rex1 in human melanoma 124
3.4.1 P-Rex1 is upregulated in human melanoma 124
3.4.2 P-Rex1 is associated with progression in human melanoma 126
3.4.3 Endogenous and ectopic P-Rex1 drives invasion through its GEF activity 126
3.5 What is the most effective molecular strategy for targeting P-Rex1? 130
3.6 Summary 132

CHAPTER 4 134

THE ROLE OF P-REX1 IN EMBRYONIC MODELS OF THE MELANOCYTE LINEAGE 134

4.1 P-REX1-DEFICIENT MICE HAVE A WHITE BELLY PHENOTYPE 136
4.2 P-REX1 DEFICIENCY IMPAIRS NORMAL MELANOBLAST MIGRATION 138
4.3 P-REX1 DEFICIENCY CAUSES A REDUCTION IN MELANOBLAST PROLIFERATION 145
4.4 ARE THE DOWNSTREAM EFFECTS OF P-REX1 UNIQUELY DRIVEN THROUGH RAC? 149
4.4.1 P-Rex1 and Rac are fundamental components of mouse coat colour phenotype 149
4.4.2 P-Rex1 promotes cell numbers using a Rac1-independent mechanism 152
4.5 SUMMARY 156

CHAPTER 5 158

EXPLORING THE ROLE OF P-REX1 IN BRAF^{V600E}-DRIVEN MELANOMA 158

5.1 P-REX1 IS UPREGULATED IN HUMAN MELANOMA DRIVEN BY BRAF^{V600E} 160
5.2 BRAF^{V600E} DRIVES PROLIFERATION OF MELANOBLASTS DURING MURINE DEVELOPMENT 162
5.3 ABLATION OF PTEN DOES NOT RESCUE THE *P-REX1$^{-/-}$* MIGRATION PHENOTYPE 164
5.4 *PTEN$^{LOX/+}$* COMBINATION WITH *BRAF^{V600E}* IS AN APPROPRIATE MODEL FOR STUDYING P-REX1 ACTIVITY 168
5.5 *PREX1* DISRUPTION DOES NOT ALTER PRIMARY MELANOMA PARAMETERS IN *TYR::CREER BRAF$^{V600E/+}$; PTEN$^{LOX/+}$* MICE 172
5.6 *PREX1* DISRUPTION DOES NOT ALTER METASTASES OR SURVIVAL IN *TYR::CREER BRAF$^{V600E/+}$; PTEN$^{LOX/+}$* MICE 176
5.7 SUMMARY 178

CHAPTER 6 180

EXPLORING THE TUMOURIGENIC ROLE OF FAK IN THE MELANOCYTE LINEAGE 180

6.1 FAK DELETION REDUCES MELANOBLAST NUMBERS DURING EMBRYOGENESIS 183
6.2 FAK DELETION MAY IMPAIR MELANOBLAST MIGRATION DURING EMBRYOGENESIS 188
6.3 FAK DISRUPTION PROMOTES A COAT COLOUR PHENOTYPE IN *TYR::NRAS$^{Q61K/°}$* MICE 190
6.4 PRIMARY MELANOMAGENESIS IS DELAYED BY FAK DELETION 193
6.5 METASTATIC AND INVASIVE MELANOMA IS PROMOTED BY FAK DELETION 198
6.6 SUMMARY 202

CHAPTER 7 204

DISCUSSION 204

7.1 P-REX1 205
7.1.1 Study relevance 205
7.1.2 Braf^{V600E} and P-Rex1 206
7.1.3 Tyr::Cre Rac$^{fl/fl}$; P-Rex1$^{-/-}$ mice 211
7.1.4 Translation 212
7.2 FAK 217
7.2.1 Study relevance 217
7.2.2 Translation 218
7.3 WORKING TOWARDS IMPROVED MOUSE MODELS 220
7.3.1 Nras^{Q61K} versus Braf^{V600E} mouse models 220
7.3.2 Allografts/xenografts 221
7.3.3 Improved assessment of melanoma parameters 222
7.3.4 Embryonic models 223

BIBLIOGRAPHY 227

List of Tables

TABLE 1.1 SYNOPSIS OF COMMON MUTATIONS AND SIGNALING PATHWAYS THAT ARE ABERRANTLY AFFECTED IN MELANOMA. 23
TABLE 1.2 MOUSE MODELS SYSTEMS USED TO DELINEATE METASTASES 47
TABLE 1.3 DETAILS OF METASTASES OBSERVED IN GENETICALLY MODIFIED MOUSE MODELS OF MELANOMA. 50
TABLE 2.1 DESCRIPTION OF ALLELES USED IN EACH MOUSE STUDIED WITHIN THIS THESIS 91
TABLE 3.1 P-REX1 DISRUPTION DRAMATICALLY REDUCES INCIDENCE OF METASTASIS IN AN *TYR::NRAS*$^{Q61K/°}$; *INK4A*$^{-/-}$ TRANSGENIC MURINE MELANOMA MODEL 114
TABLE 3.2 ENDOGENOUS P-REX1 FACILITATES METASTASES TO DISTANT SITES FOLLOWING THE INTRAVASATION STEP 120
TABLE 3.3 HIGH P-REX1 IN CELL LINES IS SENSITIVE FOR DETECTING METASTATIC MELANOMA DEVELOPMENT IN IMMUNO-DEFICIENT MICE 123
TABLE 3.4 LOW P-REX1 IN CELL LINES IS SPECIFIC FOR EXCLUDING MELANOMA DEVELOPMENT IN IMMUNO-DEFICIENT MICE 123
TABLE 5.1 P-REX1 DEPLETION DOES NOT REDUCE INCIDENCE OF METASTASIS IN A *TYR::CREER BRAF*$^{V600E/+}$; *PTEN*$^{LOX/+}$ MURINE MELANOMA MODEL 174
TABLE 5.2 THERE IS NO DIFFERENCE IN PRIMARY MELANOMA ULCERATION WHEN P-REX1 IS DEPLETED IN *TYR::CREER BRAF*$^{V600E/+}$; *PTEN*$^{LOX/+}$ MICE 175
TABLE 6.1 *FAK* DELETION DELAYS MELANOMA ONSET BUT INCREASES DISEASE AGGRESSIVENESS FOLLOWING MELANOMA ONSET 196
TABLE 7.1 RELATIVE MERITS AND LIMITATIONS OF THE TWO MAIN GENETICALLY MODIFIED MOUSE MODELS OF MELANOMA ANALYSED IN THIS THESIS. 221
TABLE 7.2 RELATIVE MERITS AND LIMITATIONS OF THE TWO MELANOBLAST REPORTER MICE ANALYSED 226

List of Figures

FIGURE 1.1 STEPWISE MODEL OF MELANOMA DEVELOPMENT 17
FIGURE 1.2 NEURAL CREST MODEL OF MELANOBLAST MIGRATION IN EMBRYOGENESIS 33
FIGURE 1.3 STEPWISE MODEL OF MELANOMA METASTASIS (DETAILED IN SECTION 1.2) 37
FIGURE 1.4 DRUG DISCOVERY CASCADE 60
FIGURE 1.5 STRUCTURE AND FUNCTION OF P-REX1 62
FIGURE 1.6 POTENTIAL P-REX1 SIGNALLING IN MELANOMA 69
FIGURE 1.7 STRUCTURE AND FUNCTION OF FAK 71
FIGURE 2.1 *DCT-LACZ* MELANOBLAST MIGRATION ASSAYS 78
FIGURE 2.2 *DCT-LACZ* MELANOBLAST CELL NUMBER ASSAYS 80
FIGURE 2.3 TYR::CRE Z/EG MELANOBLAST TECHNIQUE 82
FIGURE 3.1 P-REX1 DISRUPTION DOES NOT SIGNIFICANTLY ALTER PRIMARY MELANOMAGENESIS IN A *TYR::NRAS*$^{Q61K/°}$*; INK4A*$^{-/-}$ TRANSGENIC MURINE MELANOMA MODEL 113
FIGURE 3.2 P-REX1 DISRUPTION DRAMATICALLY REDUCES INCIDENCE OF METASTASIS IN AN *TYR::NRAS*$^{Q61K/°}$*; INK4A*$^{-/-}$ TRANSGENIC MURINE MELANOMA MODEL 116
FIGURE 3.3 ENDOGENOUS P-REX1 FACILITATES METASTATIC FREQUENCY AND ORGAN SPREAD FOLLOWING THE INTRAVASATION STEP 119
FIGURE 3.4 HIGH P-REX1 IS SENSITIVE FOR THE DEVELOPMENT OF METASTASES IN IMMUNO-DEFICIENT MICE 122
FIGURE 3.5 P-REX1 UPREGULATION IS ASSOCIATED WITH PROGRESSIVE DISEASE IN HUMAN MELANOMA ..125
FIGURE 3.6 ENDOGENOUS P-REX1 DRIVES INVASION IN HUMAN MELANOMA CELL LINES 127
FIGURE 3.7 EXOGENOUS P-REX1 DRIVES INVASION THROUGH ITS GEF ACTIVITY 129
FIGURE 3.8 ECTOPIC GEF-DEAD P-REX1 INHIBITS TUMOUR GROWTH AND PROMOTES MOUSE SURVIVAL .131
FIGURE 4.1 P-REX1 DEFICIENT MICE HAVE A 'WHITE BELLY' PHENOTYPE 137
FIGURE 4.2 P-REX1 IS PRESENT IN MOUSE MELANOBLASTS 139
FIGURE 4.3 *P-REX1*$^{-/-}$ MICE HAVE A DEFECT IN MELANOBLAST MIGRATION 141
FIGURE 4.4 *P-REX1*$^{-/-}$ MICE HAVE A DEFECT IN MELANOBLAST MIGRATION AT E13.5 AND E15.5 143
FIGURE 4.5 *P-REX1*$^{-/-}$ MICE HAVE REDUCED PROTRUSIONS AT E15.5 144
FIGURE 4.6 *P-REX1*$^{-/-}$ MICE HAVE A REDUCTION IN MELANOBLAST CELL NUMBERS USING *DCT-LACZ* REPORTER MICE 147
FIGURE 4.7 *P-REX1*$^{-/-}$ EMBRYOS HAVE A REDUCTION IN MELANOBLAST PROLIFERATION USING LIVE *EX VIVO* TIMELAPSE 148
FIGURE 4.8 P-REX1 AND RAC ARE FUNDAMENTAL COMPONENTS OF MOUSE COAT COLOUR PHENOTYPE 151
FIGURE 4.9 P-REX1 AND RAC1 ARE FUNDAMENTAL COMPONENTS OF MOUSE COAT COLOUR PHENOTYPE.153
FIGURE 4.10 P-REX1 PROMOTES AN INCREASE IN CELL NUMBER USING A RAC1-INDEPENDENT MECHANISM 155
FIGURE 5.1 P-REX1 IS UPREGULATED IN HUMAN MELANOMA DRIVEN BY ONCOGENIC BRAF 161
FIGURE 5.2 EXPRESSION OF BRAF^{V600E} INCREASES MELANOBLAST CELL NUMBERS AT E15.5 163
FIGURE 5.3 *PTEN* ABLATION DOES NOT RESCUE THE P-REX1 MIGRATION PHENOTYPE 166
FIGURE 5.4 *PTEN* ABLATION DOES NOT RESCUE THE P-REX1-NULL MIGRATION PHENOTYPE 167
FIGURE 5.5 SCHEMATIC DIAGRAM DETAILING BREEDING OF INDUCIBLE BRAF^{V600E} MELANOMA MODEL TO P-REX1 AND PTEN MICE 169
FIGURE 5.6 *PTEN*$^{LOX/+}$ COMBINATION WITH THE BRAF^{V600E} MELANOMA MODEL IS APPROPRIATE FOR STUDYING P-REX1 ACTIVITY 171
FIGURE 5.7 P-REX1 DEPLETION DOES NOT ALTER PRIMARY MELANOMA GROWTH PARAMETERS IN *TYRER::CRE BRAF*$^{V600E/+}$*; PTEN*$^{LOX/+}$ MICE 173

FIGURE 5.8 P-REX1 DISRUPTION DOES NOT ALTER METASTASES OR SURVIVAL IN *TYR::CREER BRAF*$^{V600E/+}$; *PTEN*$^{LOX/+}$ MICE 177
FIGURE 6.1 *TYR::CRE FAK*$^{FL/FL}$ MICE HAVE A DEFICIT OF MELANOBLASTS AT E15.5 185
FIGURE 6.2 THERE MAY BE FEWER EPIDERMAL MELANOBLASTS IN FAK-DELETED EMBRYOS AT E15.5 186
FIGURE 6.3 EXPRESSION OF NRAS^{Q61K} DOES NOT INCREASE CELL NUMBERS AT E15.5 187
FIGURE 6.4 *TYR::CRE FAK*$^{FL/FL}$ MICE HAVE A DEFICIT OF MELANOBLAST MIGRATION AT E15.5 189
FIGURE 6.5 *FAK* DISRUPTION PROMOTES A COAT COLOUR PHENOTYPE IN *TYR::NRAS*$^{Q61K/°}$ MICE 192
FIGURE 6.6 PRIMARY MELANOMAGENESIS IS DELAYED BY FAK DELETION 195
FIGURE 6.7 ENHANCED PROLIFERATION OCCURS AT THE INVASIVE EDGE OF FAK-DELETED MELANOMAS 197
FIGURE 6.8 METASTATIC AND INVASIVE MELANOMA IS PROMOTED BY FAK DELETION 200
FIGURE 6.9 INCREASED INVASION OCCURS IN MELANOMATOUS BRAIN LESIONS OF FAK *WILD-TYPE* AND FAK-DEPLETED MICE 201
FIGURE 7.1 THE DRUG DISCOVERY CASCADE AND P-REX1 215

Acknowledgements

Thank you to my supervisors, Owen Sansom and Brad Ozanne, for their patience and advice, and without whom this thesis would not be possible. Many thanks also to the members of their research groups, as well as to general Beatson research staff: particularly Andrew Campbell, Margaret O'Prey, Susan Mason, Colin Nixon, and all the BSU staff. Laura Machesky, Ang Li, and the Larue laboratory in Paris have also offered continuous support throughout this PhD, thanks to them.

Thanks to the MRC, and initially CRUK, for their funding of my work.

Finally, thanks to my parents, Joan and Gordon, who have always quietly encouraged and inspired me. Karen, my wife, thank you for your endless patience and support whilst you have become progressively more uncomfortable and tired with the baby. I can't wait to meet Bruce.

Declaration

I am the sole author of this thesis. I declare that the work here was performed personally unless stated otherwise.

Definitions/Abbreviations

ALK	Anaplastic lymphoma kinase
ALM	Acral lentiginous melanoma
AU	Arbitrary units
BM	Basement membrane
CDK4/6	Cyclin-dependent kinase 4/6
CGH	Comparative genomic hybridisation
CNS	Central nervous system
CSE	Chronic sun-exposed
CTC	Circulating tumour cell
CTLA-4	Cytotoxic T-lymphocyte-associated antigen 4
DAB	3,3'-diaminobenzidine
DH	Dbl homology
DMBA	7,12-dimethylbenz[α]anthracene
ECM	Extracellular matrix
EGFR	Epidermal growth factor receptor
FAK	Focal adhesion kinase
FAT	Focal adhesion targeting
FERM	Four-point-one, ezrin, radixin, moesin
FGF	Fibroblast growth factor
GAP	GTPase activating protein
GDI	Guanine-nucleotide dissociation inhibitor
GEF	Guanine Nucleotide Exchange Factor
GPCR	G-protein-coupled receptors
GRM	Glutamate metabotrophic receptor
HBSS	Hank's balanced salt solution
HDAC	histone deacetylase
HF	Hair follicle
HGF	Hepatocyte growth factor
IHC	Immunohistochemistry
IP4P	Inositol polyphosphate 4-phosphatase
KC	Keratinocyte
LMM	Lentigo malignant melanoma
LN	Lymph node
MAPK	Mitogen-activated protein kinase
MB	Melanoblast
MC	Melanocyte
MEFs	Mouse embryo fibroblasts
MITF	Microphthalmia-associated transcription factor
mTOR	mammalian Target of rapamycin
NHM	Normal human melanocytes
NHSFs	Normal human stromal fibroblasts
NM	Nodular melanoma
Non-CSE	non-chronic sun-exposed
NSCLC	Non-small cell lung cancer
N-WASP	Neural wiskott aldrich syndrome protein
PARP	poly(ADP)-ribose polymer formation

PCR	Polymerase chain reaction
PDs	Pharmacodynamics
PDGFR	Platelet-derived growth factor receptor
PH	Pleckstrin homology
P(I)3K	Phosphatidylinositol 3-kinase
PIP_3	Phosphatidylinositol (3,4,5)-triphosphate
PKs	Pharmacokinetics
P-Rex1	Phosphatidylinositol 3,4,5-trisphosphate-dependent Rac exchanger 1
PTEN	Phosphatase and tensin homolog
Rb	Retinoblastoma
ROS	Reactive oxygen species
RGP	Radial growth phase
SC	Subcutaneous
SCF	Stem cell factor
SSM	Superficial spreading melanoma
TBST	Tris-Buffered Saline Tween
TPA	12-O-tetradecanoyl-phorbol-13-acetate
TSG	Tumour-suppressor gene
TV	Tail-vein
UV	Ultraviolet
UVR	Ultraviolet Radiation
VEGF	Vascular endothelial growth factor
VGP	Vertical growth phase
WHO	World Health Organisation

Chapter 1

Introduction

1.1 Melanoma

Melanoma is the most lethal form of skin cancer, accounting for the majority of skin cancer deaths. There are approximately 132,000 new cases each year, an incidence that has been steadily rising in the Western world for the last few decades (World Health Organisation, www.who.int/uv/faq/skincancer/ en/index1.html): this increase relates to improved detection, as well as an increase in the frequency of holidays abroad (de Vries et al, 2005). 80% of melanoma cases will be cured by surgical resection, while the remaining 20% will develop metastatic disease which confers a poor prognosis: median survival is 6 months, with a 5 year survival rate of less than 5% (Gray-Schopfer et al, 2007). Primary melanomas with a Breslow depth of ≥4mm are sufficient to predispose to significant risk of metastatic disease, with a 43-47% 5-year patient survival (www.cancerresearchuk. org/type/melanoma/treatment/melanoma-statistics-and-outlook). Moreover, no treatment had been developed for metastatic patients that could offer an improvement in their overall survival until very recently.

The pathogenesis of melanoma is characterised by the two main physiological properties of other cells from the melanocyte lineage: adult melanocytes (MCs) are resistant to apoptosis, while their embryological precursors, melanoblasts (MBs), have a propensity to migrate. MCs are the pigment-producing cells in the skin that can give rise to melanoma. Their major role is lifelong protection of the skin from ultraviolet radiation (UVR) through the production of melanin and the consequent tanning response. Loss of melanin production in albinism is caused by mutations in genes involved in melanin-synthesis (tyrosinase, TRP1 and TRP2), and renders sufferers hyper-sensitive to the damaging effects of UV, producing higher than average reported rates of melanoma (Boissy et al, 1997; http://cancerhelp.cancerresearchuk.org/type/skin-cancer/about/skin-cancer-risks-

and-causes). Normal MCs in the human skin are tethered to the basement membrane (BM) of the epidermis and the hair follicle (HF), where their homeostasis is controlled by keratinocytes (KCs) (Gray-Schopfer et al, 2007). The capacity of MCs to resist apoptosis and survive the highly mutagenic skin environment is reflected in melanoma, a cancer characterised by its resistance to traditional cytotoxics that can confer clinical efficacy in the majority of human epithelial cancers (Terzian et al, 2010). Melanoma cells display resistance to drug-induced apoptosis *in vitro*, and also show low levels of spontaneous apoptosis *in vivo* (Soengas et al, 2003).

The migratory propensity of MCs is indicated by their anatomical localisation in adults, where they classically reside in the skin but also exist in the eyes, heart, inner ear, brain, and gut mucosa (Brito et al, 2008). It is hypothesised that malignant transformation of these distant visceral populations of MCs is responsible for the rare cases of melanoma which originate outwith the skin, such as primary CNS melanoma (Brito et al, 2008). MCs arise from a uniquely motile embryonic precursor population, MBs. The genetic predisposition of MBs to migrate can re-arise at an early stage in primary melanoma, where metastases can have quickly devastating effects and involve multiple viscera. It is not unusual in the clinic to discover metastatic disease without having identified a primary source of cancer (Gupta et al, 2005). Given its biological capacity for aggression, it seems likely that the relatively high 80% survival rate from melanoma is mainly possible because of early detection of primary tumours on an easily visualised organ, the skin.

1.1.1 A model of progression for melanoma

50-75% of human melanoma will occur *de novo*, with the other 25-50% arising from pre-existing naevi (Garcia-Cruz, 2009). It is likely that the stochastic occurrence of critical mutations will determine which one of these pathways of melanomagenesis may occur.

Patients who develop *de novo* melanomas may have a poorer prognosis (Kumasaka et al, 2010), although identification of which patients succumb to each pathway can be inherently difficult to assess. At present, mouse models still concentrate on mimicking the genetics, anatomy and histology of primary melanoma and its metastases, with little focus as yet on identifying whether a primary lesion has arisen from a pre-existing naevus or not. Using depilation of coat hair and prospective assessment of melanocytic lesions, a recent report assessing mouse naevi has followed the early progress made in this field using zebrafish models (Dhomen et al, 2009, Patton et al, 2005, Dovey et al, 2009).

The classical stepwise model of melanoma development describes initial proliferation and spread of MCs within the epidermis or dermis to form a benign naevus (Figure 1.1). Most naevi will generally not progress from this point, although in melanomagenesis, intra-epidermal naevi can enter the radial growth phase (RGP) where they proliferate further in the epidermis and exhibit cellular dysplasia. Following the RGP, collections of cells can progress to the more dangerous vertical growth phase (VGP), where they invade the dermis and acquire metastatic potential through involvement with the micro-vasculature and the lymphatic system. It is assumed that *de novo* melanomas will follow a similar pattern, but with quicker progression to the VGP by isolated MCs (Miller et al, 2006). The genetics associated with these various phases of melanoma development is discussed below.

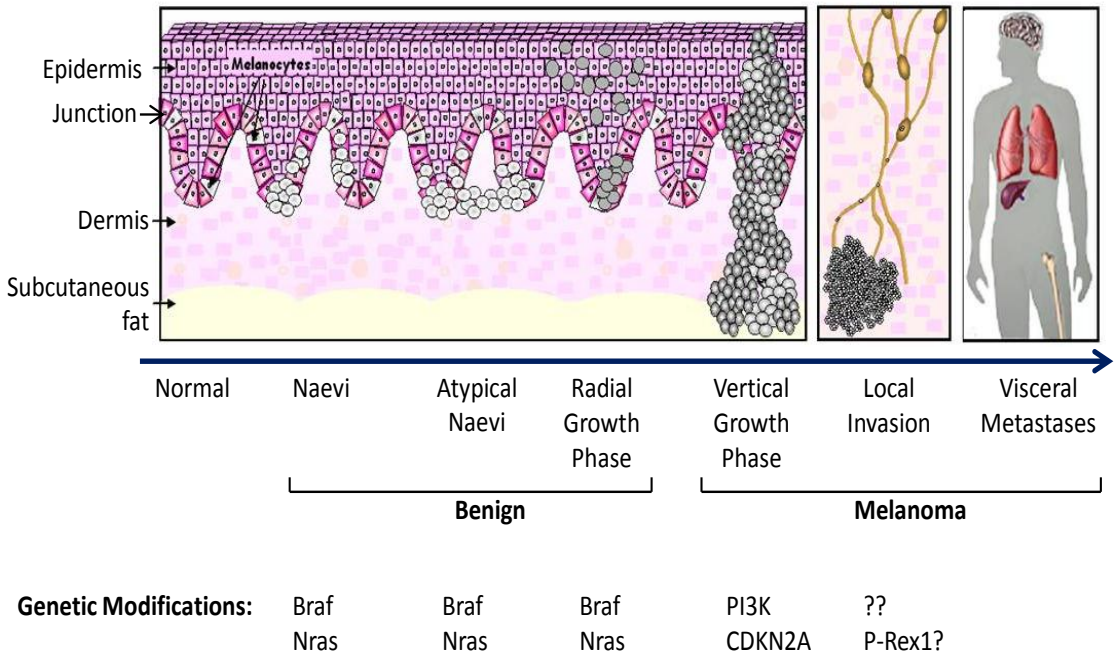

Figure 1.1 Stepwise model of melanoma development
Schematic anatomical diagram of classical melanoma progression model. Progression through various growth phases and their common associated genetics indicated below. Further details in section 1.1.1. Unpublished but adapted from figure originally provided by Gallacher laboratory, Conway Institute, Dublin.

1.1.2 Aetiology of melanoma and UVR

Risk factors for melanoma include family history, a history of previous melanoma, fair and freckling skin, large numbers of melanocytic naevi, the presence of blond/red hair, and exposure to UVR (Strizzi et al, 2011). In Scotland, a particular increase in the incidence of new melanoma cases over the past few decades is thought in part to be secondary to the large numbers of people with type I skin type (freckling skin, red/fair hair, blue/green eyes) (Whiteman et al, 2008, http://www.cancerresearchuk.org/cancer-info/cancerstats /types/skin/riskfactors /skin-cancer-risk-factors).

UVR is the most ubiquitous environmental carcinogen, and there is evidence in particular that UVB has a specific role in melanomagenesis (Zaidi et al, 2008). A strong epidemiological connection between exposure to sunlight and induction of melanoma has been established, especially through intense intermittent exposure to UVR during childhood (Elwood et al, 1997, Holman et al, 1983). Familial studies have suggested that UVR may be acting in a tumour-promoting capacity, with other genetic factors prompting tumour initiation (Serrano et al, 1996). Despite this, the mechanistic relationship between UVR and the development of genetic alterations that predispose to melanoma is still relatively poorly resolved.

One explanation for the relationship between UVR and melanoma is the ‘divergent pathway’ hypothesis (Whiteman et al, 2003). This suggests that one pathway of disease onset typically occurs at older age with lesions predominantly arising on areas of skin chronically exposed to UVR (eg head and neck) (‘Chronic sun-exposed’, CSE), while the second pathway affects younger patients with melanomas occurring in less sun-exposed anatomical areas (‘non chronic sun-exposed’, non-CSE). The second pathway to melanomagenesis is more associated with genetic risk, as evidenced by the fair skin and

high number of naevi affecting patients in this group. Patients with the largest histological subtype of melanoma, superficial spreading melanoma (SSM), will often form part of the non-CSE pathway, while patients with lentigo malignant melanoma (LMM) comprise a majority of the CSE pathway (Walker et al, 2011).

Although there are data to suggest a connection between UVR-related DNA damage and other types of skin cancer, little evidence exists which shows signature patterns of UVR damage in genes known to be mutated in melanoma. This is the case for *NRAS*, *BRAF*, and *CDKN2A* loci commonly mutated in the disease (Hocker et al, 2007, Davies et al, 2002), although it is notable that these mutations are most often related to melanoma arising from either acute intermittent sun exposure or little UVR exposure at all (non-CSE pathway). For example, oncogenic *BRAF* mutations in melanoma arise early in life at low cumulative UV exposures (Bauer et al, 2011).

Another mechanism by which UV has been proposed to promote melanomagenesis is through the induction of reactive oxygen species (ROS) (Wang et al, 2010). In particular, this is a mechanism by which UVA has been shown to induce melanoma in a manner sensitised by melanin (Kvam et al, 2004). Wang and colleagues found that UVA induces ROS in melanocytes, which have a lower nucleotide excision repair capacity for UV photoproducts than normal human stromal fibroblasts (NHSFs). UV photoproducts also induced more mutations in melanocytes than in NHSFs. This led to the proposition that UVA-induced, melanin-augmented ROS in melanocytes, allied with the reduced repair capacity of these cells, are two key factors that contribute to melanomagenesis (Wang et al, 2010).

As this thesis focuses on mouse models in the non-CSE pathway, UV-induced mouse models of melanoma have not been detailed here, although a number have been described (Kelsall et al, 1998, Broome Powell et al, 1999, Kato et al, 2000, Recio et al, 2002, Yamazaki et al, 2005, Hacker et al, 2006). The most efficient method of melanoma induction remains a single neonatal exposure of UVR, perhaps because neonatal skin has an enhanced proliferative and inflammatory capacity as well as a higher proportion of MC progenitors (Recio et al, 2002). It is arguable that this treatment might model UV-exposure in the non-CSE pathway more accurately than the CSE pathway, although often features of CSE melanoma such as solar elastosis have been described.

1.1.3 Histological subtypes of melanoma

The World Health Organisation (WHO) described four histological subtypes of melanoma: superficial spreading melanoma, nodular melanoma (NM), lentigo malignant melanoma, and acral lentiginous melanoma (ALM). The most common subtype in the Western world is SSM, accounting for approximately 70% of melanomas. SSM arises in the basal epidermis and can follow the classical model of melanoma progression described in Section 1.1.1. NM is predominantly observed in the dermis, and often involves the epidermis too. There exists conflicting hypotheses as to whether NM may be a quicker extension of the epidermal progression model seen in SSM, or whether it may represent a separate disease entity of dermal origin (Walker et al, 2011). The similar mutational constitution of both SSM and NM subtypes (frequent mutations of *BRAF* or *NRAS)* suggest that the former hypothesis is more likely, while both SSM and NM are also associated with non-CSE skin (Bastian et al, 2000, Curtin et al, 2006).

CSE skin is most frequently associated with LMM, which invariably exhibits dermal solar elastosis with a component of MC proliferation in the epidermis (Walker et al, 2011).

These melanomas are *KIT* mutated in 20% of cases, and can be p53 mutated also (Curtin et al, 2006, Hocker et al, 2007). ALM affects 10% of melanoma patients, and describes melanoma occurring in the nail apparatus or glabrous skin. It is associated with mutation or amplification of *KIT* in 40% of cases (Curtin et al, 2006), and the anatomy and similar incidence of ALM between all ethnic backgrounds helped reveal that it occurs independent of UVR damage. Mutations of *BRAF* are infrequent in patients with LMM or ALM (Lee et al, 2011).

Outwith the WHO classification, it should be remembered that ocular melanoma is the most common and lethal form of eye cancer, and can be defined and recognised by its unique genetic make-up. It mostly originates in the uveal tract rather than the conjunctiva, and has been associated with UVR (Singh et al, 1998). A striking incidence of liver metastases (50%) affects patients with uveal melanoma. Pioneering work by Bastian and colleagues identified and characterised unique activating mutations of the *GNAQ* and *GNA11* oncogenes in many cases (van Raamsdonk et al, 2009, van Raamsdonk et al, 2010). *KIT* mutations have also been identified in 33% of primary lesions (Wallander et al, 2011).

1.1.4 Molecular pathways of melanoma and their animal models

This section details the most aberrantly regulated pathways and genes in melanoma, and their contributions to the hallmarks of cancer (Hanahan et al, 2010). With the exception of SSM, the mutational signatures described here still account for less than 50% of each melanoma subtype. This is despite the development of large scale genomics studies such as comparative genomic hybridisation (CGH), which can comprehensively identify the genetic make-up of human melanoma. In part, this will be because many genetic changes identified using these techniques have yet to be functionally validated. Early efforts to

dovetail histological and genetic components of melanoma have shown considerable overlap between the two classifications, with histological features such as larger cells and increased pigmentation leading to an 82% predictability of melanomas with mutated *BRAF* (Broekaert et al, 2010). Human and mouse melanoma histology will doubtless be further analysed in this way once characterisation of functional melanoma genetics has progressed further.

Similar to other cancer types, development of melanoma is characterised by the combination of mutations that activate oncogenes (most commonly *BRAF* and *NRAS*) with mutations that lead to loss of tumour-suppressor gene (TSG) function (frequently *PTEN* or *INK4a/ARF*) (Table 1.1). As detailed below, animal models genetically modified with this combination consistently develop melanoma.

	Melanocyte	Naevus	Melanoma
BRAF status	normal	V600E	V600E
NRAS status	normal	Q61K	Q61K
MAPK status	low	increased	high
PI3K status	low	low	high
CDKN2a status	low	induced	lost
Phenotype	quiescent	senescent	malignant

Table 1.1 Synopsis of common mutations and signaling pathways that are aberrantly affected in melanoma.
The MAPK pathway is upregulated in 90% of human melanoma, most often by somatic mutation of *BRAF* (50-70%) or *NRAS* (15-30%) (www.sanger.ac.uk/genetics/CGP/cosmic/) (Cohen et al, 2002). Mutations of GNAQ and GNA11 are alternative upstream signalling mediators of this upregulation (Van Raamsdonk et al, 2009, Van Raamsdonk et al, 2010). Further details of this pathway and other mutations are covered in Sections 1.1.4.1-1.1.4.4 below.

1.1.4.1 Ras/Raf/MEK/ERK

Ras/Raf/MEK/ERK signalling. The Ras-Raf-MEK-ERK mitogen-activated protein kinase (MAPK) signalling pathway is a central oncogenic component of many human cancers. It mediates melanoma cell proliferation and regulates cell fate decisions downstream of G-protein-coupled receptors (GPCRs) and receptor tyrosine kinases (Gray-Schopfer et al, 2007). By signalling through these receptors, growth factors such as fibroblast growth factor (FGF), stem-cell factor (SCF), and hepatocyte growth factor (HGF) activate the small G protein Ras which is attached to the inner leaflet of the plasma membrane (Bohm et al, 1995). The serine/threonine kinase Raf is recruited from the cytoplasm to the plasma membrane and activated by a scaffold complex involving active Ras, with cytosolic MEK and ERK then sequentially phosphorylated and activated in turn (Kolch et al, 2000). Finally, ERK will translocate to the nucleus and activate a variety of transcription factors to stimulate downstream effectors (Strizzi et al, 2011). The complex heterogeneity of the MAPK pathway is revealed by the multiplicity and differential functions of it myriad components: three Ras (Hras, Nras, Kras), three Raf (Araf, Braf, Craf), two MEK (MEK 1/2), and two ERK (ERK1/2) proteins (Heidorn et al, 2010).

Ras/Raf/MEK/ERK in melanoma. ERK is upregulated in 90% of human melanoma, often by somatic mutation of *BRAF* (50-70%) or *NRAS* (15-30%) (Figure 1.1, Table 1.1) (www.sanger.ac.uk/genetics/CGP/cosmic/) (Cohen et al, 2002). Over 90% of melanoma *BRAF* mutations are a glutamic acid substitution for valine at position 600 ($BRAF^{V600E}$), while the most common *RAS* mutation is an *NRAS* substitution of leucine for glutamine at position 61 ($NRAS^{Q61L}$) (Davies et al, 2002, Demunter et al, 2001). Both are oncogenic gain-of-function mutations that render Braf or Nras constitutively active. On rarer occasions, the pathway can also be upregulated by mutational activation of growth factor

receptors such as c-Kit (Willmore-Payne, 2005). Downstream signalling of $Braf^{V600E}$ has been shown to regulate a variety of proteins common to both melanoma and cancer signalling, such as vascular endothelial growth factor (VEGF), microphthalmia-associated transcription factor (MITF), BRN-2 and $p16^{INK4a}$ (Gray-Schopfer et al, 2007). $Braf^{V600E}$ is also present in up to 80% of human naevi and can induce senescence in MCs, suggesting that it is not sufficient by itself to promote melanoma (Figure 1.1, Table 1.1) (Pollock et al, 2003, Michaloglou et al, 2005). The same applies to $Nras^{Q61L}$, which can also be found in a majority of human congenital naevi (Figure 1.1, Table 1.1) (56%) (Papp et al, 1999). Importantly, melanoma activating mutations of *BRAF* and *NRAS* are generally mutually exclusive, suggesting they stimulate the same linear pathway involving MAPK deregulation (Davies et al, 2002, Rajagopalan et al, 2002, Goel et al, 2006).

Ras/Raf/MEK/ERK animal models. Mouse models expressing MC-specific $BRAF^{V600E}$ or $Nras^{Q61K}$ generally confirm the capacity of these mutations to stimulate development of melanocytic lesions without full development to melanoma (Ackermann et al, 2005, Goel et al, 2009, Dhomen et al, 2009, Dankort et al, 2009). Dhomen and colleagues reported an inducible mouse model of MC-specific expression of $Braf^{V600E}$ at endogenous levels, with a primary melanoma incidence of ~70% at a median latency of 12 months (Dhomen et al, 2009); together with the information provided by other $Braf^{V600E}$ mouse models which more rarely progress to primary melanoma (Goel et al, 2009, Dankort et al, 2009), one surmises that it must require additional oncogenic insults for melanomas to develop. Consistent with this, zebrafish expressing $Braf^{V600E}$ develop 'fish naevi' in the absence of other oncogenic disruptions, and only a minority of mice expressing $Nras^{Q61K}$ will develop primary melanomas at 1 year (Ackermann et al, 2005, Patton et al, 2005). An indirect comparison of Ackermann and Dhomen mouse models would suggest that $Braf^{V600E}$ is more efficient than $Nras^{Q61K}$ at inducing primary melanoma (Ackermann et al, 2005,

Dhomen et al, 2009). However this is not paralleled by zebrafish models, with low grade melanomas consistently seen in $Nras^{Q61K}$ fish at 1 year compared to no melanomas occurring in $Braf^{V600E}$ models (Patton et al, 2005, Dovey et al, 2009).

1.1.4.2 Phosphoinositide-3-OH kinase (PI(3)K)

PI(3)K signalling. Another signalling pathway oncogenic Ras can stimulate is the PI(3)K pathway. Here, hyper-phosphorylation by members of the PI(3)K family convert phosphoinositide membrane lipids into second messengers that activate numerous downstream targets including the serine-threonine kinase Akt, which in turn can activate downstream effectors such as mammalian target of rapamycin (mTOR). PI(3)K signalling can be terminated by the lipid phosphatase phosphate and tensin homologue (PTEN). The pathway mediates hallmarks of cancer such as cell proliferation, survival, and growth, and is often upregulated in melanoma (Sansal et al, 2004). However, the differential signalling patterns of PI(3)K pathway isoforms have yet to be fully elucidated: several different isoforms of Akt and PI(3)K exist, as well as two separate complexes through which mTOR can exert its effects (Marone et al, 2008).

PI(3)K in melanoma. PTEN is a tumour-suppressor gene, mutated in germline disorders such as Cowden disease where it is associated with tumour susceptibility. This contrasts with cardio-facial-cutaneous syndrome, a BRAF/MEK germline genetic disorder which has no specific association with cancer disposition (Bentires-Alj et al, 2006). PTEN is also mutated in many spontaneous human cancers (Sansal et al, 2004). Absence or reduction of *PTEN* (by genetic or epigenetic means) occurs in the majority of primary melanomas (50-90%), although its mutation is relatively infrequent (<15%) (Figure 1.1, Table 1.1) (Inoue-Narita, 2008). Upregulated Akt occurs in 43-60% of spontaneous melanomas (Stahl et al, 2004, Dhawan et al, 2002), and *PI(3)K* activating mutations are present in only 3% of

cases (Omholt et al, 2006). The combination of Pten loss and oncogenic Braf is present in approximately 20% of human melanomas (Dankort et al, 2009). Pten loss and Nras activation were assumed to be mutually exclusive in human melanoma, due to their individual ability to activate the PI(3)K pathway, although it was later asserted that a small number of melanomas will harbour both alterations with functional consequences (Tsao et al, 2000, Nogueira et al, 2010).

PI(3)K animal models. Genetic evidence for *in vivo* co-operation of *PTEN* and *BRAF* in melanomagenesis was first reported by Dankort and colleagues (Dankort et al, 2009). In this mouse model, melanocyte-specific ablation of *PTEN* allowed progression to spontaneous melanomas driven by $Braf^{V600E}$ in 100% of mice; no melanomas were observed in those mice with $BRAF^{V600E}$ alone. In another mouse model, melanocyte-specific deletion of *PTEN* alone has been shown to predispose mice to carcinogen-induced invasive melanomas and metastases (Inoue-Narita, 2008). The loss of one copy of *PTEN* in a $Tyr::HRAS^{V12G}; CDKN2a^{-/-}$ mouse model led to more aggressive melanomagenesis and metastases, suggesting that more than one TSG loss can co-operate in melanoma (Nogueira et al, 2010). No mice carrying Akt activation have been reported in melanoma.

1.1.4.3 Senescence

Senescence signalling. The *INK4a/ARF* (*CDKN2a*) gene encodes two splice variants which can act as TSGs, $p16^{INK4a}$ and $p14^{ARF}$ ($p19^{ARF}$ in mice), by acting through the pRB and p53 pathways, respectively. Their function is to regulate cellular senescence, a cancer-protection mechanism by which cells with active oncogenes can exit the cell cycle and enter a quiescent state. Cell cycle proteins cyclin-dependent kinase 4 and 6 (CDK4/CDK6) are unable to phosphorylate and inactivate the retinoblastoma (Rb) family of tumour

suppressors as a result of binding by $p16^{INK4a}$. p53 is stabilized by $p14^{ARF}$ potentiation of its main regulatory protein, Mdm2 (Sharpless et al, 1999).

Senescence in melanoma. The *INK4a/ARF* (*CDKN2a*) gene has been identified as a susceptibility locus in both familial and sporadic melanoma, inactivated at high frequency (Chin et al, 1998). Most germline or somatic *CDKN2a* mutations in human melanoma disrupt both $p16^{INK4a}$ and $p14^{ARF}$ (Figure 1.1, Table 1.1) (Sharpless et al, 1999). $p16^{INK4a}$ is inactivated in somatic melanomas by deletions, point mutations, and transcriptional silencing by promoter methylation (Gray-Schopfer et al, 2007). $p14^{ARF}$ is genetically or epigenetically deactivated in 43% of somatic human melanomas (Freedberg et al, 2008). *p53* mutations are present in 0- 10% of all melanomas: it is thought that this low frequency is related to the frequent loss of $p14^{ARF}$, leaving *p53* mutations functionally redundant within the same pathway (Terzian et al, 2010). However, heterozygous deletion of *p53* has been reported in up to 50% of metastatic melanoma, suggesting a role in later melanoma progression (Hussein et al, 2004). Germline mutations of *CDK4* also abolish normal pRb-mediated cell cycle control and lead to melanoma susceptibility (Zuo et al, 1996).

Senescence in animal models. Animal models with ablation of the *CDKN2a/p53* loci or *CDK4* activating mutations rarely develop melanoma without other genetic alterations, although tumour development can be stimulated by UVR exposure (Chin et al, 1997, Bardeesy et al, 2001, Sharpless et al, 2001, Recio et al, 2002, Ackermann et al, 2005, Patton et al, 2005, Hacker et al, 2006, Tormo et al, 2006, Yang et al, 2007, Goel et al, 2009, Terzian et al, 2010). One of ten $p16^{INK4a}$-null mice with $p19^{ARF}$ heterozygosity was reported to develop metastatic melanoma, an effect that was increased with 7,12-dimethylbenz[α]anthracene (DMBA) treatment and not seen with $p16^{INK4a}$-null mice alone

(Krimpenfort et al, 2001). Similar to *PTEN*, the key function of *CDKN2a* in mouse and human melanoma is therefore to act as a senescence 'brake', preventing progression of naevi driven by oncogenic mutation of *NRAS* and *BRAF*. This is best demonstrated by a mouse model that combines oncogenic Nras expression with a *CDKN2a* knockout ('*Tyr::Nras*$^{Q61K/°}$*; INK4a*$^{-/-}$ mice) to recapitulate common human genetics and pathology: *Tyr::Nras*$^{Q61K/°}$ mice alone predominantly develop naevi unless they are combined with *CDKN2a* loss ('*INK4a*$^{-/-}$'), where they suffer a 94% incidence of primary melanoma at 6 months (Ackermann et al, 2005). Loss of *p16*^{INK4a} has also been demonstrated to promote tumourigenesis in senescent MCs with mutation of *BRAF* (Michaloglou et al, 2005).

Finally, it should be noted that the *CDKN2a* locus is not the only 'brake' that can prevent development of *BRAF* or *NRAS* mutated melanoma, and therefore not essential for senescence. This is best demonstrated by *CDKN2a* null patients who can still develop naevi (Pavel et al, 2003). It was also reflected and characterised further in the *Tyr::CreER Braf*$^{V600E/+}$ mouse model described earlier in section 1.1.4.1, where loss of *p16*^{INK4a} did not preclude formation of nevi and did not contribute to metastatic propensity once melanomas had developed (Dhomen et al, 2009). Consistent with this, a 'mosaic' pattern of p16^{INK4a} staining has been described in immunohistochemistry (IHC) of human naevi (Gray-Schopfer et al, 2006).

1.1.4.4 *GNAQ/GNA11* and GPCR signalling

GNAQ and *GNA11* encode members of the q class of G-protein α-subunits. Their function is to mediate signals between GPCRs and downstream effectors. Important driver mutations of *GNAQ* and *GNA11* in melanoma were recently discovered following the genetic characterisation of mice with intradermal melanocytoses histologically similar to human 'blue naevi' (rare discrete bluish moles) (Van Raamsdonk et al, 2009). Subsequent

sequencing analysis of *GNAQ* and *GNA11* in a variety of human benign and malignant melanocytic neoplasms uncovered striking results: somatic mutations of *GNAQ* (exclusively $GNAQ^{Q209L}$) were present in 45% of uveal melanoma and 22% of uveal melanoma metastases, while mutations of *GNA11* (predominantly at Q209) were found in 32% of uveal melanomas and 57% of their metastases (Van Raamsdonk et al, 2009, Van Raamsdonk et al, 2010). The limited frequency of *BRAF* and *NRAS* mutations in uveal melanoma (despite a consistent upregulation of MAPK signalling) was partly explained by these findings (Zuidervaart et al, 2005). Indeed, this was the first characterisation of mutations of these genes in human neoplasia, and the presence of *GNAQ* mutations in human cancer seems to be unique to uveal melanoma (Lamba et al, 2009). Functional examination of their Q209 mutations using cell lines and xenografts confirmed an upregulation of MAPK signalling that, like oncogenic *BRAF* and *NRAS*, was insufficient to drive melanoma without additional genetic modification.

GPCRs are a large family of cell surface receptors that can regulate multiple aspects of cellular behaviour, including MAPK signalling and motility. When ligand bound, they are activated by an associated G-protein by exchanging its GDP for a GTP. The α subunit of the G-protein can then dissociate from the β and γ subunits to further interact with a multitude of downstream intracellular signalling proteins, or target functional proteins directly depending on the α subunit type. Deregulation of GPCRs is important in melanoma: metabotrophic glutamate receptor 5 (Grm5) has been functionally implicated as a driver of melanoma, while melanoma mutations of *GRM3* have also recently been identified (Lee et al, 2008, Prickett et al, 2011).

Perhaps the earliest and most straightforward examination of GPCR signaling in melanoma was performed by Pollock and colleagues, who identified and characterised

the driver role of Grm1 by mapping an insertional mouse mutant predisposed to developing melanoma (Pollock et al, 2003). Grm1 was expressed in 7 of 19 human melanoma samples, compared to no expression observed in benign naevi. This was the first time a role for *GRM1* had been seen in human neoplasia, and the similarities between this and the *GNAQ/GNA11* study described above are striking. With the insight gleaned from functional studies such as those described in this section, it is easy to speculate that deregulated GPCR signaling might feature strongly in the large subset of melanomas which are not driven by oncogenic *NRAS* or *BRAF*.

1.1.5 What melanoblasts tell us about melanoma

A highly motile embryonic cell population called the neural crest gives rise to a number of differentiated cell types, including MBs, as they migrate through the embryo. Figure 1.2 details this prevailing and historical model of melanoblast migration in the developing mouse embryo, a focus for much of the work in this thesis. However, it should be noted that recent results have suggested there may be an alternative origin and migratory pathway of melanocyte progenitor cells in the trunk: melanocytes can arise from a stem/progenitor niche containing Schwann cell precursors (SCPs), located in nerves situated throughout the embryo (Adameyko et al, 2009).

In the neural crest model of migration, MBs in mouse embryos between E8.5 and birth migrate to populate the dermal skin and HFs using signalling from c-Kit, their major tyrosine kinase receptor. Ventral migration at E10.5-E15.5 follows an initial dorsolateral movement at E8.5-10.5 (Figure 1.2). Upward movement into the epidermis can occur from E13.5, although epidermal MCs are only found in the HFs of adult mice (Jordan & Jackson, 2000). Outside of the skin, a good example of the unique migratory capacity of

MBs is the commonly observed presence of histologically normal MC aggregates in human lymph nodes (LNs) (Gupta et al, 2005).

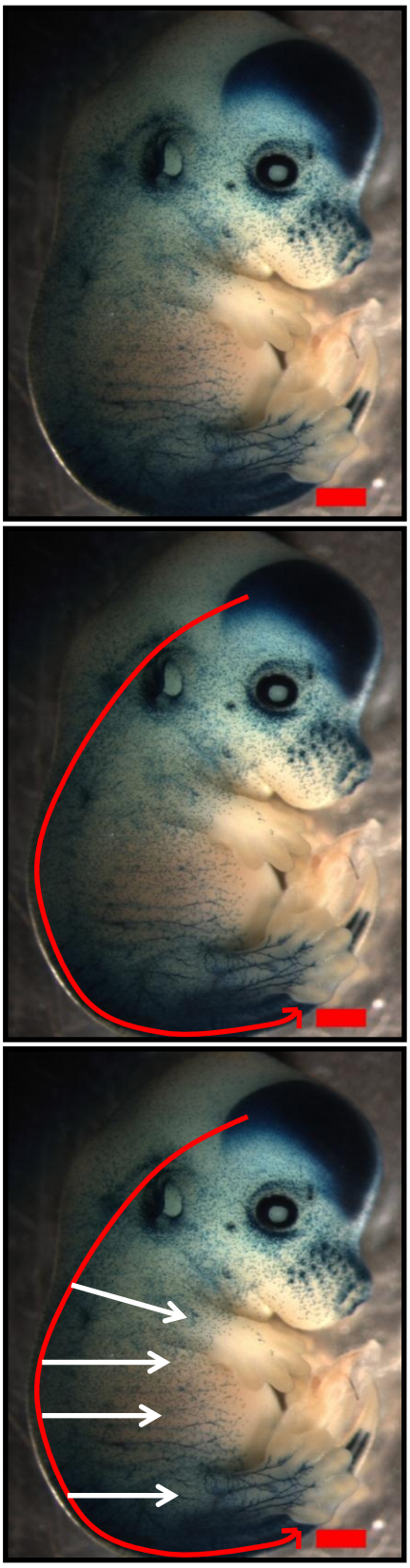

Figure 1.2 Neural crest model of melanoblast migration in embryogenesis
Representative E15.5 X-gal stained embryo derived from DCT-lacZ mice (further detail in section 1.1.5). Each blue 'dot' in the embryo represents a melanoblast. Schematic diagram indicates how dorsolateral movement of melanoblasts from the neural crest (red arrow) is followed by ventral migration (white arrows).

A number of studies have highlighted similarities between the molecular machinery involved in MB migration and melanoma invasion/metastasis, suggesting a circumstance where these physiological processes are 'hijacked' and deregulated in melanoma cells that lack major regulatory checkpoints. The capacity of *KIT* to drive MB migration as well as some subtypes of melanoma is an obvious example (Walker et al, 2011). Gupta and colleagues demonstrated using xenografts that, compared to epithelial cells, the inherent molecular predisposition of MBs for migration is crucial to metastatic melanomagenesis – rather than the mutations incurred to develop melanoma (Gupta et al, 2005). Slug, a regulator of migration and neural crest specification, was shown to be functionally required for melanoma metastasis in this study. Another example of melanoma 'hijacking' of MB molecular physiology is Nodal, an embryonic morphogen not normally expressed in adult tissues, which contributes to Notch4-mediated metastases and tumour cell plasticity after its expression re-emerges in melanomagenesis (Strizzi et al, 2011). Mutations of several other genes that are implicated in melanoma can impair hair pigmentation through their role in MB development (Inoue-Narita et al, 2008).

Melanocyte-specific constitutive expression of $BRAF^{V600E}$ during embryogenesis is lethal (Mercer et al, 2005, Dhomen et al, 2010). Embryos with melanocyte-specific expression of $BRAF^{V600E}$ succumb to hydrocephalus, micropthalmia, and ventricular septal defects, a result that again suggests the importance of MB migration to parts of the body other than skin. Developmental defects in this model were caused by overgrowth of recombined cells which upregulated MAPK signaling. It is clear therefore that MBs are more sensitive to $BRAF^{V600E}$ than adult MCs with tamoxifen-induced expression of the same construct (Dhomen et al, 2009).

Collectively, these studies that focus on the convergence of embryonic and melanoma signalling have already provided key insights regarding cancer formation and progression. It is likely that a 'developmental model' of cancer may eventually prove to be too simplistic, but there is no doubt that it is an extremely effective tool for identifying and characterising new cancer-related genes. The inherent migratory capacity of MBs suggests that their physiology could be further exploited to uncover genes involved in melanoma invasion and metastases.

1.2 Metastasis

Metastases account for over 90% of cancer-related death (Sethi et al, 2011). The pathological process of metastases involves a series of biological steps which require the co-ordinated spatiotemporal activation of a multitude of signaling pathways (Figure 1.3) (Langley et al, 2011). First, tumour cells with metastatic potential detach from the extracellular matrix (ECM) at their primary site and invade the basement membrane using localised proteolysis to become a malignant cancer. Invasion towards the vasculature follows, with eventual penetration of vessel walls ('intravasation'), the process whereby metastatic cells enter the bloodstream. Cancer cells then must withstand the shear pressures of the bloodstream as circulating tumour cells (CTCs), and can ultimately deposit in distal vascular beds by both active and passive mechanisms. Finally, 'extravasation' into the parenchyma occurs, with heterotypic signalling networks in the surrounding stroma creating an environment that promotes metastatic growth.

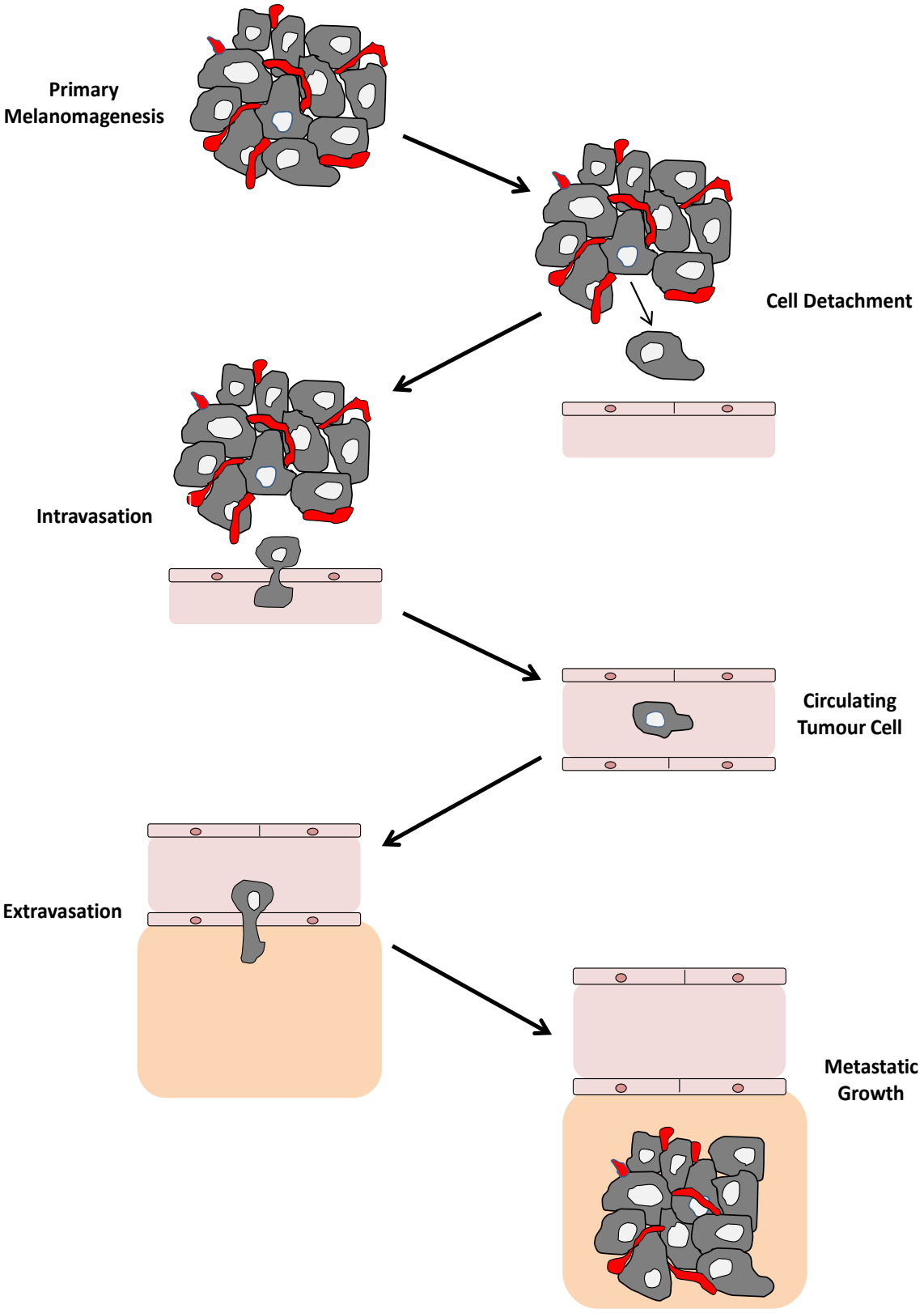

Figure 1.3 Stepwise model of melanoma metastasis (detailed in section 1.2)

The inefficiency and challenges of the metastatic process are highlighted by an estimate that only 0.01% of CTCs will eventually form secondary tumour growths (Fidler, 1970). Experimental evidence suggest that secondary growth of cancer is the most rate-limiting step of metastasis: some tumour cells will be unable to promote angiogenesis and microenvironmental support, while others will stop proliferating and lie dormant in distal organs (Chambers et al, 1995, Barkan et al, 2010). We have already mentioned that the metastatic phenotype can be contributed to by both oncogenic mutations and the inherent molecular predisposition of different cell lineages for metastases, two concepts which are not mutually exclusive and will likely both influence a final cancer outcome. This section of the introduction details the cell-autonomous and environmental mechanisms which can promote this 0.01% metastatic success, as well as describing some of the preclinical and early phase clinical trial challenges involved in assessing metastases in the future.

1.2.1 Metastatic theory

Two sets of paradigms for metastases encompass different stages of its pathological process: the linear progression and parallel progression models debate the point at which a primary tumour can develop metastatic potential, while the seed & soil and anatomical/mechanical hypotheses dispute the mechanism of metastatic organ spread.

1.2.1.1 Linear versus parallel progression models

The central tenet of the linear progression model is that metastatic potential can be determined at the primary site of cancer, where tumour cells accrue successive stages of mutation and selection in response to environmental pressures (Sethi et al, 2011). In this model, an aggressive cancer cell phenotype may be selected after survival within conditions foreign to their normal physiological organisation (hypoxia or mediators of

inflammation, for instance). Support for this theory comes from the historical demonstration that only subsets of cells in heterogeneous primary tumours can metastasise, as well as the clinical correlation of metastatic risk with primary tumour size (Fidler et al, 1972, Koscielny et al, 1984). More recently, high-powered genomic studies have suggested a common late clonal origin of metastases from primary tumours, with other non-clonal mutations required to facilitate the metastatic phenotype (Liu et al, 2009, Campbell et al, 2010, Ding et al, 2010, Yachida et al, 2010).

Parallel progression describes a process whereby primary tumour cells disseminate very early in malignant progression, possibly accruing further mutations to acquire the metastatic phenotype at secondary sites (Sethi et al, 2011). This possibility has been described preclinically with a genetically modified breast cancer mouse model (Husemann et al, 2008). One imagines that the parallel progression model may be more relevant to melanoma cells, given their inherent migratory capacity and their cumulative physiological vulnerability to mutations from lifelong UVR exposure: this thought is supported clinically by the knowledge that primary lesions only a few mm deep can predispose patients to metastases (Balch et al, 2009).

Taken together, although the recent systems biology studies described above favour the linear progression paradigm, the clinical reality is that these models of metastatic potential are not mutually exclusive and both will apply to tumour progression depending on the cancer-context. It is worth noting that either hypothesis would be consistent with the melanoma ‘phenotype switching’ model, which has identified two specific subgroups of melanoma cells in vitro by their expression of specific genes: a proliferative subgroup and an invasive subgroup. Switching between these two phenotypes in response to microenvironmental cues provides a biological rationale for the metastatic cascade, as

well as lesion heterogeneity and heterogeneity of response to treatments (Widmer et al, 2012).

1.2.1.2 Seed & soil versus anatomical/mechanical models

In 1889, Paget described the Seed and Soil hypothesis after studying a series of autopsy specimens from breast cancer patients (Paget, 1887). This model proposes that metastatic cells ('the seed') have a propensity to inhabit and grow in select host organ environments ('the soil'). A number of later experiments validated this with more detail. For instance, Kinsey showed that melanoma cells with a predilection for lung secondaries metastasised to host and ectopically explanted lungs preferentially over other organs (Kinsey, 1960). Moreover, tumour cells have been shown to selectively adhere to the vasculature of their respective target organ (Auerbach et al, 1987). It is impossible to imagine that the 50% rate of liver metastases in uveal melanoma does not conform to this model. The 'pre-metastatic niche' hypothesis extends the theory by suggesting that bidirectional signalling between primary and metastatic tumours fashions a hospitable vascular microenvironment for the survival and expansion of secondary tumours (Kaplan et al, 2005).

Nonetheless, the seed & soil hypothesis is again not mutually exclusive from the opposing anatomical/mechanical model of metastases, and it is likely that both explanations are correct to varying extents in different cancer contexts. The anatomical/mechanical model proposes that vascular and lymphatic anatomical distribution are the primary determinants of metastasis localization (Langley et al, 2011). Such a hypothesis could straightforwardly explain the propensity for liver metastases in gastro-intestinal tumours, for example. The high incidence of lung metastases in many cancers could also be considered a consequence of metastatic tumour cells becoming randomly embedded in

the tiny capillaries of the lung microvasculature. However, the experimental evidence begun by Paget suggests that this is only the beginning of the story: the challenge of understanding the cellular and molecular basis for the complex events in metastases continues and remains a difficult process. A good example of this complexity is the 'self-seeding' hypothesis: the process where CTCs re-colonise their primary site of cancer could clinically explain local recurrences after seemingly 'clean' tumour resections (Kim et al, 2009).

1.2.2 Translational considerations in metastasis

This section focuses on translational issues specific to cancer metastases in general, while section 1.4 describes and discusses translational successes in melanoma with some key examples in other cancers. Much progress up till now has come with the use of novel cytotoxic or cytostatic inhibitors, but not 'anti-metastatic' agents. In part this is because the concept and design of 'anti-metastatic' early phase clinical trials can cause many methodological difficulties. One central problem with characterising anti-metastatics is that patients referred for phase I trials nearly always already have metastatic disease: doctors will have first performed their ethical duty to try all 'evidence-based' treatment options before referring for an untested option based only on preclinical theory. This leaves us with an obvious question, how do you confirm the efficacy of a potentially new anti-metastatic drug in patients that already have metastases? The alternative would be to ethically justify administration of an unproven and potentially toxic anti-metastatic agent to patients who are seemingly cured of their cancer following primary surgery: such a trial would be costly, time-consuming, and involve large patient numbers. To add to this problem, the possible increased treatment resistance conferred by mutational

accumulation in metastases often makes pharamaceutical companies wary of developing compounds as pure ‘anti-metastatic’ targets.

Many other preclinical considerations feature in strategic decisions on how to treat metastatic disease for a given cancer. For instance, should we target the tumour microenvironment concomitant with treating the tumour itself? It is undisputed that the microenvironment plays a greatly extended role in metastases compared to primary tumourigenesis, perhaps best demonstrated by the ‘pre-metastatic niche’ concept described above (Langley et al, 2011). The success of denosumab (a human monoclonal antibody against RANK ligand) in the treatment of breast cancer-related bone metastases suggests that this may be particularly important for prevention of organ-specific spread (Stopeck et al, 2010). However, attempts to target tumour microvasculature using novel therapeutics targeted to the VEGF receptor have so far been relatively unsuccessful, with one key problem being a lack of availability of predictive biomarkers (Sethi et al, 2011).

Another consideration will be how to establish predictors of response to anti-metastatic treatment, particularly given the evidence that, in line with the linear progression model, metastatic tumours may select against and outgrow their initial driver mutations (Kim et al, 2006, Sanz-Moreno et al, 2008). Given the myriad microenvironmental and stromal contributions to metastasis, the key to identifying metastatic predictors is likely to involve a systems biology approach, including next generation sequencing of primary tumours and their metastases, as well as characterisation of transcriptomic, epigenomic, and proteomic alterations (Sethi & Kang, 2011). While these methodologies are quickly evolving, the creation of a network for publically available tumour banks (pre and post treatment) will also assume increasing importance. Finally, robust animal models will be

required to efficiently validate candidate metastatic genes as well as novel therapies targeted against their proteins.

Taken together, it seems inevitable that early phase clinical trials will require considerable upheaval to accommodate anti-metastatics. It was encouraging to see that recent clinical trial assessment of mammalian target of rapamycin (mTOR) inhibitors had evaluated their role in alternative clinical settings other than the 'last line', including one neo-adjuvant study prior to curative surgery (Baselga et al, 2009; Baselga et al, 2012). This was only possible due to the combination of the novel mTOR inhibitor with established hormonal treatments, but hopefully its success will encourage a transition towards even bolder clinical trials.

1.3 Melanoma Metastasis

Approximately 20% of melanoma sufferers over the age of 65 years will present with metastases and therefore be incurable at diagnosis. In contrast, 7% of 15-64 year olds present with metastases (www.cancerresearchuk.org/cancer-info/cancerstats /types/skin/incidence/). The five year survival of these patients is <5%, with a median survival of 6 months. Metastases to skin and lungs have a better prognosis than those to brain, bone and liver, where patients are often faced with rapidly progressive and aggressive disease that confers a life expectancy of 1-2 months (Balch et al, 2001). This section attempts to order and discuss the key *in vivo* molecular components of melanoma metastasis that have been reported.

None of the key melanoma driver mutations or TSG losses (*BRAF*, *NRAS*, *PTEN*, *CDKN2a*) have been particularly related to the development of metastases or diminished outcomes in humans. With a 50% rate of liver metastatic disease in uveal melanoma, one might have expected *GNAQ* or *GNA11* to associate with worse outcomes. However, a retrospective analysis of these patients suggested *GNAQ* and *GNA11* mutation improves overall survival in uveal melanoma compared to those patients with uncharacterised genetics (Van Raamsdonk et al, 2010). These findings are predictable given that it is not individual mutations, but mutation burden, that is important for the metastatic phenotype (Walker et al, 2011). Metastatic cells often undergo high rates of spontaneous mutation compared to benign cells, often conferring resistance to therapeutics with their mutational 'drift' (Talmadge et al, 1984). The identification of NEDD9 as a melanoma 'metastasis gene' in mouse tumours that have lost their dependence on Ras signalling suggests that the fundamental driver mutations in primary melanoma can become less important with cancer progression (Kim et al, 2006, Sanz-Moreno et al, 2008).

1.3.1 Mouse models of melanoma metastasis

The first melanoma mouse work was performed in the early 20th century, with the observation of an inbred mouse strain that was noted to have developed spontaneous melanocytic tumours (which ultimately led to derivation of the near-ubiquitous B16 cell line). Following this, a number of models employed mutagens such as UVR, DMBA, and 12-O-tetradecanoylphorbol-13-acetate (TPA). Genetically modified mouse models of melanoma were first reported in the 1990s (Damsky Jr et al, 2010).

Two prescient and contrasting thoughts will likely define the future utility of genetically modified mouse models of melanoma metastases.

1. It is impossible to observe and experimentally manipulate the entire multistep process of metastatic melanomagenesis in humans, and there is little knowledge of how faithfully *in vitro* primary and metastatic models can characterise this process (Kumasaka et al, 2010). Moreover, despite improved access to metastatic tissue with human melanoma, we still have limited insight of metastatic mechanisms compared to those of tumour initiation. Therefore, genetically modified mice still represent the primary utility for studying the metastatic process in its entirety, and one would predict that this will remain the case in the longer-term.

2. There is now a greater emphasis on a systems biology approach for studying metastases, which will ultimately lead to large numbers of novel candidate 'metastasis' genes requiring functional validation with traditional laboratory approaches. At present, genetically modified mouse models represent a potentially time-consuming and expensive bottleneck in this process.

The challenge will be to square the above two considerations into rapid, adaptable and faithfully representative models of metastatic melanoma in mice.

1.3.1.1 An optimal genetically modified model

An optimal genetically modified mouse model of metastatic melanoma helps reveal disease biology and can be used for assessment of new therapies. Ideally it will closely recapitulate characteristic human melanoma genetics and pathology, including metastases to relevant organs within a manageable and reflective timeframe. It may also be used to discover and validate driver mutations of disease onset, explore TSGs constraining disease progression, and define mechanisms of melanoma invasion and metastases. Spatial and temporal control of genetic modifications is important to accurately recapitulate spontaneous melanoma (Dankort et al, 2009). Aetiology of disease (eg. UVR) may also be represented. With all this in mind, great strides have been made in the last 20 years towards this ideal model, although even the best examples will still have several limitations.

1.3.1.2 Working towards an optimal genetically modified model

Table 1.2 delineates the current advantages and limitations of melanoma mouse model systems used to delineate metastasis. Below this, three key conceptual advances towards improved metastatic melanoma mouse models are detailed.

Mouse Model System	Advantages	Disadvantages
Allografts	• Intact immune system and correct species environment • Potential for real-time imaging with reporter genes • Multiple genetic manipulations can be investigated • Drug testing and development	• Primary tumour resection often required before metastatic development • Can only use mouse melanoma-derived cancer cells • Organ tropism not fully accurate
Germline genetically modified models	• Intact immune system and correct species environment • More accurate biological model of primary initiation, local invasion, and metastatic spread • More accurate drug testing and development possible • More accurate histology	• Difficult assessment of cell-autonomous versus non-cell-autonomous effects • Labour and resource intensive • Difficult to track metastases, primary tumour resection often required • Limited metastases and metastatic sites, often LN and lung • Restrictive timeframe of primary and metastatic development
Conditional genetically modified models	• Temporal and tissue-specific control faithfully recapitulates features of spontaneous disease. • No problem distinguishing cell-autonomous and non-cell-autonomous effects • Otherwise similar to above	• Same as last 4 bullet points above.

Table 1.2 Mouse models systems used to delineate metastases
Adapted from Sethi et al, 2011.

- *Primary tumour removal.* Other than finding the time and money required to cope with the output from high throughput sequencing analyses, a key challenge with all models mentioned in Table 1.2 is the development of efficient and standardised protocols for primary tumour removal. This is not a new idea and was reported with some success in a previous metastatic model (Kelsall et al, 1998). It is necessary because primary tumour burden will often prompt euthanisation of a mouse before full development of metastases has been possible: resection could avoid this limitation and more accurately reflect the clinical course of melanoma recurrence in humans (Francia et al, 2011). However, the technique itself can be difficult and impractical: mice often have multiple asynchronous primary tumours which are at different stages of growth and local invasion when eventually analysed histologically. More time, money and mice could optimise this technique in the short-term, investing in a future that can more accurately predict the efficacy of new anti-metastatic targets.

- *Tumour histology.* This is another issue important to genetically modified models of melanoma initiation, and will likely be important to local invasion and metastasis also. A key difference between humans and mice is the localisation of MCs and melanoma: although they characteristically reside and develop in the dermis of most mouse models, humans typically harbour MCs and develop melanomas in the epidermis or epidermal-dermal junction (Herlyn et al, 2000). It is not surprising therefore that the majority of melanoma mouse models exhibit primary melanoma more characteristic of the human NM subtype, rather than the more frequent SSM (Walker et al, 2011). A variety of spindle, epithelioid and mixed primary tumour histologies have been reported, as well as differing levels of pigmentation. Taken together or separately, the effect of these primary tumour variables on the subsequent development of

metastases remains uncharacterised. It is also unclear whether artificially manipulating mouse genetics to fully recapitulate human histology is a desirable endpoint: the success of the mutant Braf inhibitor, vemurafenib, suggests we should concentrate on mouse models that correctly reflect human melanoma genetics first (Flaherty et al, 2010).

- *Defining metastatic parameters.* One final aspect of improving mouse metastatic assessment should be readily applicable. Measures of metastases and metastatic propensity are often not reported and could easily be standardised to mimic those performed in clinical trials. This could include details such as naevi, mitotic rate, ulceration, lesion size at spread, and sites of metastases. A couple of older mouse models offered admirable macroscopic and microscopic details of their metastases, but one fears that this quality of content may have been lost with reporting some of the novel mouse models which have improved genetic recapitulation (Table 1.3) (Kelsall et al, 1998, Zhu et al, 1998).

1.3.1.3 Current optimal models of metastatic melanoma

Table 1.3 presents a synopsis and some detail of all models which have developed metastases. Modelling metastatic melanoma in mice has made great advances in the last 20 years: this section will focus on two models that most satisfactorily recapitulate the genetics, timing, and metastases of the human disease, as well as offer amenability to therapeutic treatment. Between these two models, the four most common genetic modifications in human melanoma are represented: $NRAS^{Q61K}$, $BRAF^{V600E}$, loss of *CDKN2A*, and loss of *PTEN*. Here we do not detail other reported models, such as those with mutant *HRAS* or over-expression of HGF, which are more dated and less reflective of common human melanoma genetics.

Report	Year	Genetic Modification	Carcinogen/ Induction	Histology	Metastasis detail
Nogueira et al	2010	Tyr::Hras^{G12V}; CDNK2a$^{-/-}$; PTEN$^{+/-}$	no	spindle	2/21: lung and LN
Terzian et al	2010	TPras; Mdm4$^{+/-}$	DMBA	no	7% mets in control TPras$^{O/+}$ mice: liver, lung, LN
Kumasaka et al	2010	MT::Ret; Ednrb$^{+/-}$	no	no	44% lung in MT::Ret, increased in MT::Ret; Ednrb$^{+/-}$
Goel et al	2009	Tyr::Braf$^{V600E;}$ CDKN2a$^{+/-}$	no	spindle/ epithelioid	Lung/LN/brain – no detail
Dankort et al	2009	*Tyr::CreER Braf$^{V600E/+}$; PTEN$^{lox/lox}$*	tamoxifen	spindle/ epithelioid	100% LN; lung – no detail.
Inoue-Narita et al	2008	DCT::Cre PTEN$^{fl/fl}$	DMBA/TPA	spindle	20% lung mets
Tormo et al	2006	MT::HGF/SF; CDK4$^{R24C/R24C}$	DMBA/TPA	spindle	LN in MT::HGF/SF; CDK4$^{R24C/R24C}$ and MT::HGF/SF; CDK4$^{R24C/+}$ - no details; lung in MT::HGF/SF; CDK4$^{R24C/R24C}$ only – no details
Hacker et al	2006	TPras; CDK4$^{R24C/R24C}$	UVR	no	All LN: 92% TPras; CDK4$^{R24C/R24C}$ with UVR, 60% TPras; CDK4$^{R24C/R24C}$ no UVR, 16% TPras with UVR
Yamazaki et al	2005	K14::SCF; XPA$^{-/-}$	UVR	no	11/20 to LN
Ackermann et al	2005	Tyr::Nras$^{Q61K/°}$; CDKN2a$^{-/-}$	no	epithelioid	64% LN; 36% liver or lung
Von Felbert et al	2004	MT::Ret; IL-6$^{-/-}$	no	spindle/ epithelioid	Multiple organs for MT::Ret, MT::Ret; IL-6$^{+/-}$, and MT::Ret; IL-6$^{-/-}$ - no details
Pollock et al	2003	DCT::Grm1	no	no	LNs – no details
Recio et al	2002	MT::HGF/SF; CDKN2a$^{-/-}$	UVR	no	LN/liver – no details
Krimpenfort et al	2001	INK4a$^{-/-}$; ARF$^{+/-}$	DMBA	no	1/10 without DMBA, 2/14 with DMBA: LN, lung, spleen, liver
Kato et al	2000	MT::Ret	UVR	no	1/2 mice analysed - lung met
Broome Powell et al	1999	TPras	UVR/DMBA/ TPA	no	>40% LN/lung with DMBA treatment
Otsuka et al	1998	MT::HGF/SF	no	spindle/ epithelioid	21% to various organs
Kato et al	1998	MT::Ret	no	no	13/25 to various organs
Kelsall et al	1998	Tyr::SV40E	UVR	spindle/ epithelioid	36%: lung, LN, kidney
Zhu et al	1998	TG3	no	spindle/ epithelioid	Up to 41% in organs, 100% in LNs

Table 1.3 Details of metastases observed in genetically modified mouse models of melanoma.

In 2005, Ackermann and colleagues described a *Tyr::Nras*$^{Q61K/°}$ mouse which developed a 36% incidence of lung/liver metastasis when *CDKN2a* ('*INK4a*$^{-/-}$ ') was constitutively knocked out (*Tyr::Nras*$^{Q61K/°}$*; INK4a*$^{-/-}$ mice) (Ackermann et al, 2005). 64% of these mice also had enlarged LNs, although it was impossible to ascertain if these lesions were of primary or metastatic origin. Common features of metastatic potential were reported, such as macroscopic ulceration and microscopic vascularisation. Timing of primary and metastatic melanoma typically occurred within a realistic timeframe of 6-9 months, offering an appealing window for therapeutic intervention and characterisation. Pigmented dermal primary melanomas occurred with 94% prevalence, and no primary tumour removal was attempted.

More recently, three mouse models expressing melanocyte-specific Braf^{V600E} were reported, with one study describing 100% metastatic spread when mutated *BRAF* was combined with melanocyte-specific *PTEN* deletion (*Tyr::CreER Braf*$^{V600E/+}$*; PTEN*$^{lox/lox}$ mice) (Dankort et al, 2009, Dhomen et al, 2009, Goel et al, 2009). These *Tyr::CreER Braf*$^{V600E/+}$*; PTEN*$^{lox/lox}$ mice always developed LN metastases (the issue of whether these were primary or metastatic lesions was not addressed), with an unspecified number of lung metastases also observed. Pigmented primary dermal lesions with epidermal spread were rapidly progressive, requiring euthanisation at 25-50 days after tamoxifen induction. Despite this short latency, treatment intervention with combined rapamycin and MEK inhibition was effective and induced tumour regression. No primary tumour removal was attempted. In a recent extension of this study, β-catenin was identified as a central mediator of metastasis observed in the same mouse model (Damsky et al, 2011).

The above two metastatic melanoma mouse models constitute a basis for the results of large parts of this thesis: section 7.3 in the discussion will analyse their relative merits and disadvantages in more detail.

1.3.1.4 Xenografts and other models

The deficiencies of xenograft models of metastatic melanoma have been well characterised. Some common examples are cited below (Francia et al, 2011, de Bono et al, 2010):

- Sub-cutaneous (SC)-injected tumours grow rapidly: this is not representative of human primaries, and often leads to false positive results when therapeutic interventions that target dividing cells are administered.

- Cell lines used are often genetically ill-defined, and after years of growth adapted to a laboratory, may not be indicative of the tumours from which they were derived.

- Immuno-compromised mice do not accurately recapitulate the tumour microenvironment.

- Species-specific incompatibility between mouse stroma and human tumours will not accurately recapitulate the tumour microenvironment.

- Tumours are often injected outwith their orthotopic site: it is unclear whether they would grow or respond to treatment similarly in their site of origin.

- Novel treatment studies often do not involve previous lines of therapy that would provoke resistance in a mouse, and therefore do not accurately represent patients receiving novel drugs in early phase trials.

- The primary tumours traditionally analysed in xenograft treatment studies do not reflect the high metastatic and mutational burden of patients receiving novel drugs in early phase trials.

- Endpoints are often ill-defined and unstandardised.

Nonetheless potential uses of xenografts include pharmacokinetic (PK) analyses, as well as validation and further characterization of *in vivo* results obtained with another more representative model. Moreover, orthotopic transfer and direct transfer of human tumours may offer valuable results with relatively little time and expense.

Zebrafish models of melanoma have provided excellent insights into melanomagenesis, as well as offering an adaptable resource for genetic manipulation and treatment administration (Patton et al, 2005, Patton et al, 2010). Other animals are not easily genetically modifiable and their husbandry is extremely expensive (Walker et al, 2011). Many carcinogen-induced mouse models of melanoma have been described over the past few decades (Table 1.3): as discussed earlier (section 1.1.2), more insight could be gleaned from these once we have fully established the mechanistic relationship between carcinogens such as UVR and the development of genetic alterations that predispose to melanoma.

1.4 Clinical translation and melanoma

Older cancer drugs such as tamoxifen sometimes achieved success in cancer clinical trials using a 'one size fits all' approach. For example, although no predictive evaluation of oestrogen receptor status was performed in its breakthrough breast cancer trial, the benefits of tamoxifen in the majority of women who were oestrogen receptor-positive led to a statistically significant result which was not diminished by a lack of response in the significant minority of women who were oestrogen receptor-negative (Ingle et al, 1981). It is noteable that this strategy would have catastrophically failed if it had been applied to the vast majority of translational successes in the last 15-20 years, but pressured pharmaceutical companies will often still pursue such an approach, wasting vast amounts of time, money, and resource for limited patient benefits (de Bono et al, 2010).

1.4.1 Lessons from translational research

For translational research to progress in the future, it is imperative that we recognise the reasons for prior successes and failures. Four key steps can help to achieve this:

1. *Strong biological hypothesis.* Poor validation of anticancer drug targets has been a longstanding problem that leads to clinical trial failures, and is often exacerbated by the use of unrepresentative xenograft mouse models (detailed in section 1.3.1.4). Biological concepts such as 'oncogene addiction' and 'synthetic lethality' characterise modern rational approaches, identifying predictive biomarkers and providing a therapeutic window for potential treatments. Rare success stories here include crizotinib, a small molecule inhibitor which reverses the oncogene dependence of a subset of non-small cell lung cancers (NSCLC) by targeting an anaplastic lymphoma kinase (*ALK*) fusion rearrangement, and olaparib, a small molecule which induces synthetic lethality in *BRCA*-deficient cancer patients by inhibiting poly(ADP)-ribose

polymer formation (PARP) (Fong et al, 2009, Kwak et al, 2010). The identification of *RAS* mutations as a negative predictor of success for epidermal growth factor receptor (EGFR) inhibition in colon cancer is a good example of a straightforward biological hypothesis that could easily have been considered prior to its clinical characterisation years later (Karapetis et al, 2008).

2. *Improved clinical trial design.* Consideration of clinical efficacy of novel drugs should be expedited in the early clinical trial phases. Phase I trials are traditionally designed to dose-find as well as evaluate toxicity, PKs and pharmacodynamics (PDs). Phase II/III trials, often performed years later with large patient numbers, will usually be the first assessment of treatment efficacy. However, treatment success with vemurafenib (small molecule inhibitor of $Braf^{V600E}$) has demonstrated the clear advantage of preclinical identification of enrichment biomarkers ($BRAF^{V600E}$) to instruct patient selection in phase I trials (Flaherty et al, 2010). Conversely, a number of equivocal trials with no genotyping input led to a 10 year gap between drug development and confirmation of efficacy for EGFR inhibitors (Mok et al, 2009). Characterisation of treatment benefits at phase I can lead to the expedition of later phase II/III to confirm this efficacy, and also reduce the high frequency of wasted time and money invested in failed later phase trials. If an enrichment biomarker is not available at phase I, clinical trial designs should include putative biomarkers that could predict treatment benefit, early discontinuation, or toxicity at intermediate endpoints. A network of pre- and post-treatment tumour banks will become imperative to assist this process.

3. *Re-iterative research.* Failed clinical trials can too often lead to pharmaceutical companies withdrawing development of potentially effective drugs. It is critical to biologically re-interrogate the mechanisms of action of a failed drug, as well as re-

examine clinical trial design to ensure delivery of an optimal chance of success. A common reason for clinical trial rejection that requires further biological dissection is drug resistance. EGFR-mediated resistance to vemurafenib in $Braf^{V600E}$-driven colon cancer is a recent example (Prahallad et al, 2012).

4. *Communication.* Within a framework that incorporates the sometimes opposing cultures of university academia and the pharmaceutical industry, drug development requires expert input from molecular and cell biologists, oncologists, molecular pathologists, chemists, and structural biologists. Strong communication, particularly between academia and pharmaceutical companies, will be imperative for the improvements suggested above to become possible.

1.4.2 Metastatic melanoma translation

Until very recently, no therapy administered to UK patients with metastatic melanoma could extend overall survival. Dacarbazine, a cytotoxic that has been used for years, offers limited success though an improvement in symptoms of carefully selected patients (Tarhini et al, 2006). Unlike many other cancers with developed treatment protocols, melanoma therefore offers an attractive niche for the development of targeted treatments that are tailored to their underlying genetic modifications.

1.4.2.1 Vemurafenib

In 2011, vemurafenib, a small molecule inhibitor of $Braf^{V600E}$, was reported as the first agent targeted to melanoma genetics that could offer an extension in overall survival of metastatic patients, with a hazard ratio of 0.37 compared to control patients treated with dacarbazine (Chapman et al, 2011). Response rates were 48% for vemurafenib and 5% for dacarbazine. As patient selection was strictly limited to the 50-60% of melanoma patients

carrying the *BRAF*^{V600E} mutation, toxicity was generally tolerable. Several resistance mechanisms to vemurafenib have already been described, offering important insights for oncologists to re-iteratively dissect treatment of progressing patients with further rationally designed 2nd line trials (Poulikakos et al, 2010, Heidorn et al, 2010, Hatzivassiliou et al, 2010, Johannessen et al, 2010, Nazarian et al, 2010, Gopal et al, 2010, Shao et al, 2010).

1.4.2.2 Imatinib

Similar to the protracted timeline of EGFR inhibition in cancer, imatinib in metastatic melanoma is unfortunately another paradigm of poorly considered translational research. *KIT* is mutated or amplified in 20% of LMM and 40% of ALM, two melanoma subtypes which represent a significant minority of patients (Curtin et al, 2006). Despite this, only 1 of 64 metastatic melanoma patients showed a partial treatment response in three phase II trials of imatinib in ungenotyped metastatic melanoma patients (Ugurel et al, 2005, Wyman et al, 2006, Kim et al, 2008). After a delay of 6 years, a fourth phase II trial assessed metastatic melanoma patients for *KIT* mutation or amplification, and showed a 23% response rate and 30% rate of disease stability; the mutations and amplification state of patients resistant to imatinib were also clarified in this trial, offering further opportunities for re-iterative translational research (Guo et al, 2011).

1.4.2.3 Ipilimumab

The main other metastatic melanoma success recently described is ipilimumab, a monoclonal antibody that targets cytotoxic T-lymphocyte–associated antigen 4 (CTLA-4), a negative regulator of T cells, and thereby augments T-cell activation and proliferation. Both with and without dacarbazine, this drug has also been shown to extend patient

survival, although with a smaller response rate and higher toxicity owing to its 'one size fits all' approach (Hodi et al, 2010, Robert et al, 2011).

1.4.2.4 Other agents

Other emerging agents include a variety of preclinically successful MEK and PI(3)K inhibitors which are tailored to melanoma genetics and, if they follow the example of vemurafenib development, offer exciting potential for further progress. Perhaps the most disappointing targeted therapeutic applied in melanoma trials is sorafenib, employed on the basis of its anti-VEGFR and anti-Raf activity: poor efficacy was seen in both monotherapy and combination trials (Eisen et al, 2006, Hauschild, 2009, Ott et al, 2010). Clinical efficacy through inhibition of oncogenic Ras was not achieved by farnesyl transferase inhibitors, and remains elusive for treatment of melanoma and other cancers (Flaherty et al, 2006).

1.5 Two Novel Melanoma Anticancer Targets

This thesis examines the anticancer potential of two putative melanoma targets, PIP_3-dependent Rac-exchanger 1 (P-Rex1) and focal adhesion kinase (FAK) (Figure 1.4). As both proteins have particularly important roles in physiological migration, we focus on their roles in melanoma invasion and metastases, often additionally assessing embryonic mouse models as a paradigm for their cancer phenotypes. The two metastatic melanoma mouse models described in section 1.3.1.3 provide platforms for the evaluation of P-Rex1 and FAK that can recapitulate common human genetics: *Tyr::Nras$^{Q61K/°}$; INK4a$^{-/-}$* and *Tyr::CreER Braf$^{V600E/+}$; PTEN$^{lox/+}$* mice. Throughout chapters 3-7, there is a commentary on potentially relevant translational aspects of this preclinical research.

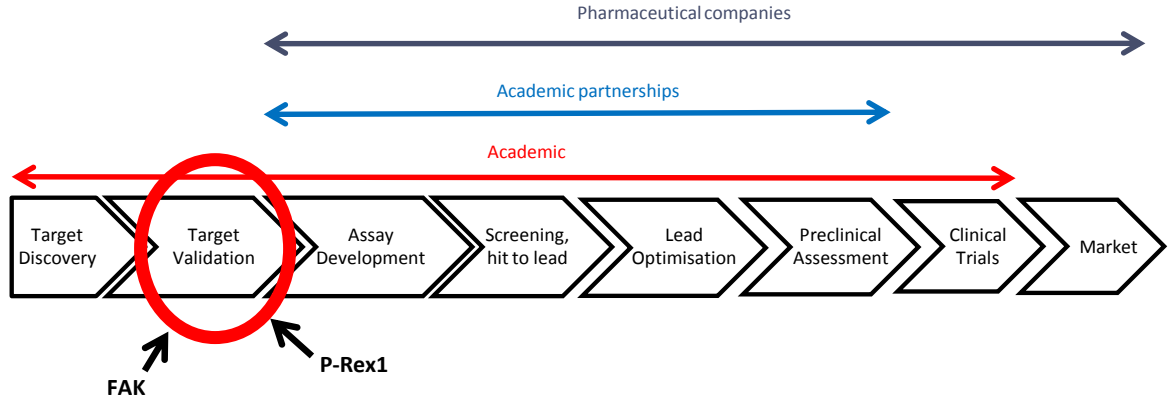

Figure 1.4 Drug discovery cascade
Schematic flowchart showing the multiple steps required to generate a novel anti-cancer inhibitor following inital target discovery. The potential roles of academia, pharma-academic partnerships, and pharmaceutical companies are indicated. This thesis focuses on a step of the cascade that can only be performed in academia, target validation. P-Rex1 and FAK are the targets studied.

1.5.1 PIP_3-dependent Rac-exchanger 1 (P-Rex1)

PREX1 encodes the P-Rex1 Dbl family of Rho guanine nucleotide exchange factors which can activate Rho family small GTPases, a major branch of the Ras superfamily of small GTPases (e.g. RhoA, Rac1/2/3 and Cdc42) (Wennerberg et al, 2005). Specifically, P-Rex1 is a guanine-nucleotide exchange factor (GEF) for Rac, whose primary cell function is induction of actin-mediated membrane ruffling and lamellipodia formation at the leading edge of cell migration (Welch et al, 2002, Hill et al, 2005, Barber et al, 2007). Stimulation of Rac-GEFs is thought the most important mechanism of Rac activation, allowing Rac to function as a bimolecular switch that is able to adopt different conformational states as a consequence of GDP or GTP-binding (Rossmann et al, 2005) (Figure 1.5a). The exchange of GDP for GTP permits Rac binding to a myriad of different downstream effectors which can initiate a diversity of cellular processes, including actin cytoskeletal control, cell cycle progression, and ROS formation (Mack et al, 2011). Most characterised of the Rac effectors are actin-associated proteins such as WASP, WAVE, and Pak (Ben-Yaacov et al, 2001, Cotteret et al, 2002); NADPH oxidase has also been identified downstream as a link to its role in ROS formation (Bokoch et al, 1995).

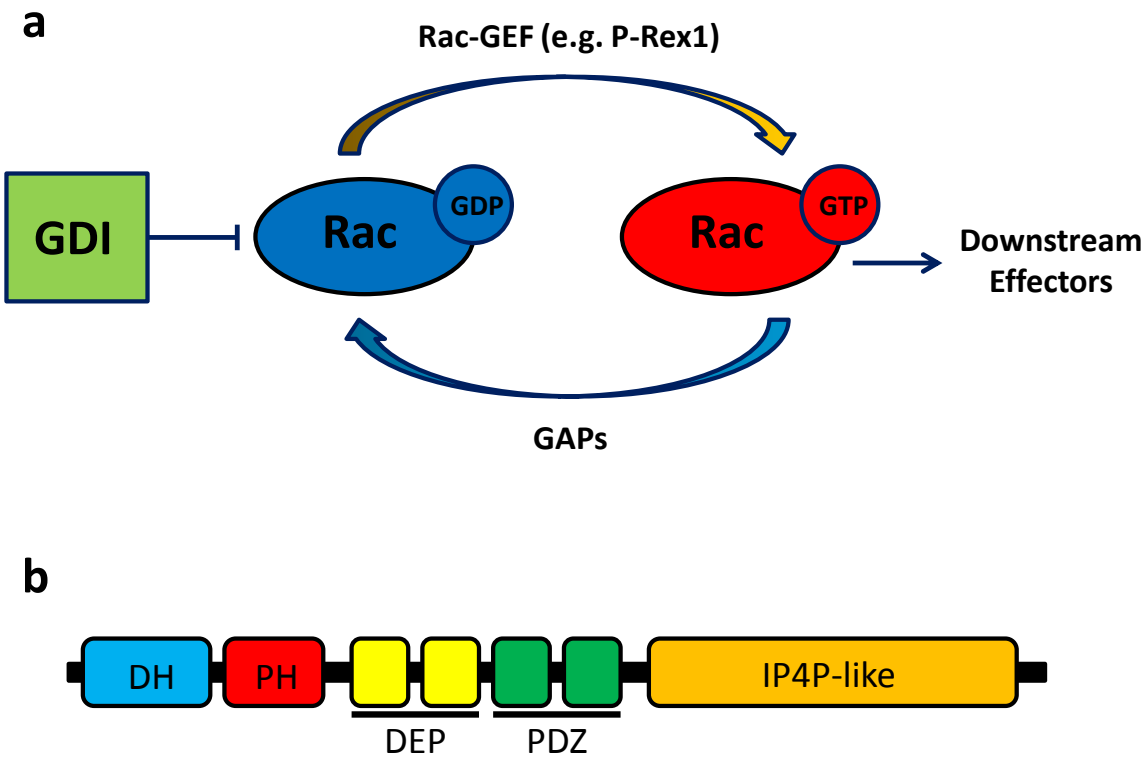

Figure 1.5 Structure and function of P-Rex1
(a) Rac-GEFs such as P-Rex1 catalyse Rac cycling from a GDP-bound inactive form to a GTP-bound active form, thus altering its conformation so that it can interact with downstream effectors. GAPs promote the intrinsic GTPase activity of Rac, returning it to its inactive GDP-bound state. GDIs sequester the inactive Rac-GDP so that it cannot be activated by GEFs. GEFs = guanine-nucleotide exchange factors, GAPs = GTPase activating proteins, GDIs = guanine-nucleotide dissociation inhibitors **(b)** Schematic diagram showing P-Rex1 domain structure (see Section 1.5.1 for further detail). DH = Dbl homology, PH = pleckstrin homology, IP4P = inositol polyphosphate 4-phosphatase.

There are three members of the P-Rex family: P-Rex1, P-Rex2a, and P-Rex2b. Normally, P-Rex1 is expressed in haematopoietic cells and the brain, while P-Rex2a and P-Rex2b are more ubiquitously expressed in other tissues, including the skeletal muscle and heart (Welch et al, 2002, Donald et al, 2004, Rosenfeldt et al, 2004). They have similar domain structure and can all exhibit GEF activity: tandem Dbl homology (DH)/pleckstrin homology (PH) domains, typical of Rho family GEFs, are followed by 2 DEP and 2 PDZ domains. An inositol polyphosphate 4-phosphatase (IP4P)-like domain follows in P-Rex1 and P-Rex2a (Figure 1.5b). P-Rex1 is a cytosolic 185kDa protein with 41 exons (Welch et al, 2002).

1.5.1.1 P-Rex1 discovery and physiological regulation

Approximately 70 Rho-family GEFs with tandem DH/PH domains have been identified to date, each exhibiting their own tissue, substrate, and upstream specificity. It is thought that they apply these different inputs to confer signalling specificity, with consequent coupling of Rac or other RhoGTPases to varying downstream effectors (Rossmann et al, 2005). Despite the large number of GEFs described, P-Rex1 was uniquely characterised as a result of its activity, using functional and biochemical purification from the cytosol of motile neutrophils (Welch et al, 2002). Before this, GEFs had previously been identified either by their homology to other known GEFs, or as oncogene products (Weiner et al, 2002).

The unique character of P-Rex1 is also evidenced by its direct stimulation from PI(3)K-stimulated phosphatidylinositol (3,4,5)-trisphosphate (PIP_3) production and the beta-gamma subunits of the heterotrimeric G proteins (Gßγ) (Welch et al, 2002, Hill et al, 2005, Barber et al, 2007). The PI(3)K pathway had only been shown to indirectly regulate other Rho-GEFs prior to P-Rex1 discovery, and P-Rex1 was also the first Rho-GEF shown to be directly stimulated by Gßγ. These two activators of P-Rex1 were shown to stimulate its

activity synergistically, raising its potential as a 'coincidence detector', designed to respond to the combined or isolated appearance of at least two different inputs that would likely bind separate P-Rex1 domains.

Myriad reports of P-Rex1 physiology over the past 10 years have detailed further functions in neuronal migration and angiogenesis, but still predominantly focus on its neutrophil role (Hill et al, 2005, Yoshizawa et al, 2005, Welch et al, 2005, Dong et al, 2005, Zhao et al, 2007, Barber et al, 2007, Waters et al, 2008, Carretero-Ortega et al, 2010, Lawson et al, 2011). A P-Rex1-deficient mouse (impaired catalytic GEF domain) exhibited no gross phenotype and a normal lifespan; further evaluation revealed that they were constitutively smaller than *wild-type* mice, with a mild neutrophilia and aberration of their normal neutrophil activity (Welch et al, 2005, Dong et al, 2005). Another report assessed the domain function of P-Rex1 using targeted deletion mutants: an *in vitro* assay measuring GTP-loading of Rac showed that the DH domain mutant was catalytically inactive, confirming it as the catalytic site of GEF activity typical to Rho-GEFs; mutation to the PH domain precluded PIP_3 stimulation and control (Hill et al, 2005). Mutation of the DEP, PDZ, or IP4P-like domains, which confer structural specificity of P-Rex1 compared to other Rho-GEFs, had no major consequences but likely have important functional interactions with the tandem DH/PH domains (Hill et al, 2005, Urano et al, 2008). Of note, the IP4P-like domain has no phosphatise activity and its role remains largely uncharacterised (Welch et al, 2002). The relative roles and contributions of P-Rex1 with another Rac-GEF, Vav, has also been assessed, while an *in vitro* study suggested P-Rex1 activity could also be controlled by protein kinase A phosphorylation (Mayeenuddin et al, 2006, Lawson et al, 2011).

1.5.1.2 P-Rex1 in cancer

In addition to its activation by both PI(3)K and GPCR signaling, a number of factors implicated a role for P-Rex1 in cancer during the early stages of its physiological characterisation:

1. *Aberrant activation of Rac in cancer*. Rac control of the actin cytoskeleton can be disrupted in cancer for invasion and metastasis (Mack et al, 2011). For example, inhibition of Rac diminishes the motility and proliferation of breast cancer cells in response to EGFR or ErbB3 ligands (Yang et al, 2006, Yang et al, 2008).

2. *Aberrant activation of Rac-GEFs in cancer*. Unlike Ras proteins, mutations of Rho-GTPases are uncommon in cancer despite the evidence for malignant deregulation of Rac. A cancer-specific role for Rac-GEFs including TIAM1, Vav1/2 and DOCK3 can alternatively contribute to this, with tumour type not necessarily related to the tissue-specific function of a given RacGEF (Minard et al, 2004, Fernandez-Zapico et al, 2005, Patel et al, 2007, Sanz-Moreno et al, 2008). For instance, Vav1 is normally expressed in haemopoietic cells, but unexpectedly upregulated in pancreatic cancer to promote proliferation in synergy with the EGF receptor (Katzav et al, 1989, Fernandez-Zapico et al, 2005). Alternatively, TIAM1 is ubiquitously expressed in human tissue and now has a role described in a number of different cancer types (Hoffmann et al, 2008). It is likely that several other Rac-GEFs will contribute to tumourigenesis in ways that are yet to be characterised (Minard et al, 2004, Fernandez-Zapico et al, 2005, Patel et al, 2007, Sanz-Moreno et al, 2008).

3. *PREX1 amplification*. *PREX1* is situated at chromosome region 20q13.13, a site commonly amplified in human cancer where a number of 'cancer-initiating' genes were recently identified (Hodgson et al, 2003, Rahman et al, 2011, Tabach et al, 2011).

4. *mTOR interaction*. mTOR, another protein commonly deregulated in human cancer, has been reported to interact with P-Rex1 to mediate Rac-driven cell migration (Hernandez-Negrete et al, 2007, Zoncu et al, 2011). This interaction was subsequently reported in ovarian cancer, whereby endogenous P-Rex1 was shown to promote mTOR complex 2-mediated Akt1 activation and cell migration (Kim et al, 2011).

The importance of P-Rex1 in cancer was confirmed in 2009, with reported roles in prostate and breast cancer in particular:

- *Prostate cancer.* Qin and colleagues showed that exogenous and endogenous P-Rex1 expression promotes migration and invasion of prostate cancer cell lines, in a manner consistent with Rac activity (Qin et al, 2009). P-Rex1 is not present in normal prostate tissue but was upregulated in metastatic cell lines. Ectopic P-Rex1 increased lamellipodia formation and facilitated LN metastases in a xenograft model, while increased P-Rex1 IHC expression in human tissue was associated with more aggressive disease. This initial study was later supplemented with a mechanism for P-Rex1 upregulation in prostate cancer, which is not frequently affected by amplification of the 20q13 locus (Wong et al, 2011). Chemical and genetic experiments validated epigenetic regulation of P-Rex1: the P-Rex1 promoter and its Sp1 binding sites were identified, and an interaction between Sp1 and histone deacetylases (HDACs) were demonstrated to regulate P-Rex1 promoter transcription. Finally, HDAC disassociation

from Sp1 was suggested as a putative mechanism for P-Rex1 derepression in invasive cancer.

- *Breast Cancer.* A clear role for P-Rex1 in breast cancer has also been demonstrated (Montero et al, 2010, Sosa et al, 2010). First, Sosa and colleagues were surprised to discover the unique upregulation of P-Rex1 relative to other Rac-GEFs in a host of luminal breast cancer cell lines. Similar to the prostate, its expression is normally minimal in breast tissue. IHC and cDNA analysis of human cancer tissue revealed the cell-autonomous association of high P-Rex1 with ER positivity, HER2 positivity and LN metastases. P-Rex1 siRNA interference diminished Rac-GTP levels, depleted cell ruffles, and reduced migration of HER2-expressing cells, and a marked impairment of xenograft tumourigenesis was also observed with P-Rex1 depletion. Second, further insight of P-Rex1 tumourigenic regulation was offered by Montero and colleagues (Montero et al, 2010). Multisite phosphorylation of P-Rex1 was identified by neuregulin stimulation of cell lines, and a serine phosphorylation/ dephosphorylation cycle that had similar kinetics to Rac activation was identified. A role for endogenous P-Rex1 in breast cancer proliferation, as well as invasion, was highlighted. Finally, a P-Rex2a study reported its inhibition of PTEN lipid phosphatase activity and stimulation of the PI(3)K pathway in cancer: a significant association of PTEN and P-Rex2a by qRT-PCR in a breast tumour dataset was demonstrated (Fine et al, 2009). To date, this is the only report of the involvement of P-Rex2 in tumourigenesis.

1.5.1.3 Aims: P-Rex1 in melanoma

A role of P-Rex1 in melanoma or any cells of the MC lineage had not been reported prior to this PhD. We hypothesised that there were several reasons for an important contribution to melanoma from P-Rex1 (Figure 1.6):

1. Deregulation of the PI(3)K pathway is a central feature of melanomagenesis, and P-Rex1 is directly stimulated by PIP_3 (see Section 1.1.4.2).

2. Amplification of the chromosome site of *PREX1*, 20q13, has been described in melanoma (Koynova et al, 2007).

3. A microarray study of melanoma cell lines identified P-Rex1 as a key gene downstream of MAPK signalling and repressed by MEK inhibition: the importance of this pathway in melanoma is also detailed earlier in the introduction (see Section 1.1.4.1) (Shields et al, 2007).

4. Although there has been a low frequency of Rac mutation characterised in cancer so far, Rac-GEFs have been implicated in melanomagenesis through their regulation of Rac, helping to delineate the contribution of Rac to invasion (http://cancer.sanger.ac.uk/cosmic/gene/overview?ln=RAC1, Uhlenbrock et al, 2004, Sanz-Moreno et al, 2008). Sanz-Moreno and colleagues showed that, in melanoma cells, Rac controlled MLC2 phosphorylation to dynamically switch between mesenchymal and amoeboid modes of cell movement; in addition, the RacGEF DOCK3 was shown to combine with NEDD9 to activate Rac, thereby reducing MLC2 phosphorylation and promoting mesenchymal movement (Sanz-Moreno et al, 2008). Conversely, ectopic TIAM1 signalling through Rac has been shown to promote a morphological change to amoeboid-type in metastatic melanoma cells (Uhlenbrock et al, 2004). Taken together, these studies suggest the upstream control of Rac by its GEFs can temperospatially control its role in invasion; one suspects that a myriad of other as yet uncharacterised RacGEFs will signal through Rac using other mechanisms to affect this process.

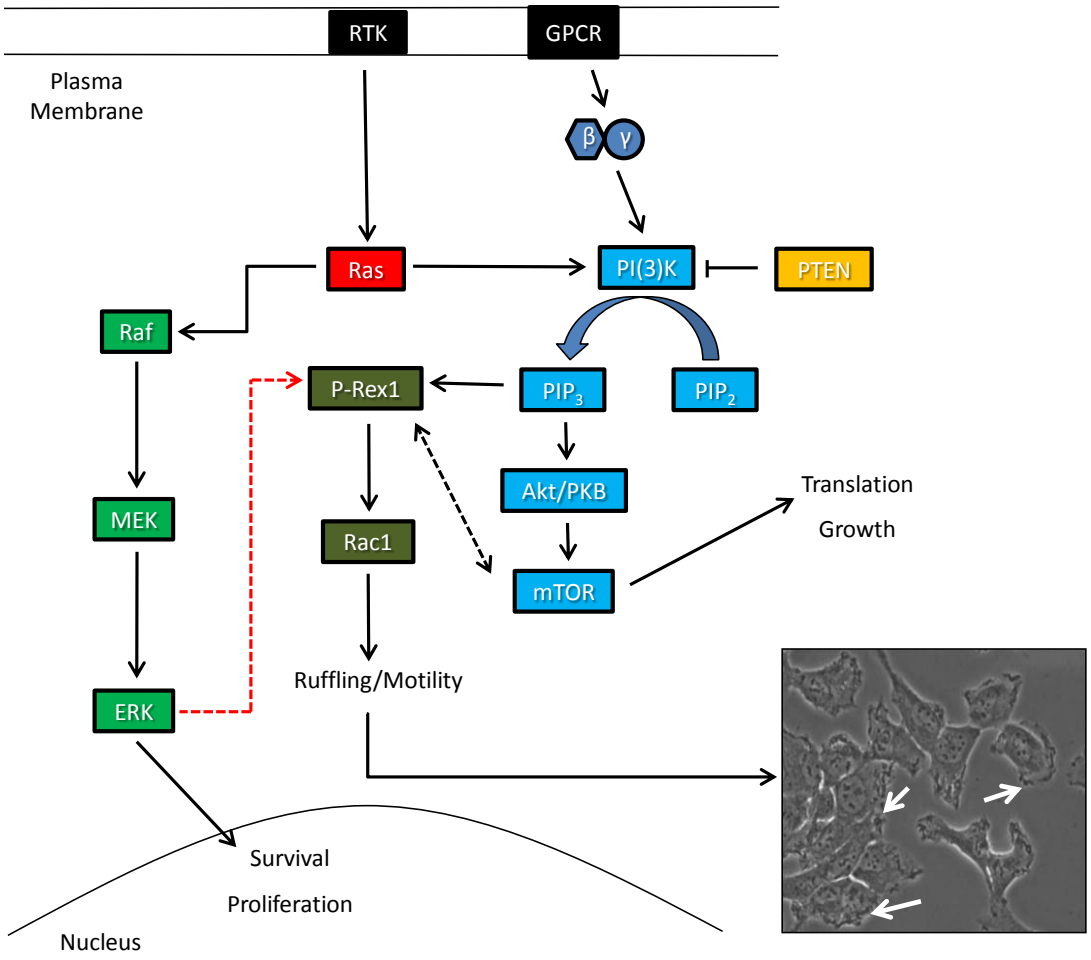

Figure 1.6 Potential P-Rex1 signalling in melanoma
P-Rex1 has been associated with several important pathways described in melanomagenesis: Ras-Raf-MEK-ERK, PI(3)K-mTOR, GPCR, and Rac signalling. Its main reported downstream function is to promote Rac-mediated migration through formation of lamellipodia and membrane ruffles (white arrows), shown here in a photomicrograph of the CHL1 melanoma-derived human cell line using 2D timelapse.

Given the the highly motile nature of melanoma cells and the known physiological and cancer-specific functions of P-Rex1, this thesis concentrates on its contribution to metastases and the invasive phenotype. P-Rex1 has not previously been characterised in genetically modified animal models of cancer that can genetically and pathologically recapitulate the human disease: this thesis described its role in the two mouse models summarised earlier in the introduction, *Tyr::Nras*$^{Q61K/°}$*; INK4a*$^{-/-}$ and *Tyr::CreER Braf*$^{V600E/+}$*; PTEN*$^{lox/lox}$ mice (Section 1.3.1.3) (chapters 3 and 5). Studies of P-Rex1 in embryonic mouse models were also used to provide mechanistic insight and consolidate our results (chapters 4 and 5). Chapter 3 also elaborates on the translational significance of our results, detailing what might be an optimal method for targeting P-Rex1.

1.5.2 Focal adhesion kinase (FAK)

FAK is a 125kDa highly conserved non-receptor tyrosine kinase and scaffold protein, first described in 1992 (Schaller et al, 1992, Hanks et al, 1992). It is expressed in a wide variety of tissues where it localises to focal adhesions. Its amino-terminal four-point-one, ezrin, radixin, moesin (FERM) domain is followed by a central catalytic domain, and then a carboxy-terminal Focal Adhesion Targeting (FAT) domain (Figure 1.7).

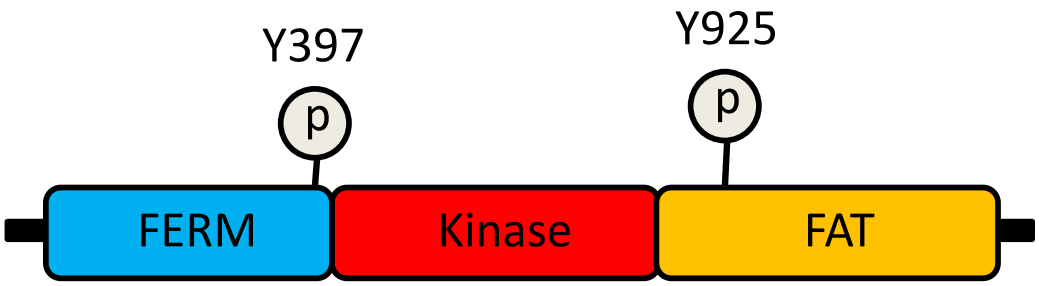

Figure 1.7 Structure and function of FAK
Schematic diagram showing FAK domain structure (see Section 1.5.2 for further detail). Its two most characterised phosphorylation sites, Y397 and Y925, are also represented. FERM = four-point-one, ezrin, radixin, moesin; FAT = Focal Adhesion Targeting.

The only other FAK family member is another non-receptor tyrosine kinase, proline-rich tyrosine kinase 2 (Pyk2), predominantly expressed in haematopoietic cells and cells of the nervous system (Lev et al, 1995). Pyk2 shares 65% sequence homology with FAK (Schultze et al, 2010). Its tyrosine phosphorylation sites are similar to those of FAK, although it generally localises to peri-nuclear sites within the cell, rather than focal adhesions (Ilic et al, 1997). Pyk2 has been shown to compensate for depleted FAK signalling in endothelial cells, demonstrating that dual inhibition of FAK and Pyk2 may be required for efficient targeting of angiogenesis (Sieg et al, 1998). An isoform of FAK with no amino-terminal, FAK related non-kinase (FRNK), has been identified and shown to function as dominant negative regulator of FAK function (Schaller et al, 1993, Richardson et al, 1996).

1.5.2.1 Regulation of FAK

FAK is regulated through a series of complex intra- and inter-molecular interactions involving all three of its domains. It has 6 sites of tyrosine phosphorylation (Y397, Y407, Y576, Y577, Y861, Y925), the most characterised of which is its major site of autophosphorylation, Y397 (Figure 1.7) (Calalb et al, 1995). Following integrin-ECM interaction, phosphorylation of FAK-Y397 leads to the recruitment of several proteins including Src. Src-dependent phosphorylation will in turn mediate phosphorylation of the other 5 FAK tyrosine residues, enhancing FAK activity and stimulating its role as a focal point of multiple pathways (Schlaepfer et al, 1999). Further data has suggested that FAK-Y397 is regulated by differential phosphorylation of the other FAK tyrosine residues (Leu et al, 2002). Associations with both the P(I)3K and MAPK pathways have been described with FAK-Y397 and FAK-Y925, respectively (Schlaepfer et al, 1999, Chen et al, 1996). FAK serine phosphorylation is also likely to play an important role within the cell, with 4 major

sites described (S732, S840, S843, and S910); in particular, FAK-732 has a described role in neuronal migration and microtubule organization (Ma et al, 2001, Xie et al, 2003).

The FERM domain of FAK resides in its amino-terminal, where it controls a myriad of complex signalling pathways. It mediates intra-molecular interactions between the FAK kinase domain and the FAK amino-terminal domain, negatively regulating both FAK phosphorylation and activity; an effect that can be reversed by its abrogation (Cooper et al, 2003). Structural evidence has suggested that this loss of activity results from the folding and binding of the FERM domain to the kinase domain, leading to a closed and inactive conformation of FAK (Dunty et al, 2004, Lietha et al, 2007). FERM is also known to functionally associate inter-molecularly with growth factors implicit in cell migration, such as the epidermal growth factor receptor (EGFR) and platelet-derived growth factor receptor (PDGFR) (Sieg et al, 2000). In the carboxy-terminal of FAK, the focal adhesion targeting (FAT) domain is required for its localisation to focal adhesions, a process shown to be dependent on its binding to the protein Paxillin (Tachibana et al, 1995).

1.5.2.2 Physiology of FAK

FAK acts as a key regulator of adhesion and migration in healthy cells (Zachary et al, 1992, Kornberg et al, 1992). Its importance in development has also been extensively characterised, with roles described in key processes such as angiogenesis and proliferation that may reflect its reported tumourigenic activity (Fonar et al, 2011, Zhao et al, 2010). Moreover, genetic manipulation of FAK has also highlighted an important pro-survival role, protecting cells from a number of potentially apoptotic insults (Sonoda et al, 1999, Sonoda et al, 2000, Xu et al, 2000, Sakurai et al, 2002, Huang et al, 2007).

The key role of FAK in cell migration is perhaps best illustrated by the developmental lethality of mice with constitutive FAK deletion, a direct consequence of defective cell movement leading to problems with embryonic gastrulation (Ilic et al, 1995). Depletion of FAK in mouse embryo fibroblasts (MEFs) has been shown to markedly impair growth-factor induced cell migration, whereas its over-expression has been shown to enhance this effect (Schlaepfer et al, 1999, Cary et al, 1996). One way by which FAK can promote this migration is through phosphorylation of neural wiskott aldrich syndrome protein (N-WASP), a mediator of the actin-related protein 2/3 (Arp2/3) complex which can regulate filopodia formation and cell spreading (Wu et al, 2004).

1.5.2.3 FAK in cancer

FAK is deregulated in human cancer, where it is thought to contribute to proliferation, invasion, survival and angiogenesis (Owens et al, 1995, Weiner et al, 1993, Ilic et al, 2003, Schaller et al, 2001). These hallmarks of cancer are promoted by FAK upregulation of a number of intracellular signalling cascades common to malignancy, such as the MAPK, PI(3)K, and JNK pathways (Schaller et al, 2001, Zhao et al, 2009). Transgenic animal models have described a role for FAK in breast and skin cancer progression and metastasis (McLean et al, 2004, Lahlou et al, 2007, Provenzano et al, 2008).

In contrast to these pro-tumourigenic properties of FAK, a conflicting picture has emerged in myriad studies analysing its expression in human cancer tissue. In various human cancers, high FAK expression has been associated with worse prognostic outcomes (Fujii et al, 2004, Lark et al, 2005, Giaginis et al, 2009, Gabriel et al, 2009, Tavernier-Tardy et al, 2009), no change in prognosis (Schmitz et al, 2005, Theocharis et al, 2003, Furuyama et al, 2006), and improved outcomes in some cases (Gabriel et al, 2006, Giaginis et al, 2009). Reduced expression of FAK in liver metastases compared to a matched colonic

adenocarcinoma primary has also been reported (Ayaki et al, 2001). However, none of these studies offer information on whether FAK may contribute to these prognoses rather than just being an association. Cell biological work is just beginning to suggest mechanisms and tumourigenic contexts in which FAK can act as a tumour suppressor (Zheng et al, 2009, Sandilands et al, 2011).

1.5.2.4 Aims: FAK in melanoma

Chapter 6 details the role of FAK in melanoma using the same genetically modified *in vivo* models described in the other results chapters. FAK is an altogether different anticancer target to P-Rex1, with a long reported role in malignancy that has led to recent evaluation of FAK kinase inhibitors in early phase trials. It seemed likely that, through its myriad biological functions, FAK would contribute to melanoma also.

Although its role in melanoma and cells of the melanocyte lineage is relatively unstudied, Meierjohann et al have described a phenotype for FAK using the Xiphophorus melanoma system as well as mouse-derived cell lines (Meierjohann et al, 2006). Stimulation of the EGFR variant, Xmrk, produced an interaction with FAK and an increase in focal contact and actin cytoskeleton turnover. Consistent with this, over-expression of dominant-negative FAK reduced Xmrk-induced migratory activity by 40% in mouse melanoma cells to the otherwise scarcely motile melanocytes turnover.

This thesis aims to clarify the role of FAK in melanomagenesis using genetically modified mouse models. The establishment of FAK as a therapeutic anticancer target also serves as a useful backdrop for some of the more translational caveats in the P-Rex1 study.

Chapter 2

Materials & Methods

2.1 Embryo analysis: ß-galactosidase (*Dct-lacZ*) staining

Time of gestation was calculated using noon on the day of detection of a vaginal plug as E0.5, but also noting and comparing the external appearance of the embryo. Embryos were dissected at E13.5 or E15.5 then fixed in 0.25% glutaraldehyde at 4°C for 45 min on a rolling platform. Embryos washed in PBS at 4°C for 15m on a rolling platform, detergent washed (2 mM $MgCl_2$, 0.01% Na-deoxycholate, 0.02% NP-40 in PBS) at room temperature x3 (30 min, 15 min x 2). ß -galactosidase substrate (1M $MgCl_2$, 0.02% NP-40, 0.01% Na-deoxycholate, 0.04% X-Gal (Promega), 5 mM $K_3Fe(CN)_6$, 5 mM $K_4Fe(CN)_6$) then added to the embryos which were incubated in darkness overnight. Embryos post-fixed in 4% paraformaldehyde for 2h at 4°C.

2.1.1 Migration assays

Cells counted and distances measured using Image J (Figure 2.1). Minitab used to compare parameters between genotypes.

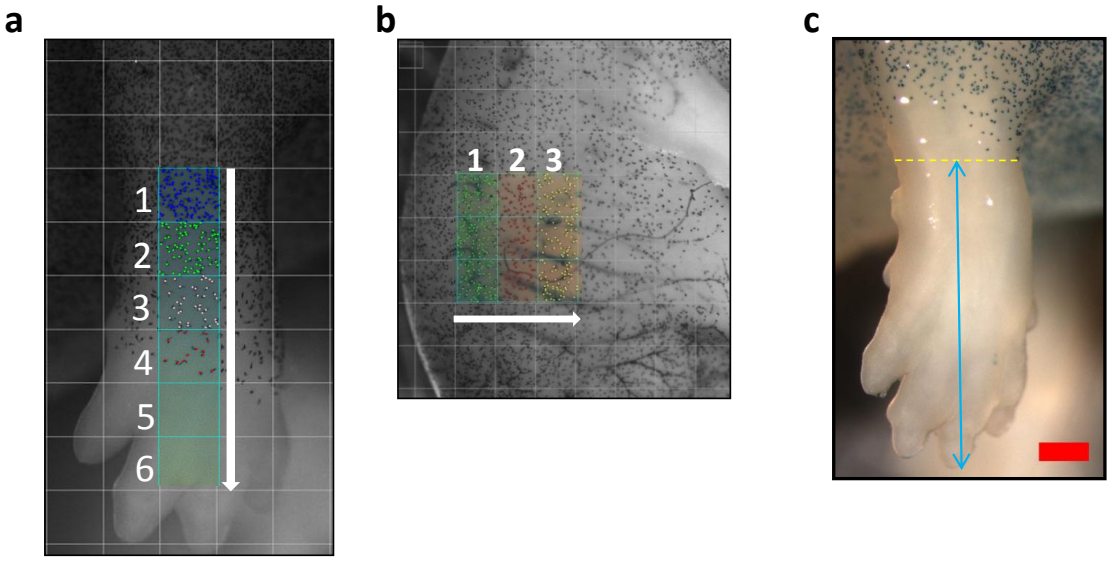

Figure 2.1 *Dct-lacZ* melanoblast migration assays
Schematic picture detailing quantification of melanoblast migration in the forepaw at E15.5. Levels 1 to 6 from top to bottom represent areas of 500µm x 500µm. Melanoblasts counted at each level and numbers compared between genotypes **(b)** As per (a), except at E13.5. Levels 1 to 3 across torso of each embryo represent areas of 500µm x 1500µm. Melanoblasts counted at each level and their numbers compared between genotypes **(c)** Schematic picture detailing alternative method for quantification of melanoblast migration in the forepaw at E15.5. The distance between 5th most distal melanoblast and the end of the forepaw was measured and compared between genotypes.

2.1.2 Melanoblast cell number assays

Cells counted using Image J (Figure 2.2). Minitab used to compare numbers between genotypes.

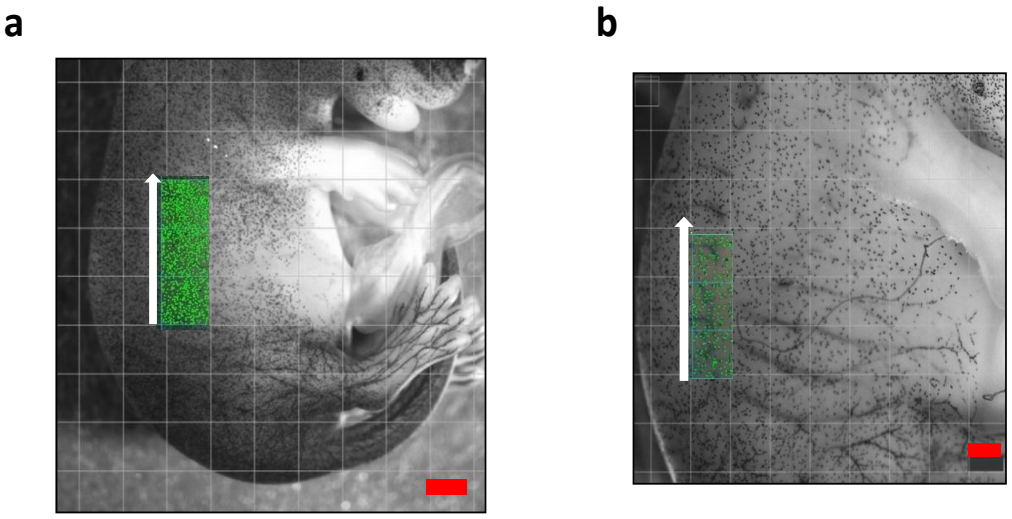

Figure 2.2 *Dct-lacZ* melanoblast cell number assays
(a) Schematic picture detailing quantification of melanoblast cell numbers at E15.5. Area represented: 1mm x 3mm **(b)** Schematic pictures detailing method for quantification of melanoblasts at E13.5. Areas represented 500µm x 1500µm. Melanoblasts were counted and their numbers compared between genotypes. For both (a) and (b), the area used for quantification of cell numbers represented the most proximal point of melanoblast migration from the neural crest which could be accurately assayed. Counting melanoblasts in more distal regions would have introduced a migrational component to the assay which we aimed to avoid.

2.2 Embryo analysis: *Ex vivo* melanoblast live imaging

Performed as described by Mort and colleagues (Figure 2.3) (Mort et al, 2010). A freshly dissected E15.5 embryonic skin sample was sandwiched between a nucleopore membrane (Whatman) and a gas permeable Lumox membrane in a Greiner Lumox culture dish (Greiner Bio-One GmbH) so that the epidermal side of skin was in contact with the Lumox membrane. To immobilize the sample, Growth Factor Reduced Matrigel (BD Bioscience) was used to cover the whole assembly and incubated at 37°C for 10 min. Culture medium (Phenol red free DMEM supplied with 10% FBS) was added. Drugs/inhibitors were added to Matrigel and medium 1 hr before imaging. Time-lapse images were captured using an Olympus FV1000 or Nikon A1 confocal microscope in a 37°C chamber with 5% CO_2 at 20× magnification for 6h with slices taken every 7.5 min.

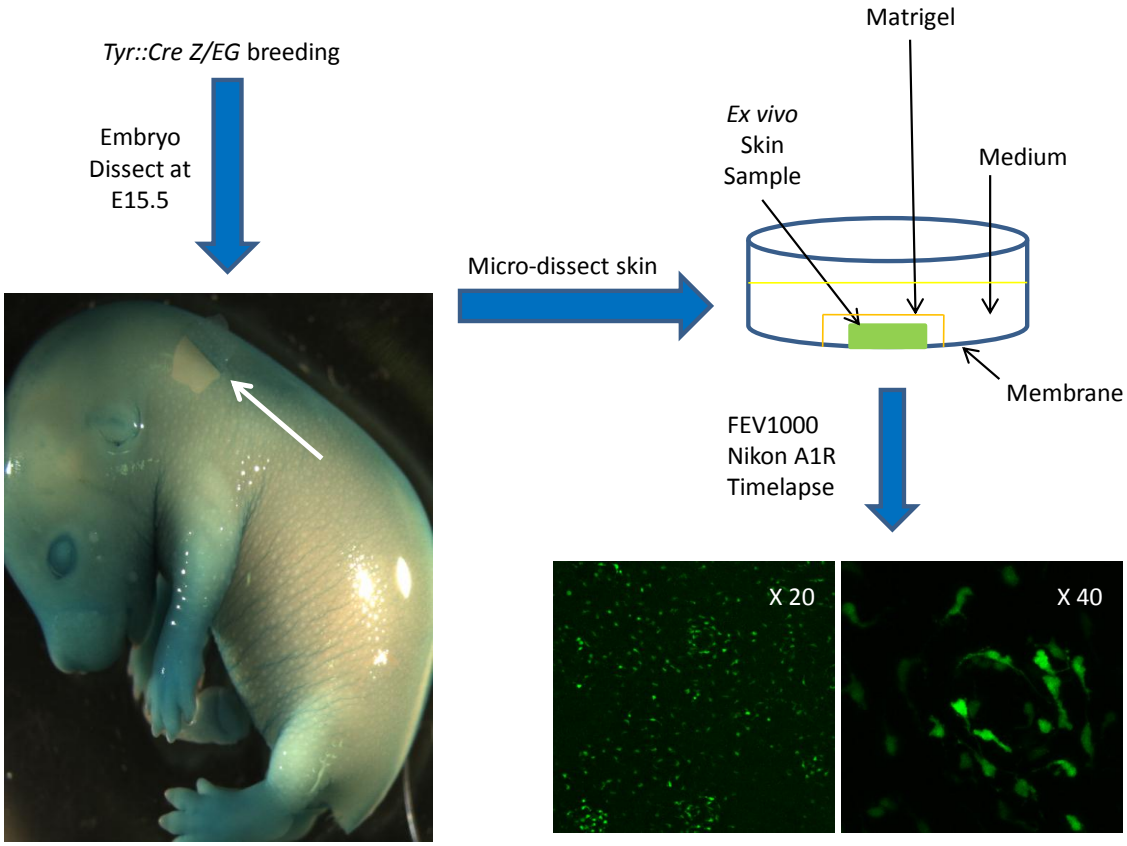

Figure 2.3 Tyr::Cre Z/EG melanoblast technique
Schematic diagram demonstrating technique for migration and cell number assessment of E15.5 embryos derived from *Tyr::Cre Z/EG* mice (further detail in section 2.2). Mouse with any gene manipulation of interest can be bred to the Tyr::Cre Z/EG reporter mice, then their melanoblast characteristics assessed. White arrow shows typical flap of skin microdissected and then placed in *ex vivo* culture, as demonstrated in the top right diagram. Each green 'dot' in the two bottom right panels represents a melanoblast under confocal imaging. Timelapse allows live assessment of cells in flank skin of embryo.

2.2.1 GFP migration assays

20 cells per timelapse sample (if possible) were manually tracked using ImageJ. ImageJ chemotaxis tool was then used to quantify co-ordinates. Timelapse images were focused on flank skin of embryo rather than limbs (as described in section 2.1.1 with *DCT-lacZ* assays). Minitab was finally used to compare speed and Euclidean distance between genotypes. Euclidean distance is the distance between two points that one would measure with a ruler, no matter what tortuous route the cell may have taken to reach that point.

2.2.2 GFP cell number assays

Number of cells present in images at 3 separate timepoints of a sample were quantified using Image J. Standard image measured at x20 magnification was 635x 635µm. Minitab was used to compare cell numbers between genotypes.

2.3 Mouse treatments, ageing and survival cohorts

For the P-Rex1 project, 80 Tyr::Nras$^{Q61K/°}$; INK4a$^{-/-}$ and 10 C57BL6 mice were monitored for up to 18 months for development of melanoma and signs of metastasis. For the FAK project, 50 Tyr::Nras$^{Q61K/°}$; INK4a$^{-/-}$ mice were monitored for up to 18 months for development of melanoma and signs of metastasis. For *Tyr::Cre Rac$^{fl/fl}$; P-Rex1$^{-/-}$* mice, 7 pups were followed until approximately 3 weeks of age, after which they were all euthanised for developing signs of a neurological defect.

All mice were checked 3x weekly for development of malignant melanoma or any other pathology. For all genetically modified and injected mice, endpoint criteria were melanomas ≥ 15mm, ulcerating melanomas, cachexia, significant weight loss, or weakness and inactivity. Upon meeting these criteria, mice were euthanised. Mice were

examined for the presence of frank metastasis upon dissection, but also visualisation of haematoxylin and eosin (H&E) stained sections for further identification of microscopic metastases. Organs/tumours were removed and fixed in 10% buffered formalin overnight at room temperature. In particular, melanomas and skin were placed on Whatman paper then subjected to vertical incision prior to formalin immersion. Fixed tissues were paraffin embedded and 5mm sections placed on sialynated/poly-L-lysine slides for IHC analysis. LN metastases were not included in this analysis due to difficulty in distinguishing them from normal melanocyte populations that can be found in lymphoid tissue.

Tumour frequency of primary melanoma was calculated as median value from weekly counting of number of melanomas per live mouse. Tumour burden of primary melanoma was calculated as median value from weekly assessment of length/breadth of largest melanoma affecting each affected live mouse (eg. Figure 5.7). Tumour frequency and burden of metastases was calculated as mean value by tallying melanocytic lesions and measuring the length/breadth of lesions from 3 histological slices of each affected organ (eg. Figure 3.3). For tumour burden: with each give mouse and timepoint, length and breadth were measured and multiplied for a final result measured in mm^2.

2.3.1 Tail vein (TV) treatments

For TV-injections into C57BL6 mice, cultured cells were maintained in antibiotic-free media for 1 week prior to injection. Cells were detached with trypsin, then blocked through suspension in complete culture media supplemented with 10 % foetal bovine serum. Cells were subjected to two rounds of washing, involving centrifugation at 100g for 5m followed by resuspension in 1 x Hanks' Balanced Salt Solution (HBSS). Cells were finally resuspended in HBSS to a concentration of 1×10^7 cells/ml and TV-injected at 1×10^6 cells/animal in a volume of 100µl.

2.3.2 Tamoxifen

For tamoxifen induction of *Tyr::CreER Braf*$^{V600E/+}$ mice, dorsal hair was shaved and 1mg in 200µl of 100% ethanol applied to shaved area once daily for 5 days.

2.4 Statistical analyses

Statistical analyses in mice were carried out using Minitab® version 15 for Windows. Cell migration, invasion, and cell number differences were determined using the Mann-Whitney test. Distinction of metastasis and primary melanoma incidence was achieved using chi-square testing. Survival differences were determined with log-rank testing. All p values were considered significant at $p = <0.05$. All appropriate value sets were tested for normality using a Kolmogorov-Smirnoff normality test.

2.5 Small Animal Regulations

All studies were conducted in accordance with UK home office guidelines. All mice were maintained under non-barrier conditions and given a standard diet (Harlan) and water *ad libitum*. All mouse experiments were performed on a C57BL6 background apart from *DCT-lacZ* experiments which were performed on mice which were 50% mixed and 50% C57BL6.

2.6 Techniques used in mouse modelling

The general principles of creating genetically modified mouse models are similar to those utilised in other forms of genetic engineering. Using recombinant DNA techniques, an isolated gene of interest is added to a genetic construct where it is combined with other genetic elements in order for it to work efficiently. These will often include a promoter to initiate transcription of the gene and control its localisation, and a selectable marker to determine which cells have been transformed by the new gene. Most commonly, the next

step is for construct DNA to be co-cultured and incorporated into embryonic stem cells, which exploits the potential to create defined mutations through homologous recombination. Successfully transformed cells are selected for and injected into mouse blastocysts. Blastocysts are then transferred into the uterus of female mice and tail biopsies of offspring taken to isolate DNA for analyses by Southern blot or PCR, resulting in the identification of transgenic founders. These founders are then bred to produce genetically modified offspring.

2.6.1 Transgenic expression or inactivation of genes

Unlike other mice used in the thesis (sections 2.6.2-2.6.4), these mice express genes in a non-physiological manner owing to ectopic promoter and enhancer elements. The random nature of transgene integration can often lead to formation of large concatamers which invariably promote over-expression. Examples of this strategy in the thesis are *Tyr::Nras*$^{Q61K/°}$*, P-Rex1*$^{-/-}$*,* and *INK4a*$^{-/-}$ mice.

2.6.2 Endogenous inactivation of tumour suppressors or oncogenes

Endogenous genetically modified mice (those described in sections 2.6.2-2.6.4) use their native promoters for genetic manipulation through the use of 'knockout' technology. In modern conditional gene mutation strategies, the gene of interest is flanked by recombinase recognition sites (eg. 'loxP' or 'flox' sites) and will be deleted in the presence of recombinase ('Cre' recombinase in this thesis) by inter-crossing with mice that express recombinase in a melanocye-specific fashion (Tyr::Cre or Tyr::CreER). An example of this technique in this thesis is *PTEN* manipulation in chapter 5. Examples of this strategy in the thesis are *Tyr::Cre PTEN*$^{lox/lox}$ *and Tyr::Cre FAK* $^{fl/fl}$ mice.

2.6.3 Endogenous expression of oncogenes

Principle is the same as described in section 2.7.1, except this time a transcriptional terminator (eg. a 'STOP' codon) is flanked by recombinase recognition sites to separate an oncogene from its tissue-specific promoter. Expression of recombinase deletes the STOP codon, allowing oncogene expression to occur. An example of this strategy in the thesis are the *Tyr::CreER Braf*$^{V600E/+}$ mice described in chapter 5.

2.6.4 Endogenous inducible oncogene expression

The *Tyr::CreER Braf*$^{V600E/+}$ model described in chapter 5 also exploits tamoxifen-regulatable oncogene activity using melanocyte-specific expression of a fusion protein incorporating Braf^{V600E} and a ligand-binding domain from the oestrogen receptor. The fusion protein is sequestered by heat shock proteins in the absence of an inducer. The presence of tamoxifen results in release of Braf^{V600E} from the oestrogen receptor fusion.

2.6.5 Reporter mouse strains

The phenotypes induced by the genetic manipulations described in this thesis are characterised by inter-crossing mice carrying genes of interest with reporter mouse strains that carry a marker gene separated from their melanocyte-specific promoter by a transcriptional terminator. The marker is transcribed when recombination deletes the transcriptional terminator. Melanocyte-specific reporter mice strains employed in this thesis are *Tyr::Cre Z/EG* and *DCT::β-galactosidase* (otherwise referred to as *DCT-lacZ*). Cells derived from *Tyr::Cre YFP* mice (MRC Human Genetics Unit, Edinburgh) were also used for Figure 4.2a.

2.7 Mouse Alleles

Mice alleles described in experiments were: *P*-Rex1 (Welch et al, 2005), *CDKN2a ('INK4a')* (Ackermann et al, 2005), *Nras*^{Q61K} (Ackermann et al, Cancer Res 2005), *Tyr::Cre* (Delmas et al, 2003), *Tyr::Cre ERT2* (Yajima et al, 2006), *Dct-lacZ* (Mackenzie et al, 1997), *Z/EG* (Novak et al, 2000), *LSL-Braf*^{V600E} (Mercer et al, 2005), *PTEN* (Backman et al, 2001), *FAK* (McLean et al, 2004), and *Rac1*$^{fl/fl}$ (Walmsley et al, 2003). Table 2.1 offers detail of mice offspring bred for study in this thesis:

Mouse (chronological order)	Allele description
Tyr::Nras$^{Q61K/°}$*; INK4a*$^{-/-}$*; P-Rex1*$^{+/+}$	One copy *Nras*^{Q61K} transgene, unconditional knockout 2 copies of *INK4a*, *wild-type P-Rex1*
Tyr::Nras$^{Q61K/°}$*; INK4a*$^{-/-}$*; P-Rex1*$^{-/-}$	One copy *Nras*^{Q61K} transgene, unconditional knockout 2 copies of *INK4a*, unconditional knockout 2 copies of *P-Rex1*
Tyr::Nras$^{Q61K/°}$*; P-Rex1*$^{+/+}$	One copy *Nras*^{Q61K} transgene, *wild-type P-Rex1*
Tyr::Nras$^{Q61K/°}$*; P-Rex1*$^{-/-}$	One copy *Nras*^{Q61K} transgene, unconditional knockout 2 copies of *P-Rex1*
P-Rex1$^{-/-}$	unconditional knockout 2 copies of *P-Rex1*
DCT-lacZ; Tyr::Nras$^{Q61K/°}$*; P-Rex1*$^{+/+}$	Melanocyte-specific expression of β-galactosidase reporter, one copy *Nras*^{Q61K} transgene, *wild-type P-Rex1*
DCT-lacZ; Tyr::Nras$^{Q61K/°}$*; P-Rex1*$^{-/-}$	Melanocyte-specific expression of β-galactosidase reporter, one copy *Nras*^{Q61K} transgene, unconditional knockout 2 copies of *P-Rex1*
DCT-lacZ; P-Rex1$^{+/+}$	Melanocyte-specific expression of β-galactosidase reporter, *wild-type P-Rex1*

DCT-lacZ; P-Rex1$^{-/-}$	Melanocyte-specific expression of β-galactosidase reporter, unconditional knockout 2 copies of *P-Rex1*
Tyr::Cre Z/EG; P-Rex1$^{+/+}$	Melanocyte-specific expression of *Z/EG* (GFP) reporter, *wild-type P-Rex1*
Tyr::Cre Z/EG; P-Rex1$^{-/-}$	Melanocyte-specific expression of *Z/EG* (GFP) reporter, unconditional knockout 2 copies of *P-Rex1*
Tyr::Cre Rac1$^{f/f}$	Melanocyte-specific knockout of 2 copies of *Rac1*
Tyr::Cre Rac1$^{f/f}$*; P-Rex1*$^{-/-}$	Melanocyte-specific knockout of 2 copies of *Rac1,* unconditional knockout 2 copies of *P-Rex1*
DCT-lacZ; Tyr::Cre Rac1$^{f/f}$	Melanocyte-specific expression of β-galactosidase reporter, melanocyte-specific knockout of 2 copies of *Rac1*
DCT-lacZ; Tyr::Cre Rac1$^{f/f}$*; P-Rex1*$^{-/-}$	Melanocyte-specific expression of β-galactosidase reporter, melanocyte-specific knockout of 2 copies of *Rac1,* unconditional knockout 2 copies of *P-Rex1*
Tyr::Cre Z/EG; Tyr::Cre Rac1$^{f/f}$	Melanocyte-specific expression of *Z/EG* (GFP) reporter, melanocyte-specific knockout of 2 copies of *Rac1*
Tyr::Cre Z/EG; Tyr::Cre Rac1$^{f/f}$*; P-Rex1*$^{-/-}$	Melanocyte-specific expression of *Z/EG* (GFP) reporter, melanocyte-specific knockout of 2 copies of *Rac1,* unconditional knockout 2 copies of *P-Rex1*
Tyr::CreER Braf$^{V600E/+}$	Melanocyte-specific expression of one copy of *Braf*^{V600E}
Tyr::Cre Z/EG; Tyr::CreER Braf$^{V600E/+}$	Melanocyte-specific expression of *Z/EG* (GFP) reporter, melanocyte-specific expression of one copy of *Braf*^{V600E}

DCT-lacZ; Tyr::Cre PTEN$^{lox/+}$; P-Rex1$^{-/-}$	Melanocyte-specific expression of β-galactosidase reporter, melanocyte-specific deletion of one copy *PTEN*, unconditional knockout 2 copies of *P-Rex1*
DCT-lacZ; Tyr::Cre PTEN$^{lox/lox}$; P-Rex1$^{-/-}$	Melanocyte-specific expression of β-galactosidase reporter, melanocyte-specific deletion of both copies *PTEN*, unconditional knockout 2 copies of *P-Rex1*
Tyr::CreER Braf$^{V600E/+}$; Tyr::Cre PTEN$^{lox/lox}$; P-Rex1$^{-/-}$	Melanocyte-specific expression of one copy of *Braf^{V600E}*, melanocyte-specific deletion of both copies *PTEN*, unconditional knockout 2 copies of *P-Rex1*
Tyr::CreER Braf$^{V600E/+}$; Tyr::Cre PTEN$^{lox/+}$; P-Rex1$^{-/-}$	Melanocyte-specific expression of one copy of *Braf^{V600E}*, melanocyte-specific deletion of one copy *PTEN*, unconditional knockout 2 copies of *P-Rex1*
Tyr::Cre FAK$^{fl/fl}$	Melanocyte-specific deletion of both copies *FAK*
Tyr::Cre FAK$^{fl/+}$	Melanocyte-specific deletion of one copy *FAK*
DCT-lacZ; Tyr::Cre FAK$^{fl/fl}$	Melanocyte-specific expression of β-galactosidase reporter, melanocyte-specific deletion of both copies *FAK*
DCT-lacZ; Tyr::Cre FAK$^{fl/+}$	Melanocyte-specific expression of β-galactosidase reporter, melanocyte-specific deletion of one copy *FAK*
DCT-lacZ; Tyr::Nras$^{Q61K/°}$; Tyr::Cre FAK$^{fl/fl}$	Melanocyte-specific expression of β-galactosidase reporter, one copy *Nras^{Q61K}* transgene, melanocyte-specific deletion of both copies *FAK*
DCT-lacZ; Tyr::Nras$^{Q61K/°}$; Tyr::Cre FAK$^{fl/+}$	Melanocyte-specific expression of β-galactosidase reporter, one copy *Nras^{Q61K}* transgene, melanocyte-specific deletion of one copy *FAK*

Tyr::Nras$^{Q61K/°}$; Tyr::Cre FAK$^{fl/fl}$	One copy *Nras^{Q61K}* transgene, melanocyte-specific deletion of both copies *FAK*
Tyr::Nras$^{Q61K/°}$; Tyr::Cre FAK$^{fl/+}$	One copy *Nras^{Q61K}* transgene, melanocyte-specific deletion of one copy *FAK*
Tyr::Nras$^{Q61K/°}$; INK4a$^{-/-}$; Tyr::Cre FAK$^{fl/fl}$	One copy *Nras^{Q61K}* transgene, unconditional knockout 2 copies of *INK4a*, melanocyte-specific deletion of both copies *FAK*
Tyr::Nras$^{Q61K/°}$; INK4a$^{-/-}$; Tyr::Cre FAK$^{fl/+}$	One copy *Nras^{Q61K}* transgene, unconditional knockout 2 copies of *INK4a*, melanocyte-specific deletion of one copy *FAK*

Table 2.1 Description of alleles used in each mouse studied within this thesis

2.8 Mouse Genotyping

Mice were genotyped by polymerase chain reaction (PCR). The majority of the samples were processed by Transnetyx Inc, although protocols were established or tested inhouse initially by various members of the R18 lab group including myself. Ear biopsies were taken at weaning. DNA was extracted from biopsies using puregene DNA extraction kit (Qiagen). Tails were lysed in 500µl cell lysis solution (Puregene) and 10µl proteinase K (20mg/ml, Sigma), and shaken overnight at 37ºC. Tails were left to cool at room temp and 200µl of protein precipitation solution (Puregene) then added to each tube, vortexed and centrifuged at top speed for 5 min. Supernatant fluid was pipetted into a clean tube containing 500µl of isopropanol, vortexed and centrifuged as before for 5 min. Supernatant was decanted and DNA pellet left to dry overnight. DNA was finally resuspended in 500µl DNA hydration solution (Puregene). PCR reactions performed in 50µl volumes using 2.5µl DNA preparation. PCR products were resolved by electrophoresis on 2% agarose gels.

CRE PCR Protocol

PCR Mix	µl
5x Colorless GoTaq Flexi Buffer*	10
$MgCl_2$ (25mM)	5
dNTPs (10mM)	0.4
Primer (100µM)	0.2 (of each)
Go Taq*	0.2
H_2O to final volume of 47.5 µl	

*GoTaq Flexi DNA Polymerase from Promega.

Primers:

Cre A = TGA CCG TAC ACC AAA ATT TG

Cre B = ATT GCC CCT GTT TCA CTA TC

Reaction Conditions: 95°C, 3min (95°C, 30s; 55°C, 30s; 72°C 1min)$_{30}$, 72°C, 5min. 15°C, hold.

Bands: Cre = ~1000bp

2.8.1 LACZ PCR Protocol

PCR Mix	µl
5x Colorless GoTaq Flexi Buffer*	10
$MgCl_2$ (25mM)	5
dNTPs (10mM)	0.4
Primer (100µM)	0.2 (of each)
Go Taq*	0.2
H_2O to final volume of 47.5 µl	

*GoTaq Flexi DNA Polymerase from Promega.

Primers:

LACZ A = CTG GCG TTA CCC AAC TTA AT

LACZ B = ATA ACT GCC GTC ACT CCA AC

Reaction Conditions: 95°C, 3min (95°C, 30s; 55°C, 30s; 72°C 1min)$_{30}$, 72°C, 5min. 15°C, hold.

Bands: LacZ = ~500bp

2.8.2 $NRAS^{Q61K}$ PCR Protocol

PCR Mix	µl
5x Colorless GoTaq Flexi Buffer*	10
$MgCl_2$ (25mM)	5
dNTPs (10mM)	0.4
Primer (100µM)	0.2 (of each)
Go Taq*	0.2
H_2O to final volume of 47.5 µl	

*GoTaq Flexi DNA Polymerase from Promega.

Primers:

NRas A = GAT CCC ACC ATA GAG GAT T

NRas B = CTG GCG TAT TTC TCT TAC C

Reaction Conditions: 94°C, 4min (94°C, 30s; 56°C, 30s; 72°C, 1min) $_{35}$ 72°C, 10min. 15°C, hold.

Bands: Nras= ~400bp

2.8.3 CDKN2A PCR Protocol

PCR Mix	µl
5x Colorless GoTaq Flexi Buffer*	10
$MgCl_2$ (25mM)	5
dNTPs (10mM)	0.4
Primer (100µM)	0.2 (of each)
Go Taq*	0.2
H_2O to final volume of 47.5 µl	

*GoTaq Flexi DNA Polymerase from Promega.

Primers:

P16 WT A = ATG ATG ATG GGC AAC GTT C

P16 WT B = CAA ATA TCG CAC GAT GTC

P16 Null A = CTA TCA GGA CAT AGC GTT GG

P16 Null B = AGT GAG AGT TTG GGG ACA GAG

Reaction Conditions: 94°C, 3min (94°C, 1min; 60°C, 1min; 72°C 1min) $_{30}$; 72°C, 10min. 15°C, hold.

Bands: WT = 236bp; null = 723bp

2.8.4 PREX1 PCR Protocol

PCR Mix	µl
5x Colorless GoTaq Flexi Buffer*	10
$MgCl_2$ (25mM)	5
dNTPs (10mM)	0.4
Primer (100µM)	0.2 (of each)
Go Taq*	0.2
H_2O to final volume of 47.5 µl	

*GoTaq Flexi DNA Polymerase from Promega.

Primers:

P-Rex1 WT A = GAC CTG AGG TTT TTT TCT GGC CTC CGT GGC

P-Rex1 WT B = GAA AGA GGC AGA AGC TGG GCA CGC CTG GCC

P-Rex1 Null A = AGG GGG AAG GCT GAG GTG CTG GTG ATG CTG

P-Rex1 Null B = TCC TCG TGC TTT ACG GTA TCG CCG CTC CCG

Reaction Conditions: 95°C, 3min (95°C, 30s; 60°C, 30s; 72°C 1min) $_{30}$; 72°C, 5min. 4°C, hold.

Bands: WT = 1kb; null = 436bp

2.8.5 $BRAF^{V600E}$ PCR Protocol

PCR Mix	µl
5x Colorless GoTaq Flexi Buffer*	10
$MgCl_2$ (25mM)	5
dNTPs (10mM)	0.4
Primer (100µM)	0.2 (of each)
Go Taq*	0.2
H_2O to final volume of 47.5 µl	

*GoTaq Flexi DNA Polymerase from Promega.

Primers:

$Braf^{V600E}$ A = GCT TGG CTG GAC GTA AAC TC

$Braf^{V600E}$ B= GCC CAG GCT CTT TAT GAG AA

$Braf^{V600E}$ C = AGT CAA TCA TCC ACA GAG ACC T

Reaction Conditions: 94°C, 5min (94°C, 30s; 60°C, 30s; 72°C, 30s) $_{35}$; 72°C, 10min. 4°C, hold.

Bands: targeted allele = 140bp (primers A+B); WT = 466bp (primers B+C); Cre-deleted allele = 518bp (primers B+C).

2.8.6 FAK PCR Protocol

PCR Mix	µl
10x Buffer	5
$MgCl_2$ (50mM)	2.5
dNTPs (10mM)	1
Primer (100µM)	0.2 (of each)
Platinum Taq*	0.2
H_2O to final volume of 47.5 µl	

*Platinum Taq (Invitrogen)

Primers:

FAK A = ATT GTG CTA TAC TCA CAT TTG GA

FAK B = TTA ATA AGA CCA GAG GAC TCA GC

FAK C = GGA AGA AGC TTG TAT ACT GTA TG

Reaction Conditions: 95°C, 5min (95°C, 45s; 64°C, 45s; 72°C, 1min)$_{35}$, 72°C, 7min. 4°C, hold.

Bands: WT = ~650bp; Flox = ~580bp

2.8.7 PTEN PCR Protocol

PCR Mix	µl
10x Buffer	5
$MgCl_2$ (50mM)	2.5
dNTPs (10mM)	0.4
Primer (100µM)	0.1 (of each)
Platinum Taq*	0.2
H_2O to final volume of 47.5 µl	

*Platinum Taq (Invitrogen)

Primers:

PTEN A = CTC CTC TAC TCC ATT CTT CCC

PTEN B = ACT CCC ACC AAT GAA CAA AC

Reaction Conditions: 95°C, 2.5min (94°C, 1min; 58°C, 1min; 72°C, 1min)$_{35}$, 72°C, 10min. 15°C, hold.

Bands: WT = 228bp; Flox = 335bp

2.8.8 Z/EG PCR Protocol

PCR Mix	µl
5x Colorless GoTaq Flexi Buffer*	10
$MgCl_2$ (25mM)	5
dNTPs (10mM)	0.4
Primer (100µM)	0.2 (of each)
Go Taq*	0.2
H_2O to final volume of 47.5 µl	

*GoTaq Flexi DNA Polymerase from Promega.

Primers:

Z/EG A = TGG TCG AGC TGG ACG GCG AC

Z/EG B = CTC GAA CTT CAC CTC GGC GC

Reaction Conditions: 95°C, 2.5min (94°C, 1min; 60°C, 30s; 72°C, 30s)$_{30}$, 72°C, 10min. 4°C, hold.

Bands: Z/EG = 300bp

2.8.9 RAC1 PCR Protocol

PCR Mix	µl
5x Colorless GoTaq Flexi Buffer*	10
$MgCl_2$ (25mM)	5
dNTPs (10mM)	0.4
Primer (100µM)	0.2 (of each)
Go Taq*	0.2
H_2O to final volume of 47.5 µl	

*GoTaq Flexi DNA Polymerase from Promega.

Primers:

RAC1 A = ATT TTG TGC CAA GGA CAG TGA CAA GCT

RAC1 B = GAA GGA GAA GAA GCT GAC TCC CAT C

RAC1 C = CAG CCA CAG GCA ATG ACA GAT GTT C

Reaction Conditions: 94°C, 5min (94°C, 30s; 55°C, 30s; 72°C, 30s)$_{30}$, 72°C, 7min. 4°C, hold.

2.9 Immunohistochemistry

IHC performed by myself except for Figures 3.1 and 3.5 (Dr William Faller). Standard paraffin sections were de-waxed in xylene (3 x 3 min) and then rehydrated through decreasing concentrations of ethanol to distilled water. Antigen retrieval was performed in 10mM citric acid (pH 6.0) by the water bath method. 5ml of Citrate antigen retrieval buffer (Thermo) diluted 1 in 10 with distilled water to a final volume of 50ml in a Coplin jar. This was placed in a cold water bath and then heated to 99.9^{o}C, prior to immersion of the slides. Slides then placed in the pre-heated solution for 20 min before being allowed to cool in the solution for 30 min at room temperature. Endogenous peroxidase activity was then blocked by incubating slides in 3% hydrogen peroxide for 10 min. Washing steps consisted of 3x 5 min immersions in Tris-Buffered Saline and Tween (TBST). Primary antibodies were incubated in the presence of 5% normal goat serum (Dako). Staining was visualised using DAB (3,3'-diaminobenzidine) chromogen in FAK project (Thermo Scientific), otherwise using Vector Red Alkaline Phosphatase Substrate Kit (Vector Labs) in P-Rex1 and Braf projects. Finally, slides were counterstained with haematoxylin, prior to dehydration in increasing concentrations of ethanol before mounting.

2.9.1 Ki67

Primary rabbit anti-Ki-67 antibody (1:200; Thermo RM-9106) applied for 1 h at room temp.

2.9.2 P-Rex1

Primary rabbit anti-P-Rex1 antibody (1:150, Sigma A001927) applied for 1 h at room temp.

2.9.3 MelanA

Primary mouse anti-melanA antibody (1:100, Abcam AB731) applied overnight at 4^{o}C.

2.9.4 S100

Primary rabbit anti-S100 antibody (1:250, Dako Z0311) applied overnight at 4^{o}C.

2.9.5 FAK

Primary rabbit anti-FAK antibody (1:200, Cell Signaling #3285) applied overnight at 4^{o}C.

2.10 Melanocyte Isolation

Performed by Dr Sam Lawn and Dr Andrew Muinonen-Martin. For melanocyte isolation from mice, pup skin was dissected at P2 then placed in ice cold PBS. Quickly it was cut into pieces and incubated in 1.5ml of collagenase type 1 and 2 at 37^{o}C, 5% CO_2 for approximately 25-50 min. Contents were transferred into 10ml wash buffer (1 x HBSS, 1mM CaCl2, 0.005% DNase) and centrifuged at 200g for 5 min at room temperature. Samples were resuspended in 2ml dissociation buffer, placed in small Petri dish and incubated at 37^{o}C, 5% CO_2 for 10 min. Thereafter, samples were put through an 18 gauge then 20 gauge needle and transferred into 10ml wash buffer for 10 min. The supernatant was centrifuged at 200g for 5 min at room temp, the pellet resuspended in 2ml PBS, then re-centrifuged at 200g for 5 min. The resuspended pellet was maintained in Hams F12 medium supplemented with 10% foetal calf serum, L-glutamine at 200µM, penicillin/streptomycin at 100 U/ml, and 200nM TPA.

2.11 Cell Culture

Performed by Dr Andrew Campbell. Normal human melanocytes (NHM) were maintained in Mln254 medium (M-254-500, Cascade Biologics) supplemented with Human

Melanocyte Growth Serum (S-002-5, Cascade Biologics) and penicillin/streptomycin at 100 U/ml. Mel224, Mel505, SK-Mel 2, 5, 23, 119, 147 and 187, CHL-1, A375 and WM266.4 were maintained in Dulbecco's Modified Eagle Medium supplemented with 10% foetal calf serum, L-glutamine at 200µM and penicillin/streptomycin at 100 U/ml. SBCL2, Lu1205, WM852, MeWo, Dauv-1, Gerlach, 888mel, 501mel, MNT-1, WM 35, 278, 793, 902b, 1552c and 1789 were maintained in RPMI 1640 supplemented with 10% foetal calf serum and penicillin/streptomycin at 100U/ml.

2.12 Immunoblotting

Performed by Dr Andrew Campbell except for Figure 6.6 (performed by myself). Cells were washed in PBS, then lysed in cell extraction buffer (50mM Tris-HCl (pH 7.6), 150mM sodium chloride, 1% Triton X-100, 0.5% deoxycholate, 0.1% SDS, 10µg/ml aprotinin, 125mM phenylmethylsulfonyl fluoride, 100µM sodium orthovanadate and 0.5mM sodium fluoride). Tissue samples were homogenised in Tissue Protein Extraction Reagent (Thermo) for 2 min at 2,200g. Protein concentration was determined by comparison of absorbance against known BSA concentrations. Lysates were then cleared by centrifugation and resolved by 10% Bis-Tris gel electrophoresis (Invitrogen). Proteins were transferred to PVDF membrane, blocked and probed with either 1:500 anti-P-Rex1 (Sigma), 1:10000 anti-β-actin (Sigma), 1:1000 anti-TIAM1 (Bethyl), 1:2000 anti-ERK2 (BD Biosciences), or 1:1000 anti-FAK (Cell Signalling) antibodies. Bound antibody was detected by incubation with anti-mouse or anti-rabbit horseradish peroxidase-conjugated secondary antibody and visualized by Enhanced Chemiluminescence (Amersham).

2.13 siRNA Treatments and RacGEF Constructs

Performed by Dr Andrew Campbell. Stable cell lines expressing Myc-epitope tagged human P-Rex1 were generated by retroviral infection using the modified Retro-X

retroviral expression system (Clontech). An Hpa I restriction site, followed by Kozak consensus translation initiation site was introduced to the 5' end of the coding sequence of myc-P-Rex1 (Hill et al, 2005), myc-P-Rex1 GEF-dead (Hill et al, 2005), or myc-Tiam1 by PCR (5' GTTAACCACCATGGAGCAGA AGCTGATC 3'), with a Cla I restriction site introduced to the 3' end in the same reaction (P-Rex1/P-Rex1 GEF-dead - 5' CCATCGATTCAGAGGTCCCCATCCACCGG 3'), with pCMV-P-Rex1, pCMV-P-Rex1 GEF-dead or pcDNA3.1-myc-Tiam1 used as template. In each case, the Hpa I-Cla I DNA fragments produced were subcloned into Hpa I and Cla I sites of the pLHCX retroviral expression vector. High-titre, replication-incompetent retroviral particles encoding the RNA of interest were produced in the Phoenix Ampho packaging line (Orbigen), for human target cells, and the Phoenix Eco packaging line (Orbigen) for murine target cells. Subsequent infection of target lines resulted in transfer of the coding region of interest, along with a selectable marker. Pooled cell lines stably expressing the construct of interest were isolated by selection with hygromycin-B (500 μg/ml) over multiple passages. Control lines were infected with retroviral particles expressing an empty pLHCX control vector transcript, and subjected to an identical selection procedure. Expression of the ectopically-introduced proteins of interest was determined by western blot and immunodetection with both epitope-tag specific and protein specific primary antibodies.

Transient knockdown of target proteins was achieved through consecutive rounds of liposome-mediated transfection with the appropriate siRNA oligonucleotides, 48 h apart. Liposomal transfection reagent (301702, HiPerFect), non-targeting control oligonucleotides (1027281, AllStars Negative Control) and P-Rex1 specific oligonucleotides (SI00692405, Hs_PREX1_3; SI03144449, Hs_PREX1_5; SI03246383, Hs_PREX1_6) were obtained from Qiagen Ltd.

2.14 Invasion Assays

Performed by Dr Andrew Campbell. Inverted matrigel invasion assays were performed as previously described (Hennigan et al, 1994). Matrigel protein matrix (BD bioscience) was allowed to polymerise in Transwell permeable inserts (Corning Ltd) over a period of 60 min at 37°C. Inserts were inverted, and cells seeded directly onto the filter surface in complete growth medium. Cells were then allowed to adhere over a period of 3h at 37°C, after which both non-adherent cells and residual growth medium were removed with 3x washes in appropriate serum-free medium. Finally, inserts were placed in serum-free tissue culture medium (containing 10% foetal calf serum) above the Matrigel matrix to act as a chemoattractant. In the case of siRNA-mediated transient knockdown experiments, invasion assays were prepared 24 h after the second round of lipofection. At 72h post-seeding, invasive cells which had entered Matrigel were stained with the fluorescent live-cell dye Calcein-AM, and visualised through confocal microscopy of optical sections obtained in the Z-plane at 15 µm intervals. Quantification was with the Area Calculator plugin for ImageJ.

2.15 RT-PCR

Performed by Dr Richard Mort. For embryo skin, E14.5 (Tyr::CreB/R26YFPR) skin was dissected in PBS on ice. Subsequently skin was digested over night in 0.05% collagenase and then dissociated mechanically using a pipette. Cells were sorted by FACS into sterile PBS and RNA prepared using the Qiagen RNAeasy plus kit. cDNA was prepared using the Roche first strand cDNA synthesis kit. Primer sequences were as follows: Prex1, Ex22_23_F, FGCACGGTGTGGTTTACGAAT; Prex1, Ex22_23_R, TCTCCAGCTTGGTGTCACAG; Prex1, Ex_37_38_F, TCTACCGCCTCATGAAGACC; Prex1, Ex_37_38_R, ATGACACACTTGGGCAACAG; Prex1, Ex1_3_F, GCCTCCGTCTGTGCGTACT; Prex1, Ex1_3_R,

CAGGATGTCCTCAATGTTGG; Dct, F, TGTGCAAGATTGCCTGTCTC; Dct, R, GTTGCTCTGCGGTTAGGAAG; Tyr, F, ATGCACCTATCGGCCATAAC; Tyr, R, ATAACAGCTCCCACCAGTGC; GAPDH_F AAGGTCATCCATGACAACTTTGG; GAPDH, R, AAGAGTGGGAGTTGCTGTTGAAG.

2.16 Microarray

Microarray analyses were performed using the Agilent microarray platform, chip ref G4112F. Raw data, including nude mouse work, were provided by Larue laboratory (Institut Curie, Paris), then analysed by myself.

2.17 Human Tissues

Human tissue was analysed from archival paraffin patient samples from St. Vincent's University Hospital, Dublin, Ireland. Quadruplicate cores from 141 consecutive melanoma patients (1994-2007) were used to construct a tissue microarray with insufficient survival data. Further samples were received from Radboud University Medical Center, Nijmegen, Netherlands. All patient specimens were used in accordance with institutional and national policies at the respective locations. All samples were formalin fixed and paraffin embedded. TMA samples were analysed independently by 2 people. Analysis in Beatson by Dr William Faller.

2.18 BRaf and NRas Mutation Status of Cell Lines

The following tables offer details of mutation status of melanoma cell lines used in chapter 3 and 5. Further data on the growth phase of the originating tumour are also described where possible. RGP = radial growth phase; Met = metastatic.

Cell Line	Braf status	Nras status	Growth phase
NHM	WT	WT	N/A
SK-Mel 23	WT	WT	Met
SK-Mel 187	WT	WT	VGP
CHL1	WT	WT	Met
Mel505	WT	WT	VGP
SK-Mel 2	WT	Q61R	Met
SK-Mel 119	WT	Q61R	Met
SK-Mel 147	WT	Q61R	Met
SBCL2	WT	Q61R	RGP
Mel224	WT	Q61R	Met
A375	V600E	WT	VGP
Colo 829	V600E	WT	Met
SK-Mel 5	V600E	WT	Met
WM35	V600I	WT	RGP
WM266.4	V600D	WT	VGP
WM278	V600E	WT	VGP
WM793	V600E	WT	VGP
WM902b	V600E	WT	VGP
WM1552c	V600E	WT	RGP
WM1789	K601E	WT	RGP

Cell Line	Braf status	Nras status
WM852	WT	Q61R
LU1205	V600E	WT
MeWo	WT	WT
A375M	V600E	WT
WM793	V600E	WT
WM983A	V600E	WT
WM983B	V600E	WT
WM1366	WT	Q61L
SK28	V600E	WT
SK29	V600E	WT
Rosi	WT	WT
Daju	V600E	WT
Dauv-1	V600E	WT
Mull	V600E	WT
Lyse	WT	Q61K
Gerlach	WT	Q61K
501Mel	V600E	WT
G1	WT	WT
T1	WT	WT
888mel	V600E	WT
Quar	V600E	WT
MNT-1	WT	WT
SKMEL3	V600E	WT

Chapter 3

The role of P-Rex1 in Nras^{Q61K}-driven models of melanoma

P-Rex1 has not previously been characterised in genetically modified animal models of cancer that can recapitulate the genetics and pathology of the human disease. As detailed at the end of the introduction (Section 1.5.1.3), several factors led to our hypothesis that P-Rex1 could contribute to invasive and metastatic melanoma: reported direct and indirect interactions with PI(3)K and MAPK pathways, amplification of its chromosome site 20q13, and the role of Rac and other Rac-GEFs already described in the disease. This chapter reports the role of endogenous and ectopic P-Rex1 in a *Tyr::Nras*$^{Q61K/°}$*; INK4a*$^{-/-}$ mouse model of melanoma, dissecting some of the results with further experimental analysis in allografts, xenografts and invasion studies of human melanoma cell lines.

3.1 P-Rex1 deficiency does not alter primary melanoma in a *Tyr::Nras$^{Q61K/°}$; INK4a$^{-/-}$* melanoma mouse model

We first assessed the role of P-Rex1 in primary melanoma development by crossing *P-Rex1$^{-/-}$* mice to a genetically modified model of metastatic malignant melanoma, *Tyr::Nras$^{Q61K/°}$; INK4a$^{-/-}$* mice (Ackermann et al, 2005, Welch et al, 2005).

Tyr::Nras$^{Q61K/°}$; INK4a$^{-/-}$; P-Rex1$^{+/+}$ mice developed primary melanoma with a similar penetrance and latency to that previously described (Figure 3.1a, Table 3.1). IHC was carried out on primary melanomas taken from *P-Rex1$^{+/+}$* and *P-Rex1$^{-/-}$* mice to confirm P-Rex1 expression in tumours (Figures 3.1b,c). 7/10 primary melanomas from *P-Rex1$^{+/+}$* mice showed staining for P-Rex1, compared to 0/9 samples from *P-Rex1$^{-/-}$* mice. Although Rac function has been shown to be required for primary squamous cell skin and lung tumour development (Kissil et al, 2007, Malliri et al, 2002), we observed no difference in incidence, latency, or tumour burden of primary melanomas between *Tyr::Nras$^{Q61K/°}$; INK4a$^{-/-}$; P-Rex1$^{+/+}$* mice and *Tyr::Nras$^{Q61K/°}$; INK4a$^{-/-}$; P-Rex1$^{-/-}$* mice (Table 3.1, Figures 3.1d,e).

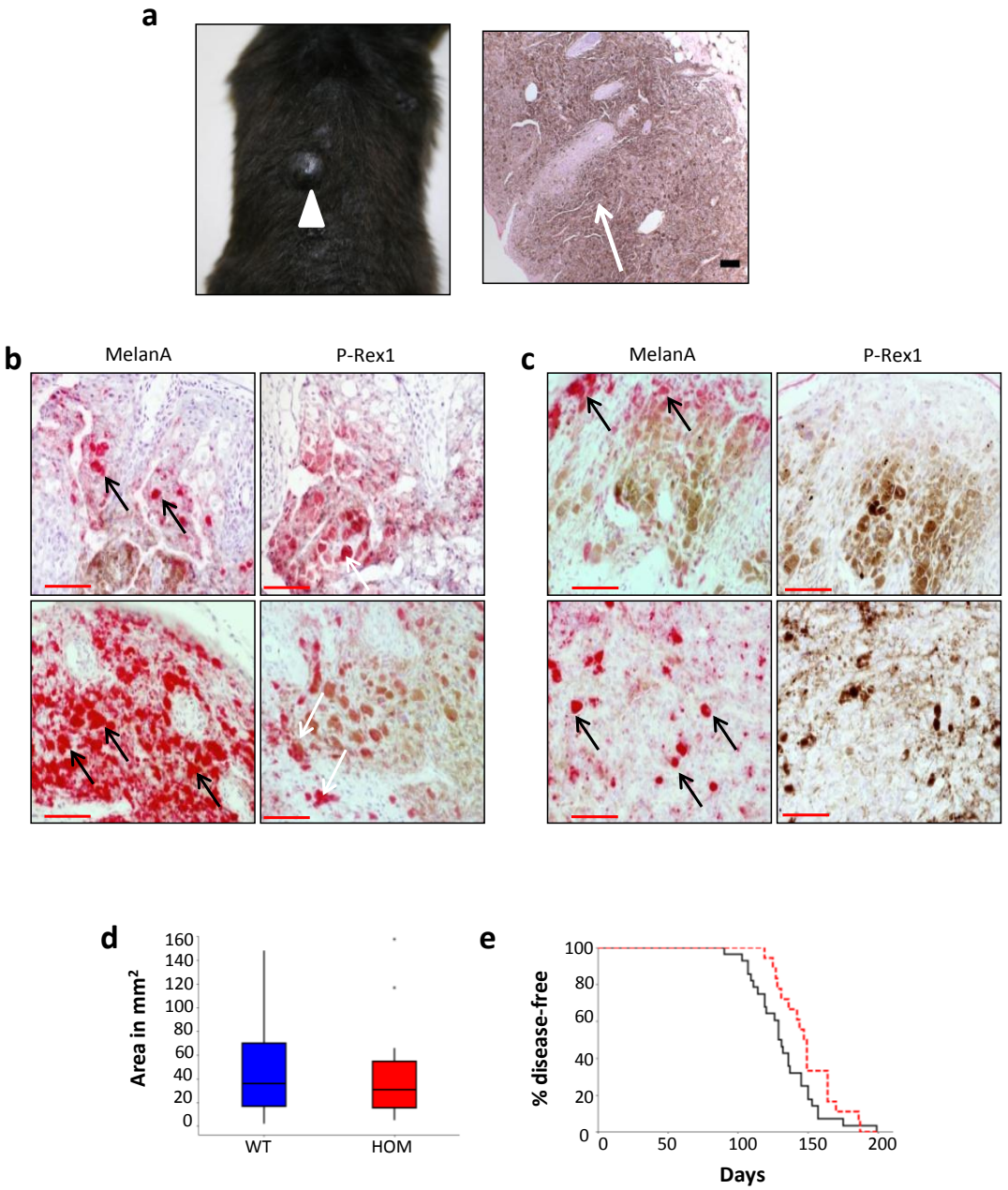

Figure 3.1 P-Rex1 disruption does not significantly alter primary melanomagenesis in a *Tyr::Nras$^{Q61K/°}$; INK4a$^{-/-}$* transgenic murine melanoma model
(a) Example of primary melanoma arising in *Tyr::Nras$^{Q61K/°}$; INK4a$^{-/-}$* transgenic mice. White arrowhead: pigmented primary skin melanoma. Accompanying photomicrograph (H&E) indicates pigmented dermal melanocytosis characteristic of these lesions (white arrow) (Scale bar=100µm). **(b)** MelanA (a common melanocyte marker; black arrows, pink staining) and P-Rex1 (white arrows, pink staining) IHC expression in two separate primary melanomas of P-Rex1$^{+/+}$ mice. Varying levels of P-Rex1 expression can be seen in mouse melanomas (n=10). Brown staining represents melanin pigment. **(c)** MelanA (black arrows, pink staining) and lack of P-Rex1 IHC expression (no pink staining) in two separate primary melanomas of P-Rex1$^{-/-}$ mice. No P-Rex1 expression was observed in melanomas from these mice (n=9). Brown staining represents melanoma pigment. **(d)** Comparison of primary tumour burden between *Tyr::Nras$^{Q61K/°}$; INK4a$^{-/-}$; P-Rex1$^{+/+}$* (blue bar, 'WT') and *Tyr::Nras$^{Q61K/°}$; INK4a$^{-/-}$; P-Rex1$^{-/-}$* (red bar, 'HOM') mice (p=0.43, Mann-Whitney, n=29; small asterisks represent outlying data) (Box and whiskers plot: box represent 25th-75th percentile of given value, line represents median value). **(e)** Kaplan-Meier analysis of primary melanoma latency between *Tyr::Nras$^{Q61K/°}$; INK4a$^{-/-}$; P-Rex1$^{+/+}$* (black line, n=27) and *Tyr::Nras$^{Q61K/°}$; INK4a$^{-/-}$; P-Rex1$^{-/-}$* (red line, n=18) cohorts (p=0.156, log-rank test). Figures (b) and (c) kindly contributed by Dr William Faller.

Genotypes	Mice with Primary Melanoma	Average Age (days)	Mice with Melanoma Metastases	Mice with Melanoma Metastases, Excluding Brain Lesions
Tyr::Nras$^{Q61K/°}$; INK4a$^{-/-}$; P-Rex1$^{+/+}$	30/41	184	13/30	6/30
Tyr::Nras$^{Q61K/°}$; INK4a$^{-/-}$; P-Rex1$^{-/-}$	30/42	211	1/30	1/30
			p=0.001	**p=0.044**

Table 3.1 P-Rex1 disruption dramatically reduces incidence of metastasis in an *Tyr::Nras$^{Q61K/°}$; INK4a$^{-/-}$* transgenic murine melanoma model
Table detailing numbers of mice within both *Tyr::Nras$^{Q61K/°}$; INK4a$^{-/-}$; P-Rex1$^{+/+}$* and *Tyr::Nras$^{Q61K/°}$; INK4a$^{-/-}$; P-Rex1$^{-/-}$* cohorts suffering from primary and metastatic melanoma (chi-square test). Metastatic sites other than brain for *Tyr::Nras$^{Q61K/°}$; INK4a$^{-/-}$; P-Rex1$^{+/+}$* cohort were lungs (4 mice), liver (3 mice), peritoneum (1 mouse); *Tyr::Nras$^{Q61K/°}$; INK4a$^{-/-}$; P-Rex1$^{-/-}$* metastasis was in lungs.

3.2 P-Rex1 deficiency impairs metastasis in a *Tyr::Nras$^{Q61K/°}$; INK4a$^{-/-}$* melanoma mouse model

Tyr::Nras$^{Q61K/°}$; INK4a$^{-/-}$; P-Rex1$^{+/+}$ mice also developed melanoma metastasis with a similar penetrance and latency to that previously described (Figure 3.2a). All metastases from *P-Rex1$^{+/+}$* mice displayed immunoreactivity for P-Rex1 similar to that of MelanA, a common melanocyte marker (11 samples; lung, liver, brain) (Figure 3.2b). A significant reduction in melanoma metastasis was observed in the *Tyr::Nras$^{Q61K/°}$; INK4a$^{-/-}$; P-Rex1$^{-/-}$* cohort (1/30 mice), with the number of metastases in control *Tyr::Nras$^{Q61K/°}$; INK4a$^{-/-}$; P-Rex1$^{+/+}$* mice the same as previously reported (13/30 mice; p=0.001; chi-square) (Table 3.1). *Tyr::Nras$^{Q61K/o}$; INK4a$^{-/-}$; P-Rex1$^{-/-}$* mice also had an improved overall survival (Figure 3.2c). The one metastasis observed in the experimental *Tyr::Nras$^{Q61K/°}$; INK4a$^{-/-}$; P-Rex1$^{-/-}$* metastasis was to the lungs. These data suggest that P-Rex1 is a central component of metastasis development in this context.

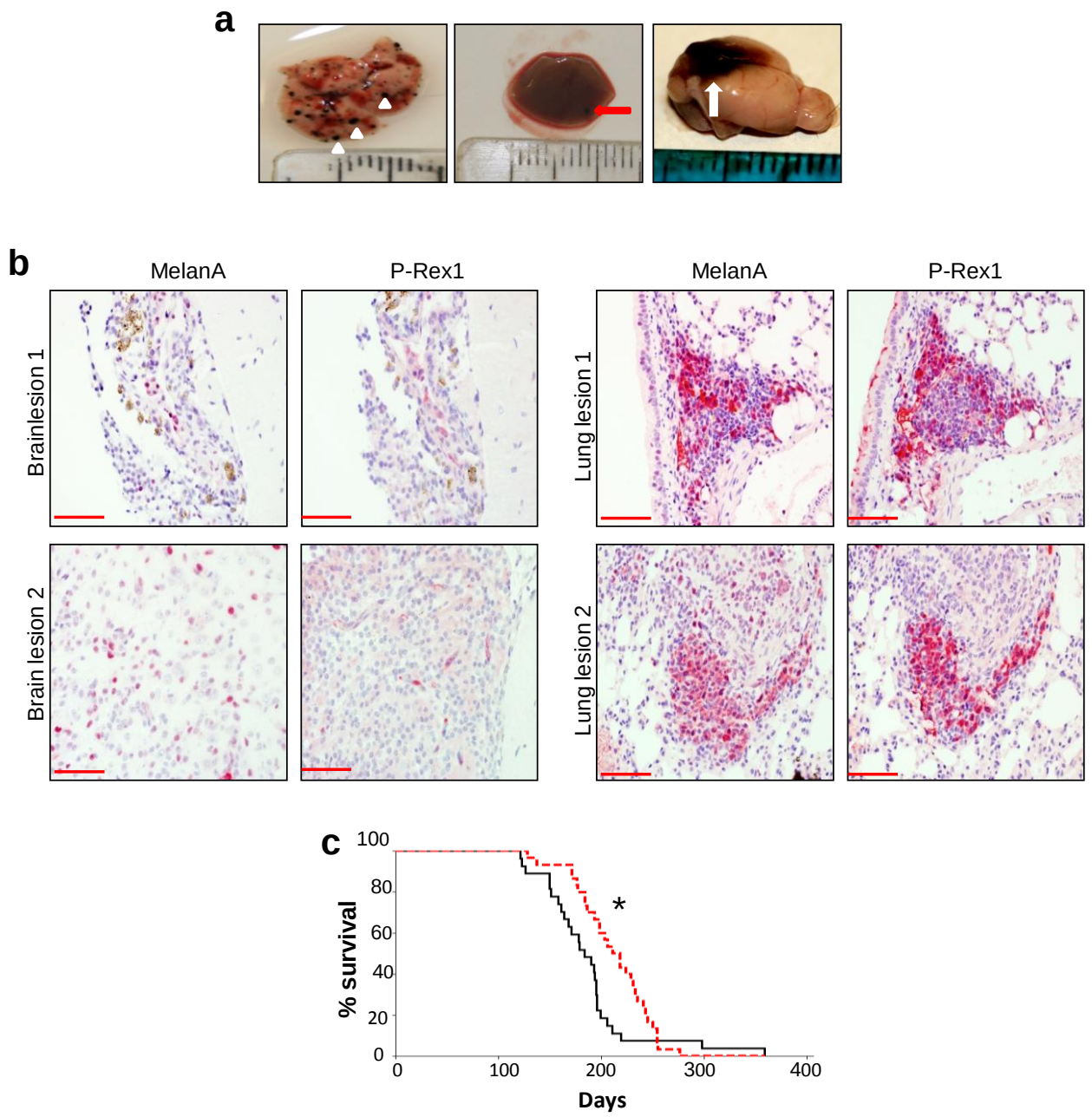

Figure 3.2 P-Rex1 disruption dramatically reduces incidence of metastasis in an *Tyr::Nras$^{Q61K/°}$; INK4a$^{-/-}$* transgenic murine melanoma model
(a) Examples of metastatic melanomas arising in *Tyr::Nras$^{Q61K/°}$; INK4a$^{-/-}$* transgenic mice. White arrowheads: multiple pigmented lung metastases; Red arrow: pigmented liver metastasis; White arrow: large pigmented brain lesion. Nras^{Q61K} expression was not confirmed in these lesions. **(b)** MelanA (common marker of cells from the melanocyte lineage) and P-Rex1 immunohistochemical expression in melanoma metastases from P-Rex1$^{+/+}$ control mice. Left four panels show expression in brain lesions, while right four panels show expression in lung metastases (pink staining). n=11. Brown staining represents melanoma pigment. **(c)** Kaplan-Meier curves detailing significant improvement in survival of *Tyr::Nras$^{Q61K/°}$; INK4a$^{-/-}$; P-Rex1$^{-/-}$* cohort (red line) compared to *Tyr::Nras$^{Q61K/°}$; INK4a$^{-/-}$; P-Rex1$^{+/+}$* cohort (black line) (*p=0.017, log-rank test, n=30 for each cohort). Figure (b) kindly contributed by Dr William Faller.

Although we were unable to exclude categorically the possibility that our melanoma brain lesions are not primary melanocytic neoplasms of the central nervous system (CNS), a significant reduction in metastases was still seen when these lesions were excluded from our analysis (Table 3.1). Consistent with findings in another genetically modified mouse model, these brain lesions extended into the cortex and exhibited locally aggressive behaviour, thus either invading the brain parenchyma from a blood-borne metastasis or the lepto-meningeal site of origin in primary CNS melanoma (Fig. 3.2b) (Goel et al, 2009). However, melanomatous brain lesions are generally infrequent in other genetically modified mouse models (see Table 1.3). Regardless of their point of origin, ablation of P-Rex1 in these lesions either suppresses local invasion or metastasic spread. In support of them being genuine metastases, no *Nras*^{Q61K} mutations were observed in a previous study of human primary CNS melanoma (Küsters-Vandevelde et al, 2010).

3.2.1 P-Rex1 deficiency impairs frequency, growth, and organ spread of metastases

We next explored the pro-metastatic role of endogenous P-Rex1 in melanoma by deriving melanocyte cell lines from the early pup skin of *Tyr::Nras*$^{Q61K/°}$*; INK4a*$^{-/-}$*; P-Rex*$^{+/+}$ and *Tyr::Nras*$^{Q61K/°}$*; INK4a*$^{-/-}$*; P-Rex1*$^{-/-}$ mice. When injected via TV into C57BL6 mice, 2/4 mice treated with *Tyr::Nras*$^{Q61K/°}$*; INK4a*$^{-/-}$*; P-Rex1*$^{-/-}$ melanocytes were found to have metastases, compared with 5/5 mice who were treated with *Tyr::Nras*$^{Q61K/°}$*; INK4a*$^{-/-}$*; P-Rex*$^{+/+}$ cells (Figures 3.3a-f, Table 3.2). A significant reduction in metastatic frequency was observed on histological analyses of the cohort injected with *Tyr::Nras*$^{Q61K/°}$*; INK4a*$^{-/-}$*; P-Rex1*$^{-/-}$ melanocytes, with a reduction in metastatic tumour burden also seen but not significant (Figures 3.3g,h; methods detailed in section 2.3). Moreover, we observed a propensity of the *Tyr::Nras*$^{Q61K/°}$*; INK4a*$^{-/-}$*; P-Rex*$^{+/+}$ cells to metastasise to distant viscera (kidney, liver, heart, spleen), metastases that were not seen in the mice TV-treated with

Tyr::Nras$^{Q61K/°}$; INK4a$^{-/-}$; P-Rex1$^{-/-}$ cells (Figures 3.3b-f, Table 3.2). Collectively, these results suggested endogenous P-Rex1 can facilitate frequency and organ spread of metastases in melanoma from the intravasation stage of the metastatic cascade (detailed in Section 1.2 and Figure 1.3), with a strong suggestion that P-Rex1 might also support their secondary growth.

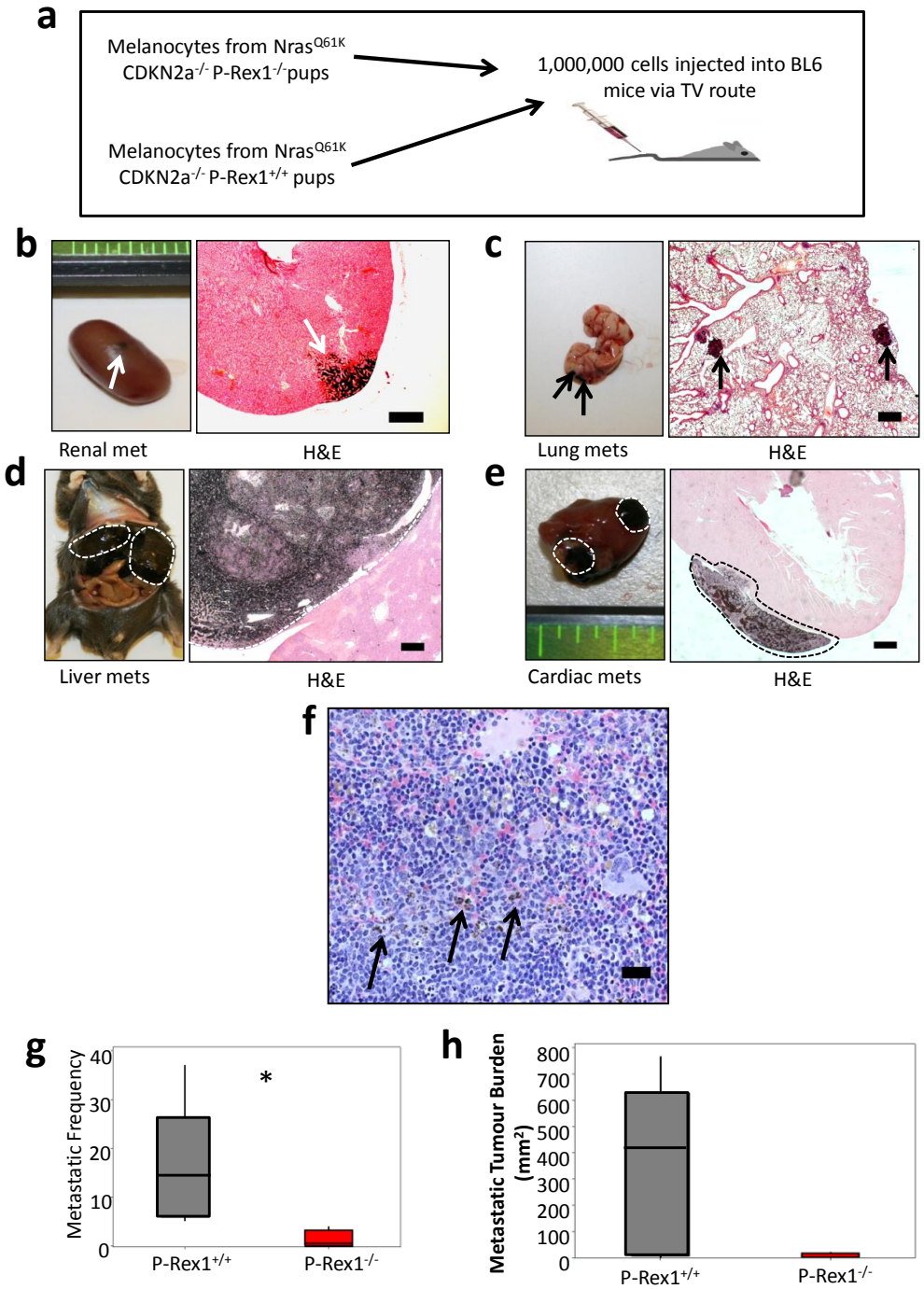

Figure 3.3 Endogenous P-Rex1 facilitates metastatic frequency and organ spread following the intravasation step

(a) Schematic diagram detailing cell type, cell numbers, injection type, and mouse background used in experiment **(b) – (f)** Metastatic melanomas affecting kidney (b, white arrow), lungs (c, black arrows), liver (d, white interrupted line), heart (e, interrupted line), and melanin in spleen (f, black arrows) of C57BL6 mice TV-treated with *Tyr::Nras$^{Q61K/°}$; INK4a$^{-/-}$; P-Rex$^{+/+}$* cells; accompanying photomicrographs (H&E, scale=500µm for all except 30µm for splenic photomicrograph). **(g)** Quantification of metastases observed in C57BL6 mice TV-treated with melanocytes derived from early pup skin of either *Tyr::Nras$^{Q61K/°}$; INK4a$^{-/-}$; P-Rex1$^{-/-}$* mice (red bar) or *Tyr::Nras$^{Q61K/°}$; INK4a$^{-/-}$; P-Rex$^{+/+}$* mice (grey bar) (*p=0.02, Mann-Whitney test; n=5) (Box and whiskers plots: boxes represent 25th-75th percentiles of given value, lines represent median values). **(h)** Quantification of metastatic tumour burden (method described in Section 2.3) observed in the same C57BL6 TV-treated mice as described in (g) (p=0.087, Mann-Whitney test; n=5) (Box and whiskers plots: boxes represent 25th-75th percentiles of given value, lines represent median values).

	Number of Metastatic Mice	Sites of Metastases
Tyr::Nras$^{Q61K/°}$; INK4a$^{-/-}$; P-Rex1$^{-/-}$	2/4	Skin (1), LN (1), Lung (1)
Tyr::Nras$^{Q61K/°}$; INK4a$^{-/-}$; P-Rex$^{+/+}$	5/5	Liver (5), kidney (5), lung (4), LN (3), Spleen (3), Peritoneal (2), Skin (2), Heart (1)

Table 3.2 Endogenous P-Rex1 facilitates metastases to distant sites following the intravasation step
Table indicating number of mice with metastases as well as range of metastatic sites between C57BL6 mice TV-treated with either *Tyr::Nras$^{Q61K/°}$; INK4a$^{-/-}$; P-Rex$^{+/+}$* murine melanocytes or *Tyr::Nras$^{Q61K/°}$; INK4a$^{-/-}$; P-Rex1$^{-/-}$* murine melanocytes.

3.3 High P-Rex1 is sensitive for the development of metastases in immuno-deficient mice

The above data in genetically modified models of cancer were also supported by analyses of immuno-deficient mice which were injected subcutaneously (SC) with a number of different melanoma cell lines, derived from human melanomas driven mostly by oncogenic Braf or Nras (section 2.8 for cell line details) (Figure 3.4). In total, 18/24 cell lines developed tumours following injection, with 4/24 also forming metastases. Microarray analysis revealed that, of the cell lines with P-Rex1 intensity above the median ('high' P-Rex1), all went on to develop tumours in immuno-deficient mice (Figs. 3.4b). This included all mice that developed metastases, and notably, the two $Nras^{Q61K}$ and $Braf^{V600E}$ cell lines with the highest P-Rex1 intensity both developed metastases. Statistical evaluation of these results confirmed high P-Rex1 was 100% statistically sensitive for detecting those cell lines that developed metastases in nude mice (Table 3.3) ($p=0.005$). We also found that P-Rex1 intensity below the median in cell lines ('low' P-Rex1) was 100% statistically specific for excluding melanoma development in immuno-deficient mice (Table 3.4) ($p=0.028$). Using qRT-PCR, this data was supported by our finding that P-Rex1 levels were highest in cell lines that form metastases - after averaging P-Rex1 levels in cell lines that formed no tumours, tumours, or metastases (Fig. 3.4c). Furthermore, the lowest expression occurred in those cell lines that do not form tumours in immuno-deficient mice (Fig. 3.4c). Unfortunately we do not have access to raw data to statistically confirm our results in Figure 3.4c.

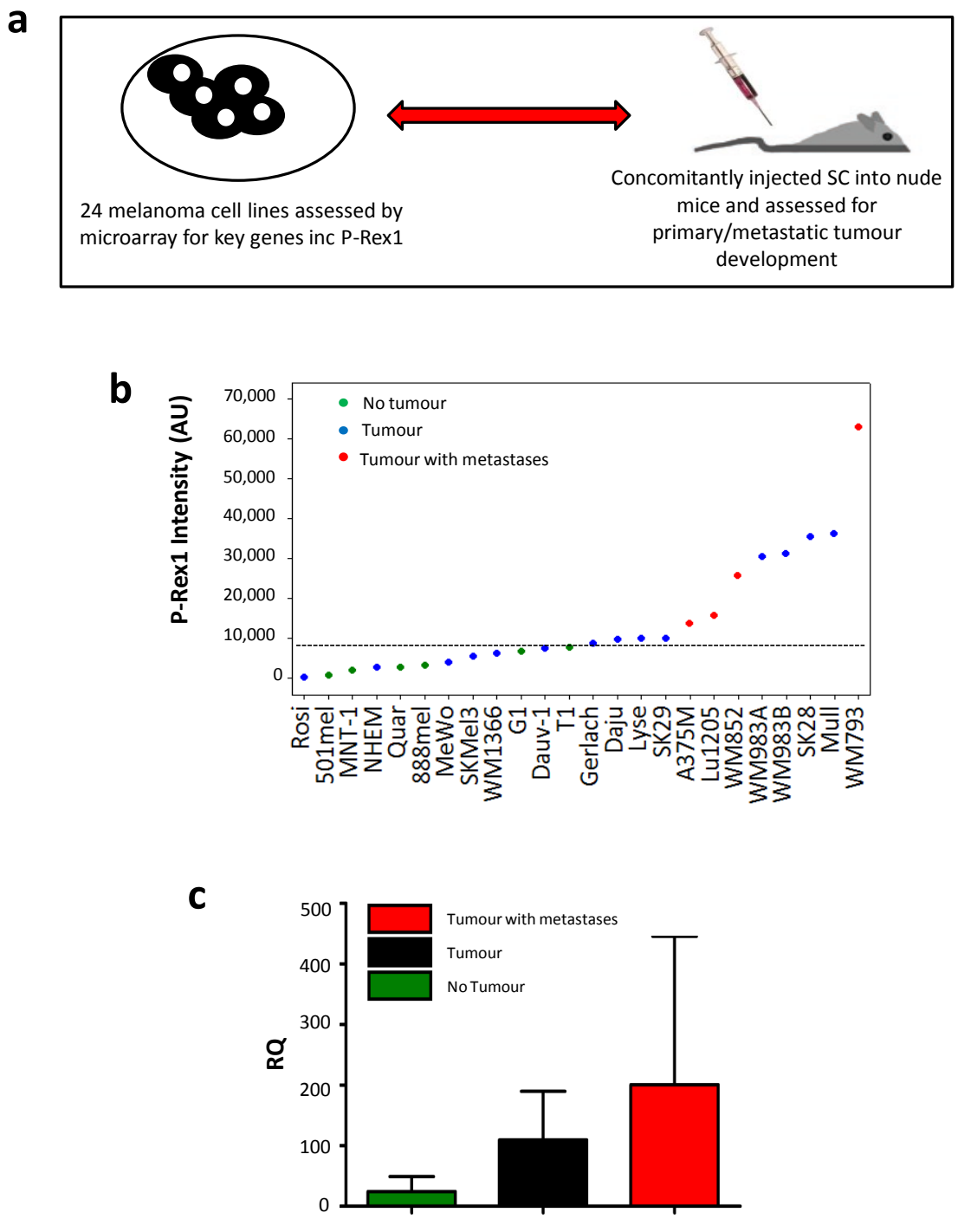

Figure 3.4 High P-Rex1 is sensitive for the development of metastases in immuno-deficient mice
(a) Schematic diagram describing experimental details. 24 melanoma cell lines were assessed by microarray for presence of key genes (including P-Rex1). They were also SC-injected into immuno-deficient mice to assess propensity to develop primary and metastatic melanomas. **(b)** Individual value plot derived from cell line microarray showing P-Rex1 intensity in melanoma-derived cell lines correlates with propensity to develop metastases in immuno-deficient mice. Interrupted line represents median P-Rex1 value. AU = arbitrary units. NHEM = normal human melanocytes. **(c)** qRT-PCR analysis showing average P-Rex1 RQ value of cell lines from each tumour group. Error bars represent the standard deviation of the triplicate measurement. RQ = relative quantity. No raw data or statistical information available for this figure which was kindly provided by Larue laboratory, Institute Curie, Paris.

	Melanoma Mets	No Melanoma Mets
High P-Rex1	4	8
Low P-Rex1	0	12
	100% sensitive (p=0.005)	**60% specific**

Table 3.3 High P-Rex1 in cell lines is sensitive for detecting metastatic melanoma development in immuno-deficient mice
P-Rex1 intensity levels my microarray divided into those above and below median value ('high' vs 'low'; chi-square test). Statistical sensitivity is defined as the probability that the test says a person has a disease when they do have the disease. Statistical specificity is defined as the probability that the test says a person does not have a disease when they are disease free.

	Primary Melanoma	No Primary Melanoma
High P-Rex1	12	0
Low P-Rex1	6	6
	66.7% sensitive	**100% specific (p=0.028)**

Table 3.4 Low P-Rex1 in cell lines is specific for excluding melanoma development in immuno-deficient mice
P-Rex1 intensity levels by microarray divided into those above and below median value ('high' vs 'low'; chi-square test). Statistical sensitivity is defined as the probability that the test says a person has a disease when they do have the disease. Statistical specificity is defined as the probability that the test says a person does not have a disease when they are disease free.

3.4 P-Rex1 in human melanoma

3.4.1 P-Rex1 is upregulated in human melanoma

To test the relevance of our data to human melanomagenesis, we first examined the protein expression of P-Rex1 in established human melanoma cell lines derived from primary or metastatic disease. Compared to normal human melanocytes (NHM), there was marked P-Rex1 overexpression in nearly all of the cell lines (Figure 3.5a). Moreover, the 3 cell lines with clearly the highest P-Rex1 expression (CHL1, SK-Mel119, Mel224) were all derived from a metastatic source (see Section 2.17), supporting our above analysis that showed high P-Rex1 intensity by microarray was sensitive for the development of metastases in immuno-deficient mice (Figure 3.4).

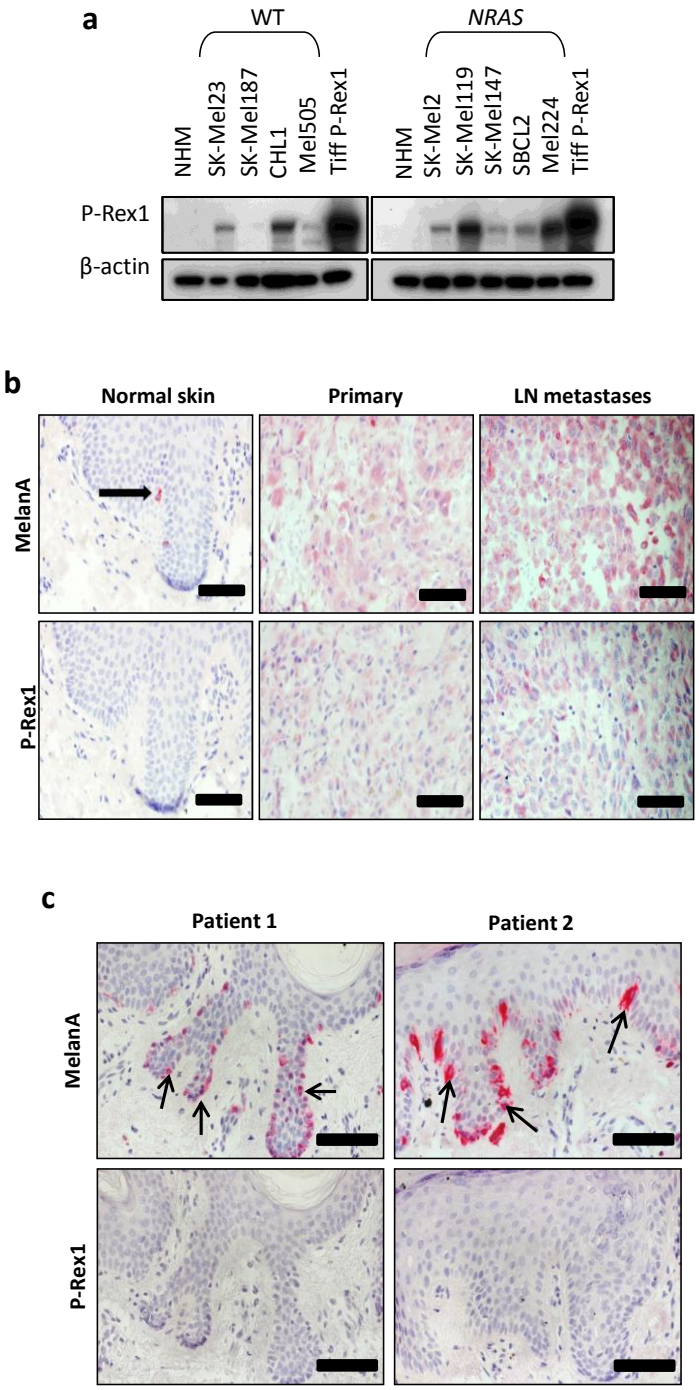

Figure 3.5 P-Rex1 upregulation is associated with progressive disease in human melanoma **(a)** Western blots illustrating endogenous expression of P-Rex1 in a panel of human melanoma derived cell lines. Cell lines with driver mutations in *NRAS* are represented ('*NRAS*' bracket), along with cell lines that are *wild-type* for *NRAS* (*'WT'* bracket). NHM = normal human melanocytes. **(b)** P-Rex1 expression increases with more aggressive disease. Photomicrographs of human tissue specimens of normal skin, primary and metastatic melanoma, immunohistochemically labelled against P-Rex1 or the melanocyte marker melanA. LN = lymph node. Scale bars = 90µm. **(c)** P-Rex1 is not detectable in normal melanocytes by immunohistochemistry. Photomicrographs of human melanocytes (black arrows) of normal skin (serial sections from 2 separate patients) immunohistochemically labelled against P-Rex1 or the melanocyte marker melanA. Similar staining of normal skin from a third patient is seen as part of Figure 3.5b (Scale bars = 90µm). Figure (a) kindly contributed by Dr Andrew Campbell, figures (b) and (c) kindly contributed by Dr William Faller.

3.4.2 P-Rex1 is associated with progression in human melanoma

We next assessed whether increased P-Rex1 activity in humans is also related to melanoma progression: this possibility was raised by both the sensitivity of high P-Rex1 for nude mouse metastasis development and the increased expression of P-Rex1 observed in melanoma-derived cell lines compared to normal melanocytes (Figures 3.4 and 3.5a). IHC for P-Rex1 was performed on human tissue specimens from skin and melanoma: although P-Rex1 expression was not detectable in melanocytes in normal skin (3 out of 3 specimens), we consistently detected it in biopsies of primary melanomas (112 out of 141 specimens) and melanoma lymph node metastases (8 out of 9 specimens) (Figures 3.5b,c). These data provided further evidence of a role for P-Rex1 in human melanoma progression, and were consistent with our prior findings in mice.

3.4.3 Endogenous and ectopic P-Rex1 drives invasion through its GEF activity

One potential way P-Rex1 could drive progression and metastatic spread is through an increased invasive capacity conferred by its DH-domain-mediated GEF activity. To examine this, we knocked down endogenous P-Rex1 in the CHL1 human melanoma cell line where P-Rex1 was upregulated in Figure 3.5a. Consistently we observed that 3D matrigel invasion was diminished following knockdown of endogenous P-Rex1 (Figures 3.6a-c).

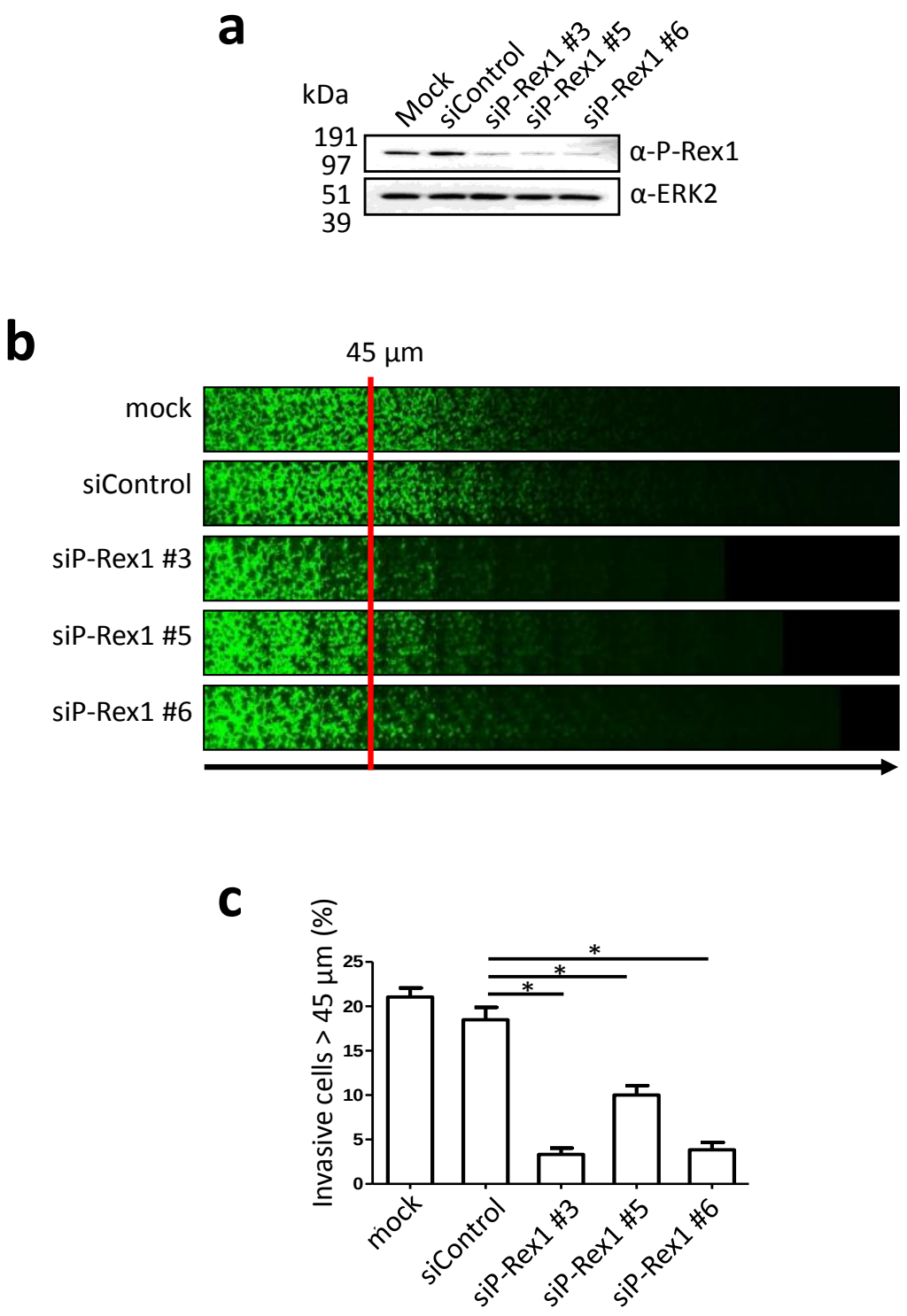

Figure 3.6 Endogenous P-Rex1 drives invasion in human melanoma cell lines
(a) Silencing P-Rex1 by siRNA as shown by western blot analysis. A mock transfection and scramble siRNA were used as controls. **(b)** Comparison of representative matrigel invasion assays of CHL1 human melanoma cell lines treated with control or P-Rex1 specific siRNA oligonucleotides. **(c)** Quantification of cells invading beyond 45µm in matrigel invasion assays of CHL1 human melanoma cell lines treated with control ('siControl') vs P-Rex1 ('siP-Rex1') specific siRNA oligonucleotides. (*p=0.005, Mann-Whitney test; n=3; error bars = +/- standard error of mean (SEM). Figure kindly contributed by Dr Andrew Campbell.

As P-Rex1 is overexpressed in the majority of human melanoma cell lines, we used the previously described melanocyte cell line derived from early pup skin of *Tyr::Nras*$^{Q61K/°}$*; INK4a*$^{-/-}$*; P-Rex1*$^{-/-}$ mice (see section 3.2.1) to examine invasion in a cell line where P-Rex1 is not endogenously expressed. These *P-Rex1*$^{-/-}$ cell lines, which were genetically manipulated to over-express empty vector ('P-Rex1$^{-/-}$'), failed to invade in 3D matrigel and organotypic assays unless they were re-constituted to express ectopic levels of P-Rex1 ('P-Rex1') (Figures 3.7a-d). Expression of ectopic levels of GEF-dead P-Rex1 ('GD P-Rex1') failed to phenocopy the invasive phenotype of cells with re-constituted *wild-type* P-Rex1, confirming the GEF activity of P-Rex1 as central to its invasive phenotype (Figures 3.7a-d). Ectopic expression of another RacGEF described in melanoma, TIAM1, also failed to phenocopy the invasion seen with P-Rex1 expression (Figures 3.7a-d) (Uhlenbrock et al, 2004). These results showed the GEF activity of P-Rex1 may have a unique role amongst RacGEFs: it functions as a vital component of invasion for cells of the melanocyte lineage, a mechanism by which it can drive melanoma progression and metastases.

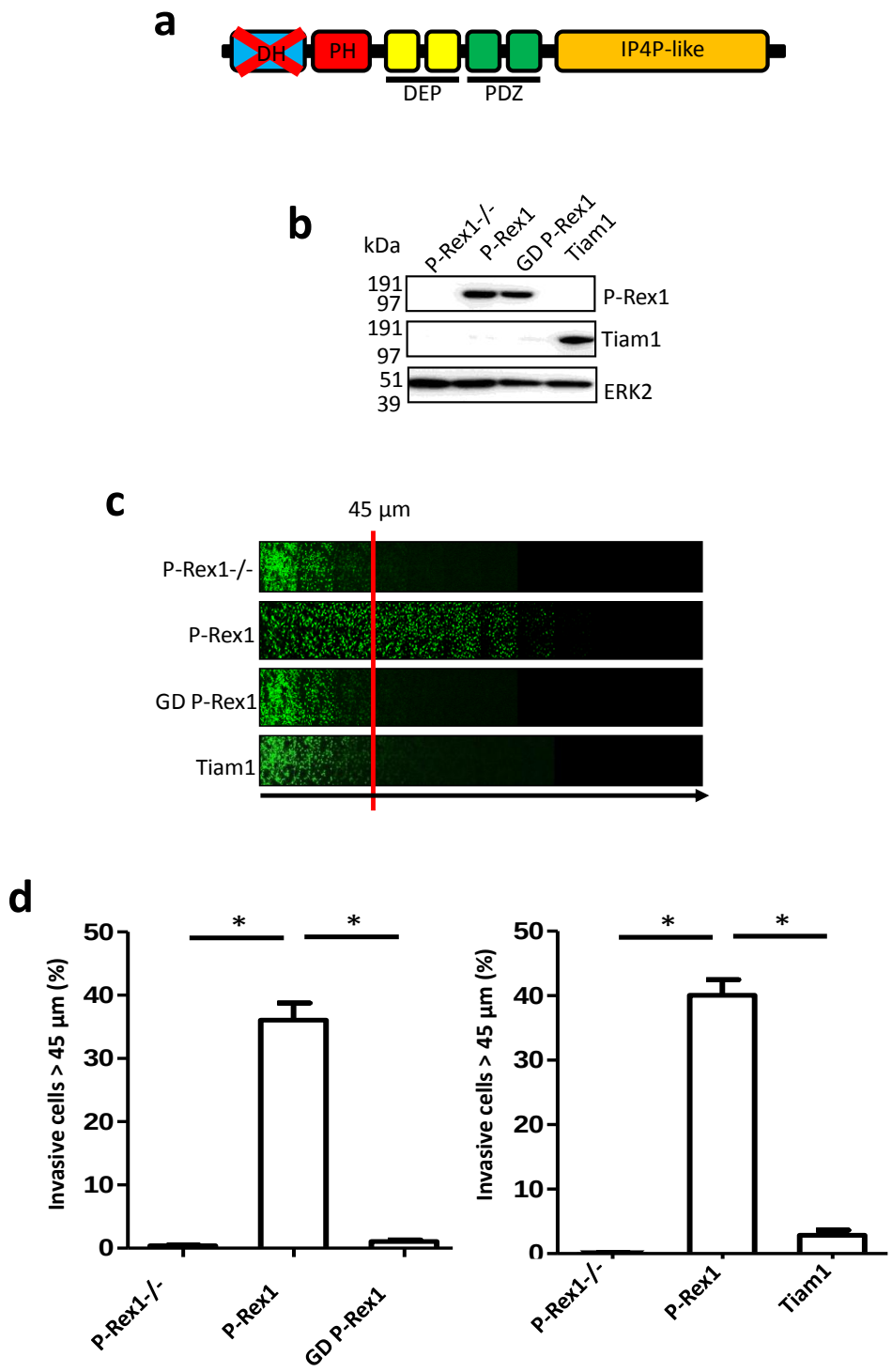

Figure 3.7 Exogenous P-Rex1 drives invasion through its GEF activity
(a) Schematic picture detailing domain structure of GEF-dead P-Rex1 mutant. 2 point mutations (E56A, N238A) are introduced to the DH domain, abolishing its GEF activity. **(b)** Westen blot confirming relative expression of 'P-Rex1', 'P-Rex1 GD', and 'Tiam1' cells is well matched. **(c)** Representative matrigel invasion assays comparing melanocytes derived from early pup skin of *Tyr::Nras$^{Q61K/°}$; INK4a$^{-/-}$; P-Rex1$^{-/-}$* mice and genetically modified to over-express P-Rex1 ('P-Rex1'), empty vector ('P-Rex1$^{-/-}$'), GEF-dead P-Rex1 ('GD P-Rex1'), or Tiam1 ('Tiam1'). **(d)** Left panel: quantification of cells invading beyond 45µm in matrigel invasion assays of P-Rex1$^{-/-}$ vs P-Rex1 vs GD P-Rex1 cells (*p=<0.0001 for both comparisons, Mann-Whitney test; n=18 quantifications from 6 samples). Right panel: quantification of cells invading beyond 45µm in matrigel invasion assays of P-Rex1$^{-/-}$ vs P-Rex1 vs Tiam1 cells (*p=<0.0001 for both comparisons, Mann-Whitney test; n=18 quantifications from 6 samples; error bars for both panels = +/- standard error of mean (SEM). Figures (b) – (d) kindly contributed by Dr Andrew Campbell.

3.5 What is the most effective molecular strategy for targeting P-Rex1?

Mutational studies have identified the DH domain of P-Rex1 as key to its GEF enzymatic activity (Hill et al, 2005). In this chapter, we have also revealed its importance to invasion of melanoma cell-lines (Figure 3.7). We next explored the importance of GEF-dead P-Rex1 *in vivo* by using the same melanocyte cell lines derived from early pup skin that were described in Section 3.4.3: 'P-Rex1$^{-/-}$', 'ectopic P-Rex1', or 'GD P-Rex1'. Cells were injected into immuno-compromised mice via subcutaneous injection (Figure 3.8a).

All injected mice developed melanoma at their site of injection with 100% consistency (Figure 3.8b). It became quickly apparent in tumour growth analysis that control 'P-Rex1$^{-/-}$' tumours were growing at a significantly different rate compared to 'ectopic P-Rex1' and 'GD P-Rex1' tumours: 'ectopic P-Rex1' tumours grew significantly more quickly than 'P-Rex1$^{-/-}$' tumours, while 'GD P-Rex1' tumours grew significantly more slowly than 'P-Rex1$^{-/-}$' tumours (Figure 3.8c). Prior to metastatic development, all mice were euthanised due to fatigue and large primary tumour burden. No difference in tumour burden was observed between melanomas of the three genotypes (Figure 3.8d). Survival analysis from time of injection till death were consistent with the differences seen in tumour growth: mice which developed 'ectopic P-Rex1' tumours required euthanisation most quickly, while mice which developed 'GD P-Rex1' tumours had the most prolonged lifespan (Figure 3.8e). These results therefore show an anti-tumour effect of GEF-dead P-Rex1, validating the DH domain of P-Rex1 as the primary molecular focus of its tumourigenic activity, and confirming that any potential small molecule inhibitor of P-Rex1 should specifically target this domain.

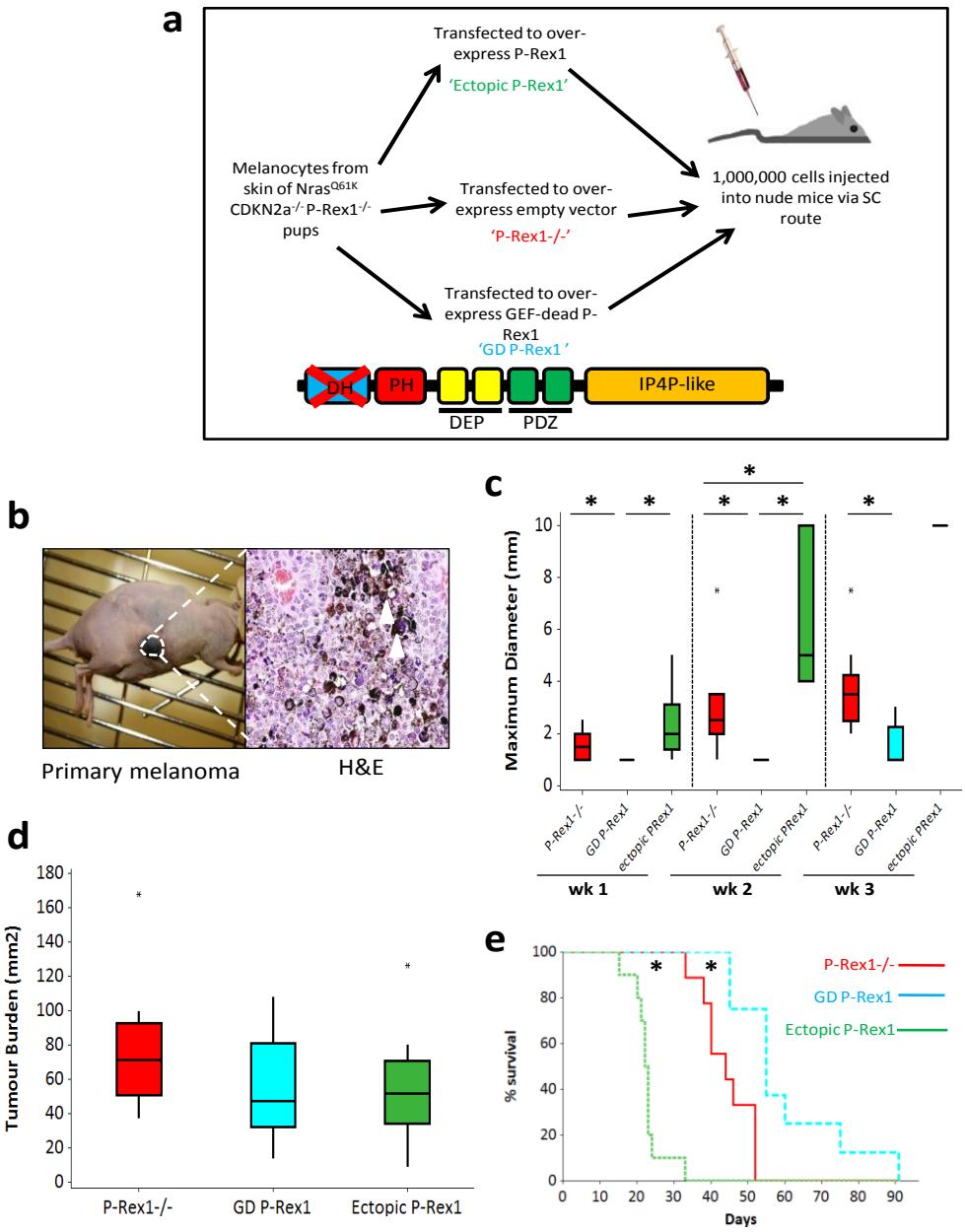

Figure 3.8 Ectopic GEF-dead P-Rex1 inhibits tumour growth and promotes mouse survival **(a)** Schematic diagram detailing cell type, cell numbers, injection type, and mice used in experiment (SC = subcutaneous). Also a reminder of domain structure of GEF-dead P-Rex1 mutant (detailed in figure 3.7a). **(b)** Example of primary melanoma arising following SC injection of nude mice. White interrupted line: pigmented primary skin melanoma. Accompanying photomicrograph (H&E) indicates pigmented melanocytosis characteristic of these lesions (white arrowheads) **(c)** Quantification and comparison of primary melanoma growth between 'P-Rex1$^{-/-}$' (red bars), 'GD P-Rex1' (blue bars), and 'ectopic P-Rex1' (green bars) treated mice (Week 1: n=9 (P-Rex1$^{-/-}$) vs n=5 (GD P-Rex1) vs n=6 (ectopic P-Rex1); Mann-Whitney; p = 0.289 (P-Rex1$^{-/-}$, ectopic P-Rex1); *p = 0.023 (GD P-Rex1, ectopic P-Rex1); *p = 0.033 (P-Rex1$^{-/-}$, GD P-Rex1)) (Week 2: n=9 (P-Rex1$^{-/-}$) vs n=5 (GD P-Rex1) vs n=3 (ectopic P-Rex1); Mann-Whitney; *p = 0.042 (P-Rex1$^{-/-}$, ectopic P-Rex1); *p = 0.037 (GD P-Rex1, ectopic P-Rex1); *p = 0.008 (P-Rex1$^{-/-}$, GD P-Rex1)) (Week 3: n=9 (P-Rex1$^{-/-}$) vs n=5 (GD P-Rex1) vs n=1 (ectopic P-Rex1); Mann-Whitney; *p = 0.011 (P-Rex1$^{-/-}$, GD P-Rex1); stats not possible for P-Rex1$^{-/-}$ vs ectopic P-Rex1 and GD P-Rex1 vs ectopic P-Rex1). **(d)** Comparison of primary melanoma tumour burden between mice treated with 'P-Rex1$^{-/-}$' (red bars, n=9), 'GD P-Rex1' (blue bars, n=6), and 'ectopic P-Rex1' cells (green bars, n=10) (P-Rex1$^{-/-}$,ectopic P-Rex1: p=0.191; P-Rex1$^{-/-}$,GD P-Rex1: p=0.377; GD P-Rex1 , ectopic P-Rex1: p=0.871; Mann-Whitney). **(e)** Kaplan-Meier curves detailing survival of nude mice SC-injected with the same cells: 'Ectopic P-Rex1', (n=10); P-Rex1$^{-/-}$ ('P-Rex1$^{-/-}$'; n=9); or GEF-dead P-Rex1 ('GD P-Rex1', n=8) (log-rank; P-Rex1$^{-/-}$ vs GD P-Rex1: p=*0.003; ectopic P-Rex1 vs GD P-Rex1: p=*0.0001; P-Rex1$^{-/-}$ vs ectopic P-Rex1: p=*0.0001).

3.6 Summary

In this chapter we have evaluated the role of the Rac-specific GEF, P-Rex1, for the first time in a genetically modified animal model of cancer. In particular we examined its role in melanoma progression, invasion and metastasis. Our results are more fully discussed with suggestions for further study in Sections 7.1.1 and 7.1.4. This summary offers a synopsis of our findings so far.

Progression. First we showed P-Rex1 has a role in progression through its upregulation in tumour compared to normal human melanocytes (Figures 3.4 and 3.5). IHC showed increased expression of P-Rex1 with the transformations from benign melanocyte to primary melanoma, and also primary melanoma to LN metastasis (Figures 3.5b,c). Despite our discovery of a role for P-Rex1 following the intravasation stage of metastasis, the increase in P-Rex1 levels observed in primary human melanoma would also suggest an early role for P-Rex1 in the metastatic phenotype; this hypothesis could perhaps be examined further with orthotopic murine injection of luciferase-labelled melanoma cell lines treated with P-Rex1 siRNA. Western blots and our microarray analysis supported these findings, with the highest P-Rex1 levels seen in cell lines with a metastatic propensity (Figures 3.4 and 3.5a).

Invasion. Matrigel invasion assays confirmed P-Rex1 is a key component of invasion in both humans and mice, channeled through its GEF activity (Figures 3.6 and 3.7). Endogenous and exogenous expression of P-Rex1 impacted on the invasive capacity of our cell lines. Ectopic expression of TIAM1 failed to phenocopy the invasion seen with P-Rex1 expression, suggesting P-Rex1 may be a unique mediator of invasion for melanoma cells.

Metastasis. Finally and most importantly, we have determined that genetic ablation of *PREX1* impairs melanoma metastases in *Tyr::Nras*^{Q61K} *INK4a*$^{-/-}$ mice (Figure 3.2). We extended this analysis using mouse allografts to show that endogenous P-Rex1 can facilitate metastatic frequency and organ spread following the intravasation stage of the metastatic cascade (Figure 3.3). An increase in metastatic growth, although it did not reach statistical significance, could suggest a potential proliferative role for P-Rex1 on top of its expected pro-invasive function, although further experiments such as immunohistochemistry staining for proliferative markers were not performed to confirm this possibility (Figure 3.3h).

Taken together, these results confirm that P-Rex1 upregulation is an important component of melanoma progression, invasion and metastatic signaling, supporting the value of pharmacological inhibition of P-Rex1 activation of Rac for treatment of metastatic or high risk primary melanomas. To finish the chapter, we confirmed that the DH domain of P-Rex1 is the most important molecular target for therapeutic intervention to curtail its tumourigenic signalling (Figure 3.8).

Chapter 4

The role of P-Rex1 in embryonic models of the melanocyte lineage

The imprint of past migratory behaviour of MBs has been suggested to confer a propensity of primary melanomas to establish distant metastases (Gupta et al, 2005, Uong et al, 2010, Strizzi et al, 2011). This chapter employs two embryonic models with which we investigate the effect of endogenous P-Rex1: *Dct-lacZ* and *Tyr::Cre Z/EG* mice. With these mice, we further delineate the mechanisms by which loss of P-Rex1 function might affect metastases and invasion in melanoma, and in turn, offer detail of how an anti P-Rex1 drug might work. There is little doubt from chapter 3 that invasion, as well as metastases, is important to the P-Rex1 effect in $Nras^{Q61K}$-driven melanoma, suggesting a putative inhibitor would have utility as an anti-invasive and anti-metastatic measure (Figures 3.6 and 3.7). Our main aims in this chapter were to validate this hypothesis, but also to investigate whether P-Rex1 may also have a proliferative or survival effect that could contribute to its metastatic role, a finding which would uncover potential cytotoxic or cytostatic effects for a putative P-Rex1 inhibitor.

We finish the chapter by combining Rac1-depleted mice with the same embryonic models to clarify whether the downstream effects of P-Rex1 are uniquely driven through Rac. We speculate that a P-Rex1 role outside of its pro-migratory/invasive function (eg survival or proliferation) might employ an alternative RhoGTPase to Rac. This in turn would suggest that Rac levels would not suffice as a downstream readout for the efficacy of a P-Rex1 inhibitor, whilst also suggesting that inhibition of Rac may not be an appropriate therapeutic alternative to targeting P-Rex1.

4.1 P-Rex1-deficient mice have a white belly phenotype

Prior to characterising the cancer phenotypes described in chapter 3, we had already identified an *in vivo* relevance for P-Rex1 by back-crossing the *P-Rex1*$^{-/-}$ mouse to mice of a pure C57BL6 background (Welch et al, 2005). We identified a 'white belly' phenotype with 100% penetrance in *P-Rex1*$^{-/-}$ mice when on a pure C57BL6 background (Figure 4.1a). Belly spots or spotting phenotypes in mice have been identified before with deregulation of other genes ('Color Genes', www.espcr.org/micemut). Given the importance of oncogenic Nras in human melanoma (see Section 1.1.4.1) and the known activation of P-Rex1 by the PI(3)K pathway downstream of Nras (see Section 1.5.1.1), we also crossed *P-Rex1*$^{-/-}$ mice to the *Tyr::Nras*$^{Q61K/°}$ mice (*Tyr::Nras*$^{Q61K/°}$*; P-Rex1*$^{-/-}$) described in chapter 3 (Ackermann et al, 2005). A white belly phenotype was also evident in these mice (Figure 4.1a), a finding which directly led to the money and time invested to assess the metastatic effects of P-Rex1 knockout in the *Tyr::Nras*$^{Q61K/°}$ cancer model (Chapter 3). Depigmentation affecting the feet was also observed in *Tyr::Nras*$^{Q61K/°}$*; P-Rex1*$^{-/-}$ mice (Figure 4.1a). Tissue sections of bellies from *P-Rex1*$^{-/-}$ and *Tyr::Nras*$^{Q61K/°}$*; P-Rex1*$^{-/-}$ mice suggested no melanocytes were present throughout the skin in the white belly area (Figure 4.1b). Thus expression of Nras^{Q61K} was not able to overcome the 'white belly' induced by ablation of *PREX1*.

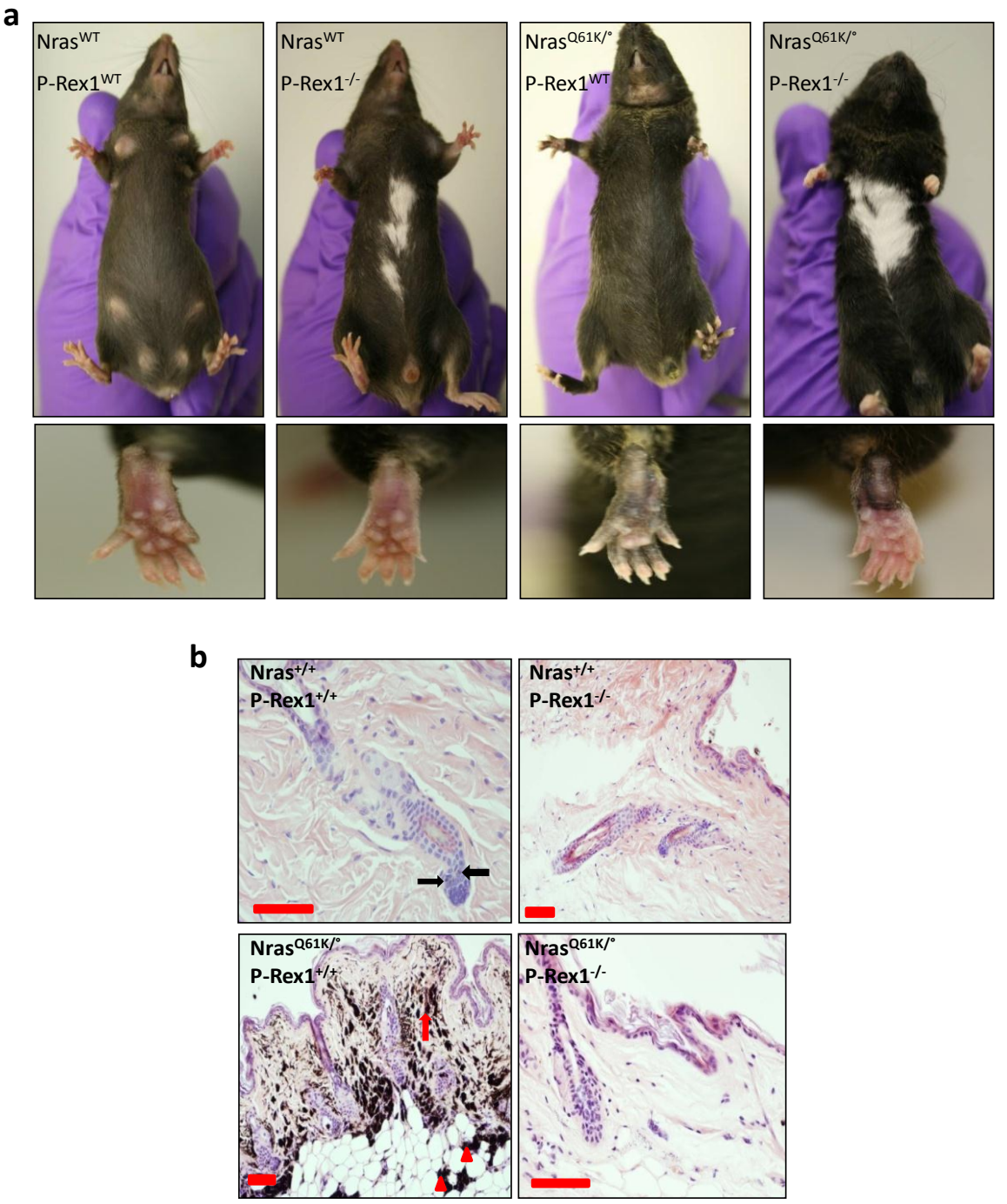

Figure 4.1 P-Rex1 deficient mice have a 'white belly' phenotype
(a) Belly and feet of *P-Rex1*$^{+/+}$ and *P-Rex1*$^{-/-}$ mice in combination with both *Nras*$^{+/+}$ and *Nras*$^{Q61K/°}$ transgenic modification. **(b)** Photomicrographs (H&E) of belly skin from the four genotypes represented in (a). Normal melanocyte situation in a C57BL6 mouse is in the bulge of the hair follicles (black arrows show melanin pigment deposition). Melanocytes and deposition of melanin in the dermis (red arrow) and adipose tissue (red arrowheads) are seen in *Nras*$^{Q61K/°}$ mice. No melanocytes or pigment deposition were observed in belly skin of *P-Rex1*$^{-/-}$ mice. Scale bars = 100µm.

4.2 P-Rex1 deficiency impairs normal melanoblast migration

The belly, feet, and tail are the furthermost points of mouse melanoblast migration from the neural crest during embryogenesis. In line with this and the pro-metastatic role of P-Rex1 described in chapter 3, we hypothesised that the areas of depigmentation in *P-Rex1*$^{-/-}$ mice predominantly represented a defect of melanoblast migration during embryogenesis, rather than an impaired proliferative capacity or indeed an inability to produce melanin pigment in adult melanocytes. Examining each of these possibilities would offer further insight into the tumourigenic mechanisms used by P-Rex1 in its pro-metastatic role. Before testing our hypothesis, we first ensured the presence of *PREX1* in melanoblasts (Figure 4.2a). The confirmed presence of P-Rex1 in motile melanoblasts compared to the lack of P-Rex1 expression previously described in non-motile adult melanocytes was consistent with its Rac-specific role and influence on the actin cytoskeleton in migratory cells such as melanoblasts or melanoma (Figure 3.5, Figure 4.2a). However, the mechanism by which P-Rex1 may be switched ‘off’ or ‘on’ at different stages of the melanocyte lineage is as yet unknown.

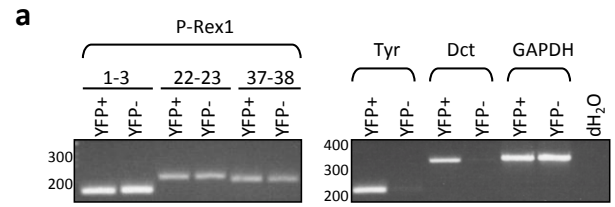

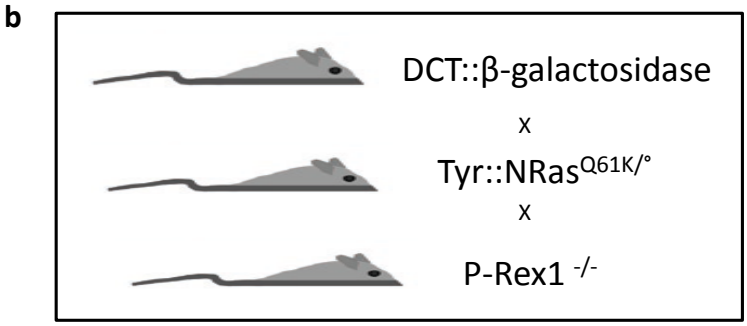

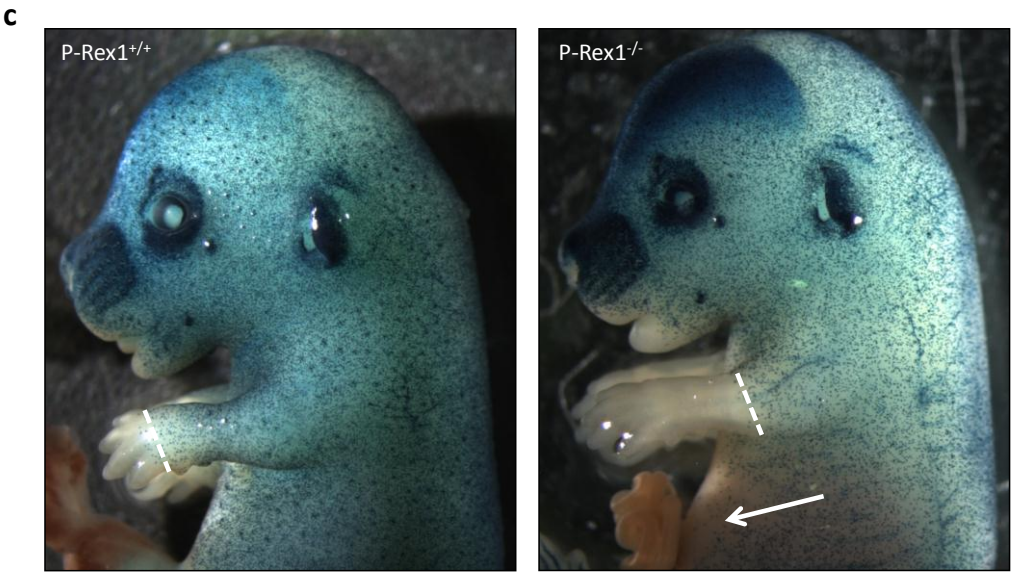

Figure 4.2 P-Rex1 is present in mouse melanoblasts
(a) RT-PCR of P-Rex1 mRNA in E14.5 embryo skin following FACS selection of cells enriched for melanoblasts (YFP+) compared to the rest of the embryo skin (YFP-). Mice expressing YFP were inter-crossed with mice expressing the melanocyte-specific Tyr::Cre, then skin cells isolated from their progeny and FACS-sorted. Tyrosinase and Dct controls confirm melanoblast enrichment of YFP+ cells. DCT = dopachrome tautomerase, a common marker of cells of the melanocyte lineage along with tyrosinase. **(b)** Schematic diagram detailing breedings of *DCT::β-galactosidase* melanoblast reporter mice to P-Rex1 and $Nras^{Q61K}$ mice. To label melanoblasts with β-galactosidase, $P\text{-}Rex1^{-/-}$ and $Nras^{Q61K}$ mice mice were inter-crossed with reporter *DCT::β-galactosidase* mice that express *β-galactosidase* in a melanocyte-specific fashion (see Section 2.7.4). Progeny were then analysed using techniques described in Section 2.1. **(c)** Representative photos of melanoblast distribution observed in *wild-type* and *P-Rex1*$^{-/-}$ embryos at E15.5. White arrow indicates melanoblast sparing of belly, white interrupted lines represent most distal point of melanoblast migration along forepaw. Figure (a) kindly contributed by Dr Richard Mort, MRC Human Genetics Unit, Edinburgh.

To address whether melanoblast number, pigmentation, or migratory behaviour was altered, we next analysed *P-Rex1*$^{-/-}$ mice and *Tyr::Nras*$^{Q61K/°}$*; P-Rex1*$^{-/-}$ mice which had been intercrossed to mice carrying the *DCT::β-galactosidase* transgene (hereon referred to as *DCT-lacZ*), a melanoblast reporter line (Figure 4.2b) (Mackenzie et al, 1997). Melanoblast sparing of the feet and belly was apparent in both *DCT-lacZ P-Rex1*$^{-/-}$ and *DCT-lacZ Tyr::Nras*$^{Q61K/°}$*; P-Rex1*$^{-/-}$ mice at E15.5, excluding a defect in melanin production as a cause for their depigmentation (Figure 4.2c, Figure 4.3).

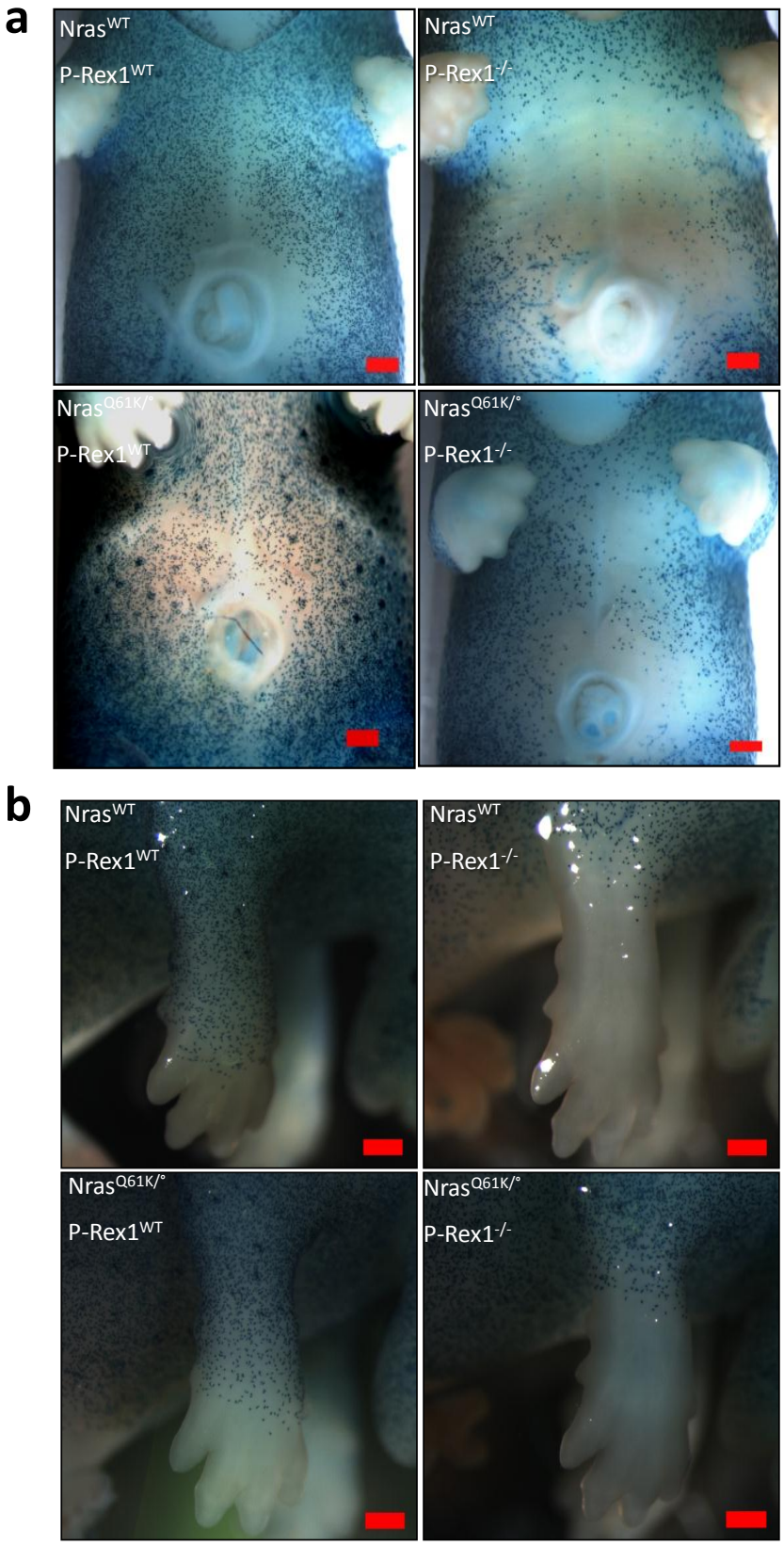

Figure 4.3 *P-Rex1*$^{-/-}$ mice have a defect in melanoblast migration
To label melanoblasts with β-galactosidase, P-Rex1$^{-/-}$ and Nras^{Q61K} mice mice were inter-crossed with reporter *DCT::β-galactosidase* mice that express *β-galactosidase* in a melanocyte-specific fashion (see Section 2.7.4). Progeny were then analysed using techniques described in Section 2.1. **(a)** E15.5 representative pictures comparing melanoblast migration to the belly in X-gal stained embryos. Scale bars = 500µm. **(b)** Comparison of melanoblast migration along forepaw in X-gal stained embryos at E15.5. A migratory deficit is evident in both *P-Rex1*$^{-/-}$ (with either *Nras*$^{+/+}$ or *Nras*$^{Q61K/°}$) embryos. Scale bars = 500µm.

Using the melanoblast migration assays detailed before (Figure 2.1a,b), analysis of E13.5 and E15.5 embryos showed a statistical difference in melanoblast migration between *DCT-lacZ P-Rex1*$^{-/-}$ and *DCT-lacZ P-Rex1*$^{+/+}$ mice (Figures 4.4a-f). This was not overcome by *Nras*$^{Q61K/°}$ expression (Figures 4.4c,f). These results were recapitulated using an alternative migration assay at E15.5 (detailed in figure 2.1c), applied to preclude any biasing effects of cell-cell contact inhibition should cell numbers be different between genotypes (Figures 4.4g,h). Consistent with a migratory defect, melanoblasts on the flank of the *DCT-lacZ P-Rex1*$^{-/-}$ mice had fewer protrusions than *DCT-lacZ P-Rex1*$^{+/+}$ controls (Figures 4.5a,b). More recently, we were able to confirm a migratory deficit in E15.5 skin using live *ex vivo* timelapse (technique detailed in Figure 2.3), which revealed a statistical reduction in both speed and Euclidean distance travelled by GFP-expressing melanoblasts with ablated *PREX1* (Figures 4.5c,d).

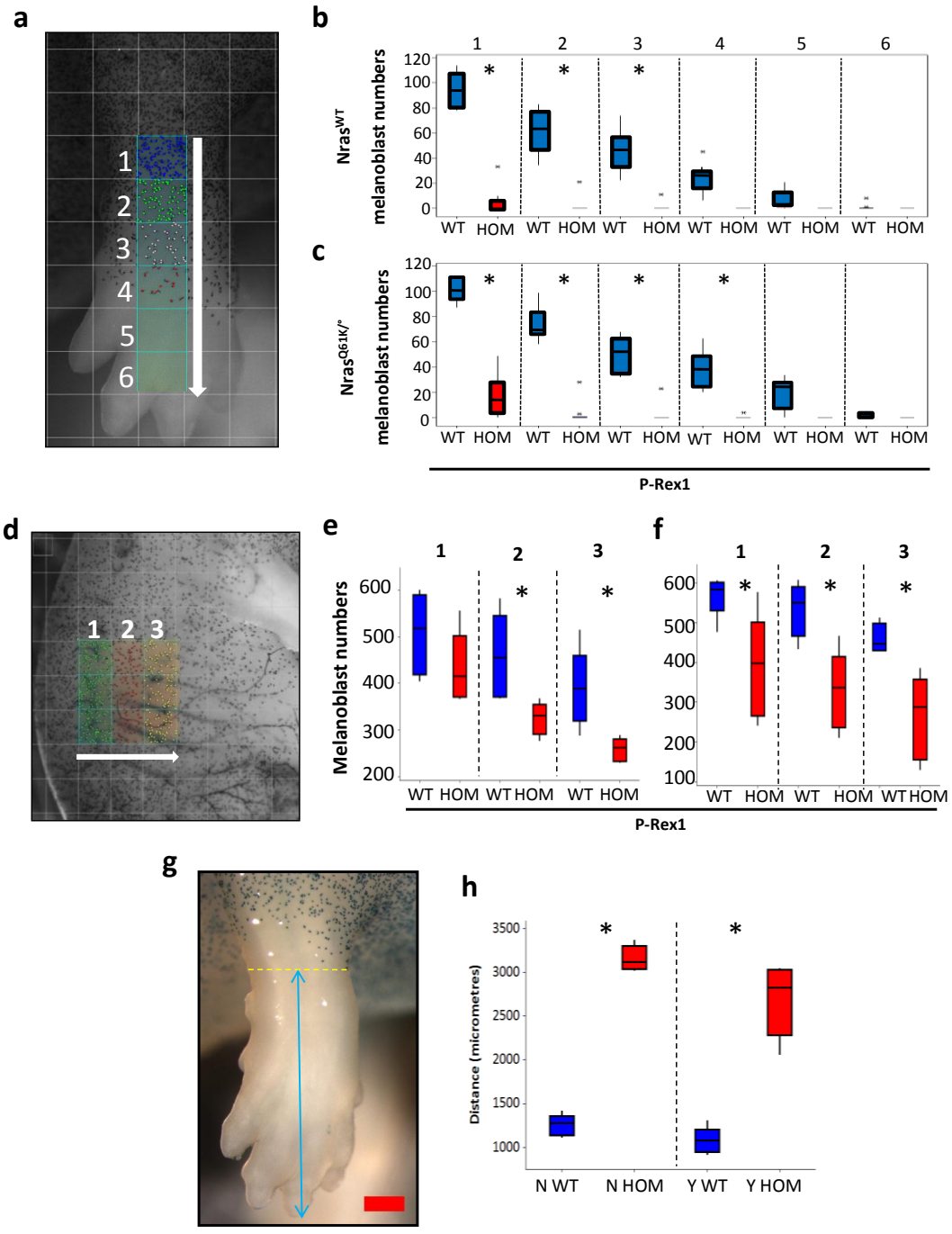

Figure 4.4 *P-Rex1*$^{-/-}$ mice have a defect in melanoblast migration at E13.5 and E15.5
(a) Schematic picture showing method of quantification of melanoblast migration used for (b) and (c) **(b,c)** Comparison of melanoblast migration between *P-Rex1*$^{+/+}$ ('WT', blue bars) and *P-Rex1*$^{-/-}$ ('HOM', red bars) mice. Upper panel (b) represents *Nras*$^{+/+}$ embryos (*p=0.01/0.02, Levels 2/3; Mann-Whitney test, n=5), lower panel (c) represents *Nras*$^{Q61K/°}$ embryos (*p=0.02/0.02/0.01, Levels 1/2/3; Mann-Whitney test, n=5) (All box and whiskers plots: boxes represent 25th-75th percentiles of given value, lines represent median values). **(d)** Schematic picture showing method of quantification of melanoblast cell migration used for (e) and (f) **(e,f)** Comparison of melanoblast migration between *P-Rex1*$^{+/+}$ ('WT', blue bars) and *P-Rex1*$^{-/-}$ ('HOM', red bars) mice along torso in X-gal stained embryos at E13.5. Left panel (e) represents *Nras*$^{+/+}$ embryos (*p=0.016/0.021 at levels 2/3, Mann-Whitney test; n=5), right panel (f) represents *Nras*$^{Q61K/°}$ embryos (*p=0.021/0.021/0.012 at levels 1/2/3, Mann-Whitney test; n=5) **(g)** Schematic picture detailing alternative method for quantification of melanoblast migration used in (h) **(h)** Quantification and comparison of migration as described in (g): *P-Rex1*$^{+/+}$ ('N WT', blue bars) and *P-Rex1*$^{-/-}$ mice ('N HOM', red bars) (left hand panel; *p=0.012, Mann-Whitney; n=5); *Tyr::Nras*$^{Q61K/°}$*; P-Rex1*$^{+/+}$ ('Y WT', blue bars) and *Tyr::Nras*$^{Q61K/°}$*; P-Rex1*$^{-/-}$ ('Y HOM', red bars) mice (right hand panel; *p=0.012; Mann-Whitney, n=5). All migration assay detail found in chapter 2.

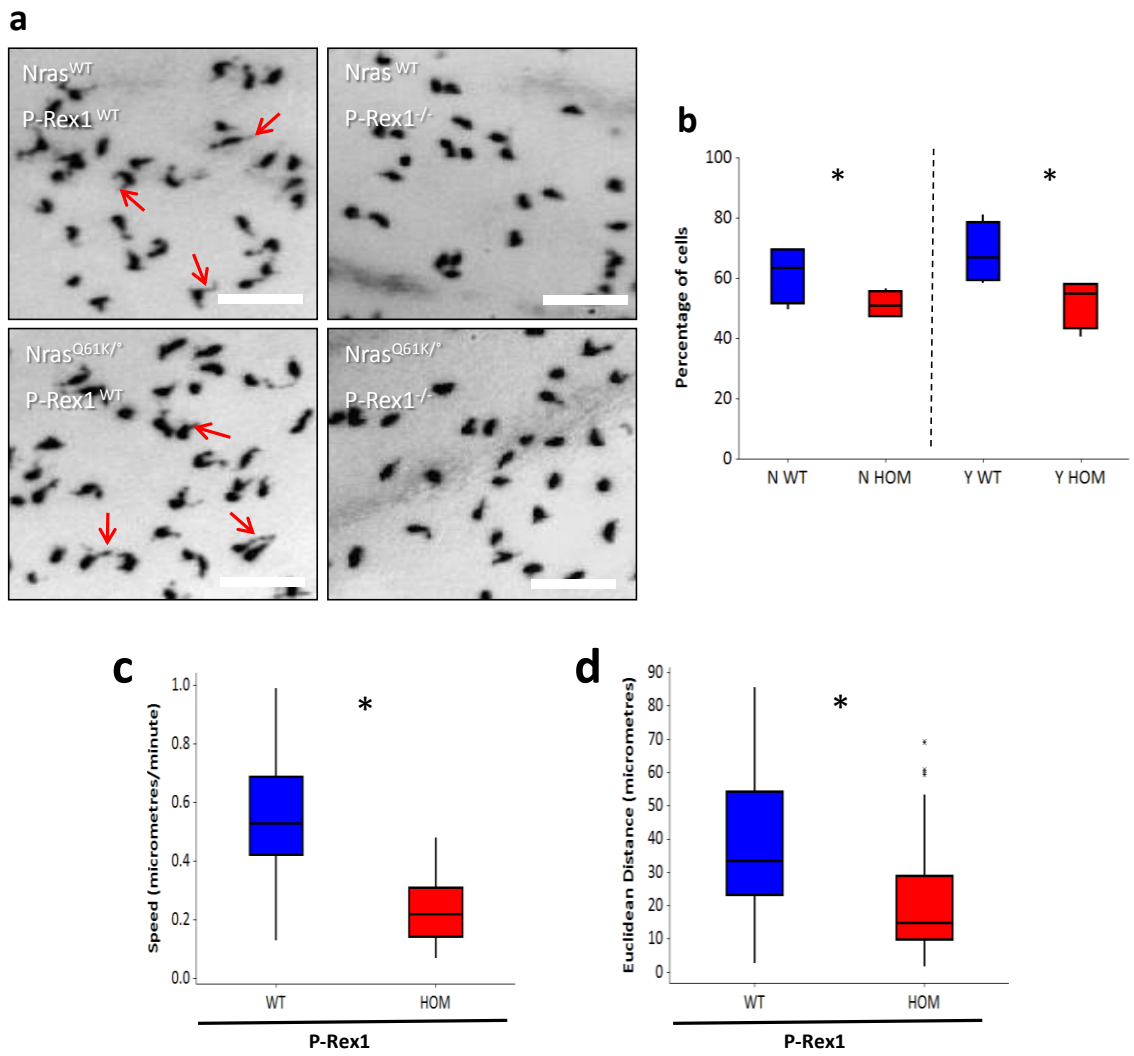

Figure 4.5 *P-Rex1*$^{-/-}$ mice have reduced protrusions at E15.5
(a) Representative pictures at E15.5 of melanoblast morphology and protrusions (red arrows) on the flank of X-gal stained embryos. Scale bars = 100µm. **(b)** Quantification and comparison of percentage of cells with 1+ protrusions: *P-Rex1*$^{+/+}$ ('N WT', blue bars) and *P-Rex1*$^{-/-}$ mice ('N HOM', red bars) (left hand panel; *p=0.05, Mann-Whitney; n=4); *Tyr::Nras*$^{Q61K/°}$*; P-Rex1*$^{+/+}$ ('Y WT', blue bars) and *Tyr::Nras*$^{Q61K/°}$*; P-Rex1*$^{-/-}$ ('Y HOM', red bars) mice (right hand panel; *p=0.03; Mann-Whitney, n=4). **(c)** Quantification and comparison of individual melanoblast speed at E15.5 under live confocal timelapse: *P-Rex1*$^{+/+}$ ('WT', blue bars) and *P-Rex1*$^{-/-}$ ('HOM', red bars) compared (*p=0.00001; Mann-Whitney, n=60). **(d)** Quantification and comparison of Euclidean distance travelled by individual melanoblasts at E15.5 under live confocal timelapse: *P-Rex1*$^{+/+}$ ('WT', blue bars) and *P-Rex1*$^{-/-}$ ('HOM', red bars) compared (*p=0.00001; Mann-Whitney, n=60).

4.3 P-Rex1 deficiency causes a reduction in melanoblast proliferation

Recent reports have implied a role for P-Rex1 in proliferation as well as migration (Qin et al, 2009, Montero et al, 2010). A clue to the effect of P-Rex1 on proliferation was also offered by its possible effect on metastatic tumour burden in chapter 3 (Figure 3.3h). We therefore investigated this possibility more closely using our two melanoblast model systems as potential surrogates for the metastatic effect seen in chapter 3. A proliferative role for P-Rex1 could have important implications for its potential as a novel anticancer target.

A melanoblast cell number assay at E13.5 (detailed in Figure 2.2b) showed no difference in cell numbers between *DCT-lacZ P-Rex1*$^{-/-}$ mice and *DCT-lacZ P-Rex1*$^{+/+}$ mice unless *DCT-lacZ P-Rex1*$^{-/-}$ was inter-crossed with *Tyr::Nras*$^{Q61K/°}$ (Figures 4.6a,b). There was however a small but significant reduction of E15.5 cell numbers (assay detailed in Figure 2.2a) in *DCT-lacZ P-Rex1*$^{-/-}$ mice compared to *DCT-lacZ P-Rex1*$^{+/+}$, and *DCT-lacZ Tyr::Nras*$^{Q61K/°}$*; P-Rex1*$^{-/-}$ mice compared to *DCT-lacZ Tyr::Nras*$^{Q61K/°}$*; P-Rex1*$^{+/+}$ mice (Figures 4.6c,d). This difference is likely to represent a proliferative deficit in *P-Rex1*$^{-/-}$ melanoblasts: cell death was not observed in E15.5 whole skin from *P-Rex1*$^{+/+}$ or *P-Rex1*$^{-/-}$ mouse embryos using live *ex vivo* imaging described in Section 2.2 (Figure 4.7a). Moreover, it is well characterised that cells of the melanocyte lineage are noteworthy by their resistance to apoptosis, owing to a lifetime of UV damage occurring in the skin (Terzian et al, 2010). A significant reduction in E15.5 cell numbers was again seen in *P-Rex1*$^{-/-}$ embryos compared to *P-Rex1*$^{+/+}$ controls using this technique (Figure 4.7b). Collectively, these results would be consistent with previous reports of a role for Rac in cell cycle control, as well as the proliferative defect observed when P-Rex1 was knocked down in breast cancer cell lines (Moore et al, 1997, Michaelson et al, 2008, Qin et al, 2009, Montero et al, 2011). They

suggest that a small proliferative defect is accompanied by a marked migration defect in *P-Rex1*$^{-/-}$ mice.

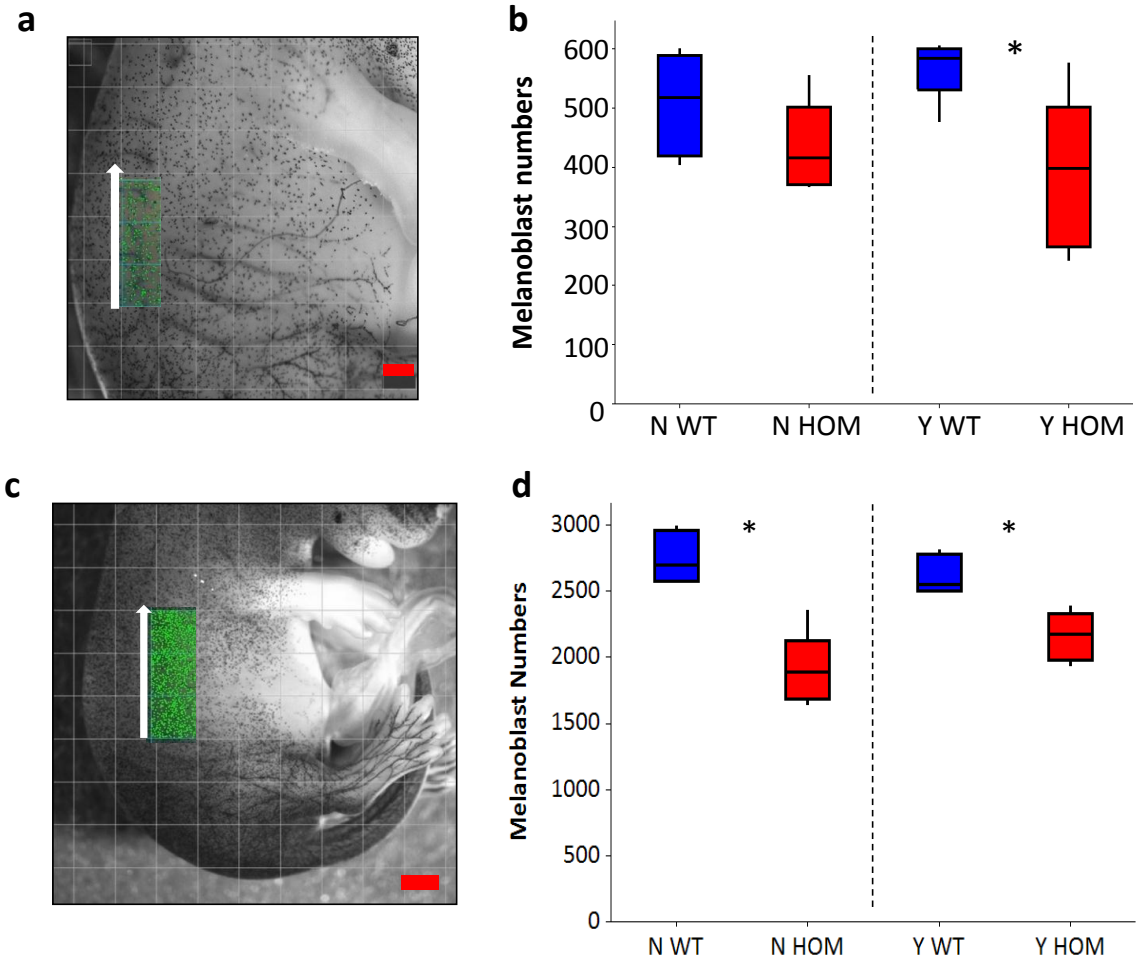

Figure 4.6 *P-Rex1*$^{-/-}$ mice have a reduction in melanoblast cell numbers using *DCT-lacZ* reporter mice
(a) Schematic pictures detailing method for quantification of melanoblast numbers used in (b) **(b)** Comparison of E13.5 melanoblast numbers between *P-Rex1*$^{+/+}$ (N WT, blue bars) and *P-Rex1*$^{-/-}$ (N HOM, red bars) mice (left hand panel), and also between *Tyr::Nras*$^{Q61K/°}$*; P-Rex1*$^{+/+}$ (Y WT, blue bars) and *Tyr::Nras*$^{Q61K/°}$*; P-Rex1*$^{-/-}$ (Y HOM, red bars) mice (right hand panel) (*p =0.02, Mann-Whitney test; n=5) **(c)** Schematic picture detailing method for quantification of melanoblast cell numbers used in (d) **(d)** Comparison of E15.5 melanoblast numbers between *P-Rex1*$^{+/+}$ ('N WT', blue bars) and *P-Rex1*$^{-/-}$ ('N HOM', red bars) mice (left hand panel), and also between *Tyr::Nras*$^{Q61K/°}$*; P-Rex1*$^{+/+}$ ('Y WT', blue bars) and *Tyr::Nras*$^{Q61K/°}$*; P-Rex1*$^{-/-}$ ('Y HOM', red bars) mice (right hand panel). (left panel: *p =0.01; right panel: *p =0.01; Mann-Whitney test, n=5). (Box and whiskers plots: boxes represent 25th-75th percentiles of given value, lines represent median values). All cell number assay details found in chapter 2.

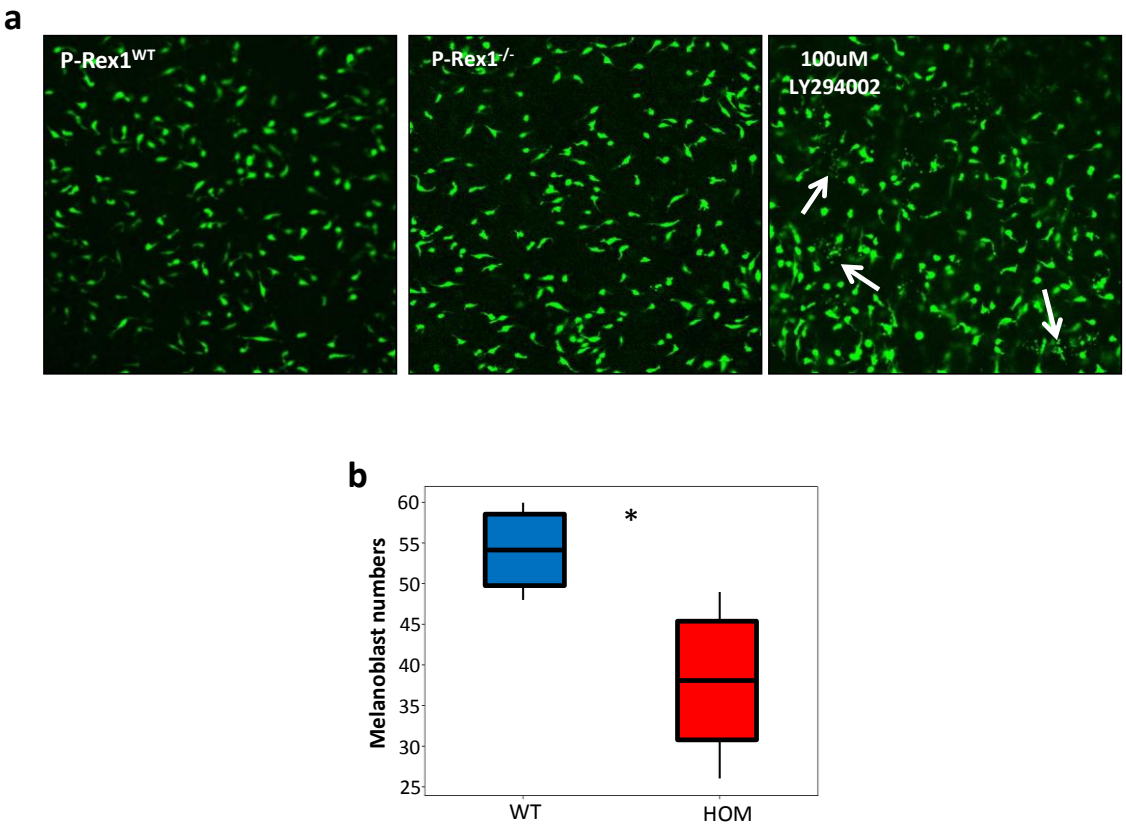

Figure 4.7 *P-Rex1*$^{-/-}$ embryos have a reduction in melanoblast proliferation using live *ex vivo* timelapse
To label melanoblasts with GFP, *P-Rex1*$^{-/-}$ mice were inter-crossed with reporter *Tyr::Cre Z\EG* mice which express GFP in a melanocyte-specific fashion (see Section 2.7.4). Progeny were then analysed using technique described in Section 2.2. **(a)** E15.5 representative pictures comparing *ex vivo* numbers of melanoblasts expressing green fluorescent protein in the skin. Last panel, used as a positive control, shows apoptotic blebbing (white arrows) induced following treatment with 100µM LY294002, an inhibitor of the pro-survival PI(3)K pathway. This is not observed in *P-Rex1*$^{-/-}$ skin despite reduction in cell numbers. **(b)** *Ex vivo* quantification and comparison of numbers of melanoblasts expressing green fluorescent protein in the skin: *P-Rex1*$^{+/+}$ ('WT', blue bars) and *P-Rex1*$^{-/-}$ ('HOM', red bars) compared (*p=0.0216; Mann-Whitney, n=5).

4.4 Are the downstream effects of P-Rex1 uniquely driven through Rac?

Another important question with P-Rex1 signalling was to establish whether its downstream effects were mediated specifically by Rac alone. As mice with melanocyte-specific *RAC1* abrogation require early adult euthanisation due to neurological problems (Li et al, 2011), our embryonic reporter models offered the most appropriate way to assess this question *in vivo*.

4.4.1 P-Rex1 and Rac are fundamental components of mouse coat colour phenotype

Earlier in the chapter we described the 'white belly' phenotype of mice with P-Rex1 deletion (Figure 4.8a). Considering the Rho-GTPase signalling mechanisms that might be responsible for melanoblast migration to the perimeter of the P-Rex1-null white belly, it seemed likely that other Rac-GEFs might activate Rac and potentially other Rho-GTPases too (Figure 4.8a). Constitutive deletion of *RAC1* is embryonically lethal, but a coat colour defect of mice with melanocyte-specific *RAC1* abrogation (*Tyr::Cre Rac$^{fl/fl}$*) has recently been described: these mice have an even larger belly spot on their ventral side, suggesting that other GEFs (and potentially P-Rex1) can stimulate alternative Rho-GTPases to enable melanoblast migration to the perimeter of the *Tyr::Cre Rac$^{fl/fl}$* white belly (Figure 4.8b) (Li et al, 2011, Sugihara et al, 1998).

To confirm whether P-Rex1 was Rac-specific, we hypothesised that the offspring of a mating between *P-Rex1$^{-/-}$* mice and *Tyr::Cre Rac$^{fl/fl}$* mice (*Tyr::Cre Rac$^{fl/fl}$; P-Rex1$^{-/-}$*) would exhibit the same coat colour phenotype as *Tyr::Cre Rac$^{fl/fl}$* mice alone. However, we discovered that P-Rex1 has a major additional function to that which it confers through Rac: *Tyr::Cre Rac$^{fl/fl}$; P-Rex1$^{-/-}$* mice display a dramatic alteration in coat colour phenotype from *Tyr::Cre Rac$^{fl/fl}$* mice (Figure 4.8c) (n=7). In detail, the ventral and dorsal coats of

these mice are almost entirely white, with hypopigmented limbs and tail also. Greying pigmented areas were only observed in the head coat, as if melanoblasts could not escape beyond this point in the early stages of development. We conclude from this experiment that P-Rex1 and Rac *together* constitute fundamental signalling components of the mouse coat colour phenotype, with minimal rescue of melanoblast development conferred by other GEFs or Rho-GTPases (Figure 4.8c). It is also clear that P-Rex1 must be able to exert phenotypic effects through Rho-GTPases other than Rac.

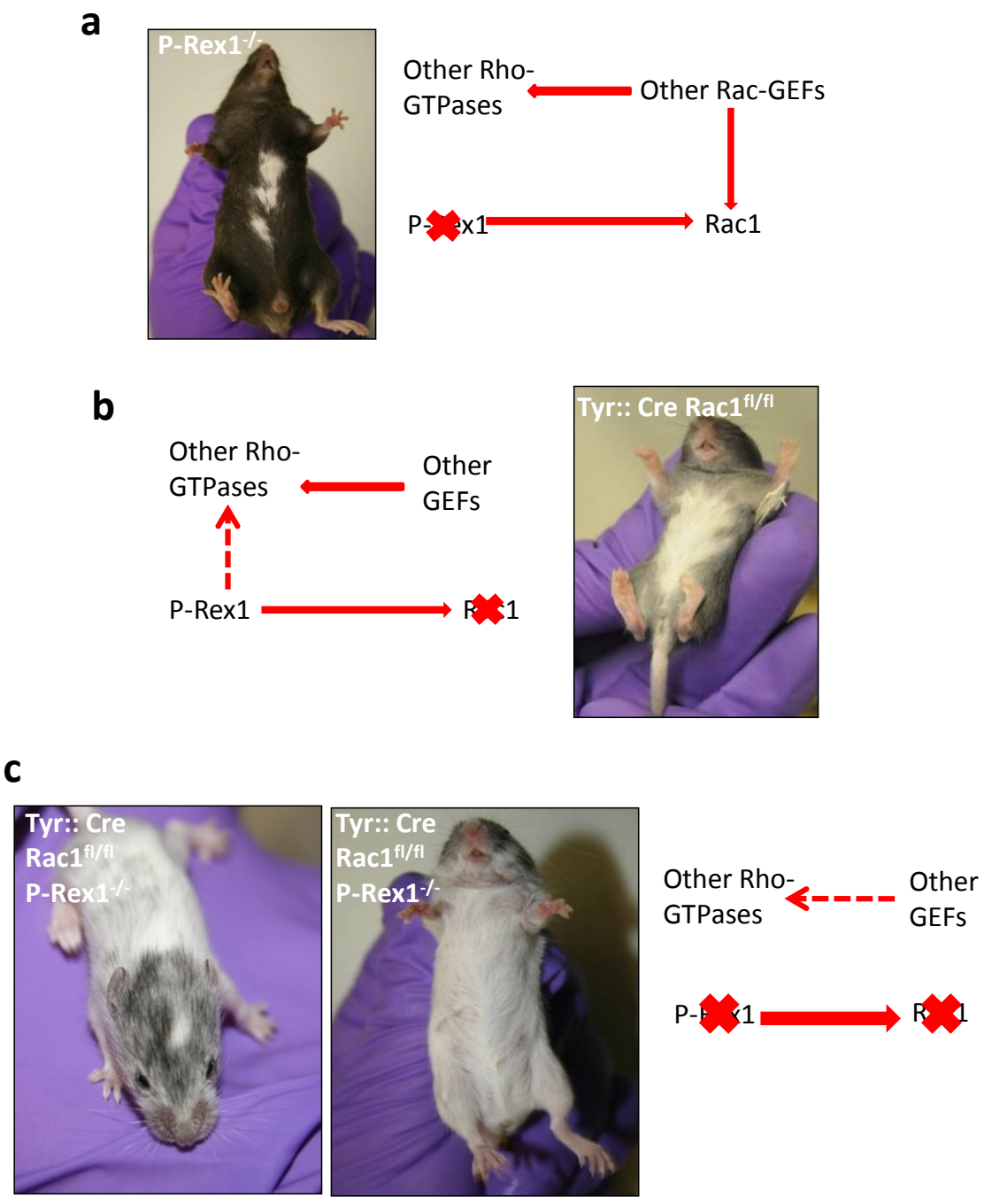

Figure 4.8 P-Rex1 and Rac are fundamental components of mouse coat colour phenotype **(a)** Schema detailing potential signalling mechanisms which could influence migration of melanoblasts to the level of the 'white belly' in the absence of P-Rex1. **(b)** Schema detailing potential P-Rex1 and Rho-GTPase signalling mechanisms which could influence migration of melanoblasts to the level of the 'white belly' in the absence of Rac1. **(c)** Representative pictures showing coat colour phenotype of *Tyr::Cre Rac1$^{fl/fl}$; P-Rex1$^{-/-}$* mice. Schema shows potential 'escape' signalling mechanisms by which melanoblasts may migrate and contribute to the minimal pigmentation observed in these mice. Picture in (b) kindly contributed by Dr Ang Li and Professor Laura Machesky, Beatson Institute.

4.4.2 P-Rex1 promotes cell numbers using a Rac1-independent mechanism

To explore the Rac-independent effects of P-Rex1 further, we crossed *Tyr::Cre Rac*$^{fl/fl}$*; P-Rex1*$^{-/-}$ mice to mice carrying the reporter *DCT-lacZ* transgene. Relative to *Tyr::Cre Rac*$^{fl/fl}$mice or *P-Rex1*$^{-/-}$ embryos alone, *Tyr::Cre Rac*$^{fl/fl}$*; P-Rex1*$^{-/-}$ embryos at E15.5 displayed a substantial reduction in melanoblast numbers across their entire body (Figures 4.9a,b). Closer microscopic examination of cell morphology revealed amoeboid cell-rounding, consistent with what has been described in *Tyr::Cre Rac*$^{fl/fl}$mice or *P-Rex1*$^{-/-}$ melanoblasts alone (Fig. 4.9c). Unfortunately, quantification and comparison of melanoblasts with this technique was impossible as the Machesky laboratory, who kindly gifted the *Tyr::Cre Rac*$^{fl/fl}$ photomicrographs, had destroyed their embryos. In any case, application of the previously described *DCT-lacZ* assays to differentiate between cell numbers and migration would not have been accurate with so few melanoblasts present in *Tyr::Cre Rac*$^{fl/fl}$*; P-Rex1*$^{-/-}$ mice. It was therefore necessary to use live imaging to delineate whether the coat colour phenotype of *Tyr::Cre Rac*$^{fl/fl}$*; P-Rex1*$^{-/-}$ mice occurs as a result of migratory failure, proliferative failure, or even cell death.

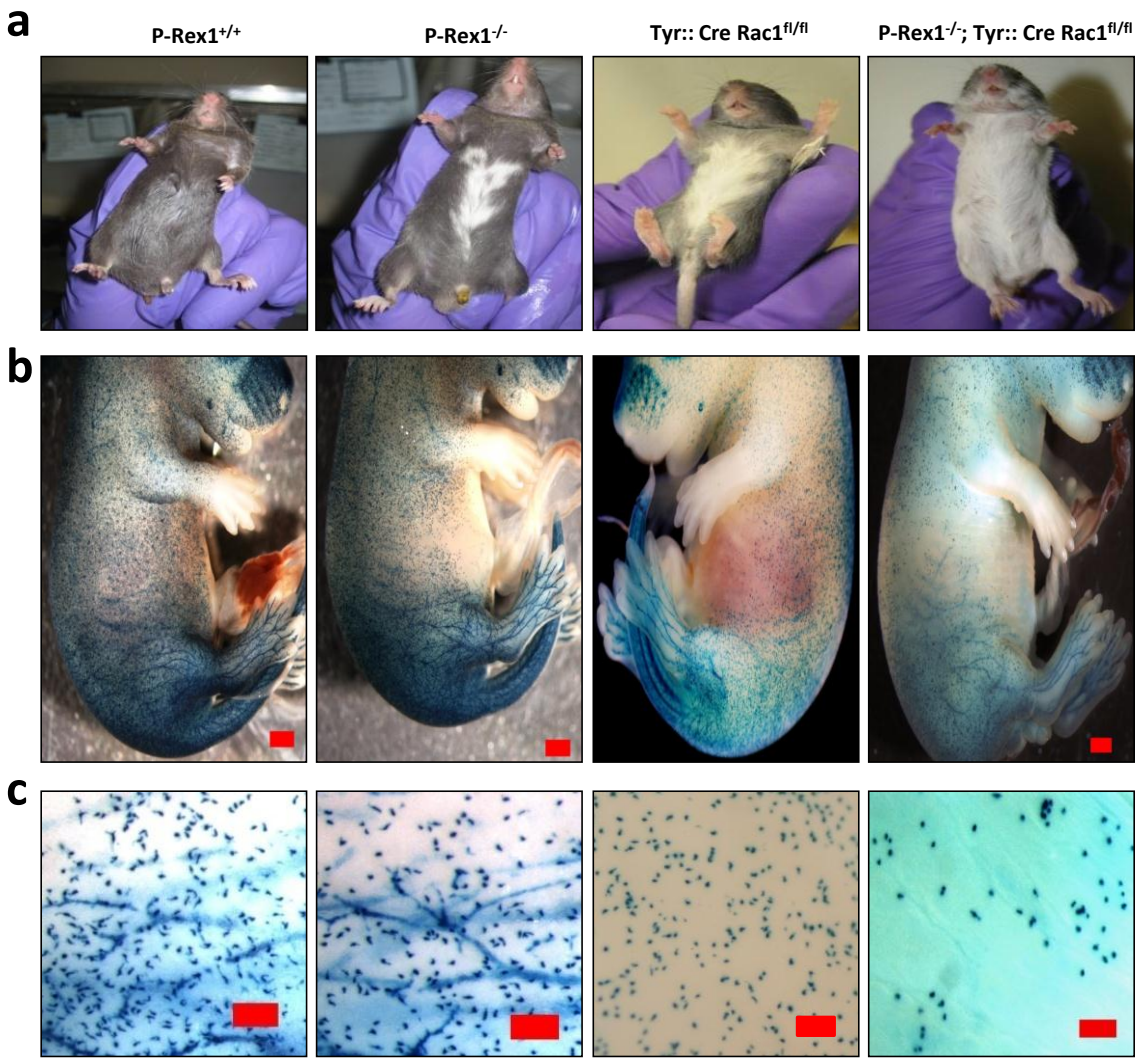

Figure 4.9 P-Rex1 and Rac1 are fundamental components of mouse coat colour phenotype
(a) Bellies of *Tyr::Cre Rac1*$^{fl/fl}$ and *P-Rex1*$^{-/-}$ mice in isolation and combination. **(b)** Representative photos of *DCT-lacZ* melanoblast distribution observed in *wild-type*, *P-Rex1*$^{-/-}$, *Tyr::Cre Rac1*$^{fl/fl}$ and *Tyr::Cre Rac1*$^{fl/fl}$*; P-Rex1*$^{-/-}$ embryos at E15.5 (scale bars=1mm; n=3). Melanoblast sparing is evident in *Tyr::Cre Rac1*$^{fl/fl}$*; P-Rex1*$^{-/-}$ embryos in particular. **(c)** Representative pictures at E15.5 of *wild-type*, *P-Rex1*$^{-/-}$, *Tyr::Cre Rac1*$^{fl/fl}$ and *Tyr::Cre Rac1*$^{fl/fl}$*; P-Rex1*$^{-/-}$ melanoblast sparing on the flank of X-gal stained embryos. (Scale bars = 200µm; n=3). *Tyr::Cre Rac1*$^{fl/fl}$ pictures kindly contributed by Dr Ang Li and Professor Laura Machesky, Beatson Institute.

Mice with the *Z/EG* double reporter transgene were crossed to *Tyr::Cre Rac$^{fl/fl}$; P-Rex1$^{-/-}$* mice, driving GFP expression in the melanoblast lineage. First observations again suggested a marked reduction in melanoblast numbers in the flank skin of *Tyr::Cre Rac$^{fl/fl}$; P-Rex1$^{-/-}$* E15.5 embryos compared to *Tyr::Cre Rac$^{fl/fl}$* or *P-Rex1$^{-/-}$* embryos alone (Figure 4.10a). Cell quantification suggested a small but significant reduction in *Tyr::Cre Rac$^{fl/fl}$; P-Rex1$^{-/-}$* melanoblast speed of migration compared to *Tyr::Cre Rac$^{fl/fl}$* or *P-Rex1$^{-/-}$* embryos alone (Figure 4.10b). However, this speed reduction was not matched by any difference in Euclidean distance travelled by melanoblasts of the same three genotypes (Figure 4.10c). As expected, *wild-type* melanoblasts had a significant increase in speed, numbers and Euclidean distance travelled relative to all other genotypes (Figures 4.10b-d). Finally, there was a dramatic reduction in melanoblast numbers between *Tyr::Cre Rac$^{fl/fl}$; P-Rex1$^{-/-}$* embryos and all other genotypes, with no difference in numbers observed between *Tyr::Cre Rac$^{fl/fl}$* and *P-Rex1$^{-/-}$* embryos (Figure 4.10d). As no cell death was seen in all timelapse movies of any genotype, our suspicion is that P-Rex1 contributes to coat colour phenotype by promoting cell proliferation using a Rac1-independent mechanism. However, we cannot completely exclude the possibility that P-Rex1 might contribute to this phenotype by promoting melanoblast survival (discussed further in section 7.3.4).

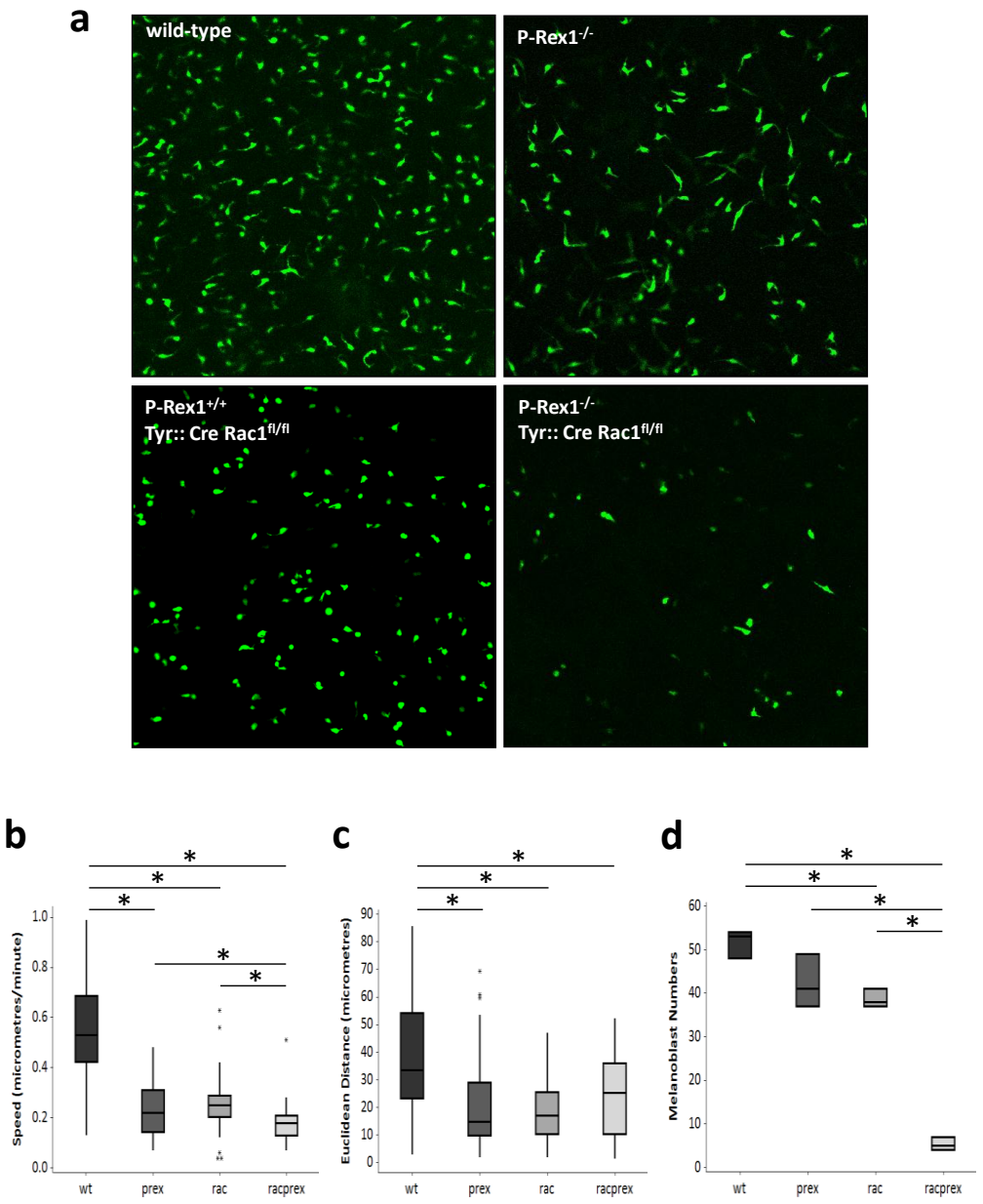

Figure 4.10 P-Rex1 promotes an increase in cell number using a Rac1-independent mechanism

(a) Representative pictures comparing *ex vivo* numbers of melanoblasts expressing green fluorescent protein in the skin of *wild-type*, *P-Rex1*$^{-/-}$, *Tyr::Cre Rac1*$^{fl/fl}$ and *Tyr::Cre Rac1*$^{fl/fl}$*; P-Rex1*$^{-/-}$ embryos at E15.5 (n=3). **(b)** Quantification and comparison of individual melanoblast speed at E15.5 under live confocal timelapse: *wild-type* ('wt', n=60 cells), *P-Rex1*$^{-/-}$('prex', n=56 cells), *Tyr::Cre Rac1*$^{fl/fl}$('rac', n=60 cells) and *Tyr::Cre Rac1*$^{fl/fl}$*; P-Rex1*$^{-/-}$('racprex', n=45 cells)$^{-}$ cells compared ('wt' vs 'prex': *p=0.00001; 'wt' vs 'rac': *p=0.00001; 'wt' vs 'racprex': *p=0.00001; 'prex' vs 'rac': p=0.1417; 'prex' vs 'racprex': *p=0.0097; 'rac' vs 'racprex': *p=0.00001; Mann-Whitney; 3 timelapses per genotype). **(c)** Quantification and comparison of euclidean distance travelled by individual melanoblasts at E15.5 under live confocal timelapse: *wild-type* ('wt', n=60 cells), *P-Rex1*$^{-/-}$('prex', n=56 cells), *Tyr::Cre Rac1*$^{fl/fl}$('rac', n=60 cells) and *Tyr::Cre Rac1*$^{fl/fl}$*; P-Rex1*$^{-/-}$('racprex', n=45 cells)$^{-}$ cells compared ('wt' vs 'prex': *p=0.00001; 'wt' vs 'rac': *p=0.00001; 'wt' vs 'racprex': *p=0.00001; 'prex' vs 'rac': p=0.8165; 'prex' vs 'racprex': p=0.1099; 'rac' vs 'racprex': p=0.064; Mann-Whitney; 3 timelapses per genotype). **(d)** *Ex vivo* quantification and comparison of numbers of melanoblasts expressing green fluorescent protein in the skin: *wild-type* ('wt', n=60 cells), *P-Rex1*$^{-/-}$('prex', n=56 cells), *Tyr::Cre Rac1*$^{fl/fl}$('rac', n=60 cells) and *Tyr::Cre Rac1*$^{fl/fl}$*; P-Rex1*$^{-/-}$ ('racprex', n=45 cells)$^{-}$ cells compared ('wt' vs 'prex': p=0.1; 'wt' vs 'rac': *p=0.01; 'wt' vs 'racprex': *p=0.002; 'prex' vs 'rac': p=0.429; 'prex' vs 'racprex': p=*0.01; 'rac' vs 'racprex': p=*0.0002; Mann-Whitney; 3 timelapses per genotype). *Tyr::Cre Rac1*$^{fl/fl}$ pictures and movies kindly contributed by Dr Ang Li and Professor Laura Machesky, Beatson Institute.

4.5 Summary

Mechanistic experiments in this chapter have highlighted the key similarities between the molecular machinery involved in the movement of melanoblasts and that of metastatic melanoma cells. Our results here are more fully discussed with suggestions for further study in Sections 7.1.1, 7.1.3, 7.1.4, and 7.3.4. This summary offers a synopsis of our findings in this chapter.

We have shown in this chapter that genetic ablation of *PREX1* impaired migration of melanoblasts, evidenced by a 'white belly' phenotype that reflected the diminished metastases seen in *Tyr::Nras*^{Q61K} *INK4a*$^{-/-}$ mice (Figures 3.2, 3.3, 4.1, and 4.4). A potential pathophysiological link with the incidence of metastases therefore fits with the physiological role of P-Rex1 seen in melanoblast migration. The predominant role of P-Rex1 in invasion and migration is also suggested by its presence in motile melanoblasts and its upregulation in the metastatic melanoma cell lines observed in chapter 3 (Figures 3.4, 3.5, and 4.2). Consistent with this, an association between P-Rex1 and number of melanoblast protrusions was observed (Figure 4.5). Outside of it migratory/invasive role, a small proliferative deficit was also observed in *P-Rex1*$^{-/-}$ embryos, a finding which was consistent with the trend towards diminished metastatic tumour burden noted in chapter 3 (Figures 3.3h, 4.6 and 4.7). Taken together, these results therefore confirm an anti-metastatic role for a putative P-Rex1 inhibitor, but also raise the possibility that therapeutic intervention may confer anti-proliferative cytostatic effects.

A proliferative effect for P-Rex1 was again suggested when, using the same embryonic models, it was shown to promote cell numbers in the absence of Rac1 (Figures 4.8, 4.9, and 4.10). There has previously been another suggestion that P-Rex1 can exert proliferative effects using a Rac-independent mechanism in cancer (Montero et al, 2010).

This finding potentially carries at least two important caveats for development of a putative P-Rex1 inhibitor. First, as a downstream readout is crucial to understanding the pharmacodynamics of a lead compound in drug development, it is important to be aware that a reduction in Rac activity does not fully represent a biological 'hit' of P-Rex1: it must also signal through an as yet unidentified Rho-GTPase(s). Second, a Rac-independent mechanism for P-Rex1 could confer proliferative effects on cancer beyond its pro-metastatic migratory potential driven through Rac: this has implications for cytostatic or cytotoxic effects of P-Rex1 inhibition, on top of an expected anti-metastatic role. Such an inhibitor would be much more straightforward to justify in the context of drug development (see Section 1.2.2 for more detail).

Chapter 5

Exploring the role of P-Rex1 in Braf^{V600E}-driven melanoma

We have shown in chapters 3 and 4 that P-Rex1 can influence metastases, migration, invasion and proliferation in the context of oncogenic Nras. However, human melanoma driver mutations in *BRAF* occur more commonly than those in *NRAS*, contributing to 50-60% of all cases (Davies et al, 2002).This chapter therefore describes our investigation of P-Rex1 in melanomas driven by oncogenic $Braf^{V600E}$. A relevance of P-Rex1 to $Braf^{V600E}$-driven tumours was a clear possibility given the identification of P-Rex1 as a transcriptional target of ERK signalling in melanoma, as well as the common downstream MEK-ERK signalling shared by Braf and Nras (Shields et al, 2007).

There have now been a number of high profile success stories in cancer where targeted antibody or small molecule inhibitors are applied to specific genotypic subsets of patients with a given cancer (Slamon et al, 2001, Kwak et al, 2010, Flaherty et al, 2010). One report has already identified P-Rex1 as having particular relevance to the specific ER+ (+/- ErbB2) subset of breast tumours (further detail in section 1.5.1.2) (Sosa et al, 2010). Such a finding could improve the efficacy, toxicity, and cost-benefit profile of any putative P-Rex1 inhibitors, enabling a straightforward genetic selection for patient enrichment in early phase clinical trials (see Section 1.4 for further details).

5.1 P-Rex1 is upregulated in human melanoma driven by $Braf^{V600E}$

To test the relevance of our data to human melanomagenesis, we started by assessing the expression of P-Rex1 in established human melanoma cell lines derived from primary or metastatic $Braf^{V600E}$-driven melanoma. Compared to normal human melanocytes, upregulation of P-Rex1 was observed in nearly all of the cell lines (Figure 5.1). This immunoblotting also suggested that this over-expression was less than that observed in melanomas driven by $Nras^{Q61K}$ (Figure 3.5a; immunoblot performed at the same time as that in Figure 5.1). However, review of our previous microarray data showed no difference in P-Rex1 intensity between melanoma cell lines with $Nras^{Q61}$ mutations (WM852, WM1366, Lyse, Gerlach) or $Braf^{V600E}$ (the majority of other cell lines) (Figure 3.4).

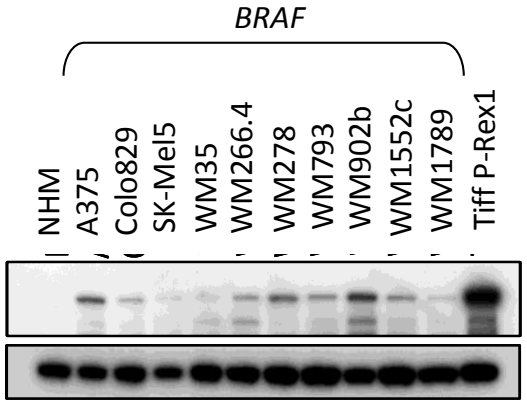

Figure 5.1 P-Rex1 is upregulated in human melanoma driven by oncogenic Braf
Western blot illustrating endogenous expression of P-Rex1 in a panel of human melanoma derived cell lines. Cell lines with driver mutations in *BRAF* are represented.NHM = normal human melanocytes. Figure kindly contributed by Dr Andrew Campbell.

5.2 Braf^{V600E} drives proliferation of melanoblasts during murine development

In line with the embryonic detail described in chapter 4, we next wanted to delineate the developmental effects of *PREX1* ablation on the *BRAF^{V600E}* mutation in melanoblasts. However, this experiment was virtually precluded by the reported *in utero* mortality of Braf^{V600E}-expressing embryos following recombination with the constitutively active melanocyte-specific *Tyr::Cre* (Dhomen et al, 2010). We were able to at least characterise the phenotype of Braf^{V600E} expression (without P-Rex1 depletion) in melanoblasts using *ex vivo* live timelapse of E15.5 wholemount skin (detailed in Figure 2.3). A large increase in melanoblast numbers was noted in *Tyr::Cre Braf^{V600E}* embryos compared to *wild-type* controls (Figure 5.2a). This result fell short of statistical significance, most likely as a consequence of the limited embryo numbers obtained due to the common *in utero* death of *Tyr::Cre Braf^{V600E}* embryos prior to dissection. Consistent with other reports, it is likely that a potential difference in cell number is accounted for by an increase in proliferation, given that no cell death was observed in samples from either cohort (Figure 5.2b) (Dhomen et al, 2010). No difference in cell speed or Euclidean distance travelled was noted between the two cohorts (Figures 5.2c,d).

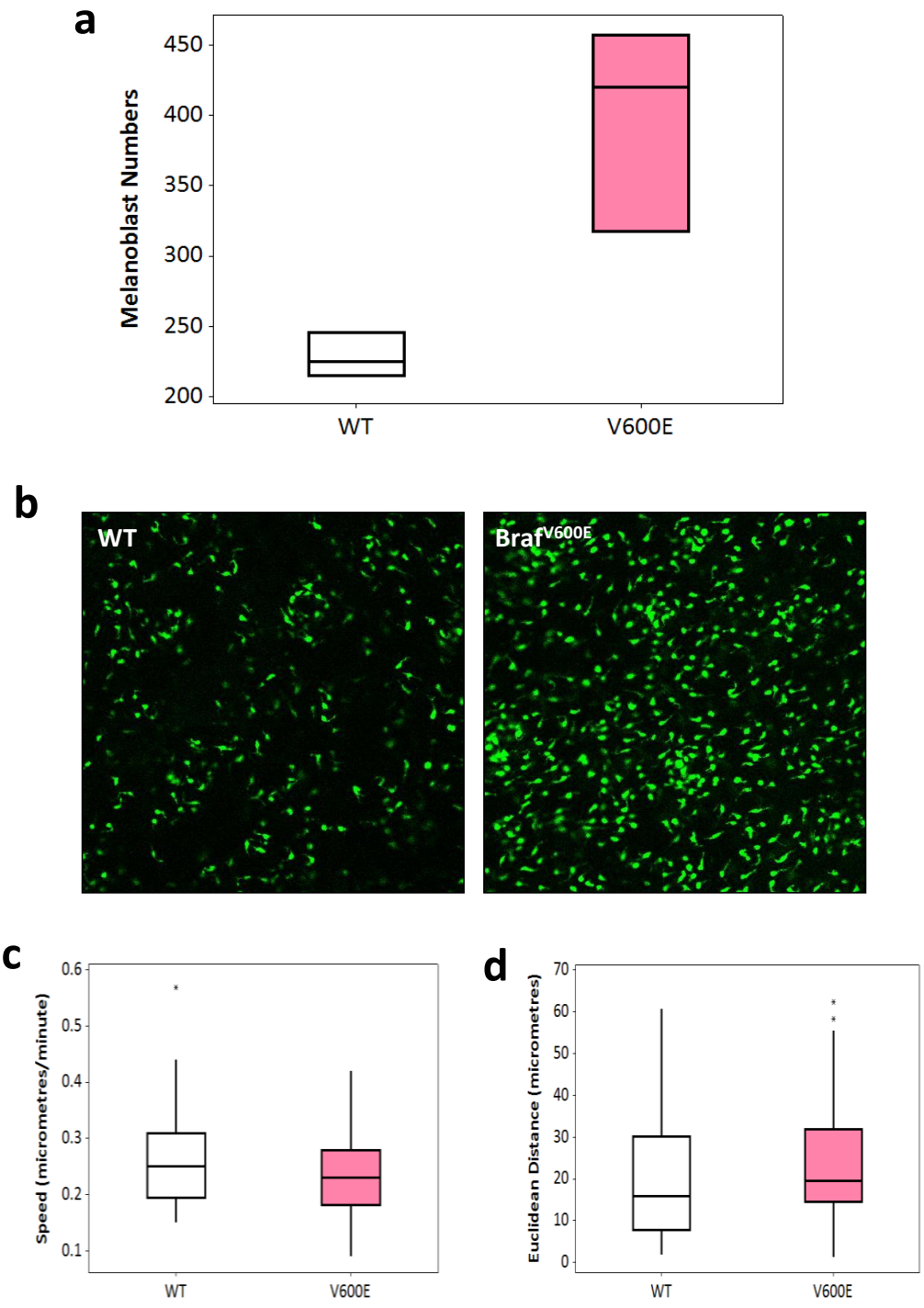

Figure 5.2 Expression of Braf^{V600E} increases melanoblast cell numbers at E15.5
(a) *Ex vivo* quantification and comparison of numbers of melanoblasts expressing green fluorescent protein in the skin: *wild-type* ('WT', white bars) and *Tyr::CreER Braf^{V600E}* ('V600E', pink bars) compared (p=0.081; Mann-Whitney; n=3 embryos, 3 slices counted per embryo). **(b)** Representative pictures comparing *ex vivo* numbers of *WT* and *Tyr::CreER Braf^{V600E}* melanoblasts expressing green fluorescent protein in the skin. No cell death was seen in any sample. **(c)** Quantification and comparison of individual melanoblast speed at E15.5 under live confocal timelapse: : *wild-type* ('WT', white bars) and *Tyr::CreER Braf^{V600E}* ('V600E', pink bars) compared (p=0.099; Mann-Whitney; n=60 cells, 20 per timelapse). **(d)** Quantification and comparison of Euclidean distance travelled by individual melanoblasts at E15.5 under live confocal timelapse: *wild-type* ('WT', white bars) and *Tyr::CreER Braf^{V600E}* ('V600E', pink bars) compared (*p=0.054; Mann-Whitney; n=60, 20 per timelapse). (Box and whiskers plots: boxes represent 25th-75th percentiles of given value, lines represent median values).

5.3 Ablation of PTEN does not rescue the *P-Rex1*$^{-/-}$ migration phenotype

Metastases were rare and required a prolonged latency period when conditional expression of Braf^{V600E} was induced in a melanoma mouse model (Dhomen et al, 2009). However, the inducible melanocyte-specific combination of *PTEN* ablation and expression of Braf^{V600E} has been reported to confer metastatic melanoma with 100% penetrance and short latency in mice (Dankort et al, 2009). This second model therefore seemed more appropriate for assessing a potential anti-metastatic effect of *P-Rex1* deletion in melanomas driven by oncogenic Braf.

As P-Rex1 is known to be directly stimulated by PI(3)K-stimulated phosphatidylinositol (3,4,5)-trisphosphate (PIP_3) production, we first ensured ablation of *PTEN* did not rescue the *P-Rex1*$^{-/-}$ migratory phenotype (detailed in Figure 4.4) by upregulating the PI(3)K pathway (Welch et al, 2002). It was necessary to assess this embryologically as melanocyte-specific *PTEN* ablation using the constitutively active *Tyr::Cre* is lethal in the late stages of development or shortly after birth (Lionel Larue, personal communication; Delmas et al, 2003). This lethality is consistent with the early neurological defects and death seen when PTEN was conditionally depleted by Cre recombinase under the control of an alternative melanocyte-specific promoter, Dct (Inoue-Narita, 2008). *P-Rex1*$^{-/-}$ and *Tyr::Cre Pten*$^{lox/lox}$ mice were inter-crossed to mice carrying the reporter *DCT-lacZ* transgene (Figure 5.3a). Initial inspection suggested that P-Rex1 depletion still inhibited melanoblast migration when either one or two copies of *PTEN* were concomitantly ablated (Figure 5.3b). This finding was quantitatively confirmed using an E15.5 migration assay (described in Figure 2.1) (Figures 5.4a-c). Notably, homozygous deletion of *PTEN* also increased melanoblast numbers compared to *Tyr::Cre Pten*$^{lox/+}$ mice (regardless of P-

Rex1 genotype): this was consistent with the increase of melanoblast numbers seen when *PTEN* was deleted under the control of the Dct promoter (Inoue-Narita, 2008).

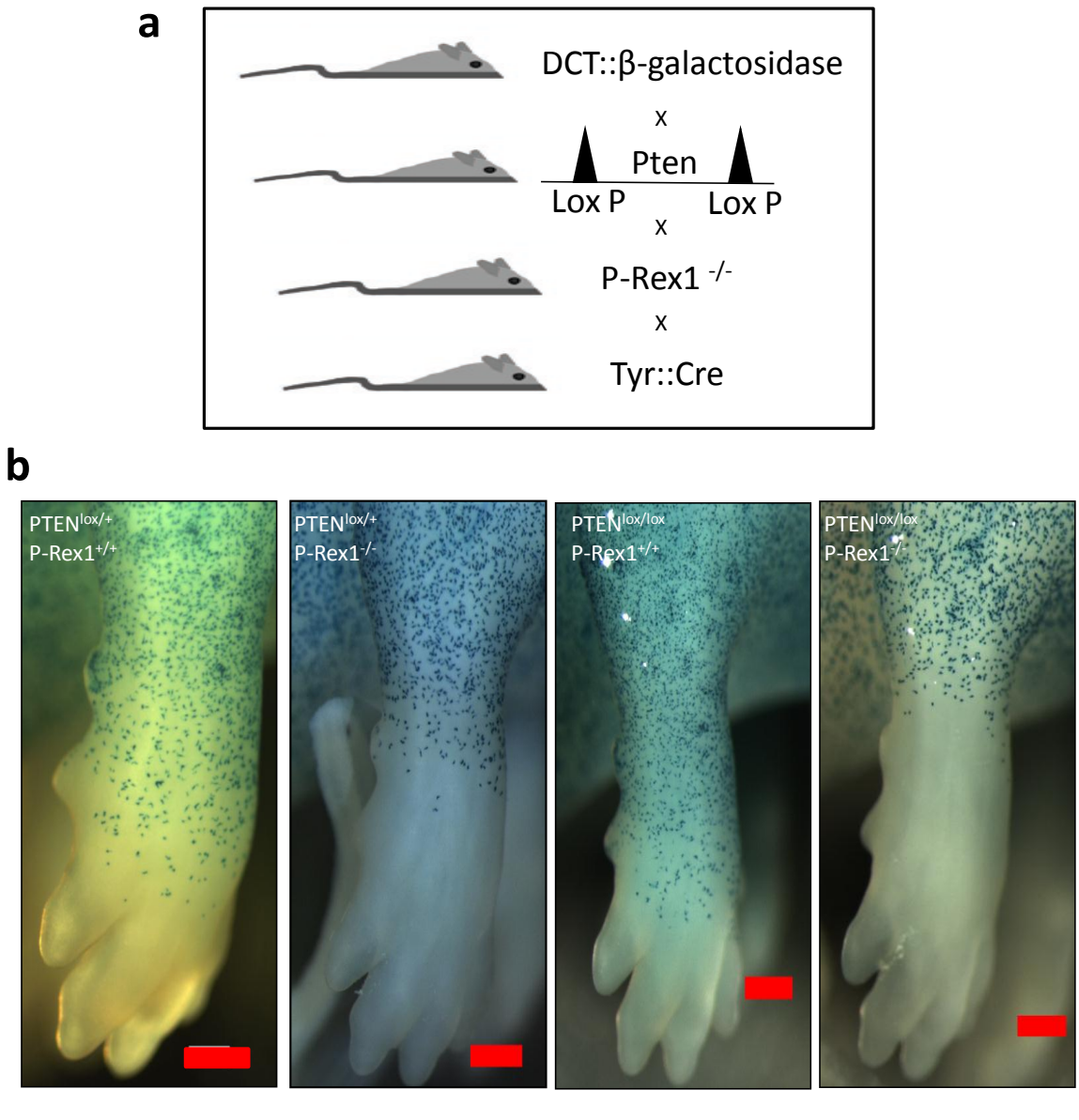

Figure 5.3 *PTEN* ablation does not rescue the P-Rex1 migration phenotype
(a) Schematic diagram detailing breedings of *DCT-lacZ* melanoblast reporter mice to *PREX1* and *PTEN* gene modifications. **(b)** Comparison of melanoblast migration along forepaw in X-gal stained embryos at E15.5. A migratory deficit is evident in both *P-Rex1*$^{-/-}$ (with either *PTEN*$^{lox/+}$ or *PTEN*$^{lox/lox}$) embryos. Scale bars = 500µm.

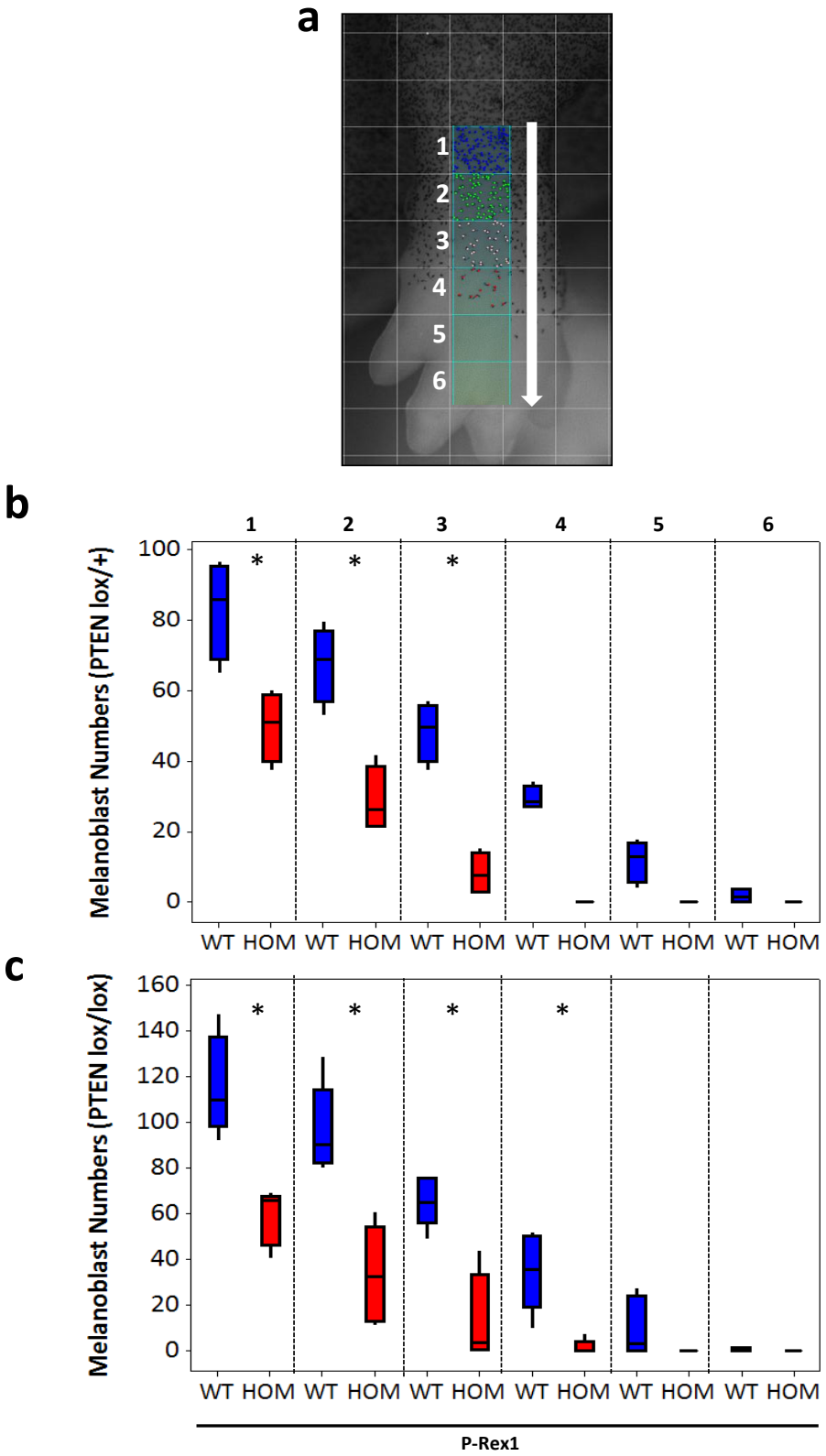

Figure 5.4 *PTEN* ablation does not rescue the P-Rex1-null migration phenotype
(a) Schematic picture showing method of quantification of melanoblast migration used for (b) and (c) **(b,c)** Comparison of melanoblast migration between *P-Rex1*$^{+/+}$ ('WT', blue bars) and *P-Rex1*$^{-/-}$ ('HOM', red bars) mice. Upper panel (b) represents *PTEN*$^{lox/+}$ embryos (*p=0.03, Levels 1/2/3; Mann-Whitney test, n=4), lower panel (c) represents *PTEN*$^{lox/lox}$ embryos (*p=0.012, Levels 1/2/3/4; Mann-Whitney test, n=5) (All box and whiskers plots: boxes represent 25th-75th percentiles of given value, lines represent median values).

5.4 *Pten*$^{lox/+}$ combination with *Braf*^{V600E} is an appropriate model for studying P-Rex1 activity

We next assessed whether heterozygous or homozygous melanocyte-specific disruption of *PTEN* (in combination with Braf^{V600E} expression) is a more appropriate model for characterising any putative anti-metastatic effects of P-Rex1 depletion. To avoid problems with embryonic lethality, Pten$^{lox/lox}$, *Braf*$^{V600E/+}$, and *P-Rex1*$^{-/-}$ mice were inter-crossed to mice carrying a melanocyte-specific inducible Tyr::CreER promoter (Figure 5.5) (Yajima et al, 2006). Using this model, no *PTEN* deletion or expression of Braf^{V600E} would occur until mice were shaved and induced using skin painting with topical tamoxifen (Dhomen et al, 2009).

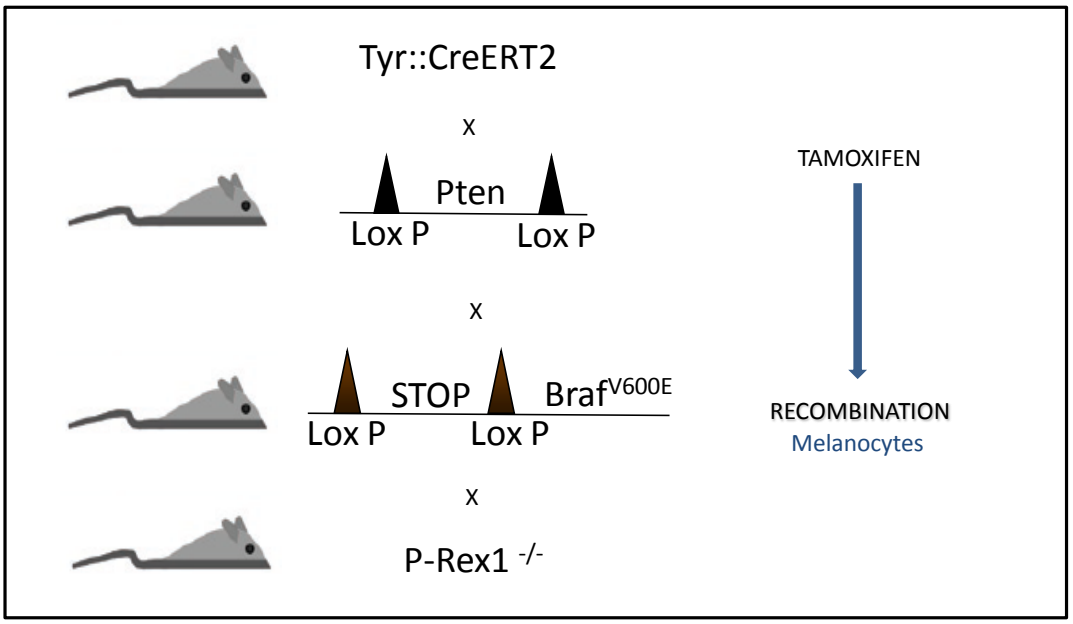

Figure 5.5 Schematic diagram detailing breeding of inducible Braf^{V600E} melanoma model to P-Rex1 and PTEN mice
Offspring are shaved and painted with topical tamoxifen to induce recombination in melanocytes (detailed in section 2.3.2).

Comparison of survival between the first 6 painted *Tyr::CreER Braf$^{V600E/+}$; Pten$^{lox/lox}$* mice and *Tyr::CreER Braf$^{V600E/+}$; Pten$^{lox/+}$* mice revealed a considerably shortened overall survival for *Tyr::CreER Braf$^{V600E/+}$; Pten$^{lox/lox}$* mice, with nearly all requiring euthanisation due to overgrowth or ulceration of primary melanoma (Figures 5.6a,b). We therefore concluded that *Tyr::CreER Braf$^{V600E/+}$; Pten$^{lox/+}$* mice would be a more appropriate model for investigation of P-Rex1: the longer survival of these mice would allow more time for metastases to develop, without their survival extending for a period that was too prolonged. Both epithelioid and spindle cells were observed in the dermis of induced *Tyr::CreER Braf$^{V600E/+}$; Pten$^{lox/+}$* mice, with a predominance of melanomas macroscopically non-pigmented (Figures 5.6b,c). As is characteristic of many genetically modified melanoma mouse models, the presence of both of these cell types is consistent with the nodular histological subtype of primary melanoma (detailed further in section 1.3.1.2). P-Rex1 expression was consistently observed in all melanomas, whether characterised by spindle or epithelioid cell morphology (Figures 5.6c).

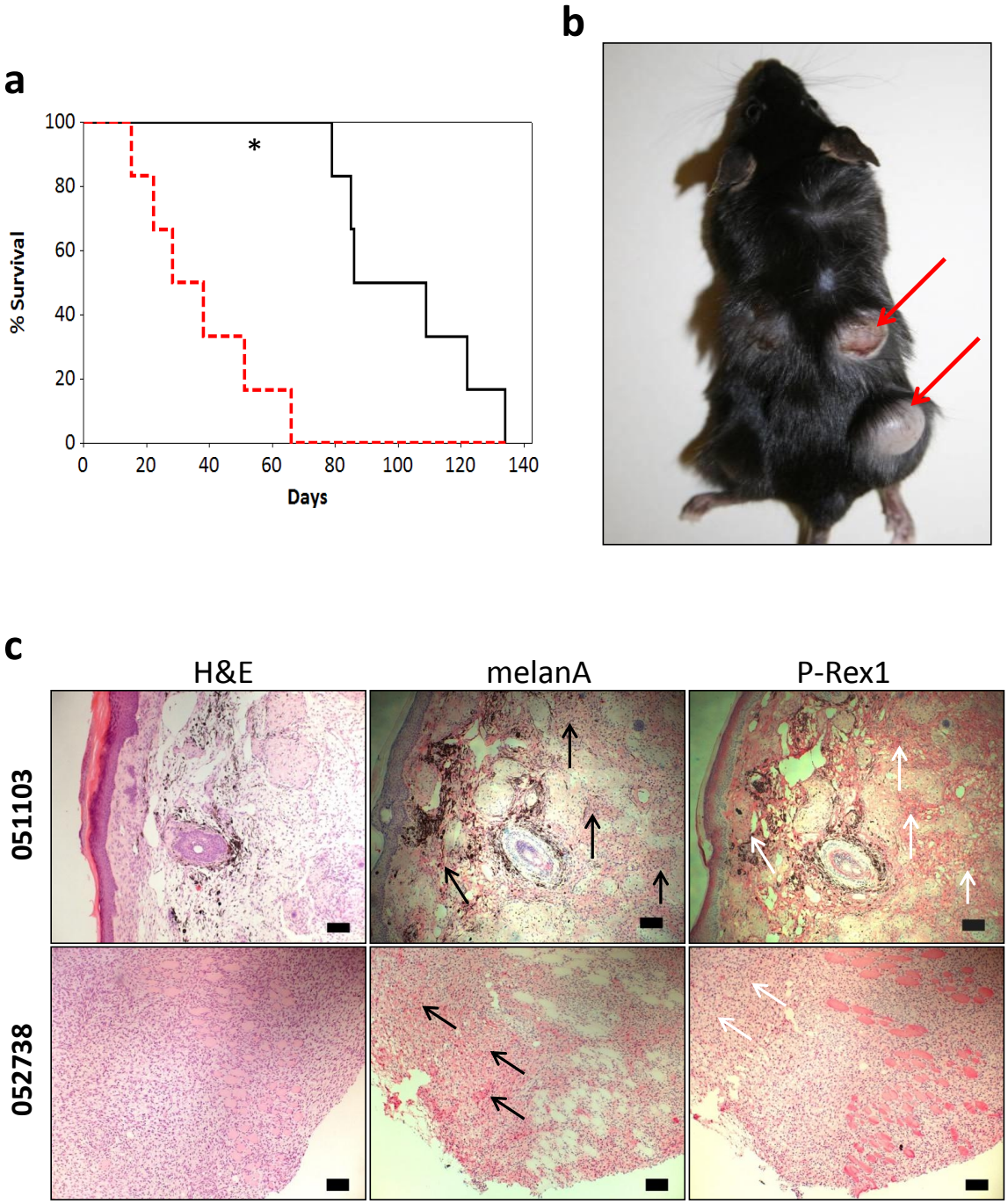

Figure 5.6 *PTEN*$^{lox/+}$ combination with the Braf^{V600E} melanoma model is appropriate for studying P-Rex1 activity

(a) Kaplan-Meier curves detailing significant survival improvement of first 6 mice from *TyrER::Cre Braf*$^{V600E/+}$*; PTEN*$^{lox/+}$ cohort (black line) compared to first 6 from *TyrER::Cre Braf*$^{V600E/+}$*; PTEN*$^{lox/lox}$ cohort (red line) (*p=0.001, log-rank test, n=6). **(b)** Example of primary melanomas arising in *TyrER::Cre Braf*$^{V600E/+}$*; PTEN*$^{lox/+}$ transgenic mice. Red arrows: non-pigmented primary skin melanomas. **(c)** Representative H&Es and melanA/P-Rex1 immunohistochemistry showing consistent expression of P-Rex1 in two melanomas characterised by different cell populations. Pink staining represents expression of melanA (black arrows) or P-Rex1 (white arrows), black/brown areas are melanin pigment. 057238/051103 =mouse identification numbers. 051103 melanoma predominantly composed of epithelioid cells, 057238 predominantly composed of spindle cells with hyperchromatic nuclei compared to 051103 (n=3) (Scale bars = 100µm, 30µm for inserts).

5.5 *PREX1* disruption does not alter primary melanoma parameters in *Tyr::CreER Braf$^{V600E/+}$; PTEN$^{lox/+}$* mice

Consistent with our analysis of *Tyr::Nras$^{Q61K/°}$; INK4a$^{-/-}$* mice in Chapter 3, we could not confirm an alteration of primary melanoma characteristics when P-Rex1 was reduced in *Tyr::CreER Braf$^{V600E/+}$; PTEN$^{lox/+}$* mice. 100% of mice in both cohorts developed primary melanoma after induction with tamoxifen (Table 5.1). No difference in rate of growth was observed between *Tyr::CreER Braf$^{V600E/+}$; PTEN$^{lox/+}$; P-Rex1$^{-/-}$* mice and control *Tyr::CreER Braf$^{V600E/+}$; PTEN$^{lox/+}$; P-Rex1$^{+/+}$* mice (Figure 5.7a). In the experimental *Tyr::CreER Braf$^{V600E/+}$; PTEN$^{lox/+}$; P-Rex1$^{-/-}$* cohort, there was a trend towards diminished tumour burden as a consequence of fewer primary melanomas developed per mouse following tamoxifen induction, but no statistically significant change seen (Figures 5.7b,c). There was no difference in ulceration incidence or median size at which ulceration occurred (Table 5.2). Finally, primary melanoma latency following tamoxifen induction was not altered (Figure 5.7d).

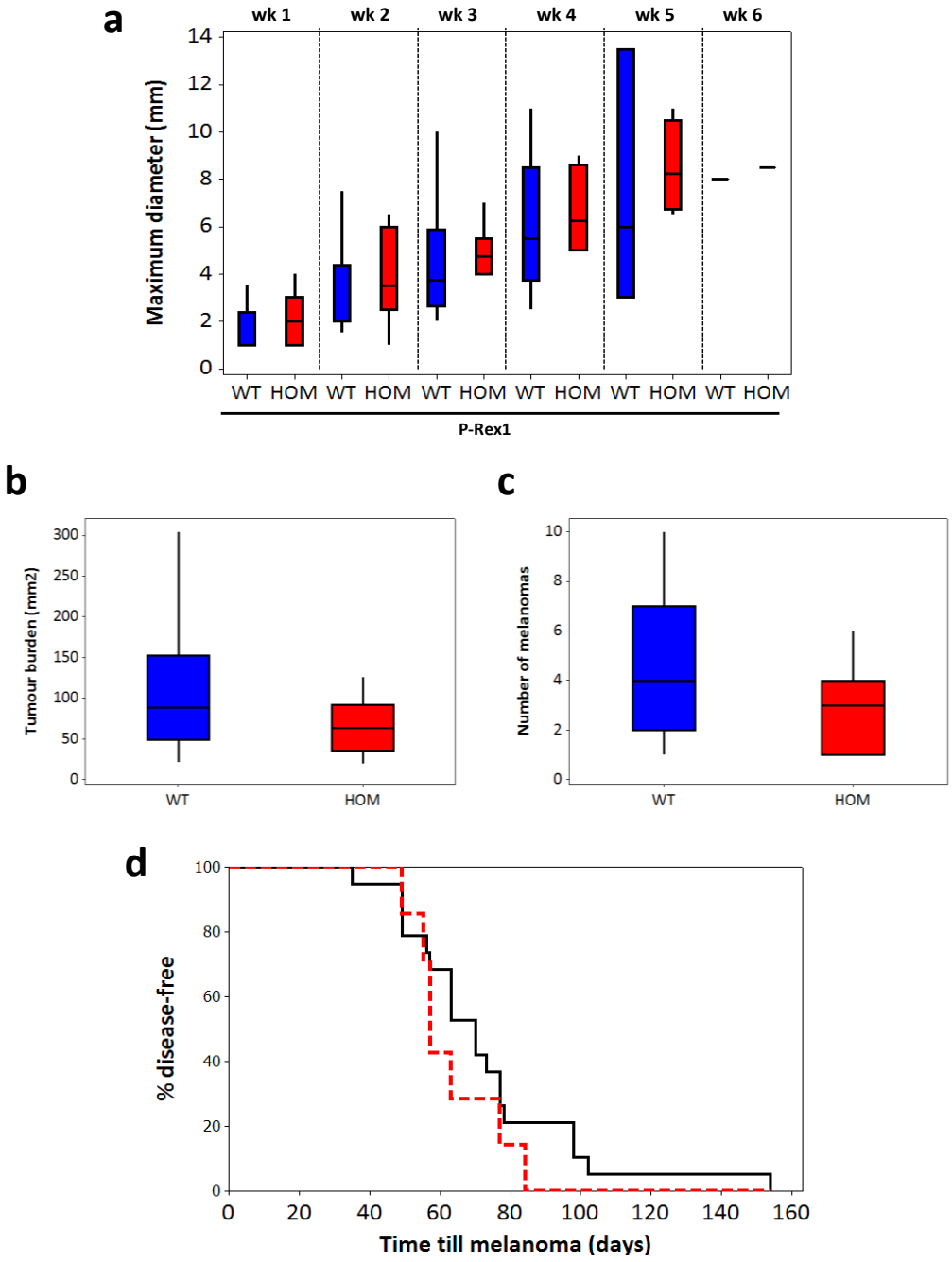

Figure 5.7 P-Rex1 depletion does not alter primary melanoma growth parameters in *TyrER::Cre Braf$^{V600E/+}$; PTEN$^{lox/+}$* mice

(a) Quantification and comparison of first 6 weeks primary melanoma growth between *TyrER::Cre Braf$^{V600E/+}$; PTEN$^{lox/+}$; P-Rex1$^{+/+}$* mice ('WT', blue bars) compared to first 6 weeks from *TyrER::Cre Braf$^{V600E/+}$; PTEN$^{lox/+}$; P-Rex1$^{-/-}$* mice ('HOM', red bars) (Week 1: n=16 vs n=7, Mann-Whitney, p=0.229; Week 2: n=16 vs n=7, Mann-Whitney, p=0.3; Week 3: n=16 vs n=6, Mann-Whitney, p=0.285; Week 4: n=13 vs n=4, Mann-Whitney, p=0.734; Week 5: n=3 vs n=4, Mann-Whitney, p=0.596; Week 6: n=1 vs n=2, statistical assessment not possible). **(b)** Comparison of primary melanoma tumour burden between *TyrER::Cre Braf$^{V600E/+}$; PTEN$^{lox/+}$; P-Rex1$^{+/+}$* mice ('WT', blue bars, n=23) and *TyrER::Cre Braf$^{V600E/+}$; PTEN$^{lox/+}$; P-Rex1$^{-/-}$* mice ('HOM', red bars, n=7) (p=0.155, Mann-Whitney) **(c)** Quantification and comparison of primary melanoma frequency observed between *TyrER::Cre Braf$^{V600E/+}$; PTEN$^{lox/+}$; P-Rex1$^{+/+}$* mice ('WT', blue bars, n=23) and *TyrER::Cre Braf$^{V600E/+}$; PTEN$^{lox/+}$; P-Rex1$^{-/-}$* mice ('HOM', red bars, n=7) (p=0.162, Mann-Whitney) (Box and whiskers plots: boxes represent 25th-75th percentiles of given value, lines represent median values). **(d)** Kaplan-Meier analysis of primary melanoma latency between *TyrER::Cre Braf$^{V600E/+}$; PTEN$^{lox/+}$; P-Rex1$^{+/+}$* (black line, n=19) and *TyrER::Cre Braf$^{V600E/+}$; PTEN$^{lox/+}$; P-Rex1$^{-/-}$* (red line, n=7) cohorts (p=0.286, log-rank test).

Genotype	Mice with Primary Melanoma	Mice with Melanoma Metastases
TyrER::Cre Braf$^{V600E/+}$; PTEN$^{lox/+}$; P-Rex1$^{+/+}$	25/25	3/10
TyrER::Cre Braf$^{V600E/+}$; PTEN$^{lox/+}$; P-Rex1$^{-/-}$	7/7	2/7

Table 5.1 P-Rex1 depletion does not reduce incidence of metastasis in a *Tyr::CreER Braf$^{V600E/+}$; PTEN$^{lox/+}$* murine melanoma model
Table detailing numbers of mice within both *Tyr::CreER Braf$^{V600E/+}$; PTEN$^{lox/+}$; P-Rex1$^{+/+}$* and *Tyr::CreER Braf$^{V600E/+}$; PTEN$^{lox/+}$; P-Rex1$^{-/-}$* cohorts suffering from primary and metastatic melanoma. Metastatic sites were all observed in the lung, except for 1 liver lesion in the *Tyr::CreER Braf$^{V600E/+}$; PTEN$^{lox/+}$; P-Rex1$^{-/-}$* cohort.

Genotype	Number of mice assessed for ulceration	Number of mice with ulceration	Median diameter of melanoma at ulceration (mm)
TyrER::Cre $Braf^{V600E/+}$; $PTEN^{lox/+}$; P-$Rex1^{+/+}$	23/25	19/23	7
TyrER::Cre $Braf^{V600E/+}$; $PTEN^{lox/+}$; P-$Rex1^{-/-}$	7/7	7/7	7.5

Table 5.2 There is no difference in primary melanoma ulceration when P-Rex1 is depleted in *Tyr::CreER $Braf^{V600E/+}$; $PTEN^{lox/+}$* mice
Table detailing incidence of ulceration and size of tumour at which ulceration occurs.

5.6 *PREX1* disruption does not alter metastases or survival in *Tyr::CreER Braf$^{V600E/+}$; PTEN$^{lox/+}$* mice

Contrary to what we observed in chapter 3 when P-Rex1 was ablated in *Tyr::Nras$^{Q61K/°}$; INK4a$^{-/-}$* mice, no difference in metastatic incidence was observed between age-matched *Tyr::CreER Braf$^{V600E/+}$; PTEN$^{lox/+}$; P-Rex1$^{-/-}$* mice and control *Tyr::CreER Braf$^{V600E/+}$; PTEN$^{lox/+}$; P-Rex1$^{+/+}$* mice (Table 5.1). However, only 7 mice were assessable in the *Tyr::CreER Braf$^{V600E/+}$; PTEN$^{lox/+}$; P-Rex1$^{-/-}$* cohort. Across both cohorts, one liver and four lung metastases were seen, with mild staining intensity of the melanocyte marker, S100, observed in these lesions (Figure 5.8a; Table 5.1). There was no difference in survival between the two cohorts, measured from induction or time of primary melanoma development (Figures 5.8b,c).

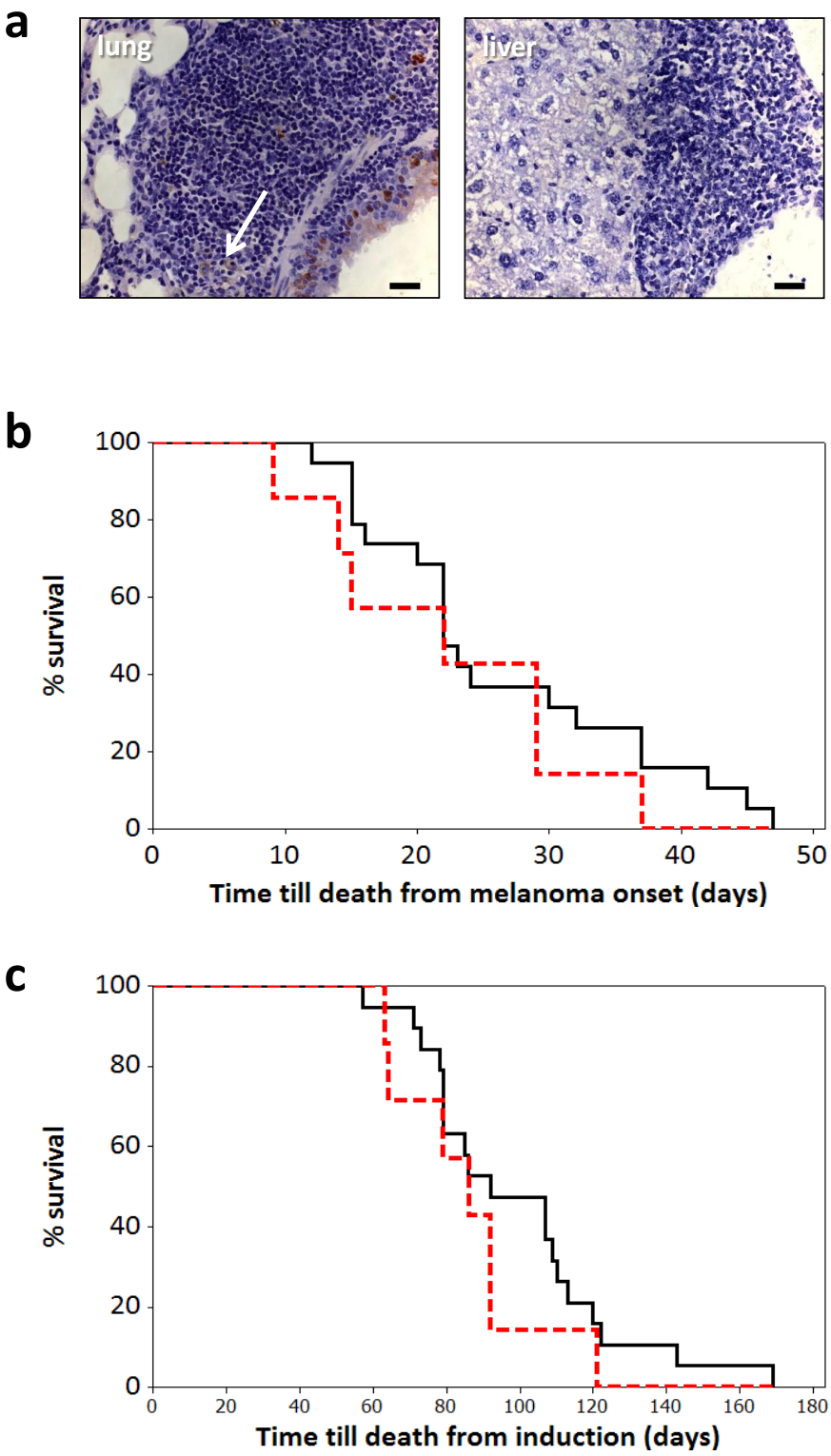

Figure 5.8 P-Rex1 disruption does not alter metastases or survival in *Tyr::CreER Braf$^{V600E/+}$; PTEN$^{lox/+}$* mice
(a) Representative photomicrographs of IHC showing lung and liver metastasis with rare expression of the melanocyte marker S100 (white arrow) (n=5 across both cohorts; Scale bars = 30μm) **(b)** Kaplan-Meier analysis of time till death after melanoma onset: comparison between *Tyr::CreER Braf$^{V600E/+}$; PTEN$^{lox/+}$; P-Rex1$^{+/+}$* (black line, n=19) and *Tyr::CreER Braf$^{V600E/+}$; PTEN$^{lox/+}$; P-Rex1$^{-/-}$* (red line, n=7) cohorts (p=0.311, log-rank test). **(c)** Kaplan-Meier analysis of time till death from tamoxifen induction: comparison between *Tyr::CreER Braf$^{V600E/+}$; PTEN$^{lox/+}$; P-Rex1$^{+/+}$* (black line, n=19) and *Tyr::CreER Braf$^{V600E/+}$; PTEN$^{lox/+}$; P-Rex1$^{-/-}$* (red line, n=7) cohorts (p=0.303, log-rank test).

5.7 Summary

This chapter describes several important features of P-Rex1 function which expand our knowledge of the potential use of a P-Rex1 inhibitor in the clinic. We have analysed and discussed these in more detail in sections 7.1.2 and 7.3.1. This summary offers a synopsis of our findings in chapter 5.

Importantly, we have not been able to prove an effect of P-Rex1 depletion on $Braf^{V600E}$-driven melanomas that matches its anti-metastatic effects in $Nras^{Q61K}$-driven tumours. There was no reduction in metastases or survival observed in P-Rex1-null $Braf^{V600E}$-driven melanomas (Table 5.1, Figure 5.8). Moreover, extensive analyses of $Braf^{V600E}$ primary tumours did not suggest any difference in tumour growth, burden, frequency, timing of onset, or ulceration without endogenous P-Rex1 (Table 5.2, Figure 5.7). It should be noted that metastases observed using the $Braf^{V600E}$-driven model were limited, perhaps reflecting the rarity of metastatic success described by Fidler in 1970 (Fidler, 1970) (detailed in section 1.2). Other possible reasons for the small number of $Braf^{V600E}$-driven metastases, and the apparent metastatic discrepancy with P-Rex1 depletion between $Braf^{V600E}$-driven and $Nras^{Q61K}$-driven models, are discussed in detail in section 7.1.2.

For the first time in this thesis, this chapter uncouples our P-Rex1 embryonic phenotype from the phenotype which we might have expected in our cancer model. The persisting migrational deficit observed when *PTEN* was ablated in P-Rex1-depleted embryos suggested we would again see a metastasis reduction with P-Rex1 manipulation in the *TyrER::Cre* $Braf^{V600E/+}$*;* $PTEN^{lox/+}$ cancer model (Figures 5.3, 5.4). As already mentioned, this was not the case and there was no change in metastases with P-Rex1 depletion (Table 5.1, Figure 5.8). Sections 7.1.2 and 7.3.1 detail why the *TyrER::Cre* $Braf^{V600E/+}$*;* $PTEN^{lox/+}$ cancer model may not be optimal for study of metastases, a potential reason why there

was no fit between the cancer and embryonic phenotypes on this occasion. The possibility that we may have missed a P-Rex1 effect due to use of a sub-optimal model is supported by the clear upregulation of P-Rex1 observed in human melanoma cell lines driven by $Braf^{V600E}$ (Figure 5.1). However, as mentioned in section 1.1.5, it is possible that a 'developmental' hypothesis for cancer using embryonic models may prove to be too simplistic in this case, unable to offer an insight of the complicated mutational and biological processes involved in $Braf^{V600E}$-driven metastases.

Finally, in this chapter we have established important practical considerations for the future utility of murine *TyrER::Cre* $Braf^{V600E/+}$ cancer models. Their optimal use in our hands was in combination with heterozygous $PTEN^{lox/+}$ mice, rather than the $PTEN^{lox/lox}$ mice previously reported (Figure 5.6) (Dankort et al, 2009). It is also clear that their greatest current advantage is for the study of primary melanomas rather than metastases, at least until a facility and protocol for primary tumour removal can be efficiently set up (see sections 1.3.1.2, 7.1.2 and 7.3.1).

Chapter 6

Exploring the tumourigenic role of FAK in the melanocyte lineage

In chapters 3-5, we have established a melanomagenic role for P-Rex1 using a number of different cancer and embryonic genetically modified mouse models. This chapter focuses on validating the diversity of these models by assessing an alternative molecule described in tumourigenesis, FAK. FAK has been described as a key player in cancer for several years, and has been characterised as pro-migratory using a Xiphophorus model of melanoma (see section 1.5.2, Meierjohann et al, 2006). It represents an altogether different type of anticancer target to P-Rex1 for the following reasons:

1. *Expression.* Unlike P-Rex1, FAK is widely expressed in human cells, suggesting that finding a therapeutic window for its inhibition in tumourigenesis may be less straightforward (Schaller et al, 1992, Hanks et al, 1992). Other than in large bowel cancers (5 mutations in 47 cancers analysed), there is little evidence from the cancer genome project that FAK can contribute to cancer secondary to its mutation rather than changes in expression levels (total of 14 mutations in 1503 cancer samples), so targeting a mutant form of FAK would not be an appropriate strategy for narrowing the therapeutic window (http://cancer.sanger.ac.uk/cosmic/gene/analysis ?ln=PTK2#histo). Despite this, several small molecule inhibitors of FAK have been developed and are now in advanced clinical assessment (Sui et al, 2008).

2. *Cancer biology.* Through its complex involvement in various downstream signalling networks such as MAPK, PI(3)K, Src, and EGFR, FAK has confirmed roles in cancer-related processes such as angiogenesis, surv`ival and migration (Weiner et al, 1993, Owens et al, 1995, Schaller et al, 2001, Ilic et al, 2003). This contrasts with the solitary Rac-specific downstream role reported for P-Rex1 in cancer invasion, but also suggests that optimising the benefits of FAK inhibition could be a complicated

process. It is also unclear how the many roles of FAK relate to its kinase activity compared to its intra- and inter-molecular protein-protein interactions.

3. *Possible role in tumour inhibition.* A pro-tumourigenic role for P-Rex1 through its capacity to induce migration is intuitive and has been straightforwardly described in the previous chapters, as well as other reports (Qin et al, 2009). Despite a majority of literature asserting that the same is the case for FAK, there are conflicting data that suggest FAK upregulation can be beneficial in certain tumour contexts (Gabriel et al, 2006, Giaginis et al, 2009, Zhao et al, 2009). This might support the cell biological hypothesis that downregulation of FAK might permit primary melanoma cells to become more migratory by reducing their focal adhesions to the extra-cellular matrix (Schultze et al, 2010).

Currently melanoma is a cancer where there is a relative deficit of translational research involving FAK. Given the cancer-specific roles described above, we deemed it would be important to analyse FAK in more detail using our mouse models.

6.1 FAK deletion reduces melanoblast numbers during embryogenesis

As highlighted throughout this thesis, mechanistic and observational studies have revealed key similarities between the molecular machinery involved in signalling of melanoblasts and that of melanoma cells (detailed in section 1.1.5) (Gupta et al, 2005, Uong et al, 2010, Strizzi et al, 2011). In line with the role of FAK in development of other cell lineages, we first explored its role in development of melanocyte precursors, looking for parallels that could offer insight into a potential cancer phenotype (Fonar et al, 2011, Zhao et al, 2010).

Embryonic lethality at E8.5 occurs when *FAK* is ablated in mice (Ilic et al, 1995, Furuta et al, 1995). To address whether melanoblast behaviour is altered by *FAK* abrogation, we therefore inter-crossed mice with a melanocyte-specific *FAK* deletion, *Tyr::Cre FAK*$^{fl/fl}$, to mice carrying the *DCT-lacZ* transgene, the melanoblast reporter line described in chapter 4 (McLean et al, 2004, Mackenzie et al, 1997). Consistent with the reported role of FAK in proliferation and anoikis, there was a statistically significant reduction of E15.5 melanoblast numbers in *DCT-lacZ; Tyr::Cre FAK*$^{fl/fl}$ mice compared to *DCT-lacZ; Tyr::Cre FAK*$^{+/+}$ mice (Figures 6.1a,b).

Given the importance of oncogenic Nras in human melanoma (see Section 1.1.4.1) and the known interaction of FAK with a number of cancer-associated pathways (see Section 1.5.2.3), we also crossed *Tyr::Cre FAK*$^{fl/fl}$ mice to the *Tyr::Nras*$^{Q61K/°}$ mice (*Tyr::Nras*$^{Q61K/°}$*; P-Rex1*$^{-/-}$) described in chapter 3 (Ackermann et al, 2005). The *FAK*$^{fl/fl}$ cell number phenotype shown in Figure 6.1b was overcome by expression of *Tyr::Nras*$^{Q61K/°}$ (Figures 6.1a,c). Examination of melanoblast morphology revealed possible apoptotic bodies present in both *DCT-lacZ; Tyr::Cre FAK*$^{fl/fl}$ mice and *DCT-lacZ; Tyr::Nras*$^{Q61K/°}$; *Tyr::Cre FAK*$^{fl/fl}$ mice,

which were not present in their relative *wild-type* FAK controls (Figure 6.2). An alternative hypothesis was that these areas represent an increased dermal localisation of melanoblasts when FAK is conditionally deleted (Figure 6.2, arrows). Comparison of E15.5 cell numbers when *Tyr::Nras*$^{Q61K/^{\circ}}$ was expressed with or without FAK disruption did not show a change in melanoblast cell numbers (Figures 6.3a,b).

Collectively, these findings do no yet convey a clear physiological picture of the role of FAK in melanocyte embryology: there is an undoubted cell number deficit induced by its deletion and overcome by expression of *Tyr::Nras*$^{Q61K/^{\circ}}$, but further delineation of the relative contributions of proliferation, apoptosis, and dermal mislocalisation to this phenotype is required. This will start with clarification of what these potential dermal or apoptotic bodies are, followed by their quantification.

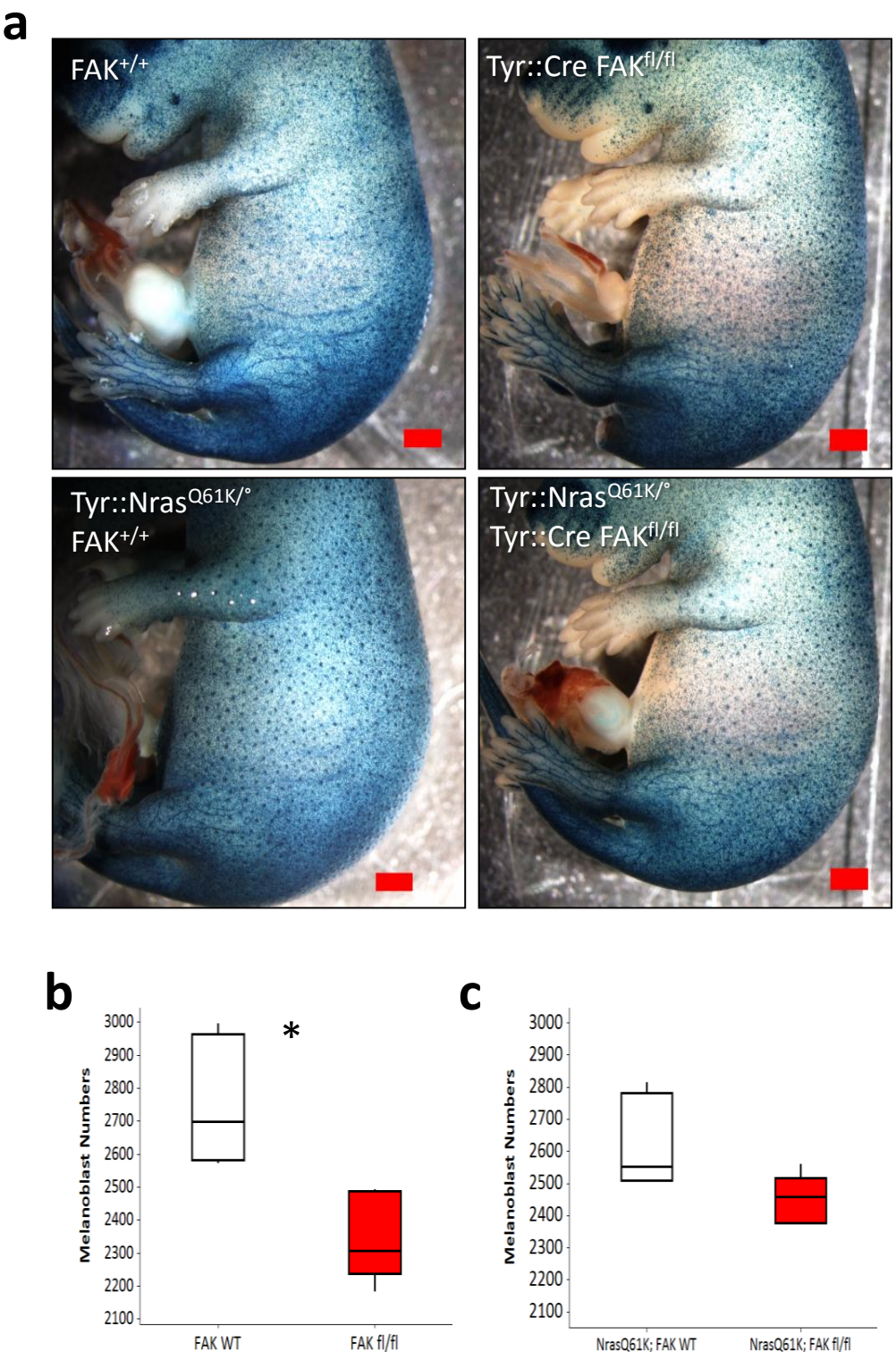

Figure 6.1 *Tyr::Cre FAK$^{fl/fl}$* mice have a deficit of melanoblasts at E15.5
(a) Representative pictures at E15.5 comparing cell numbers on the flank of X-gal stained embryos in *wild-type*, *Tyr::Cre FAK$^{fl/fl}$*, *Tyr::Nras$^{Q61K/°}$; FAK$^{+/+}$* and *Tyr::Nras$^{Q61K/°}$; Tyr::Cre FAK$^{fl/fl}$* mice. Scale bars = 1mm **(b)(c)** Comparison of E15.5 melanoblast numbers between *wild-type* ('FAK WT', white bars) and *Tyr::Cre FAK$^{fl/fl}$* ('FAK fl/fl', red bars) mice (b), and also between *Tyr::Nras$^{Q61K/°}$; FAK$^{+/+}$* ('NrasQ61K; FAK WT', white bars) and *Tyr::Nras$^{Q61K/°}$; Tyr::Cre FAK$^{fl/fl}$* (NrasQ61K; FAK fl/fl', red bars) mice (c). (b: *p =0.012; c: p =0.06; Mann-Whitney test, n=5) (Box and whiskers plots: boxes represent 25th-75th percentiles of given value, lines represent median values).

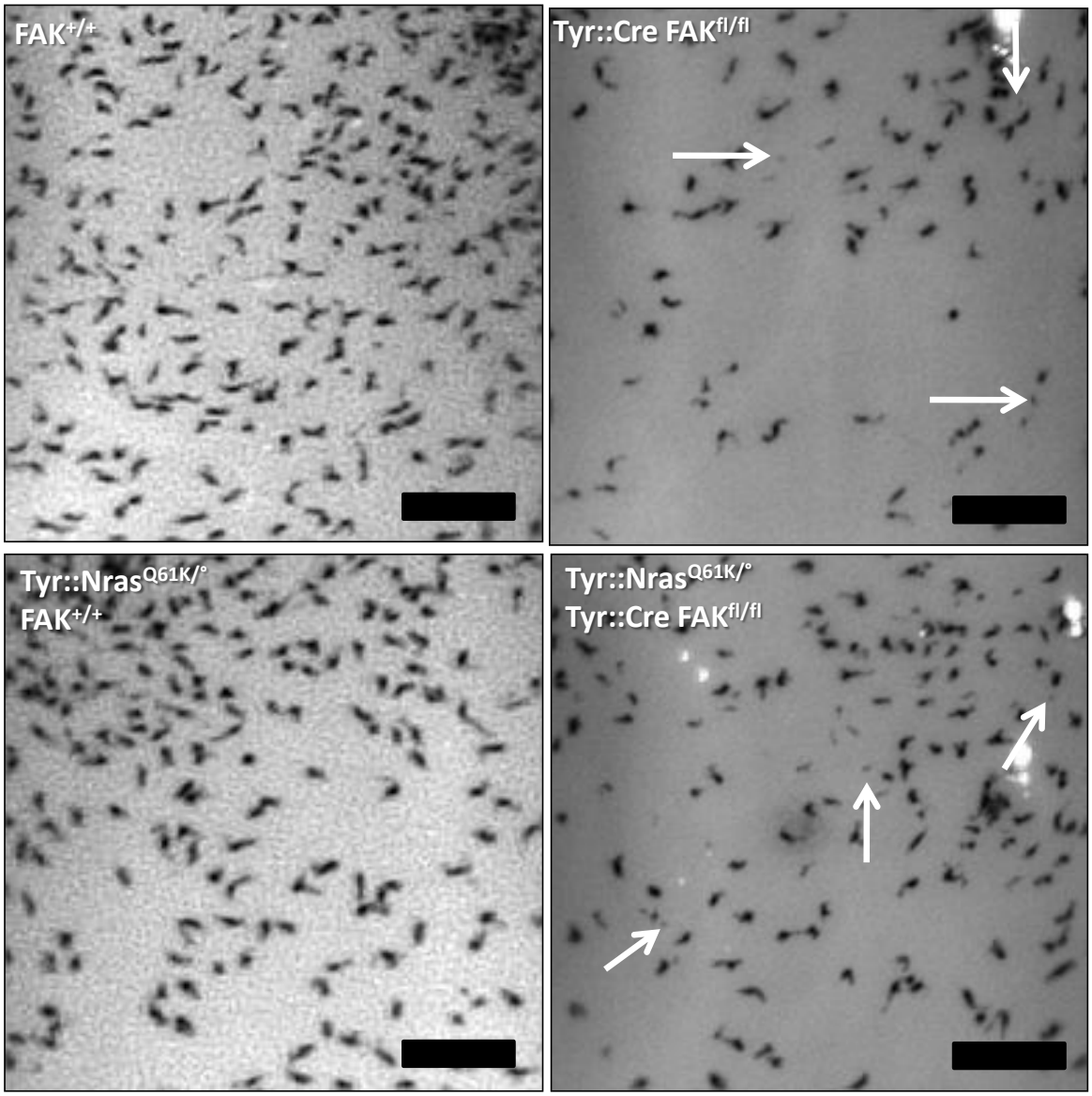

Figure 6.2 There may be fewer epidermal melanoblasts in FAK-deleted embryos at E15.5
Representative pictures at E15.5 comparing melanoblasts on forearms of X-gal stained embryos of *wild-type*, *Tyr::Cre FAK*$^{fl/fl}$, *Tyr::Nras*$^{Q61K/°}$*; FAK*$^{+/+}$ and *Tyr::Nras*$^{Q61K/°}$*; Tyr::Cre FAK*$^{fl/fl}$ mice. Scale bars = 200µm. White arrows likely show either apoptotic bodies or a dermal localisation of melanoblasts (n=4).

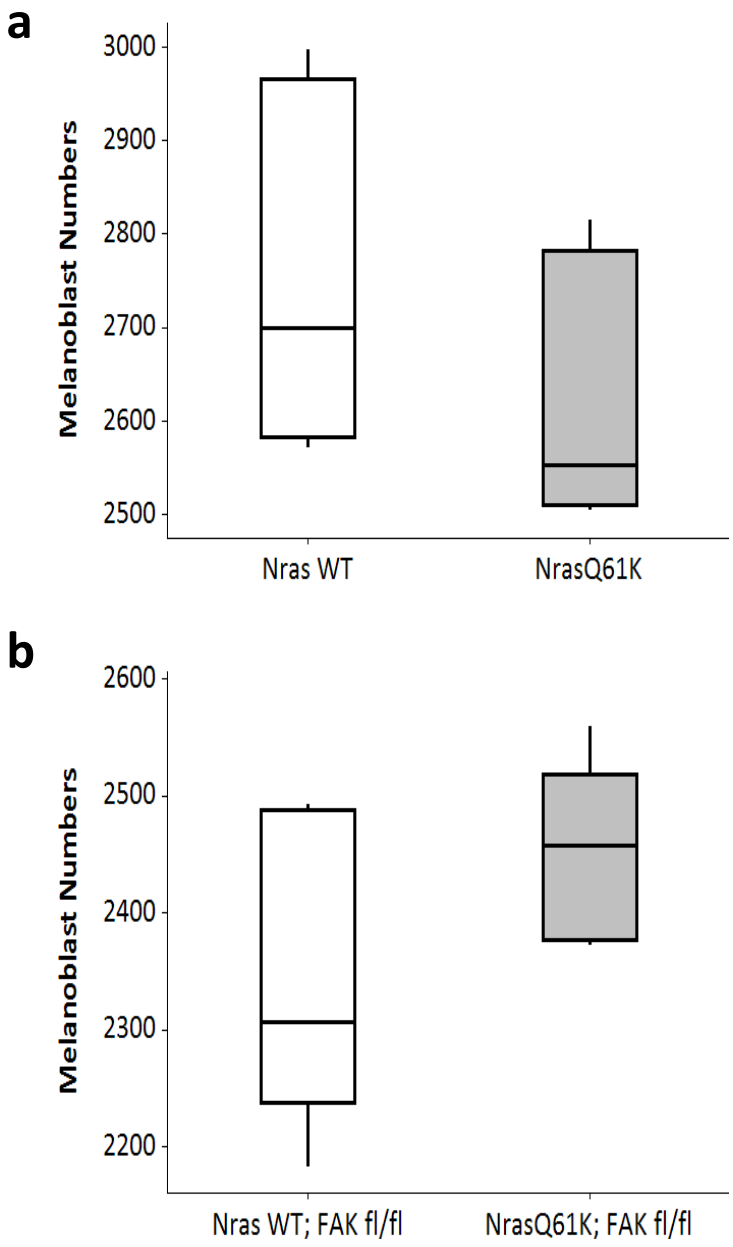

Figure 6.3 Expression of Nras^{Q61K} does not increase cell numbers at E15.5
(a) Comparison of E15.5 melanoblast numbers between *wild-type* ('Nras WT', white bars) and *Tyr::Nras$^{Q61K/°}$* ('NrasQ61K', grey bars) (p =0.21; Mann-Whitney test; n=5) (Box and whiskers plots: boxes represent 25th-75th percentiles of given value, lines represent median values). **(b)** Comparison of E15.5 melanoblast numbers between *Tyr::Cre FAK$^{fl/fl}$* ('Nras WT; FAK fl/fl', white bars) mice and *Tyr::Nras$^{Q61K/°}$; Tyr::Cre FAK$^{fl/fl}$* (NrasQ61K; FAK fl/fl', grey bars) mice (p =0.403; Mann-Whitney test; n=5)

6.2 FAK deletion may impair melanoblast migration during embryogenesis

Using the melanoblast migration assay detailed in Figure 2.1c, a statistical reduction in melanoblast migration between *DCT-lacZ; Tyr::Cre FAK*$^{fl/fl}$ and *DCT-lacZ; Tyr::Cre FAK*$^{+/+}$ mice was observed (Figure 6.4a,b). Again this phenotype was overcome by *Nras*$^{Q61K/°}$ expression (Figure 6.4c). No increase in cell rounding when FAK was deleted (through a reduction in focal adhesion) was evident on inspection of melanoblast morphology (Figure 6.2). As well as differing with the morphological changes seen with P-Rex1 ablation in figure 4.5, this result contrasts with a study showing an increase in cells with amoeboid morphology when FAK was knocked down using RNA interference in a breast cancer cell line (Golubovskaya et al, 2009).

Collectively, our embryo results show that the developmental phenotype of FAK deletion in melanoblasts potentially parallels its reported proliferative and migratory role in epithelial cell tumourigenesis. Although our migratory results parallel those described with dominant-negative FAK using a *Xiphophorus* melanoma model, it should be stressed that so far only one assay has been used to quantify migration in *Tyr::Cre FAK*$^{fl/fl}$ mice: their lack of a white belly spot or any cell morphological change (Figure 6.4c) might suggest that our result in Figure 6.4a,b could be artefact, resulting from the reduction in cell numbers described in Section 6.1 and Figure 6.1 (Meierjohann et al, 2006). This possibility is discussed further in Section 7.3.4.

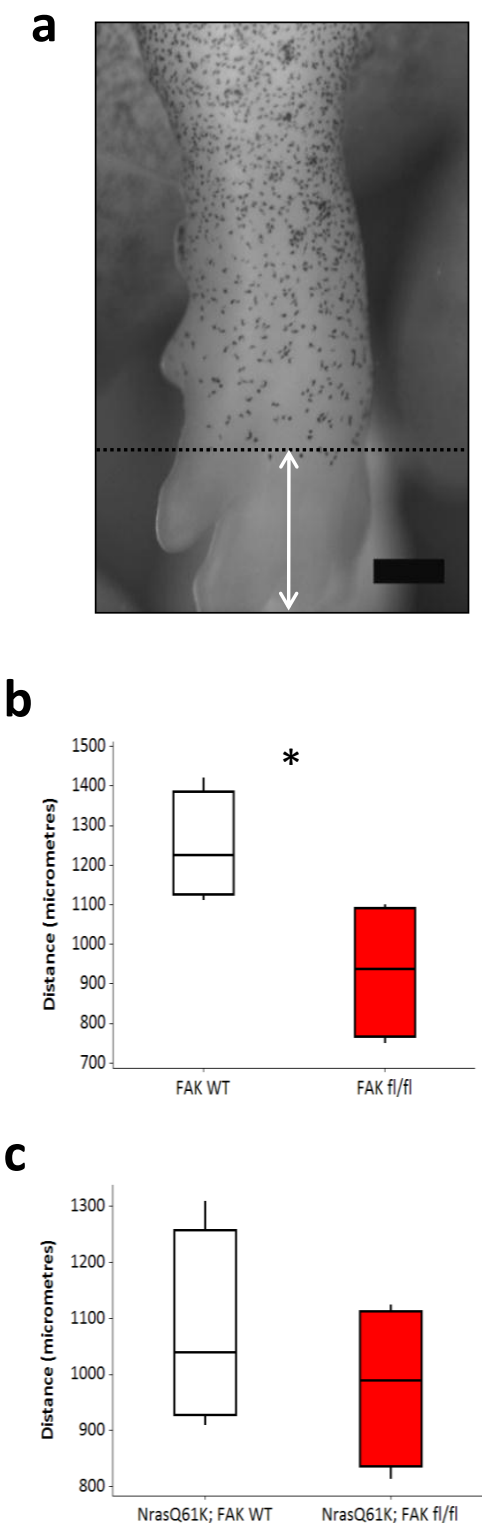

Figure 6.4 *Tyr::Cre FAK$^{fl/fl}$* mice have a deficit of melanoblast migration at E15.5
(a) Schematic picture showing method for quantification of melanoblast migration used in (b) and (c) (detailed in Figure 2.1c) **(b) (c)** Comparison of E15.5 melanoblast migration *wild-type* ('FAK WT', white bars) and *Tyr::Cre FAK$^{fl/fl}$* ('FAK fl/fl', red bars) mice (e), and also between *Tyr::Nras$^{Q61K/°}$; FAK$^{+/+}$* ('NrasQ61K; FAK WT', white bars) and *Tyr::Nras$^{Q61K/°}$; Tyr::Cre FAK$^{fl/fl}$* ('NrasQ61K; FAK fl/fl', red bars) mice (f). (b: *p =0.03; f: c =0.47; Mann-Whitney test, n=4) (Box and whiskers plots: boxes represent 25th-75th percentiles of given value, lines represent median values).

6.3 FAK disruption promotes a coat colour phenotype in *Tyr::Nras$^{Q61K/°}$* mice

Many mouse coat colour phenotypes resulting from genetically manipulated oncogenes have offered insights into melanomagenesis, notably including Kit (www.espcr.org/micemut, Berlin et al, 2012). In line with this, as well as the key role FAK has in normal cell physiology, we next investigated the health and phenotype of adult mice with melanocyte-specific *FAK* disruption.

Mice were interbred as described in the developmental analysis above, but this time omitting the *DCT-lacZ* reporter and allowing the mice to litter and age until ill health necessitated euthanisation. No change in coat colour or condition was detected for up to 12 months in experimental *Tyr::Cre FAK$^{fl/fl}$* mice when compared to *FAK$^{+/+}$* controls. However, a coat colour phenotype was noted from the age of 3 months when melanocyte-specific expression of the *Tyr::Nras$^{Q61K/°}$* transgene was combined with FAK deletion (Figure 6.5a). In detail, these *Tyr::Nras$^{Q61K/°}$; Tyr::Cre FAK$^{fl/fl}$* mice consistently exhibited glossier coats compared to *Tyr::Nras$^{Q61K/°}$; Tyr::Cre FAK$^{fl/+}$* mice and *Tyr::Nras$^{Q61K/°}$; Tyr::Cre FAK$^{+/+}$* controls (100% penetrance) (Figure 6.5a). While *Tyr::Nras$^{Q61K/°}$; Tyr::Cre FAK$^{+/+}$* and *Tyr::Nras$^{Q61K/°}$; Tyr::Cre FAK$^{fl/+}$* mice developed skin hypertrophy, blackening of skin, greying of hair, and hair loss from early adulthood, *Tyr::Nras$^{Q61K/°}$; Tyr::Cre FAK$^{fl/fl}$* mice persistently maintained a full healthy coat of black hair more characteristic of *wild-type* C57BL6 mice. Histological inspection and quantification of skin sections from *Tyr::Nras$^{Q61K/°}$; Tyr::Cre FAK$^{fl/fl}$* mice showed a reduction in tissue thickness and melanin deposition compared to *Tyr::Nras$^{Q61K/°}$; Tyr::Cre FAK$^{fl/+}$* mice (Figure 6.5b,c). In summary, endogenous FAK has an important role in melanocyte homeostasis when combined with oncogenic *Nras^{Q61K}*. Thus, divergent effects of endogenous FAK signalling in melanocyte homeostasis and development exist:

expression of oncogenic *Nras*^{Q61K} rescues the *FAK*$^{fl/fl}$ phenotypes of melanoblasts but can promote an adult coat colour phenotype not seen in *Tyr::Cre FAK*$^{fl/fl}$ mice alone.

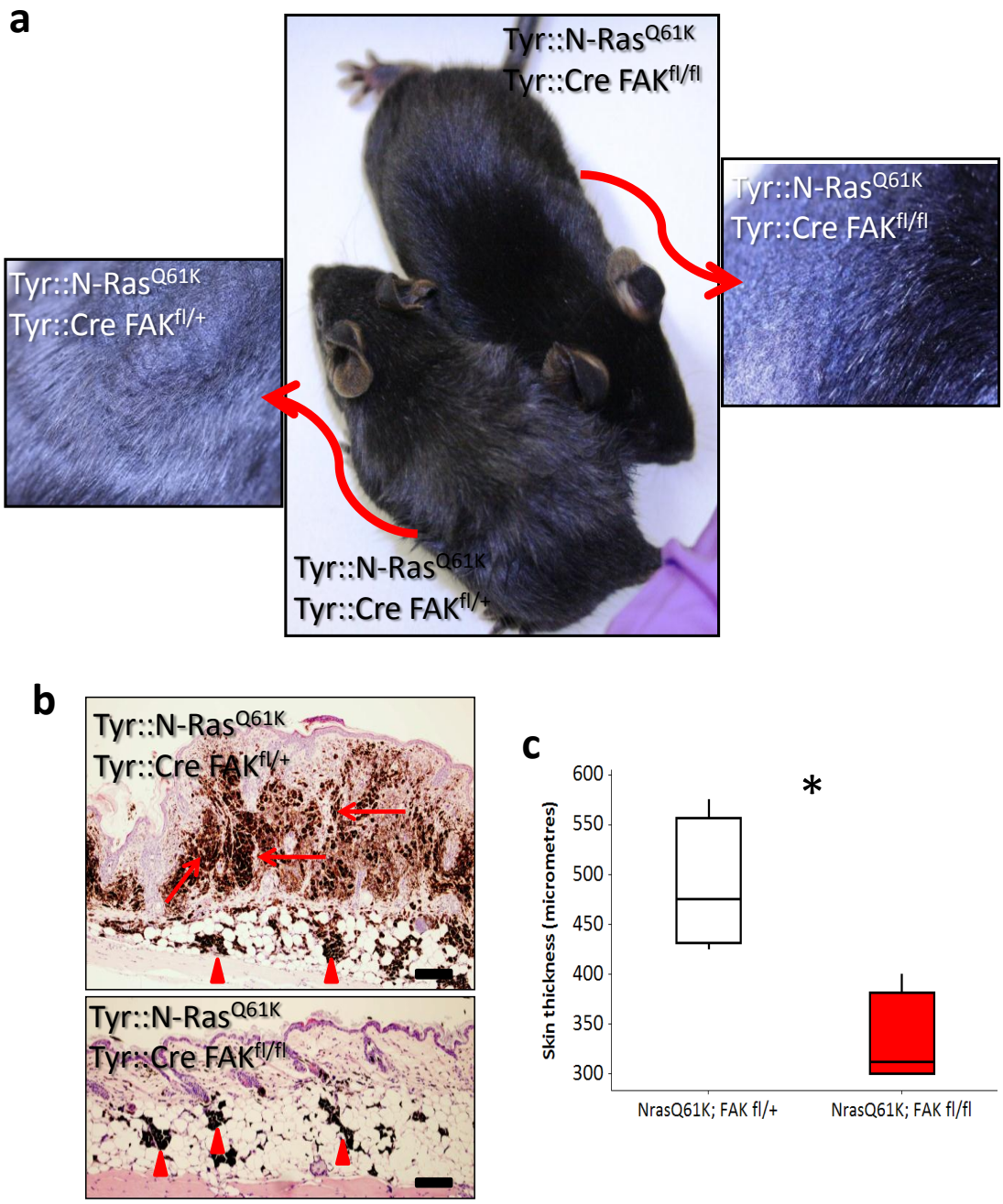

Figure 6.5 *FAK* disruption promotes a coat colour phenotype in *Tyr::Nras$^{Q61K/°}$* mice
(a) Coats of *Tyr::Nras$^{Q61K/°}$; Tyr::Cre FAK$^{fl/+}$* mice and *Tyr::Nras$^{Q61K/°}$; Tyr::Cre FAK$^{fl/fl}$* mice. Inserts show shaved area of back skin. **(b)** Photomicrographs (H&E) of back skin from the two genotypes represented in (a). Melanocytes and deposition of melanin in the dermis (red arrow) and adipose tissue (red arrowheads) are indicated (Scale bars=100µm). **(c)** Quantification of back skin thickness from epidermis to adipose tissue compared between *Tyr::Nras$^{Q61K/°}$; Tyr::Cre FAK$^{fl/+}$* (NrasQ61K; FAK fl/+', white bars) and *Tyr::Nras$^{Q61K/°}$; Tyr::Cre FAK$^{fl/fl}$* ('NrasQ61K; FAK fl/fl', red bars) mice (*p =0.012; Mann-Whitney test, n=4) (Box and whiskers plots: boxes represent 25th-75th percentiles of given value, lines represent median values).

6.4 Primary melanomagenesis is delayed by FAK deletion

Disruption of endogenous FAK has been shown to retard primary cancer formation and progression (McLean et al, 2004, Lahlou et al, 2007, Provenzano et al, 2008). Given our previous results combining *FAK* deletion with expression of oncogenic Nras, we crossed *Tyr::Cre FAK$^{fl/fl}$* and *Tyr::Cre FAK$^{fl/+}$* mice to the *Tyr::Nras$^{Q61K/°}$; INK4a$^{-/-}$* genetically modified model of metastatic malignant melanoma, assessing whether FAK may also be important for primary melanoma development and/or metastasis.

Having observed similar coat colour phenotypes between mice expressing one or two copies of *wild-type* FAK (described in section 6.3), we first confirmed that control *Tyr::Nras$^{Q61K/°}$; INK4a$^{-/-}$; Tyr::Cre FAK$^{fl/+}$* mice developed primary melanoma with a similar incidence and latency to that previously described with *Tyr::Nras$^{Q61K/°}$; INK4a$^{-/-}$* mice (Table 6.1; Figures 6.6a,b; Figure 3.1e and Table 3.1). As this was the case, it allowed us to continue our experiments efficiently, using littermate *Tyr::Nras$^{Q61K/°}$; INK4a$^{-/-}$; Tyr::Cre FAK$^{fl/+}$* controls to compare with our experimental *Tyr::Nras$^{Q61K/°}$; INK4a$^{-/-}$; Tyr::Cre FAK$^{fl/fl}$* mice.

No difference in incidence of primary melanomas between *Tyr::Nras$^{Q61K/°}$; INK4a$^{-/-}$; Tyr::Cre FAK$^{fl/+}$* mice and *Tyr::Nras$^{Q61K/°}$; INK4a$^{-/-}$; Tyr::Cre FAK$^{fl/fl}$* mice was observed (Table 6.1). Consistent with prior studies of FAK in genetically modified cancer models of other tumour types, we observed significant prolongation of melanoma onset when *FAK* was abrogated (median 167 days vs 113 days; p=0.0001) (Figure 6.6b, Table 6.1). This prolongation did not correlate with any difference in primary tumour burden between the two cohorts (Figure 6.6c).

We next derived cell lines from the primary melanomas of *Tyr::Nras$^{Q61K/°}$; INK4a$^{-/-}$* mice with *wild-type* FAK, *FAK$^{fl/+}$*, or *FAK$^{fl/fl}$*. Western Blotting performed at 8-10 passages in culture revealed FAK expression in *Tyr::Nras$^{Q61K/°}$; INK4a$^{-/-}$; Tyr::Cre FAK$^{fl/fl}$* mice comparable to that seen in *Tyr::Nras$^{Q61K/°}$; INK4a$^{-/-}$; FAK$^{+/+}$* mice (Figure 6.6d). This suggested there was a propensity for melanoma cell populations which have escaped conditional *FAK* deletion, as a result of the inherent inefficiencies of Cre recombinase technology in mouse modelling, to outgrow those with *FAK* deletion (see Sections 2.6.2 and 2.6.3). Further *in vitro* characterisation of endogenous FAK depletion in our mice was therefore precluded, and we alternatively investigated using IHC.

First, we confirmed with IHC that there was no *in vivo* outgrowth of *Tyr::Nras$^{Q61K/°}$; INK4a$^{-/-}$; Tyr::Cre FAK$^{fl/fl}$* melanomas by escaping populations of melanoma cells expressing *wild-type* FAK: FAK expression could not be visualised in *FAK$^{fl/fl}$* melanomas (Figure 6.6e). Preliminary IHC assessment showed enhanced proliferation at the invasive edge of FAK-depleted melanomas, although we were unable to effectively compare or quantify this observation with *Tyr::Nras$^{Q61K/°}$; INK4a$^{-/-}$; FAK$^{fl/+}$* controls given their saturation with melanin pigment (Figure 6.7). Tissue 'bleaching' of melanin pigment is a technique that can be employed in the future to characterise this result further and ensure an unbiased approach. Collectively, our findings suggest that, consistent with our results in melanocyte embryogenesis, *FAK* disruption can affect onset of primary melanoma driven by oncogenic Nras.

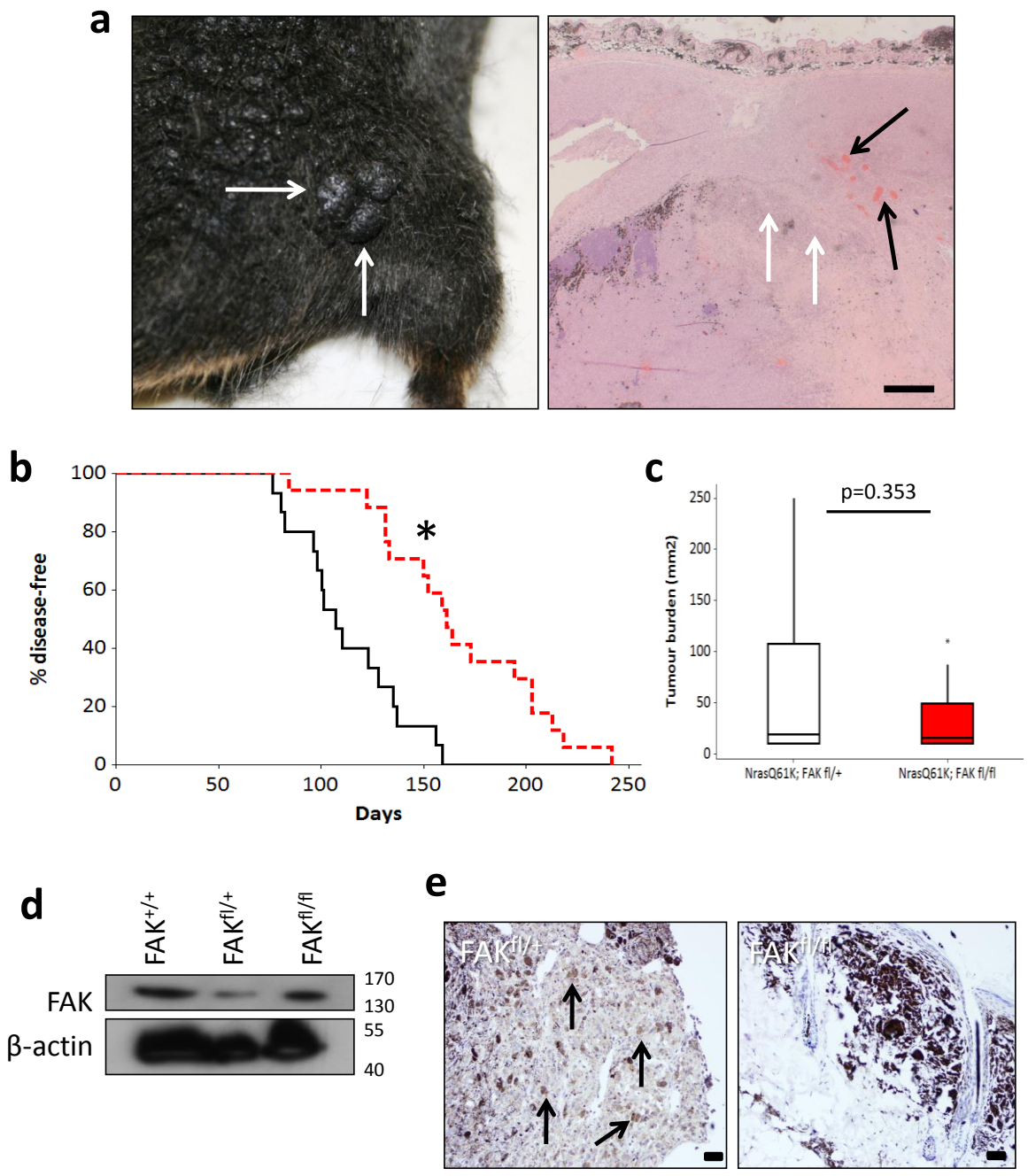

Figure 6.6 Primary melanomagenesis is delayed by FAK deletion
(a) Primary pigmented melanoma arising in *Tyr::Nras$^{Q61K/°}$; INK4a$^{-/-}$; Tyr::Cre FAK$^{fl/+}$* transgenic mice (white arrows). Accompanying photomicrograph (H&E) indicates muscle invasion (white arrows) as well as vascular involvement (black arrows) (Scale bars=500µm). **(b)** Kaplan-Meier analysis of primary melanoma latency between *Tyr::Nras$^{Q61K/°}$; INK4a$^{-/-}$; Tyr::Cre FAK$^{fl/+}$* (black line, n=15) and *Tyr::Nras$^{Q61K/°}$; INK4a$^{-/-}$; Tyr::Cre FAK$^{fl/fl}$* (red line, n=16) cohorts (*p=0.0001, log-rank test). **(c)** Comparison of primary melanoma tumour burden between *Tyr::Nras$^{Q61K/°}$; INK4a$^{-/-}$; Tyr::Cre FAK$^{fl/+}$* (NrasQ61K; FAK fl/+', white bars, n=15) and *Tyr::Nras$^{Q61K/°}$; INK4a$^{-/-}$; Tyr::Cre FAK$^{fl/fl}$* ('NrasQ61K; FAK fl/fl', red bars, n=16) mice (p =0.353; Mann-Whitney test) (Box and whiskers plots: boxes represent 25th-75th percentiles of given value, lines represent median values). **(d)** Western blots illustrating endogenous expression of FAK in melanoma cell lines derived from *Tyr::Nras$^{Q61K/°}$; INK4a$^{-/-}$* vs *Tyr::Nras$^{Q61K/°}$; INK4a$^{-/-}$; Tyr::Cre FAK$^{fl/+}$* vs *Tyr::Nras$^{Q61K/°}$; INK4a$^{-/-}$; Tyr::Cre FAK$^{fl/fl}$* mice **(e)** Photomicrographs of adult mouse melanomas immunohistochemically labelled against FAK. Black arrows indicate FAK upregulation (brown staining) in control *Tyr::Nras$^{Q61K/°}$; INK4a$^{-/-}$; Tyr::Cre FAK$^{fl/+}$* melanomas, not observed in the *Tyr::Nras$^{Q61K/°}$; INK4a$^{-/-}$; Tyr::Cre FAK$^{fl/fl}$* cohort. Black melanin pigment is clearly distinct from brown Fak staining (Scale bars = 100µm; n=4).

Genotypes	Number of Mice with Primary Melanoma	Number of Metastatic Mice	Mean time till primary melanoma (days)	Mean time from melanoma to death (days)	Mean Survival (days)
Tyr::Nras$^{Q61K/°}$; INK4a$^{-/-}$; FAK$^{fl/+}$	15/16	8/15	113	76	182
Tyr::Nras$^{Q61K/°}$; INK4a$^{-/-}$; FAK$^{fl/fl}$	16/19	9/16	167	44	198
			p=0.0001	**p=0.03**	**p=0.166**

Table 6.1 *FAK* deletion delays melanoma onset but increases disease aggressiveness following melanoma onset
Table comparing numbers and melanoma parameters of mice within *Tyr::Nras$^{Q61K/°}$; INK4a$^{-/-}$; Tyr::Cre FAK$^{fl/+}$* and *Tyr::Nras$^{Q61K/°}$; INK4a$^{-/-}$; Tyr::Cre FAK$^{fl/fl}$* cohorts suffering from primary and metastatic melanoma. (Chi-square test used for primary and metastatic melanoma incidence, log-rank test to compare survival and melanoma onset).

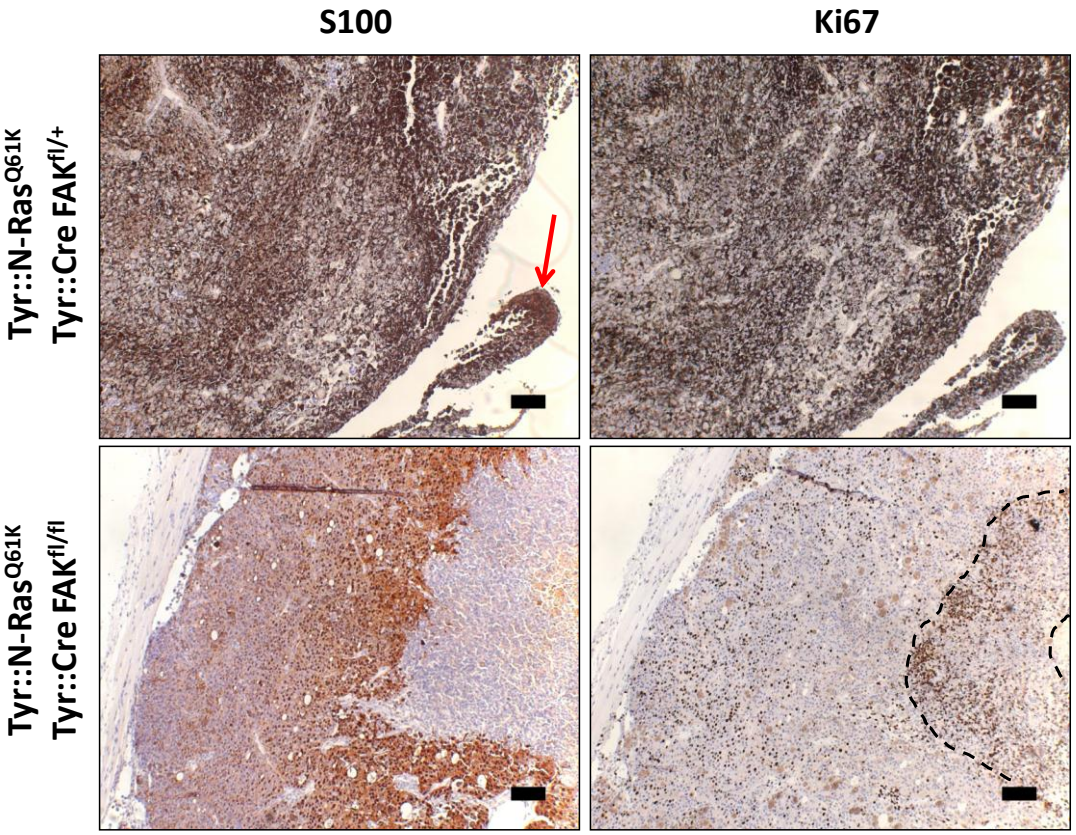

Figure 6.7 Enhanced proliferation occurs at the invasive edge of FAK-deleted melanomas
Photomicrographs of adult mouse melanomas immunohistochemically labelled against the melanocyte marker S100 or proliferative marker Ki67. Saturation with melanin pigment precluded clear analysis of *Tyr::Nras$^{Q61K/°}$; INK4a$^{-/-}$; Tyr::Cre FAK$^{fl/+}$* melanomas, although melanoma cell presence was confirmed (brown staining, red arrow). This one *Tyr::Nras$^{Q61K/°}$; INK4a$^{-/-}$; Tyr::Cre FAK$^{fl/fl}$* melanoma was less pigmented, showing clear S100 upregulation (brown staining) as well as enhanced Ki67 at the invasive edge of tumour (black interrupted line) (Scale bars = 100µm; n=1).

6.5 Metastatic and invasive melanoma is promoted by FAK deletion

An ambivalent picture is described in reports characterising the role of FAK in human cancer, with both pro-tumourigenic and tumour suppressive roles suggested. Of interest, although studies of primary cancers predominantly suggest a pro-tumourigenic role for FAK, reduction in FAK expression has been noted in human metastatic tissue compared to a matched sample of primary adenocarcinoma (Ayaki et al, 2001). Cell biology studies of invasion and survival have also shown an inhibitory effect of FAK in certain contexts (Schaller et al, 2004, Zheng et al, 2009, Sandilands et al, 2011).

In chapter 3, our control *Tyr::Nras$^{Q61K/°}$; INK4a$^{-/-}$* mice developed visceral melanotic lesions in line with the initial report describing this model (31% of cases; Figures 6.8a,b), offering an opportunity for seamless *in vivo* analysis of FAK between primary and metastatic tumours. We therefore continued our mouse breeding until sufficient data were available to assess the effect of *FAK* ablation on melanoma metastasis.

In contrast to our primary melanoma results, *Tyr::Nras$^{Q61K/°}$; INK4a$^{-/-}$; Tyr::Cre FAK$^{fl/fl}$* mice showed a clear propensity to deteriorate rapidly after they had developed primary melanoma (median 44 days vs 76 days; p=0.03) (Figure 6.8c, Table 6.1), despite there being no difference in number of mice affected by metastases between the two cohorts (Table 6.1). These results are consistent with the findings and paradoxical mechanism reported by Zheng and colleagues, whereby loss of FAK promotes tumour cell invasion in the context of Ras signalling (Zheng et al, 2009). Moreover, this acceleration of invasion and metastases precluded any overall survival benefit offered by prolongation of primary tumour onset when *FAK* is deleted (median 198 days vs 182 days; p=0.166) (Figure 6.8d, Table 6.1). IHC performed so far has shown proliferating malignant cells in the brain

lesions of both FAK-depleted and *FAK*$^{fl/+}$ controls (Figure 6.9a). The limited number of lung metastases seen in experimental *Tyr::Nras*$^{Q61K/°}$*; INK4a*$^{-/-}$*; FAK*$^{fl/fl}$ mice has so far precluded comparison with the proliferation observed in heterozygous controls (Figure 6.9b). Taken together, our results confirm a paradoxical and biphasic role for FAK in tumourigenesis: pro-oncogenic in the context of primary tumour onset, and tumour suppressive following development of primary melanoma. The mechanisms behind this have yet to be fully delineated.

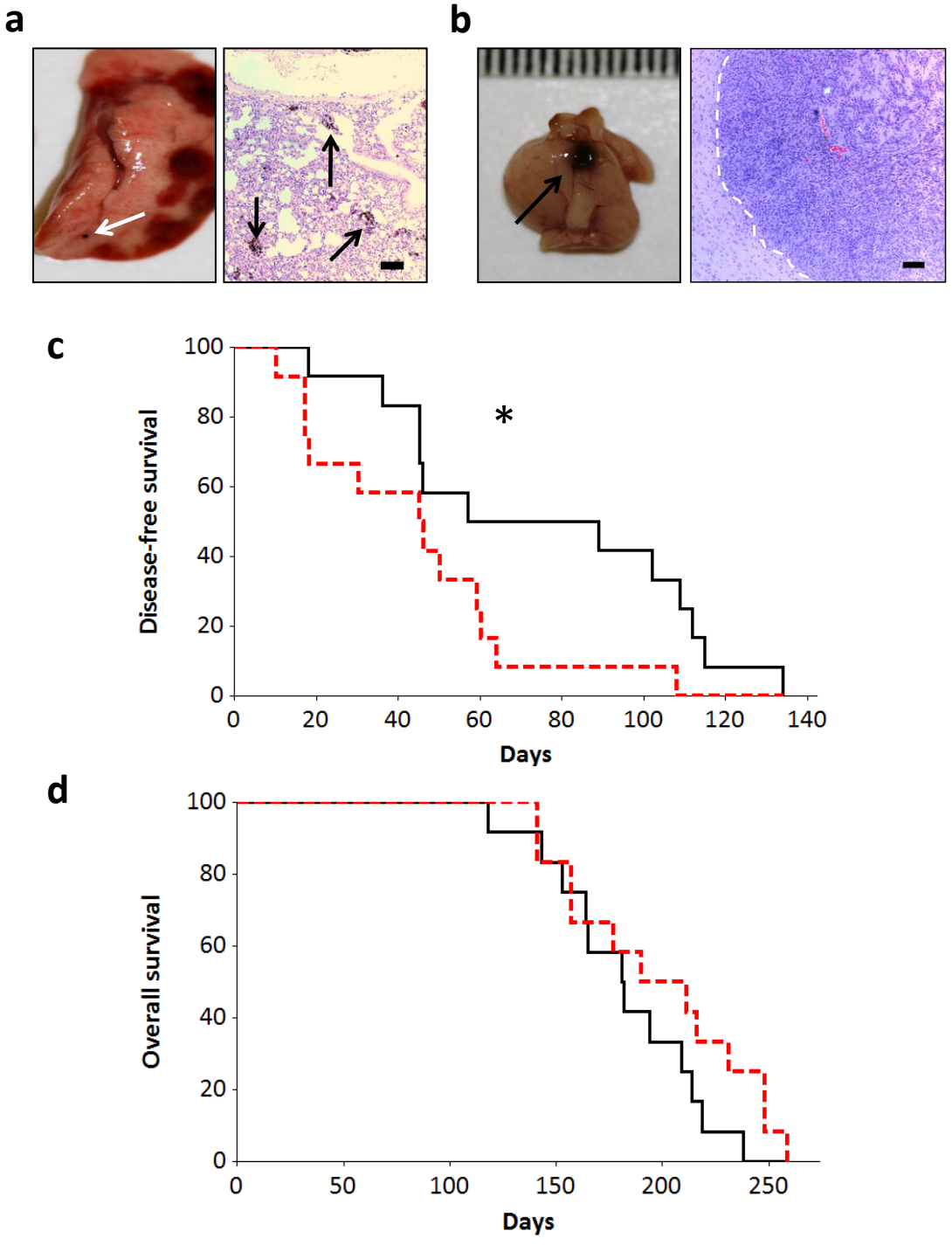

Figure 6.8 Metastatic and invasive melanoma is promoted by FAK deletion
(a) Representative picture showing typical metastatic pigmented melanoma (white arrow) arising in lungs of *Tyr::Nras$^{Q61K/°}$; INK4a$^{-/-}$* transgenic mice with both FAK genotypes. Accompanying photomicrograph (H&E) shows multiple pigmented lung lesions (black arrows) (Scale bars=100µm). **(b)** Representative picture showing typical pigmented brain lesion (black arrow) arising in *Tyr::Nras$^{Q61K/°}$; INK4a$^{-/-}$* transgenic mice with both *FAK* genotypes. Accompanying photomicrograph (H&E) shows clear demarcation between normal brain and tumour (white interrupted line) (Scale bars=100µm). **(c)** Kaplan-Meier analysis of time from onset of primary melanoma till death from melanoma. *Tyr::Nras$^{Q61K/°}$; INK4a$^{-/-}$; Tyr::Cre FAK$^{fl/+}$* (black line, n=12) and *Tyr::Nras$^{Q61K/°}$; INK4a$^{-/-}$; Tyr::Cre FAK$^{fl/fl}$* (red line, n=12) cohorts were compared (*p=0.03, log-rank test). **(d)** Kaplan-Meier analysis of overall survival: time from birth till death from melanoma. *Tyr::Nras$^{Q61K/°}$; INK4a$^{-/-}$; Tyr::Cre FAK$^{fl/+}$* (black line, n=12) and *Tyr::Nras$^{Q61K/°}$; INK4a$^{-/-}$; Tyr::Cre FAK$^{fl/fl}$* (red line, n=12) cohorts were compared (p=0.166, log-rank test).

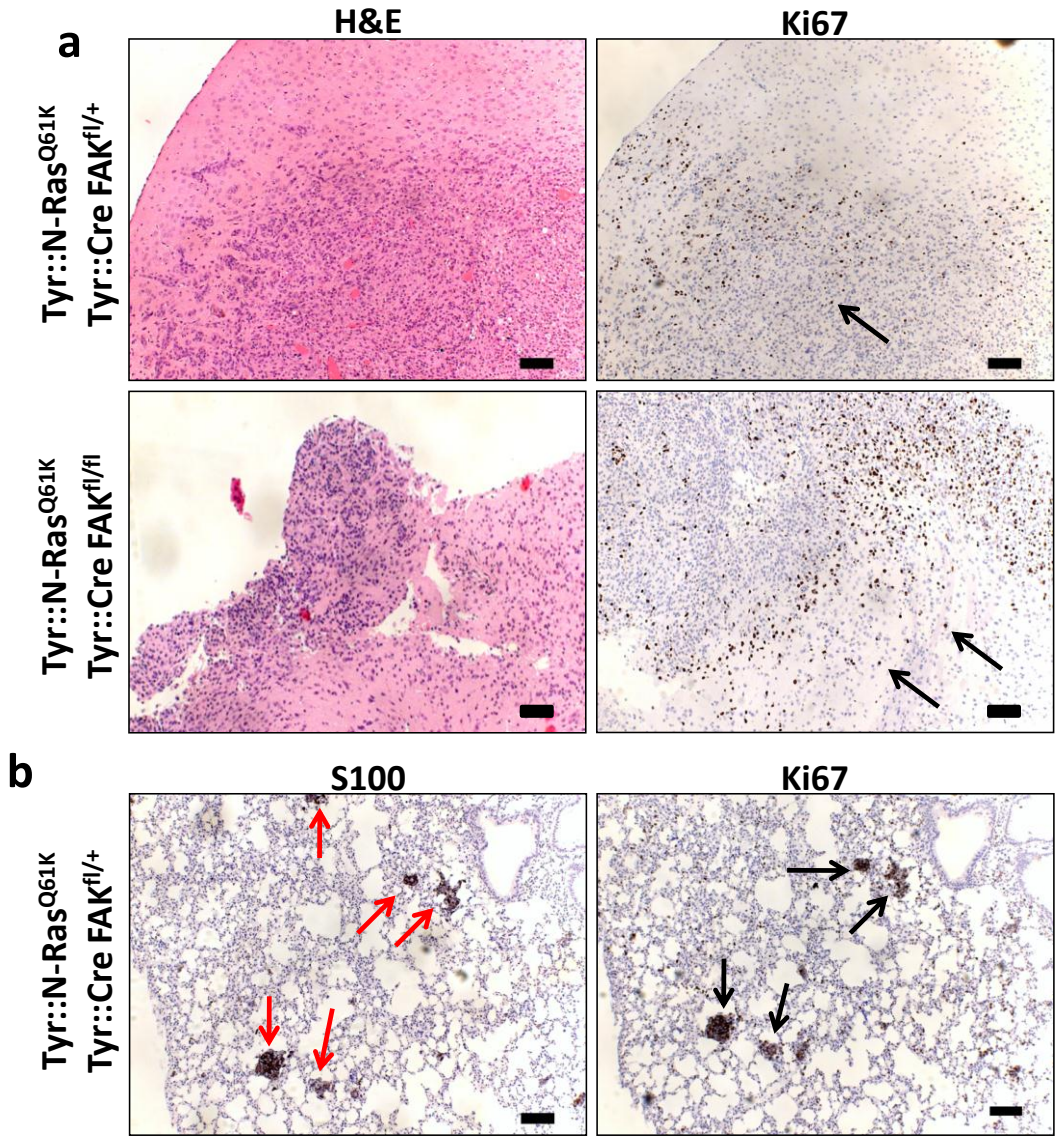

Figure 6.9 Increased invasion occurs in melanomatous brain lesions of FAK *wild-type* and FAK-depleted mice

Photomicrographs of adult mouse melanoma lesions in brain (a) and lungs (b): H&E, or immunohistochemically labelled against the melanocyte marker S100 or the proliferative marker Ki67. **(a)** Ki67 upregulation in *Tyr::Nras$^{Q61K/°}$; INK4a$^{-/-}$; Tyr::Cre FAK$^{fl/+}$* and *Tyr::Nras$^{Q61K/°}$; INK4a$^{-/-}$; Tyr::Cre FAK$^{fl/fl}$* brain lesions (black arrows) (Scale bars = 100µm; n=4) **(b)** Lung metastases (red arrows) seen in control *Tyr::Nras$^{Q61K/°}$; INK4a$^{-/-}$; FAK$^{fl/+}$* mice exhibited proliferation (black arrows) concordant with S100 expression (red arrows) (Scale bars = 100µm; n=4).

6.6 Summary

Here we describe a tumour suppressor function of FAK for the first time using genetically modified mouse models of cancer. This chapter is analysed and discussed in greater detail in Sections 7.2.1 and 7.2.2.

In summary, we have shown divergent functions for endogenous FAK in both a physiological and pathophysiological context. In normal murine physiology, *FAK* disruption compromises melanoblast cell numbers in development, but has no long-term effect on melanocyte homeostasis (Figures 6.1 and 6.5). Combined expression of oncogenic Nras with FAK deletion apparently reverses these effects, promoting a rescue of the embryonic cell number deficit and an adult coat colour phenotype not seen in *Tyr::Cre FAK$^{fl/fl}$* mice alone (Figures 6.1 and 6.5). Finally and most importantly, FAK signalling promotes primary tumour formation but slows development of invasion and metastases in a *Tyr::Nras$^{Q61K/°}$; INK4a$^{-/-}$* murine model of melanoma (Figures 6.6 and 6.8). These final cancer results support the cell biology hypothesis that downregulation of FAK initially diminishes its pro-survival function to delay primary melanoma onset, but eventually primary melanoma cells will form and become more migratory as a consequence of their reduced focal adhesions to the extra-cellular matrix (Schultze et al, 2010). This is discussed further in Section 7.2.1.

Mechanistic experiments in our study have again contended the orthodoxy that key similarities often exist between the molecular machinery involved in melanoblast and melanoma signalling (see section 1.1.5 for more detail). Genetic ablation of *FAK* impaired melanoblast cell numbers, reflecting the delayed onset of primary melanomas seen in *Tyr::Nras$^{Q61K/°}$; INK4a$^{-/-}$; Tyr::Cre FAK$^{fl/fl}$* mice (Figures 6.1 and 6.6). However, a divergent role for FAK in motility was revealed by the contrasting effect of inhibition of melanoma

invasion and metastasis compared to its limited effect on melanoblast migration observed in *DCT-lacZ* mice expressing *Tyr::Nras*$^{Q61K/^{\circ}}$ (Figures 6.4 and 6.8).

Another noteable result from these experiments was that E15.5 expression of oncogenic Nras did not significantly increase melanoblast cell numbers relative to wild-type embryos, suggesting that any hyper-proliferative effect induced by Nras^{Q61K} occurs following birth: this contrasts with the non-significant increase in melanocyte numbers observed in Braf^{V600E}-expressing embryos (Figure 5.2a and 6.3). Given the coat colour phenotype we have described in adult *Tyr::Nras*$^{Q61K/^{\circ}}$*; Tyr::Cre FAK*$^{fl/fl}$ mice, it is tempting to speculate that FAK ablation induces its phenotype in mice only once melanocyte numbers have increased to an undefined post-natal threshold in response to Nras^{Q61K} expression.

In conclusion, this chapter contends a context-dependent role for FAK as both a tumour promoter and tumour suppressor in cancer. Our experiments provide stringent preclinical validation of a role for FAK in melanoma using informative genetically defined mouse models that recapitulate common human mutations. The biological and structural complexity of FAK likely confers the variable functions described in this study (see sections 1.5.2 and 7.2.1). We suggest considerable thought must be given to the appropriate clinical application of FAK inhibitors in the medium to long-term (discussed in detail in section 7.2.2).

Chapter 7

Discussion

The end of each results chapter offers a synopsis of results accumulated for each topic. Rather than re-iterate these, this discussion aims to dissect some key questions that have arisen from the data in each chapter, with reference to what further investigations could be applied in the future.

7.1 P-REX1

7.1.1 Study relevance

Possibly the most surprising aspect of endogenous P-Rex1 loss in our analysis is its capacity to induce such profound phenotypes. P-Rex1 is only one of approximately 70 Dbl-GEFs which can activate a host of Rho-GTPases, yet there is no question of any functional redundancy in the case of melanoma (Rossmann et al, 2005). In fact, it has been identified on at least two occasions for its striking functional contribution in other contexts, both physiological and cancer-specific (Welch et al, 2002, Sosa et al, 2010). In this study, metastases within the context of $Nras^{Q61K}$-driven melanoma are largely reliant on P-Rex1, despite the mutational drift and diversity of signalling you might expect at this stage. Other signalling molecules that can induce such striking phenotypes include Atf2 and Ikkb, deletion of which nearly abrogated melanoma using similar *in vivo* models (Shah et al, 2010, Yang et al, 2010).

In explanation of this biological impact, it seems likely that P-Rex1 can contribute to the metastatic phenotype outside of its activation of Rac-mediated invasion; there have been suggestions of alternative cancer-specific functions for P-Rex1 in this thesis as well as another report, but nothing that has fully been characterised as yet (Montero et al, 2010). For instance, a role for P-Rex1 in proliferation has been implicated on a number of occasions here: melanoblast cell number differences, secondary growth following TV-injection, and the *Tyr::Cre* $Rac^{fl/fl}$*; P-Rex1*$^{-/-}$ double knockout phenotype (Figure 3.3h,

Figure 4.6, Figure 4.10). Although our results in *Tyr::Cre Rac$^{fl/fl}$; P-Rex1$^{-/-}$* embryos might suggest that endogenous P-Rex1 can only exert significant proliferative effects when Rac1 is disrupted, the non-significant trend towards secondary growth observed after TV-injection of P-Rex1$^{+/+}$ melanocytes raises the prospect that this process might become Rac-independent in cancer (Figure 3.3h). This possibility is supported by one of the P-Rex1 breast cancer studies, which showed a decrease in Rac-GTP that was far less pronounced than the deficit of proliferation induced by P-Rex1 siRNA interference; consistent with our study, no increase in apoptosis was seen in breast cancer cells when P-Rex1 was abrogated (Montero et al, 2010).

The P-Rex1 cancer phenotype is also significant when one considers the biological complexity of metastasis, which requires the co-ordinated spatiotemporal activation of a multitude of signalling pathways for its different steps: local invasion, intravasation, vascular migration, extravasation, and colonisation (detailed in Figure 1.3). P-Rex1 might have been expected to be an insignificant part of this process, but our results suggest that its abrogation can exploit the fragility and inefficiency of the metastatic process (Fidler, 1970).

7.1.2 Braf^{V600E} and P-Rex1

A significant finding in this thesis was that the pro-metastatic effect of endogenous P-Rex1 in Nras^{Q61K}-driven mouse melanoma was not matched by any cancer phenotype in Braf^{V600E}-driven models. This is despite a common upregulation of MAPK signalling by both models (Dhomen et al, 2009, Dankort et al, 2009). This result could be explained by biological nuances of P-Rex1 signalling, or deficiencies of the Braf^{V600E} model used for this study. Biological explanations include:

1. *P-Rex1 expression.* As shown by comparison of Figure 3.5a with Figure 5.1 (immunoblots from both figures were performed together), P-Rex1 upregulation in human *BRAF* mutant melanoma cell lines is not as marked as in cell lines expressing mutant *NRAS* or with neither mutation. Review of our microarray data did not support this finding, suggesting there was no difference in P-Rex1 intensity levels between melanoma cell lines with $Nras^{Q61}$ (WM852, WM1366, Lyse, Gerlach) or $Braf^{V600E}$ (the majority of other cell lines) (Figure 3.4). However, there remains a possibility that the lack of a phenotype in the $Braf^{V600E}$-driven model could therefore represent a threshold effect, whereby P-Rex1 can only exert its pro-tumourigenic effects at a certain level of upregulation. The first step in delineating this further will be more detailed analyses of P-Rex1 protein and RNA levels in cell lines expressing mutant Braf or Nras.

2. *Alternative Rac-GEFs.* Other Rac-GEFs have been implicated in melanomagenesis and cancer (Uhlenbrock et al, 2004, Sanz-Moreno et al, 2008, Minard et al, 2004, Fernandez-Zapico et al, 2005, Patel et al, 2007). It is therefore likely that more RacGEFs will feature in melanoma than are presently reported, perhaps suggesting that alternative RacGEFs could compensate for P-Rex1 depletion in $Braf^{V600E}$-driven cancer. Neutrophil studies have already suggested a relative reciprocity and functional redundancy of P-Rex1 function with another Rac-GEF, Vav (Mayeenuddin et al, 2006).

3. *Endogenous $Braf^{V600E}$.* The potential effect of P-Rex1 levels mentioned above may be modulated by the relative expression of *$Tyr::Nras^{Q61K/+}$* and *$Tyr::CreER\ Braf^{V600E}$* in the two mouse models. Transgenic expression of $Nras^{Q61K}$ in the first model will likely simulate its ectopic expression in melanoma, whereas expression of $Braf^{V600E}$ in the second model was designed to reflect its endogenous expression. Direct activation of

P-Rex1 by PI(3)K signalling (downstream of $Nras^{Q61K}$) was described on its discovery, and it has also been highlighted as a downstream target for ERK signalling (Welch et al, 2002, Shields et al, 2007). However the relative quantities and patterns of differential inputs required to induce a functional effect of P-Rex1 is less clear.

4. *Synergistic activation of P-Rex1.* The direct synergistic activation of P-Rex1 by both PIP_3 and Gßγ was described in its initial characterisation (Welch et al, 2002). At present, we are unaware of the biochemical nature of the interaction between MAPK signalling and P-Rex1 (Shields et al, 2007). It may also be the case that synergy of inputs from MAPK and PI(3)K effectors are what is necessary to induce a phenotypically meaningful effect of endogenous P-Rex1 in melanoma: this is more likely to be provided by the *Tyr::Nras$^{Q61K/°}$* model, as opposed to the *Tyr::CreER Braf^{V600E}* which retains *PTEN* heterozygosity.

5. *Alternative Braf^{V600E} mouse.* This $Braf^{V600E}$-driven mouse used in this study was not the same as that in which metastases were reported with *PTEN* ablation: the relative expression of $Braf^{V600E}$ in these mice is unreported (Dhomen et al, 2009, Dankort et al, 2009).

Despite the plausibility of these factors above, it also should be acknowledged that study of P-Rex1 is not optimal in the *Tyr::CreER Braf^{V600E}* model for the following reasons:

1. *Primary tumour removal.* Under UK home office guidelines, many mice required euthanisation for overgrowth or ulceration of their primary melanomas prior to looking unwell. In this context, metastases may not have had sufficient time to occur. The issue of primary tumour removal is detailed in the introduction (Section 1.3.1.2)

and may become necessary for further *in vivo* studies of P-Rex1-facilitated metastases: the short-term difficulty of optimising such a technique would likely be outweighed by the benefit of having a model that can directly reflect the clinical course of melanoma in humans (Francia et al, 2011).

2. *Limited metastatic detail.* In line with the previous description of what is required from an optimal melanoma mouse model (Section 1.3.1.2), a criticism of the *Tyr::CreER* $Braf^{V600E/+}$*;* $Pten^{lox/lox}$ model described by Dankort and colleagues is the limited metastatic detail offered (Dankort et al, 2009). 100% LN metastases are reported, along with an unspecified number of lung metastases. However, normal populations of melanocytes have frequently been described in mice and human lymph nodes, a possibility which would confound this analysis (Otsuka et al, 1998, Gupta et al, 2005). In contrast to the *Tyr::*$Nras^{Q61K/°}$ mouse report, no qualification for this possibility was mentioned. For this reason, LNs were excluded from our metastatic analysis of both $Nras^{Q61K}$- and $Braf^{V600E}$-driven models, and our results may have been more striking if we had not done this.

3. *Limited mouse numbers.* Breeding of this cohort was particularly difficult given the limited life expectancy of *Tyr::CreER* $Braf^{V600E/+}$*;* $PTEN^{lox/lox}$*;* $P\text{-}Rex1^{-/-}$ mice useful for deriving a population of heterozygous $PTEN^{lox/+}$progeny (Figure 5.6a). Our analysis was therefore limited to only 7 mice in the experimental *Tyr::CreER* $Braf^{V600E/+}$*;* $PTEN^{lox/+}$*;* $P\text{-}Rex1^{-/-}$ cohort.

The potential lack of relevance for P-Rex1 in $Braf^{V600E}$-driven melanoma has important translational implications: therapeutic inhibition of P-Rex1 may not have an effect in this context. In this era of personalised medicine, such a finding can improve the efficiency of

early phase clinical trial design, whilst potentially improving the clinical outcomes and toxicity profiles of its participants (de Bono et al, 2010).

7.1.3 *Tyr::Cre Rac$^{fl/fl}$; P-Rex1$^{-/-}$* mice

Although the proliferative defect contributing to the *Tyr::Cre Rac$^{fl/fl}$; P-Rex1$^{-/-}$* coat colour phenotype is mentioned above (section 7.1.1), we have not yet speculated which Rho-GTPase might be employed to stimulate this phenotype in the absence of Rac1. Two other isoforms of Rac (Rac2 and Rac3) can be stimulated by P-Rex1 in other cell types, including neutrophils and neurones (Welch et al, 2005, Yoshizawa et al, 2005). However, the dominant Rac isoform in cells of the melanocyte lineage is Rac1, suggesting that an alternative Rho-GTPase may be responsible for this effect (Uhlenbrock et al, Sci 2004, Sanz-Moreno et al, 2008, Laura Machesky, personal communication).

RhoG is possibly the most likely candidate for P-Rex1 interaction. This Rho-GTPase is the most structurally similar to Rac, and has been shown to co-operate with Rac for induction of cell transformation (Roux et al, 1997). Moreover, there are distinct regulatory and functional similarities between P-Rex1 and Vav proteins, which have been characterised as the predominant GEFs required for RhoG activation (Samson et al, 2010, Lawson et al, 2011). One of our main future aims in the laboratory will therefore be to assess the possibility of a novel RhoG activation by P-Rex1. *Tyr::CreER Rac$^{fl/fl}$* melanocytes have been derived from our mice models and can readily be assessed for RhoG and its interaction. The functional consequences of P-Rex1 interference in the presence or absence of Rac can also be further dissected *in vitro*.

7.1.4 Translation

The vast majority of small molecule inhibitors in existing preclinical and clinical development target the tyrosine kinase activity of a given protein, but this strategy is clearly inappropriate in the case of P-Rex1. Targeting a new class of compound can be unappealing to large pharmaceutical companies, who usually have a massive library of potential inhibitors of a given target available to perform high-throughput screens. However, this approach often ends in failure, and more adventurous pharmaceutical-academic collaborations are vital to improve the current low success rate in translational drug development.

P-Rex1 and other GEFs represent a novel challenge in drug development, but one that has already been shown not to be insurmountable (Vigil et al, 2010, Mardilovich et al, 2012). Development of small molecules targeted against P-Rex1 has recently begun (Heidi Welch, personal communication). The great hope is that GEF targeting in different cancer contexts could be applicable to all tumours driven by Ras. This thesis and other studies have demonstrated several features of P-Rex1 signalling which should be considered in the development of any putative P-Rex1 inhibitors (Figure 7.1):

1. *Cytostatic potential.* The introduction to this thesis highlights the clinical difficulties involved in confirming efficacy of an inhibitor considered to be an 'anti-metastatic' (Section 1.2.2). In short, we do not currently have a clinical trial framework in the UK that can optimise the potential of such agents. Thus the additional cytostatic potential of a P-Rex1 inhibitor, most strikingly demonstrated by the Rac-independent proliferative deficit observed in *Tyr::Cre* $Rac^{fl/fl}$*; P-Rex1*$^{-/-}$ embryos, creates a more appealing therapeutic prospect.

2. *Patient selection.* Strategies for inhibiting Ras have been a perennial therapeutic challenge (Flaherty et al, 2006). Our findings suggest that targeting P-Rex1 signalling might have great relevance to melanomas driven or co-driven by oncogenic Nras: a significant subset who have very limited treatment options (Heidorn et al, 2010). In breast cancer, Sosa and collegues have clearly shown a specificity of P-Rex1 in ER (+/- HER2) positive disease (Sosa et al, 2010). Finally, prostate cancer studies of P-Rex1 have suggested it is derepressed by HDAC inhibition, and thus might be a negative predictor of efficacy in this treatment context: the upregulation of P-Rex1 here appears to confound the hypothesis that HDAC inhibitors would confer efficacy through derepression of TSGs alone (Wong et al, 2011).

3. *Therapeutic window.* The lack of P-Rex1 expression in most other normal human cell types offers a clear therapeutic window and basis for selective inhibition (Welch et al, 2002, de Bono et al, 2010). In combination with the possibilities of patient selection described above, this treatment window offers potential to improve patient outcomes and toxicity, as well as expedite the clinical trial process.

4. *Targeting the DH domain.* Figure 3.8 provides preliminary evidence that targeting the catalytic DH domain of P-Rex1 may be the most effective strategy for therapeutic intervention. In fact the dominant negative effect observed suggests it may have a more beneficial effect than ablating P-Rex1 altogether. This result dovetails nicely with our invasion assays in Figure 3.7, which show that ectopic expression of the GEF-dead P-Rex1 mutant did not match the invasion observed with ectopic P-Rex1. An important future aim will be to ascertain the mechanism(s) responsible for the dominant-negative effect of the P-Rex1 GEF-dead mutant.

5. *Pharmacodynamics.* A downstream readout of biological P-Rex1 suppression is necessary for putative inhibitors, acting as a surrogate or intermediate endpoint by which early clinical trials may be expedited. Rac is the predominant biomarker which might fulfil this role, although one wonders if RhoG or another Rho-GTPase may add value given the Rac-independent role of P-Rex1 discussed in sections 7.1.1 and 7.1.3.

6. *Rac targeting.* A cursory assessment of P-Rex1 might incorrectly suggest that its effects can be straightforwardly diminished by Rac inhibitors, which are already in clinical development. There are a number of reasons why this is not the case. First, we have shown and discussed that P-Rex1 has significant Rac-independent effects that will likely contribute to a cancer phenotype. Second, Rac is ubiquitously expressed in human cells, and thus its inhibition could induce significant toxicity whilst assessing for a narrow therapeutic window. Finally, Rac can also regulate the actin cytoskeleton in a manner that minimises invasion of melanoma cells, thus suggesting it can act as an anti-metastatic which should not be inhibited in some contexts (Uhlenbrock et al, 2004). Taken together, the invasive character of Rac is GEF-dependent and does not mimic all the phenotypic features of P-Rex1: upstream control by an inhibitor of P-Rex1 with a large therapeutic window seems a more desirable option.

a

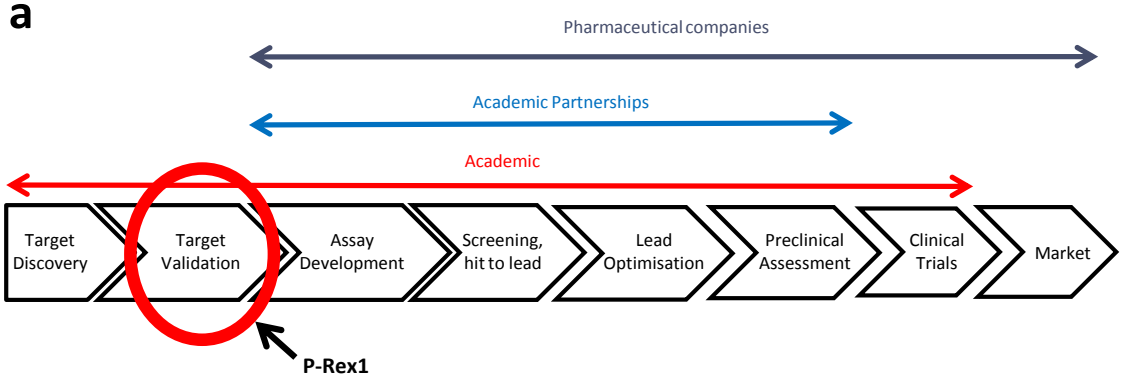

b

Target	V	A	D	T	S
P-Rex1	●	●	●	●	●

Validation; Assay; Druggability; Toxicity; Structure-based drug design

Figure 7.1 The drug discovery cascade and P-Rex1
(a) Reminder of drug development cascade described in Figure 1.4 **(b)** Common traffic lights system applied for consideration of potential novel drug targets. Red, amber or green dots are estimated by myself, and suggest suitability of a given target for each respective category. Validation ('V') suggests how well characterised P-Rex1 has been as an anticancer target. Assay ('A') describes feasibility of developing an *in vitro* assay for large scale assessment of P-Rex1. Druggability ('D') conveys whether the target class of P-Rex1 (ie GEFs) is known and whether there are inhibitors developed against that class. Toxicity ('T') shows potential for selective inhibition of P-Rex1, thereby reducing side-effects. Structure-based drug design suitability ('S') describes the limited structural knowledge we currently have of P-Rex1.

Finally, it is also worth noting that Figure 3.4 and Tables 3.3/3.4 in chapter 3 also reveal detail of the potential of P-Rex1 as a prognostic biomarker in melanoma. For instance, microarray revealed that P-Rex1 levels above the median ('high' P-Rex1) were 100% statistically sensitive for the detection of metastatic melanoma. It is tempting to speculate that 'low' P-Rex1 detected in the biopsy of a patient with newly-diagnosed primary melanoma could therefore exclude the possibility of metastases and guide treatment accordingly. Similarly, we also showed that 'low' P-Rex1 was 100% statistically specific for excluding primary melanoma: this could be of clinical use for excluding melanoma in a suspected skin lesion. Even in the absence of a P-Rex1 inhibitor, this sort of biomarker assessment could straightforwardly be incorporated in any melanoma clinical trial.

7.2 FAK

7.2.1 Study relevance

One of the key advances in our FAK study has been consolidation and tempero-spatial clarification of the disparate reports describing the role of FAK in tumourigenesis, something that would likely not have been elucidated without the use of genetically modified mouse models (Fujii et al, 2004, Lark et al, 2005, Giaginis et al, 2009, Gabriel et al, 2009, Tavernier-Tardy et al, 2009, Schmitz et al, 2005, Theocharis et al, 2003, Furuyama et al, World J Surg 2006, Gabriel et al, 2006). Our results also support the cell biology hypothesis that downregulation of FAK might permit primary melanoma cells to become more migratory by reducing their focal adhesions to the extra-cellular matrix (Schultze et al, 2010).

The structural and biological complexities of FAK help explain its myriad roles within normal cell physiology as well as tumourigenesis (detailed in Section 1.5.2). Multiple FAK tyrosine phosphorylation residues have been identified and implicated in regulation of its kinase activity, with a number of serine phosphorylation residues also implicated in its function (Zheng et al, 2009). In addition to its physiological responses to integrin signalling, FAK mediates downstream signalling of common cancer-associated receptors such as the platelet-derived growth factor receptor (PDGFR), epidermal growth factor receptor (EGFR) and vascular endothelial growth factor receptor (VEGFR) (Garces et al, 2006, Sieg et al, 2000).The four-point-one, ezrin, radixin, moesin (FERM) domain of FAK is pivotal to this control of downstream signalling and its upstream biological responses. It has key roles in regulation of FAK kinase activity, FAK auto-inhibition, and sub-cellular localisation of FAK mediated by scaffolding interactions (Frame et al, 2010). The variable nature of FAK function described in this study would likely be clarified further by systemic

investigation of the differential roles FAK plays in response to a number of factors including: upstream receptor signalling, phosphorylation status, kinase/scaffold activity, and sub-cellular localisation.

Future studies will focus on confirming a mechanism for the tumour suppressive capacity of FAK in melanoma, as well as establishing a definitive human relevance to the mouse data compiled so far. The divergent role of FAK in $Nras^{Q61K}$- driven melanoma could be explained by a cell line study which revealed a mechanism for a paradoxical pro-migratory role of FAK depletion in the context of Ras signalling: one initial step in our project will therefore be to confirm whether this mechanism also applies to our animal model results (Zheng et al, 2009).

7.2.2 Translation

In contrast to our analysis of P-Rex1, the analysis of FAK here is an example of the benefits of re-iterative research promoted in the introductory chapter (Section 1.4.1). The heterogeneous nature of FAK signalling suggests there is a need for considerable detailed thought to be given to the application of clinical FAK inhibition. Presently there are a number of ATP-competitive FAK small molecule inhibitors being tested in early phase clinical trials, with no clear clinical activity identified in initial results from four years ago (Siu et al, 2008). It is prescient that a final report of these data are still awaited at a time when an edition of the British Medical Journal scrutinised the pharmaceutical industry's compliance with the mandatory reporting of clinical trial results (Prayle et al, 2012).

Our results suggest a clinical investigator should always consider common upstream receptor signalling mechanisms of a patient's cancer before intervening with FAK

inhibition. For instance, our study shows that abrogation of FAK would be inappropriate and could accelerate metastases in patients with melanoma driven by $Nras^{Q61K}$, a finding that might extend to all patients with cancer driven by Ras signalling (Zheng et al, 2009, Lu et al, 2001). On a preclinical level, more investigation is required to delineate how scaffold vs kinase FAK activity can modulate its role in survival, proliferation, and migration; targeting the kinase activity of FAK may not always be an appropriate strategy, and characterisation of the tumourigenic relevance of FAK biochemistry will assist in the generation of a new generation of 'smarter' FAK small molecule inhibitors (Siesser et al, 2006).

7.3 Working towards improved mouse models

This section uses our experience of the various mouse models described in this thesis to document the practical advantages and limitations of each technique. I hope that this might serve as a useful reference for other researchers to plan their potential experiments.

7.3.1 $Nras^{Q61K}$ versus $Braf^{V600E}$ mouse models

Despite their mutual signalling through the MAPK pathway, these are two markedly different mouse models which carry relative advantages and disadvantages. Table 7.1 details the merits and limitations of each model, but two general rules are worth considering before a choice is made:

1. *Primary versus metastatic melanomagenesis*. In our hands, *Tyr::Nras$^{Q61K/°}$; INK4a$^{-/-}$* mice have been a useful metastatic model with limited value for primary melanoma study, whereas the *Tyr::CreER Braf$^{V600E/+}$; PTEN$^{lox/+}$* mice offer an excellent platform for primary melanoma analyses but rarely succumb to metastases.

2. *Additional allograft/xenograft studies*. These are likely necessary to complement and detail a metastatic result uncovered using the *Tyr::Nras$^{Q61K/°}$; INK4a$^{-/-}$* model: for instance, to detail whether a deficit of metastases may have occurred after the intravasation stage or before. In contrast, primary melanomagenesis assessed using the *Tyr::CreER Braf$^{V600E/+}$; PTEN$^{lox/+}$* does not necessarily require a further cell line injection study.

Varying levels of pigmentation between the two models can also cause practical difficulties, although nothing that is insurmountable (Table 7.1).

Mouse Model System	Advantages	Disadvantages
Tyr::Nras$^{Q61K/°}$; INK4a$^{-/-}$	• Good metastatic model with appropriate organ spread. • Characteristic human mutations. • Pigmented, mets easily assessed on dissection. • Rare euthanisation for primary tumour outgrowth: allows mets to develop. • Cell lines easily derived.	• Limited value as primary tumour model: multiple tiny tumours grow, rather than single discrete lesions. • Pigmentation precludes immunofluorescence, IHC achieved with difficulty. • *INK4a$^{-/-}$* prompts lymphoma in some mice, require exclusion from cohort and increased mouse numbers.
Tyr::CreER Braf$^{V600E/+}$; PTEN$^{lox/+}$	• Inducible, temperospatial control. • Excellent primary tumour model: initiation, growth and ulceration easily assessed. • Characteristic human mutations. • Little pigmentation: straightforward IHC and immunofluorescence possible. • Healthy mice, no other illnesses.	• Rare metastases, primary tumour resection likely required: frequent euthanisation for primary tumour outgrowth precludes metastases. • Little pigmentation: mets not easily assessed on dissection. • Cell lines not derived easily

Table 7.1 Relative merits and limitations of the two main genetically modified mouse models of melanoma analysed in this thesis.

7.3.2 Allografts/xenografts

A key advance in this thesis is the characterisation of P-Rex1 in animal models of cancer which recapitulate the common human genetics of the disease. Prior P-Rex1 cancer studies have shown an effect on both primary tumour growth and LN metastases using xenotransplantation of human cancer cell lines into immunodeficient mice (Qin et al, 2009, Sosa et al, 2010, Montero et al, 2010). However this technique often fails to

recapitulate the characteristics of the original tumour they are meant to represent, and their use for informative studies of novel cancer target validation has become increasingly contentious (see Section 1.3.1.4) (Becher et al, 2006, Sausville et al, 2006).

Despite this criticism, this thesis argues there is still a role for allograft and xenograft study, particularly in the context of metastasic melanoma where we still do not have a genetically modified mouse model that can recapitulate its different stages fully. It has recently been recommended that metastatic melanoma research should involve two animal models, with genetically modified models complementing traditional xenograft analyses: our experience here suggests that this is broadly correct, except we believe xenografts (or allografts) must be utilised for validation and delineation *after* initial characterisation using a genetically valid model (Sethi et al, 2011). For instance, our P-Rex1 results in *Tyr::Nras*$^{Q61K/°}$*; INK4a*$^{-/-}$ mice was validated using TV allograft injections to further define the nature of the P-Rex1 effect on metastases (Figure 3.3); this allowed us to bypass the potential time-limitation and technical difficulty involved in primary tumour removal. A xenograft study would likely have complemented our results this way too.

7.3.3 Improved assessment of melanoma parameters

The importance of conscientious and efficient documentation of melanoma parameters is highlighted in the introduction to this thesis (Section 1.3.1.2). Measurement of metastases and propensity for metastases should routinely occur in a manner that can accurately reflect what might occur in a human clinical trial. Our experience in this thesis has evolved to include increasing amounts of melanoma detail in chapters 5 and 6:

- *Primary melanoma.* Standard practice should record time of induction (if applicable), time of onset, anatomical site, rate of growth, ulceration, and size at which ulceration

occurs. Survival measures may not be of particular use if otherwise healthy mice only require euthanisation because of their primary tumour burden. The dermal localisation of most mouse melanoma precludes assessment of Breslow thickness for metastatic propensity, although a practiced pathologist could alternatively offer information about mitotic rate.

- *Metastic Melanoma.* Standard practice should record anatomical sites on dissection, and survival measures from birth, induction (if applicable), and tumour onset. Our FAK analysis demonstrated the benefits of these different survival analyses, offering biologically relevant results with the measurement of survival from tumour onset that would not have been elicited had survival been measured from birth alone. CT or CT-PET offer the best means of recording metastatic site, number, and size, although thorough assessment of these measures with dissection and histological analysis can provide a less costly alternative. As discussed earlier, potential LN lesions should be interpreted with caution, and excluded if there is any doubt between malignancy and benign overgrowth.

7.3.4 Embryonic models

With our analyses of P-Rex1 and FAK, this thesis both reaffirms and challenges the conventional wisdom that embryonic phenotypes can simulate cancer-specific events: whereas a reduction in metastasis with P-Rex1 ablation is mirrored by a deficit of MB migration, the increased invasion observed with FAK depletion was not apparent on embryonic assessment. It is easy to speculate that the likely reality is somewhere in between: embryonic migratory detail offers excellent information about potential mechanisms of melanoma metastases, but by itself is not sufficient as a tool for cancer assessment.

We have utilised two reporter models for embryonic assessment of P-Rex1 and FAK, *DCT-lacZ* mice and mice carrying the *Z/EG* double reporter transgene (Mackenzie et al, 1997, Novak et al, 2000, Mort et al, 2010). Again, the use of both can validate and further delineate initial results, and in this case we would suggest that the relative values of each model make them inter-changeable for embryonic assessment (Table 7.2).

In our analysis, a lack of cell death observed using a 6 hour timelapse of GFP-expressing melanoblasts often is assumed to indicate that a cell number difference (perhaps elicited using the *DCT-lacZ* model) might be accounted for by a proliferative impairment or enhancement. The limitations of cell death assessment over such a small timeframe are obvious, although the characteristic resistance to cell death in cells of the MC lineage supports this method (Gray-Schopfer et al, 2007). In addition, we would concede that our methods in our embryonic assessment of the *Tyr::Cre* $Rac^{fl/fl}$*; P-Rex1*$^{-/-}$ coat cannot exclude the possibility of a large amount of early MB death.

For assessment of melanoblast migration, our techniques and analyses have evolved over the past three years. The live imaging offered by use of the *Z/EG* double reporter remains a near gold standard for migratory assessment, albeit over a potentially limited timeframe. However, these GFP-expressing mice are often beset by delays such as breeding difficulty, poor litter sizes, and limited microscope availability: *DCT-lacZ* mice can therefore offer a worthy and straightforward alternative. Our migration assays in *DCT-lacZ* mice have measured both cell numbers at the distal point of MB migration (Figures 2.1a,b), and distances from the end of the forepaw to the 5th last melanoblast (Figure 2.1c). It might be reasoned that the former migratory analysis is limited by concerns regarding cell-cell interactions if a phenotype also reveals an alteration of cell numbers. With P-Rex1-null mice, we reasoned that the cell number method could straightforwardly

be justified by the clear belly spot and forepaw melanoblast migration difference represented in Figure 4.1 and Figure 4.3. Moreover, we were latterly able to confirm this migratory difference using the *Z/EG* reporter mice (Figure 4.5c,d). However, FAK mice have no belly phenotype and we have not yet been able to assess its phenotype in GFP-expressing melanoblasts: we therefore concluded that it was more appropriate to use the *DCT-lacZ* analysis of distance (Figure 2.1c), in an effort to exclude potential confounding cell-cell interactions conferred by the cell number deficit elicited (Figure 6.4).

Finally, it should be noted that the processes of cell division and cell migration cannot be completely uncoupled using the migration and cell number assays covered in this thesis. For this reason, the precise temperospatial functions of around 80 genes implicated in melanocyte development remain largely uncharacterised (Lamoreux et al, 2010). Recent efforts to mathematically model murine melanoblast distribution have shown that their rate of proliferation in the dermis is similar to their rate of migration from the dermis to epidermis (Luciani et al, 2011). To minimise this potential limitation in this thesis, our aim was to assess each given phenotype using all the assays and reporter models described in Sections 2.1 and 2.2, thereby consolidating any initial findings with an alternative assay.

Embryo Model System	Advantages	Disadvantages
DCT-lacZ	• Good litter sizes, breed well • Straightforward staining method • Visualisation of whole anatomy • Single cell detail possible • Migration and cell numbers assessable • Simple microscopy	• Limited tempero-spatial detail, 'snapshots' of each timepoint used to make deductions.
Z/EG	• Excellent tempero-spatial information allows assay of distance, speed, and cell numbers. • Information on cell death available. • Confocal microscopy reveals excellent single cell morphological detail.	• Breed poorly, small litters • Precarious and expensive technique, improves with experience. • Limited anatomy visualised • Confocal microscope availability can be difficult, low throughput.

Table 7.2 Relative merits and limitations of the two melanoblast reporter mice analysed

Bibliography

Ackermann, J., M. Frutschi, et al. (2005). “Metastasizing melanoma formation caused by expression of activated N-RasQ61K on an INK4a-deficient background.” Cancer Res **65**: 4005-11.

Adameyko, I., F. Lallemend, et al. (2009). “Schwann cell precursors from nerve innervation are a cellular origin of melanocytes in skin.” Cell **139**(2): 366-79.

Auerbach, R., W.C. Lu, et al. (1987). “Specificity of adhesion between murine tumor cells and capillary endothelium: an in vitro correlate of preferential metastasis in vivo.” Cancer Res **47**(6): 1492-6.

Ayaki, M., K. Komatsu, et al. (2001). “Reduced expression of focal adhesion kinase in liver metastases compared with matched primary human colorectal adenocarcinomas.” Clin. Cancer Res **10**: 3106-12.

Backman, S.A., V. Stambolic, et al. (2001). “Deletion of Pten in mouse brain causes seizures, ataxia and defects in soma size resembling Lhermitte-Duclos disease.” Nat Genet **29**(4): 396-403.

Balch, C.M., S.J. Soong, et al. (2001). “Prognostic factors analysis of 17,600 melanoma patients: validation of the American Joint Committee on Cancer melanoma staging system.” J Clin Oncol **19**(16): 3622-34.

Balch, C.M., J.E. Gershenwald, et al. (2009). “Final version of 2009 AJCC melanoma staging and classification.” J Clin Oncol **27**(36): 6199-206.

Barber, M.A., S. Donald, et al. (2007). "Membrane translocation of P-Rex1 is mediated by G protein betagamma subunits and phosphoinositide 3-kinase." J Biol Chem **282**: 29967-76.

Bardeesy, N., B.C. Bastian, et al. (2001). "Dual inactivation of RB and p53 pathways in RAS-induced melanomas." Mol Cell Biol **21**(6): 2144-53.

Barkan, D., J.E., Green, et al. (2010). "Extracellular matrix: a gatekeeper in the transition from dormancy to metastatic growth." Eur J Cancer **46**(7): 1181-8.

Baselga, J., V. Semiglazov, et al. (2009). "Phase II randomized study of neoadjuvant everolimus plus letrozole compared with placebo plus letrozole in patients with estrogen receptor-positive breast cancer." J Clin Oncol **27**(16): 2630-7.

Baselga, J., M. Campone, et al. (2012). "Everolimus in postmenopausal hormone-receptor-positive advanced breast cancer." N Engl J Med **366**(6): 520-9.

Bastian, B.C., M. Kashani-Sabet, et al. (2000). "Gene amplifications characterize acral melanoma and permit the detection of occult tumor cells in the surrounding skin." Cancer Res **60**(7): 1968-73.

Bauer, J., P. Büttner, et al. (2011). "BRAF mutations in cutaneous melanoma are independently associated with age, anatomic site of the primary tumor, and the degree of solar elastosis at the primary tumor site." Pigment Cell Melanoma Res **24**(2): 345-51.

Becher, O.J. and E.C. Holland. (2006). "Genetically engineered models have advantages over xenografts for preclinical studies." Cancer Res **66**(7): 3355-8.

Bentires-Alj, M., M. I. Kontaridis, et al. (2006). “Stops along the RAS pathway in human genetic disease.” Nature Medicine **12**: 283-5.

Ben-Yaacov, S., R. Le Borgne, et al. (2001). “Wasp, the Drosophila Wiskott-Aldrich syndrome gene homologue, is required for cell fate decisions mediated by Notch signaling.” J Cell Biol. **8;152**(1): 1-13.

Berlin, I., F. Luciani, et al. (2012). “General strategy to analyse coat colour phenotypes in mice.” Pigment Cell Melanoma Res **25**(1): 117-9.

Böhm, M., G. Moellmann, et al. (1995). “Identification of p90RSK as the probable CREB-Ser133 kinase in human melanocytes.” Cell Growth Differ **6**(3): 291-302.

Boissy, R.E. and J.J. Nordlund. (1997). “Molecular basis of congenital hypopigmentary disorders in humans: a review.” Pigment Cell Res **10**(1-2): 12-24.

Bokoch, G.M. (1995). Regulation of the phagocyte respiratory burst by small GTP-binding proteins. Trends Cell Biol **5**(3): 109-13.

Brito, F.C. and L. Kos. (2008). “Timeline and distribution of melanocyte precursors in the mouse heart.” Pigment Cell Melanoma Res **21**(4): 464-70.

Broekaert, S.M., R. Roy, et al. (2010). “Genetic and morphologic features for melanoma classification.” Pigment Cell Melanoma Res **23**(6): 763-70.

Broome Powell, M., P.R. Gause, et al. (1999). “Induction of melanoma in TPras transgenic mice.” Carcinogenesis **20**(9): 1747-53.

Calalb, M.B., T.R. Polte, et al. (1995). “Tyrosine phosphorylation of focal adhesion kinase at sites in the catalytic domain regulates kinase activity: a role for Src family kinases.” Mol Cell Biol **15**(2): 954-63.

Campbell, P.J., S. Yachida, et al. (2010). “The patterns and dynamics of genomic instability in metastatic pancreatic cancer.” Nature **467**(7319): 1109-13.

Carretero-Ortega, J., C.T. Walsh, et al. (2010). “Phosphatidylinositol 3,4,5-triphosphate-dependent Rac exchanger 1 (P-Rex-1), a guanine nucleotide exchange factor for Rac, mediates angiogenic responses to stromal cell-derived factor-1/chemokine stromal cell derived factor-1 (SDF-1/CXCL-12) linked to Rac activation, endothelial cell migration, and in vitro angiogenesis.” Mol Pharmacol **77**(3): 435-42.

Cary, L.A., J.F. Chang, et al. (1996). “Stimulation of cell migration by overexpression of focal adhesion kinase and its association with Src and Fyn.” J Cell Sci **109**(Pt 7): 1787-94.

Chambers, A.F., I.C. MacDonald, et al. (1995). “Steps in tumor metastasis: new concepts from intravital videomicroscopy.” Cancer Metastasis Rev **14**(4): 279-301.

Chapman, P.B., A. Hauschild, et al. (2011). “Improved survival with vemurafenib in melanoma with BRAF V600E mutation.” N Engl J Med **364**(26): 2507-16.

Chen, H.C., P.A. Appeddu, et al. (1996). “Phosphorylation of tyrosine 397 in focal adhesion kinase is required for binding phosphatidylinositol 3-kinase.” J Biol Chem **271**(42): 26329-34.

Chin, L., J. Pomerantz, et al. (1997). “Cooperative effects of INK4a and ras in melanoma susceptibility in vivo.” Genes Dev **11**(21): 2822-34.

Chin, L., G. Merlino, et al. (1998). “Malignant melanoma: modern black plague and genetic black box.” Genes Dev **12**(22): 3467-81.

Cohen, C., A. Zavala-Pompa, et al. (2002). “Mitogen-actived protein kinase activation is an early event in melanoma progression.” Clin Cancer Res **8**(12): 3728-33.

Cooper, L.A., T.L. Shen, et al. (2003). “Regulation of focal adhesion kinase by its amino-terminal domain through an autoinhibitory interaction.” Mol Cell Biol **23**(22): 8030-41.

Coterett, S., and J. Chernoff. (2002). “The evolutionary history of effectors downstream of Cdc42 and Rac.” Genome Biol **3**(2): REVIEWS0002.

Curtin, J.A., K. Busam, et al. (2006). “Somatic activation of KIT in distinct subtypes of melanoma.” J Clin Oncol **24**(26): 4340-6.

Damsky, W.E. Jr and M. Bosenberg. (2010). “Mouse melanoma models and cell lines.” Pigment Cell Melanoma Res **23**(6): 853-9.

Damsky, W.E., D.P. Curley, et al. (2011). “β-catenin signaling controls metastasis in Braf-activated Pten-deficient melanomas.” Cancer Cell **20**(6): 741-54.

Dankort, D., D.P Curley, et al. (2009). “Braf(V600E) cooperates with Pten loss to induce metastatic melanoma.” Nat Genet **41**(5): 544-52.

Davies, H., G.R. Bignell, et al. (2002). “Mutations of the BRAF gene in human cancer.” Nature **417**(6892): 949-54.

de Bono, J.S. and A. Ashworth. (2010). “Translating cancer research into targeted therapeutics.” Nature **467**(7315): 543-9.

Delmas, V., S. Martinozzi, et al. (2003). “Cre-mediated recombination in the skin melanocyte lineage.” Genesis **36**(2): 73-80.

Demunter, A., M. Stas, et al. (2001). “Analysis of N- and K-ras mutations in the distinctive tumor progression phases of melanoma.” J Invest Dermatol **117**(6): 1483-9.

De Vries, E., J.W. Coebergh. (2005). “Melanoma incidence has risen in Europe.” BMJ **331**(7518): 698.

Dhawan, P., A.B. Singh, et al. (2002). “Constitutive activation of Akt/protein kinase B in melanoma leads to up-regulation of nuclear factor-kappaB and tumor progression.” Cancer Res **62**(24): 7335-42.

Dhomen, N., J.S. Reis-Filho, et al. (2009). “Oncogenic Braf induces melanocyte senescence and melanoma in mice.” Cancer Cell **15**(4): 294-303.

Dhomen, N., S. Da Rocha Dias, et al. (2010). “Inducible expression of (V600E) Braf using tyrosinase-driven Cre recombinase results in embryonic lethality.” Pigment Cell Melanoma Res **23**(1): 112-20.

Ding, L., M.J. Ellis, et al. (2010). “Genome remodelling in a basal-like breast cancer metastasis and xenograft.” Nature **464**(7291): 999-1005.

Donald, S., K. Hill, et al. (2004). “P-Rex2, a new guanine-nucleotide exchange factor for Rac.” FEBS Lett **572**(1-3): 172-6.

Dong, X., Z. Mo, et al. (2005). “P-Rex1 is a primary Rac2 guanine nucleotide exchange factor in mouse neutrophils.” Curr Biol **15**(20): 1874-9.

Dovey, M., R.M. White, et al. (2009). Oncogenic NRAS co-operates with p53 loss to generate melanoma in zebrafish.” Zebrafish **6**: 397-404.

Dunty, J.M., V. Gabarra-Niecko, et al. (2004). “FERM Domain Interaction Promotes FAK Signaling.” Mol Cell Biol **24**(12): 5353–5368.

Eisen, T., T. Ahmad, et al. (2006). “Sorafenib in advanced melanoma: a Phase II randomised discontinuation trial analysis.” Br J Cancer **95**(5): 581-6.

Elwood, J.M. and J. Jopson. (1997). “Melanoma and sun exposure: an overview of published studies.” Int J Cancer **73**(2): 198-203.

Fernandez-Zapico, M.E., N. C. Gonzalez-Paz, et al. (2005). “Ectopic expression of VAV1 reveals an unexpected role in pancreatic cancer tumorigenesis.” Cancer Cell **7**(1): 39-49.

Fidler, I.J. (1970). “Metastasis: guantitative analysis of distribution and fate of tumor embolilabeled with 125 I-5-iodo-2'-deoxyuridine.” J Natl Cancer Inst **45**(4): 773-82.

Fidler, I.J. and S. Lieber. (1972). "Quantitative analysis of the mechanism of glucocorticoid enhancement of experimental metastasis." Res Commun Chem Pathol Pharmacol **4**(3): 607-13.

Fine, B., C. Hodakoski, et al. (2009). "Activation of the PI3K pathway in cancer through inhibition of PTEN by exchange factor P-REX2a." Science **325**(5945): 1261-5.

Flaherty, K.T. (2006). "Chemotherapy and targeted therapy combinations in advanced melanoma." Clin Cancer Res **12**: 2366s-2370s.

Flaherty, K.T., I. Puzanov, et al. (2010). "Inhibition of mutated, activated BRAF in metastatic melanoma." N Engl J Med **363**(9): 809-19.

Fonar, Y. and D. Frank. (2011). "FAK and WNT Signaling: The Meeting of Two Pathways in Cancer and Development." Anticancer Agents Med Chem **11**(7): 600-6.

Fong, P.C., D.S. Boss, et al. (2009). "Inhibition of poly(ADP-ribose) polymerase in tumors from BRCA mutation carriers." N Engl J Med **361**(2): 123-34.

Frame, M.C., H. Patel, et al. (2010). "The FERM domain: organizing the structure and function of FAK." Nat Rev Mol Cell Biol **11**(11): 802-14.

Francia, G., W. Cruz-Munoz, et al. (2011). "Mouse models of advanced spontaneous metastasis for experimental therapeutics." Nat Rev Cancer **11**(2): 135-41.

Freedberg, D.E., S.H. Rigas, et al. (2008). "Frequent p16-independent inactivation of p14ARF in human melanoma." J Natl Cancer Inst **100**(11): 784-95.

Fujii, T., K. Koshikawa, et al. (2004). “Focal adhesion kinase is overexpressed in hepatocellular carcinoma and can be served as an independent prognostic factor.” J Hepatol **41**(1): 104-11.

Furuta, Y., D. Ilic, et al. (1995). “Mesodermal defect in late phase of gastrulation by a targeted mutation of focal adhesion kinase, FAK.” Oncogene **11**(10): 1989-95.

Furuyama, K., R. Doi, et al. (2006). “Clinical significance of focal adhesion kinase in resectable pancreatic cancer.” World J Surg **30**(2): 219-26.

Gabriel, B., A. zur Hausen, et al. (2006). “Weak expression of focal adhesion kinase (pp125FAK) in patients with cervical cancer is associated with poor disease outcome.” Clin Cancer Res **12**(8): 2476-83.

Gabriel, B., A. Hasenburg, et al. (2009). “Expression of focal adhesion kinase in patients with endometrial cancer: a clinicopathologic study.” Int J Gynecol Cancer **19**(7): 1221-5.

Garces, C.A., E.V. Kurenova, et al. (2006). “Vascular endothelial growth factor receptor-3 and focal adhesion kinase bind and suppress apoptosis in breast cancer cells.” Cancer Res **66**(3): 1446-54.

Garcia-Cruz, A., A. Flórez, et al. (2009). “Observational cross-sectional study comparing Breslow thickness of melanoma arising from naevi and melanoma de novo.” Br J Dermatol **161**(3): 700-2.

Giaginis, C.T., S. Vgenopoulou, et al. (2009). “Expression and clinical significance of focal adhesion kinase in the two distinct histological types, intestinal and diffuse, of human gastric adenocarcinoma.” Pathol Oncol Res **15**(2): 173-81.

Goel, V.K., A.J. Lazar, et al. (2006). "Examination of mutations in BRAF, NRAS, and PTEN in primary cutaneous melanoma." J Invest Dermatol **126**(1): 154-60.

Goel, V.K., N. Ibrahim, et al. (2009). "Melanocytic nevus-like hyperplasia and melanoma in transgenic BRAFV600E mice." Oncogene **28**(23): 2289-98.

Golubovskaya, V.M., M. Zheng, et al. (2009). "The direct effect of focal adhesion kinase (FAK), dominant-negative FAK, FAK-CD and FAK siRNA on gene expression and human MCF-7 breast cancer cell tumorigenesis." BMC Cancer **9**: 280.

Gopal, Y.N., W. Deng, et al. (2010). "Basal and treatment-induced activation of AKT mediates resistance to cell death by AZD6244 (ARRY-142886) in Braf-mutant human cutaneous melanoma cells." Cancer Res **70**(21): 8736-47.

Gray-Schopfer, V.C., S.C. Cheong, et al. (2006). "Cellular senescence in naevi and immortalisation in melanoma: a role for p16?" Br J Cancer **95**(4): 496-505.

Gray-Schopfer, V., C. Wellbrock, et al. (2007). "Melanoma biology and new targeted therapy." Nature **445**: 851-57.

Guo, J., L. Si, et al. (2011). "Phase II, open-label, single-arm trial of imatinib mesylate in patients with metastatic melanoma harboring c-Kit mutation or amplification." J Clin Oncol **29**(21): 2904-9.

Gupta, P.B., C. Kuperwasser, et al. (2005). "The melanocyte differentiation program predisposes to metastasis after neoplastic transformation." Nat Genet **37**: 1047-54.

Hacker, E., H.K. Muller, et al. (2006). “Spontaneous and UV radiation-induced multiple metastatic melanomas in Cdk4R24C/R24C/TPras mice.” Cancer Res **66**(6): 2946-52.

Hanahan, D. and R.A. Weinberg. (2011). “Hallmarks of cancer: the next generation.” Cell **144**(5): 646-74.

Hanks, S.K., M.B. Calalb, et al. (1992). “Focal adhesion protein-tyrosine kinase phosphorylated in response to cell attachment to fibronectin.” Proc Natl Acad Sci U S A **89**(18): 8487-91.

Hatzivassiliou, G., K. Song, et al. (2010). “RAF inhibitors prime wild-type RAF to activate the MAPK pathway and enhance growth.” Nature **464**(7287): 431-5.

Hauschild, A., S.S. Agarwala, et al. (2009). “Results of a phase III, randomized, placebo-controlled study of sorafenib in combination with carboplatin and paclitaxel as second-line treatment in patients with unresectable stage III or stage IV melanoma.” J Clin Oncol **27**(17): 2823-30.

Heidorn, S.J., C. Milagre, et al. (2010). “Kinase-dead BRAF and oncogenic RAS cooperate to drive tumor progression through CRAF.” Cell **140**(2): 209-21.

Hennigan, R.F., K.L. Hawker, et al. (1994). “Fos-transformation activates genes associated with invasion.” Oncogene **9**: 3591-600.

Herlyn, M., C. Berking, et al. (2000). “Lessons from melanocyte development for understanding the biological events in naevus and melanoma formation.” Melanoma Res **10**(4): 303-12.

Hernández-Negrete, I., J. Carretero-Ortega, et al. (2007). “P-Rex1 links mammalian target of rapamycin signaling to Rac activation and cell migration.” J Biol Chem **282**(32): 23708-15.

Hill, K., S. Krugmann, et al. (2005). "Regulation of P-Rex1 by phosphatidylinositol (3,4,5)-trisphosphate and Gbetagamma subunits." J Biol Chem **280**: 4166-73.

Hocker, T. and H. Tsao. (2007). "Ultraviolet radiation and melanoma: a systematic review and analysis of reported sequence variants." Hum Mutat **28**(6): 578-88.

Hodgson, J.G., K. Chin, et al. (2003). "Genome amplification of chromosome 20 in breast cancer." Breast Cancer Res Treat **78**(3): 337-45.

Hodi, F.S., S.J. O'Day, et al. (2010). "Improved survival with ipilimumab in patients with metastatic melanoma." N Engl J Med **363**(8): 711-23.

Hoffmann, M.J., R. Engers. (2008). "TIAM1 (T-cell lymphoma invasion and metastasis 1)." Atlas Genet Cytogenet Oncol Haematol

Holman, C.D., B.K. Armstrong, et al. (1983). "A theory of the etiology and pathogenesis of human cutaneous malignant melanoma." J Natl Cancer Inst **71**(4): 651-6.

Huang, D., M. Khoe, et al. (2007). "Focal adhesion kinase mediates cell survival via NF-kappaB and ERK signaling pathways." Am J Physiol Cell Physiol **292**(4): C1339-52.

Hüsemann, Y., J.B. Geigl, et al. (2008). "Systemic spread is an early step in breast cancer." Cancer Cell **13**(1): 58-68.

Hussein, M.R. (2004). "The TP53 tumor suppressor gene and melanoma tumorigenesis: is there a relationship?" Tumour Biol **25**(4): 200-7.

Ilić, D., Y. Furuta, et al. (1995). “Reduced cell motility and enhanced focal adhesion contact formation in cells from FAK-deficient mice.” Nature **377**(6549): 539-44.

Ilić, D., C.H. Damsky, et al. (1997). “Focal adhesion kinase: at the crossroads of signal transduction.” J Cell Sci **110**(4): 401-7.

Ilic, D., B. Kovacic, et al. (2003). “Focal adhesion kinase is required for blood vessel morphogenesis.” Circ Res **92**(3): 300-7.

Ingle, J.N., D.L. Ahmann, et al. (1981). “Randomized clinical trial of diethylstilbestrol versus tamoxifen in postmenopausal women with advanced breast cancer.” N Engl J Med **304**(1): 16-21.

Inoue-Narita, T., K. Hamada, et al. (2008). “Pten deficiency in melanocytes results in resistance to hair graying and susceptibility to carcinogen-induced melanomagenesis.” Cancer Res **68**(14): 5760-8.

Johannessen, C.M., J.S. Boehm, et al. (2010). “COT drives resistance to RAF inhibition through MAP kinase pathway reactivation.” Nature **468**(7326): 968-72.

Jordan, S.A. and I.J. Jackson. (2000). “MGF (KIT ligand) is a chemokinetic factor for melanoblast migration into hair follicles.” Dev Biol **225**(2): 424-36.

Kaplan, R.N., R.D. Riba, et al. (2005). “VEGFR1-positive haematopoietic bone marrow progenitors initiate the pre-metastatic niche.” Nature **438**(7069): 820-7.

Karapetis, C.S., S. Khambata-Ford, et al. (2008). “K-ras mutations and benefit from cetuximab in advanced colorectal cancer.” N Engl J Med **359**(17): 1757-65.

Kato, M., N. Ohgami, et al. (2007). “Protective effect of hyperpigmented skin on UV-mediated cutaneous cancer development.” J Invest Dermatol **127**(5): 1244-9.

Katzav, S., D. Martin-Zanca, et al. (1989). “Vav, a novel human oncogene derived from a locus ubiquitously expressed in hematopoietic cells.” EMBO J **8**(8): 2283-90.

Kelsall, S.R. and B. Mintz. (1998). “Metastatic cutaneous melanoma promoted by ultraviolet radiation in mice with transgene-initiated low melanoma susceptibility.” Cancer Res **58**(18): 4061-5.

Kim, M., J.D. Gans, et al. (2006). “Comparative oncogenomics identifies NEDD9 as a melanoma metastasis gene.” Cell 125(7): 1269-81.

Kim, K.B., O. Eton, et al. (2008). “Phase II trial of imatinib mesylate in patients with metastatic melanoma.” Br J Cancer **99**(5): 734-40.

Kim, M.Y., T. Oskarsson, et al. (2009). “Tumor self-seeding by circulating cancer cells.” Cell **139**(7): 1315-26.

Kim, E.K., S.J. Yun, et al. (2011). “Selective activation of Akt1 by mammalian target of rapamycin complex 2 regulates cancer cell migration, invasion, and metastases.” Oncogene **30**: 2954-63.

Kinsey, D.L. (1960). “An experimental study of preferential metastasis.” Cancer **13**: 674-6.

Kissil, J.L., M.J. Walmsley, et al. (2007). “Requirement for Rac1 in a K-ras induced lung cancer in the mouse.” Cancer Res **67**: 8089-94.

Kolch, W. (2000). “Meaningful relationships: the regulation of the Ras/Raf/MEK/ERK pathway by protein interactions.” Biochem J **351**(2): 289-305.

Kornberg, L., H.S. Earp, et al. (1992). “Cell adhesion or integrin clustering increases phosphorylation of a focal adhesion-associated tyrosine kinase.” J Biol Chem **267**(33): 23439-42.

Koscielny, S., M. Tubiana, et al. (1984). “Breast cancer: relationship between the size of the primary tumour and the probability of metastatic dissemination.” Br J Cancer **49**(6): 709-15.

Koynova, D.K., E.S. Jordanova, et al. (2007). “Gene-specific fluorescence in-situ hybridization analysis on tissue microarray to refine the region of chromosome 20q amplificationin melanoma.” Melanoma Res **17**(1): 37-41.

Krimpenfort, P., K.C. Quon, et al. (2001). “Loss of p16Ink4a confers susceptibility to metastatic melanoma in mice.” Nature **413**(6851): 83-6.

Kumasaka, M.Y., I. Yajima, et al. (2010). “A novel mouse model for de novo melanoma.” Cancer Res **70**(1): 24-9.

Küsters-Vandevelde, H.V., A. Klaasen, et al. (2009). “Activating mutations of the GNAQ gene: a frequent event in primary melanocytic neoplasms of the central nervous system.” Acta Neuropathol **119**: 317-23.

Kvam, E., R.M. Tyrrell. (2004). “Melanin synthesis may sensitize melanocytes to oxidative damage by ultraviolet A irradiation and protect melanocytes from direct DNA damage by ultraviolet B radiation.” Pigment Cell Res **17**: 549-550.

Kwak, E.L., Y.J. Bang, et al. (2010). “Anaplastic lymphoma kinase inhibition in non-small-cell lung cancer.” N Engl J Med **363**(18): 1693-703.

Lahlou, H., V. Sanguin-Gendreau, et al. (2007). “Mammary epithelial-specific disruption of the focal adhesion kinase blocks mammary tumor progression.” Proc Nat Acad Sci **104**(51): 20302-7.

Lamba, S., L. Felicioni, et al. (2009). “Mutational profile of GNAQQ209 in human tumors.” PLoS One **4**(8): e6833.

Lamoreux, M.L., V. Delmas, et al. (2010). “The colors of mice: a model genetic network.” Hoboken, NJ: Wiley-Blackwell.

Langley, R.R. and I.J. Fidler. (2011). “The seed and soil hypothesis revisited--the role of tumor-stroma interactions in metastasis to different organs.” Int J Cancer **128**(11): 2527-35.

Lark, A.L., C.A. Livasy, et al. (2005). “High focal adhesion kinase expression in invasive breast carcinomas is associated with an aggressive phenotype.” Mod Pathol **18**(10): 1289-94.

Lawson, C.D., S. Donald, et al. (2011). “P-Rex1 and Vav1 cooperate in the regulation of formyl-methionyl-leucyl-phenylalanine-dependent neutrophil responses.” J Immunol **186**(3): 1467-76.

Lee, H.J., B. Wall, et al. (2008). “G-protein-coupled receptors and melanoma.” Pigment Cell Melanoma Res **21**(4): 415-28.

Lee, J.H., J.W. Choi, et al. (2011). "Frequencies of BRAF and NRAS mutations are different in histological types and sites of origin of cutaneous melanoma: a meta-analysis." Br J Dermatol **164**(4): 776-84.

Leu, T.H. and M.C. Maa. (2002). "Tyr-863 phosphorylation enhances focal adhesion kinase autophosphorylation at Tyr-397." Oncogene **21**(46): 6992-7000.

Lev, S., H. Moreno, et al. (1995). "Protein tyrosine kinase PYK2 involved in Ca(2+)-induced regulation of ion channel and MAP kinase functions." Nature **376**(6543): 737-45.

Li, A., Y. Ma, et al. (2011). "Rac1 drives melanoblast organization during mouse development by orchestrating pseudopod- driven motility and cell-cycle progression." Dev Cell **21**(4): 722-34.

Lietha, D., X. Cai, et al. (2007). "Structural basis for the autoinhibition of Focal Adhesion Kinase." Cell **129**(6): 1177–1187.

Liu, W., S. Laitinen, et al. (2009). "Copy number analysis indicates monoclonal origin of lethal metastatic prostate cancer." Nat Med **15**(5): 559-65.

Lu, Z., G. Jiang, et al. (2001). "Epidermal growth factor-induced tumor cell invasion and metastasis initiated by dephosphorylation and downregulation of focal adhesion kinase." Mol Cell Biol **21**(12): 4016-31.

Luciani, F., D. Champeval, et al. (2011). "Biological and mathematical modeling of melanocyte development." Development **138**(18): 3943-54.

Ma, A., A. Richardson, et al. (2001). “Serine phosphorylation of focal adhesion kinase in interphase and mitosis: a possible role in modulating binding to p130(Cas).” Mol Biol Cell **12**(1): 1-12.

Mack, N.A., H.J. Whalley, et al. (2011). “The diverse roles of Rac signaling in tumorigenesis.” Cell Cycle **10**(10): 1571-81.

Mackenzie, M.A., S.A. Jordan, et al. (1997). “Activation of the receptor tyrosine kinase Kit is required for the proliferation of melanoblasts in the mouse embryo.” Dev Biol **192**: 99-107.

Malliri, A., R.A. van der Kammen, et al. (2002). “Mice deficient in the Rac activator Tiam1 are resistant to Ras-induced skin tumours.” Nature **417**: 867-71.

Mardilovich, K., M.F. Olson, et al. (2012). “Targeting Rho GTPase signaling for cancer therapy.” Future Oncol **8**(2): 165-77.

Marone, R., V. Cmiljanovic, et al. (2008). “Targeting phosphoinositide 3-kinase: moving towards therapy.” Biochim Biophys Acta **1784**(1): 159-85.

Mayeenuddin, L.H. and J.C. Garrison. (2006). “Phosphorylation of P-Rex1 by the cyclic AMP-dependent protein kinase inhibits the phosphatidylinositiol (3,4,5)-trisphosphate and Gbetagamma-mediated regulation of its activity.” J Biol Chem **281**(4): 1921-8.

McLean, G.W., N.H. Komiyama, et al. (2004). “Specific deletion of focal adhesion kinase suppresses tumor formation and blocks malignant progression.” Genes Dev **18**(24): 2998-3003.

Meierjohann, S., E. Wende, et al. (2006). “The oncogenic epidermal growth factor receptor variant Xiphophorus melanoma receptor kinase induces motility in melanocytes by modulation of focal adhesions.” Cancer Res **66**(6): 3145-52.

Mercer, K., S. Giblett, et al. (2005). “Expression of endogenous oncogenic V600EB-raf induces proliferation and developmental defects in mice and transformation of primary fibroblasts.” Cancer Res **65**(24): 11493-500.

Michaelson, D., W. Abidi, et al. (2008). “Rac1 accumulates in the nucleus during the G2 phase of the cell cycle and promotes cell division.” J Cell Biol **181**: 485-96.

Michaloglou, C., L.C. Vredeveld, et al. (2005). “BRAFE600-associated senescence-like cell cycle arrest of human naevi.” Nature **436**(7051): 720-4.

Miller, A.J. and M.C. Mihm Jr. (2006). “Melanoma.” N Engl J Med **355**(1): 51-65.

Minard, M.E., L.S. Kim, et al. (2004). “The role of the guanine nucleotide exchange factor Tiam1 in cellular migration, invasion, adhesion and tumor progression.” Breast Cancer Res Treat **84**(1): 21-32.

Mok, T.S., Y.L. Wu, et al. (2009). “Gefitinib or carboplatin-paclitaxel in pulmonary adenocarcinoma.” N Engl J Med **361**(10): 947-57.

Montero, J.C., S. Seoane, et al. (2011). “P-Rex1 participates in Neuregulin–ErbB signal transduction and its expression correlates with patient outcome in breast cancer.” Oncogene **30**: 1059-71.

Moore, K.A., R. Sethi, et al. (1997). "Rac1 is required for cell proliferation and G2/M progression." Biochem J **326**: 17-20.

Mort, R.L., L. Hay, et al. (2010). "Ex vivo live imaging of melanoblast migration in embryonic mouse skin." Pigment Cell Melanoma Res **23**(2): 299-301.

Nazarian, R., H. Shi, et al. (2010). "Melanomas acquire resistance to B-RAF(V600E) inhibition by RTK or N-RAS upregulation." Nature **468**(7326): 973-7.

Nogueira, C., K.H. Kim, et al. (2010). "Cooperative interactions of PTEN deficiency and RAS activation in melanoma metastasis." Oncogene **29**(47): 6222-32.

Novak, A., C. Guo, et al. (2000). "Z/EG, a double reporter mouse line that expresses enhanced green fluorescent protein upon Cre-mediated excision." Genesis **28**(3-4): 147-55.

Omholt, K., D. Kröckel, et al. (2006). "Mutations of PIK3CA are rare in cutaneous melanoma." Melanoma Res **16**(2): 197-200.

Otsuka, T., H. Takayama, et al. (1998). "c-Met autocrine activation induces development of malignant melanoma and acquisition of the metastatic phenotype." Cancer Res **58**(22): 5157-67.

Ott, P.A., A. Hamilton, et al. (2010). "A phase II trial of sorafenib in metastatic melanoma with tissue correlates." PLoS One **5**(12): e15588.

Owens, L.V., L. Xu, et al. (1995). "Overexpression of the focal adhesion kinase (p125FAK) in invasive human tumors." Cancer Res **55**(13): 2752-5.

Paget, J. (1887). "The Morton Lecture on Cancer and Cancerous Diseases." Br Med J **2**(1403): 1091-4.

Papp, T., H. Pemsel, et al. (1999). "Mutational analysis of the N-ras, p53, p16INK4a, CDK4, and MC1R genes in human congenital melanocytic naevi." J Med Genet **36**(8): 610-4.

Patel, V., H.M. Rosenfeldt, et al. (2007). "Persistent activation of Rac1 in squamous carcinomas of the head and neck: evidence for an EGFR/Vav2 signaling axis involved in cell invasion." Carcinogenesis **28**(6): 1145-52.

Patton, E.E., H.R. Widlund, et al. (2005). "BRAF mutations are sufficient to promote nevi formation and cooperate with p53 in the genesis of melanoma." Curr Biol **15**(3): 249-54.

Patton, E.E., D.L. Mitchell, et al. (2010). "Genetic and environmental melanoma models in fish." Pigment Cell Melanoma Res **23**(3): 314-37.

Pavel, S., N.P. Smit, et al. (2003). "Homozygous germline mutation of CDKN2A/p16 and glucose-6-phosphate dehydrogenase deficiency in a multiple melanoma case." Melanoma Res **13**(2): 171-8.

Pollock, P.M., K. Cohen-Solal, et al. (2003). "Melanoma mouse model implicates metabotropic glutamate signaling in melanocytic neoplasia." Nat Genet **34**(1): 108-12.

Poulikakos, P.I., Y. Persaud, et al. (2011). "RAF inhibitor resistance is mediated by dimerization of aberrantly spliced BRAF(V600E)." Nature **480**(7377): 387-90.

Prahallad, A., C. Sun, et al. (2012). "Unresponsiveness of colon cancer to BRAF(V600E) inhibition through feedback activation of EGFR." Nature **483**(7387): 100-3.

Prayle, A.P., M.N. Hurley, et al. (2012). “Compliance with mandatory reporting of clinical trial results on ClinicalTrials.gov: cross sectional study.” BMJ **344**: d7373.

Prickett, T.D., X. Wei, et al. (2011). “Exon capture analysis of G protein-coupled receptors identifies activating mutations in GRM3 in melanoma.” Nat Genet **43**(11): 1119-26.

Provenzano, P.P., D.R. Inman, et al. (2008). “Mammary epithelial-specific disruption of focal adhesion kinase retards tumor formation and metastasis in a transgenic mouse model of human breast cancer.” Am J Pathol **173**(5): 1551-65.

Qin, J., Y. Xie, et al. (2009). “Upregulation of PIP3-dependent Rac exchanger 1 (P-Rex1) promotes prostate cancer metastasis.” Oncogene **28**: 1853-63.

Rahman, M.T., K. Nakayama, et al. (2011). “Prognostic and therapeutic impact of the chromosome 20q13.2 ZNF217 locus amplification in ovarian clear cell carcinoma.” Cancer doi: 10.1002/cncr.26598. [Epub ahead of print].

Rajagopalan, H., A. Bardelli, et al. (2002). “Tumorigenesis: RAF/RAS oncogenes and mismatch-repair status.” Nature **418**(6901): 934.

Recio, J.A., F.P. Noonan, et al. (2002). “Ink4a/arf deficiency promotes ultraviolet radiation-induced melanomagenesis.” Cancer Res **62**(22): 6724-30.

Richardson, A. and T. Parsons. (1996). “A mechanism for regulation of the adhesion-associated proteintyrosine kinase pp125FAK.” Nature **380**(6574): 538-40.

Robert, C., L. Thomas, et al. (2011). "Ipilimumab plus dacarbazine for previously untreated metastatic melanoma." N Engl J Med **364**(26): 2517-26.

Rosenfeldt, H., J. Vázquez-Prado, et al. (2004). "P-REX2, a novel PI-3-kinase sensitive Rac exchange factor." FEBS Lett **572**(1-3): 167-71.

Rossman, K.L., C.J. Der, et al. (2005). "GEF means go: turning on RHO GTPases with guanine nucleotide-exchange factors." Nat Rev Mol Cell Biol **6**: 167-80.

Roux, P., C. Gauthier-Rouvière, et al. (1997). "The small GTPases Cdc42Hs, Rac1 and RhoG delineate Raf-independent pathways that cooperate to transform NIH3T3 cells." Curr Biol **7**(9): 629-37.

Sakurai, S., Y. Sonoda, et al. (2002). "Mutated focal adhesion kinase induces apoptosis in a human glioma cell line, T98G." Biochem Biophys Res Commun **293**(1): 174-81.

Samson, T., C. Welch, et al. (2010). "Endogenous RhoG is rapidly activated after epidermal growth factor stimulation through multiple guanine-nucleotide exchange factors." Mol Biol Cell **21**(9): 1629-42.

Sandilands, E., B. Serrels, et al. (2011). "Autophagic targeting of Src promotes cancer cell survival following reduced FAK signalling." Nat Cell Biol **14**(1): 51-60.

Sansal, I. and W.R. Sellers. (2004). "The biology and clinical relevance of the PTEN tumor suppressor pathway." J Clin Oncol **22**(14): 2954-63.

Sanz-Moreno, V., G. Gadea, et al. (2008). “Rac activation and inactivation control plasticity of tumor cell movement.” Cell **135**(3): 510-23.

Sausville, E.A. and A.M. Burger. (2006). “Contributions of human tumor xenografts to anticancer drug development.” Cancer Res **66**(7): 3351-4.

Schaller, M.D., C.A. Borgman, et al. (1992). “pp125FAK a structurally distinctive protein-tyrosine kinase associated with focal adhesions.” Proc Natl Acad Sci U S A **89**(11): 5192-6.

Schaller, M.D., C.A. Borgman, et al. (1993). “Autonomous expression of a noncatalytic domain of the focal adhesion-associated protein tyrosine kinase pp125FAK.” Mol Cell Biol **13**(2): 785-91.

Schaller, M.D. (2001). “Biochemical signals and biological responses elicited by the focal adhesion kinase.” Biochim Biophy Acta **1540**(1): 1-21.

Schaller, M.D. (2004). “FAK and paxillin: regulators of N-cadherin adhesion and inhibitors of cell migration?” J Cell Biol **166**(2): 157-9.

Schlaepfer, D.D., C.R. Hauck, et al. (1999). “Signaling through focal adhesion kinase.” Prog Biophys Mol Biol **71**(3-4): 435-78.

Schmitz, K.J., F. Grabellus, et al. (2005). “High expression of focal adhesion kinase (p125FAK) in node-negative breast cancer is related to overexpression of HER-2/neu and activated Akt kinase but does not predict outcome.” Breast Cancer Res **7**(2): R194-203.

Schultze, A. and W. Fiedler. (2010). “Therapeutic potential and limitations of new FAK inhibitors in the treatment of cancer.” Expert Opin Investig Drugs **19**(6): 777-88.

Serrano, M., H. Lee, et al. (1996). “Role of the INK4a locus in tumor suppression and cell mortality.” Cell **85**(1): 27-37.

Sethi, N. and Y. Kang . (2011). “Unravelling the complexity of metastasis - molecular understanding and targeted therapies.” Nat Rev Cancer **11**(10): 735-48.

Shah, M., A. Bhoumik, et al. (2010). “A role for ATF2 in regulating MITF and melanoma development.” PLoS Genet **6**(12): e1001258.

Shao, Y. and A.E. Aplin. (2010). “Akt3-mediated resistance to apoptosis in B-RAF-targeted melanoma cells.” Cancer Res **70**(16): 6670-81.

Sharpless, N.E. and R.A. DePinho. (1999). “The INK4A/ARF locus and its two gene products.” Curr Opin Genet Dev **9**(1): 22-30.

Sharpless, N.E., N. Bardeesy, et al. (2001). “Loss of p16Ink4a with retention of p19Arf predisposes mice to tumorigenesis.” Nature **413**(6851): 86-91.

Shields, J.M., N.E. Thomas, et al. (2007). “Lack of extracellular signal-related kinase mitogen-activated protein kinase signaling shows a new type of melanoma.” Cancer Res **67**: 1502-12.

Sieg, D.J., D. Ilić, et al. (1998). “Pyk2 and Src-family protein-tyrosine kinases compensate for the loss of FAK in fibronectin-stimulated signaling events but Pyk2 does not fully function to enhance FAK- cell migration.” EMBO J **17**(20): 5933-47.

Sieg, D.J., C.R. Hauck, et al. (2000). “FAK integrates growth-factor and integrin signals to promote cell migration.” Nat Cell Biol **2**(5): 249-56.

Siesser, P.M. and S.K. Hanks. (2006). “The signaling and biological implications of FAK overexpression in cancer.” Clin Cancer Res **12**(11): 3233-7.

Singh, A.D., P. De Potter, et al. (1998). “Lifetime prevalence of uveal melanoma in white patients with oculo(dermal) melanocytosis.” Ophthalmology **105**(1): 195-8.

Slamon, D.J., B. Leyland-Jones, et al. (2001). “Use of chemotherapy plus a monoclonal antibody against HER2 for metastatic breast cancer that overexpresses HER2.” N Engl J Med **344**(11): 783-92.

Soengas, M.S. and S.W. Lowe. (2003). “Apoptosis and melanoma chemoresistance.” Oncogene **22**(20): 3138-51.

Sonoda, Y., S. Watanabe, et al. (1999). “FAK is the upstream signal protein of the phosphatidylinositol 3-kinase-Akt survival pathway in hydrogen peroxide-induced apoptosis of a human glioblastoma cell line.” J Biol Chem **274**(15): 10566-70.

Sonoda, Y., Y. Matsumoto, et al. (2000). “Anti-apoptotic role of focal adhesion kinase (FAK). Induction of inhibitor-of-apoptosis proteins and apoptosis suppression by the overexpression of FAK in a human leukemic cell line, HL-60.” J Biol Chem **275**(21): 16309-15.

Sosa, M.S., C. Lopez-Haber, et al. (2010). “Identification of the Rac-GEF P-Rex1 as an essential mediator ErbB signaling in breast cancer.” Mol Cell **40**(6): 877-92.

Stahl, J.M., A. Sharma, et al. (2004). “Deregulated Akt3 activity promotes development of malignant melanoma.” Cancer Res **64**(19): 7002-10.

Stopeck, A.T., A. Lipton, et al. (2010). “Denosumab compared with zoledronic acid for the treatment of bone metastases in patients with advanced breast cancer: a randomized, double-blind study.” J Clin Oncol **28**(35): 5132-9.

Strizzi, L., K.M. Hardy, et al. (2011). “Embryonic signaling in melanoma: potential for diagnosis and therapy.” Lab Invest **00**: 1-6.

Sugihara, K., N. Nakatsuji, et al. (1998). “Rac1 is required for the formation of three germ layers during gastrulation.” Oncogene **17**(26): 3427-33.

Tabach, Y., I. Kogan-Sakin, et al. (2011). “Amplification of the 20q chromosomal arm occurs early in tumorigenic transformation and may initiate cancer.” PLoS One **6**(1): e14632.

Tachibana, K., T. Sato, et al. (1995). “Direct association of pp125FAK with paxillin, the focal adhesion- targeting mechanism of pp125FAK.” J Exp Med **182**(4): 1089–1099.

Talmadge, J.E., K. Benedict, et al. (1984). “Development of biological diversity and susceptibility to chemotherapy in murine cancer metastases.” Cancer Res **44**(9): 3801-5.

Tarhini, A.A. and S.S. Agarwala. (2006). “Cutaneous melanoma: available therapy for metastatic disease.” Dermatol Ther **19**(1): 19-25.

Tavernier-Tardy, E., J. Cornillon, et al. (2009). “Prognostic value of CXCR4 and FAK expression in acute myelogenous leukemia.” Leuk Res **33**(6): 764-8.

Terzian, T., E.C. Torchia, et al. (2010). “p53 prevents progression of nevi to melanoma predominantly through cell cycle regulation.” Pigment Cell Melanoma Res **23**(6): 781-94.

Theocharis, S.E., G.P. Kouraklis, et al. (2003). “Focal adhesion kinase expression is not a prognostic predictor in colon adenocarcinoma patients.” Eur J Surg Oncol **29**(7): 571-4.

Tormo, D., A. Ferrer, et al. (2006). “Rapid growth of invasive metastatic melanoma in carcinogen-treated hepatocyte growth factor/scatter factor-transgenic mice carrying an oncogenic CDK4 mutation.” Am J Pathol **169**(2): 665-72.

Tsao, H., X. Zhang, et al. (2000). “Relative reciprocity of NRAS and PTEN/MMAC1 alterations in cutaneous melanoma cell lines.” Cancer Res **60**(7): 1800-4.

Ugurel, S., R. Hildenbrand, et al. (2005). “Lack of clinical efficacy of imatinib in metastatic melanoma.” Br J Cancer **92**(8): 1398-405.

Uhlenbrock, K., A. Eberth, et al. (2004). “The RacGEF TIAM1 inhibits migration and invasion of metastatic melanoma via a novel adhesive mechanism.” J Cell Sci **117**: 4863-71.

Uong, A. and L.I. Zon. (2010). “Melanocytes in development and cancer.” J Cell Physiol **222**: 38-41.

Urano, D.,A. Nakata, et al. (2008). “Domain-domain interaction of P-Rex1 is essential for the activation and inhibition by G protein betagamma subunits and PKA.” Cell Signal **20**(8): 1545-54.

Van Raamsdonk, C.D., V. Bezrookove, et al. (2009). “Frequent somatic mutations of GNAQ in uveal melanoma and blue naevi.” Nature **457**(7229): 599-602.

Van Raamsdonk, C.D., K.G. Griewank, et al. (2010). “Mutations in GNA11 in uveal melanoma.” N Engl J Med **363**(23): 2191-9.

Vigil, D., K.L. Rossman, et al. (2010). “Ras superfamily GEFs and GAPs: validated and tractable targets for cancer therapy?” Nature Rev Cancer **10**: 842-57.

Walker, G.J., H.P. Soyer, et al. (2011). “Modelling melanoma in mice.” Pigment Cell Melanoma Res **24**(6): 1158-76.

Wallander, M.L., L.J. Layfield, et al. (2011). “KIT mutations in ocular melanoma: frequency and anatomic distribution.” Mod Pathol **24**(8): 1031-5.

Walmsley, M.J., S.K. Ooi, et al. (2003). “Critical roles for Rac1 and Rac2 GTPases in B cell development and signaling.” Science **302**(5644): 459-62.

Wang, H.T., B. Choi, et al. (2010). “Melanocytes are deficient in repair of oxidative DNA damage and UV-induced photoproducts.” PNAS **107(27)**: 12180-5

Waters, J.E., M.V. Astle, et al. (2008). “P-Rex1 - a multidomain protein that regulates neurite differentiation.” J Cell Sci **121**(Pt 17): 2892-903.

Weiner, T.M., E.T. Liu, et al. (1993). “Expression of focal adhesion kinase gene and invasive cancer.” Lancet **342**(8878): 1024-5.

Weiner, O.D. (2002). “Rac activation: P-Rex1 - a convergence point for PIP(3) and Gbetagamma?” Curr Biol **12**(12): R429-31.

Welch, H.C., W.J. Coadwell, et al. (2002). “P-Rex1, a PtdIns(3,4,5)P3- and Gbetagamma-regulated guanine-nucleotide exchange factor for Rac.” Cell **108**: 809-21.

Welch, H.C., A.M. Condliffe, et al. (2005). “P-Rex1 regulates neutrophil function.” Curr Biol **15**: 1867-73.

Wellbrock, C., L. Ogilvie, et al. (2004). “V599EB-RAF is an oncogene in melanocytes.” Cancer Res **64**(7): 2338-42.

Wennerberg, K., K.L. Rossman, et al. (2005). “The Ras superfamily at a glance.” J Cell Sci **118**: 843-6.

Whiteman, D.C., P. Watt, et al. (2003). “Melanocytic nevi, solar keratoses, and divergent pathways to cutaneous melanoma.” J Natl Cancer Inst **95**(11): 806-12.

Whiteman, D.C., C.A.Bray, et al. (2008). “Changes in the incidence of cutaneous melanoma in the west of Scotland and Queensland, Australia: hope for health promotion?”. Eur J Cancer Prev **17**(3): 243-50.

Widmer, D.S., P.F. Cheng, et al. (2012). “Systematic classification of melanoma cells by phenotype-specific gene expression mapping.” Pigment Cell Melanoma Res **25**(3): 343-53.

Willmore-Payne, C., J.A. Holden, et al. (2005). “Human malignant melanoma: detection of BRAF- and c-kit-activating mutations by high-resolution amplicon melting analysis.” Hum Pathol **36**(5): 486-93.

Wong, C.Y., H. Wuriyanghan, et al. (2011). “Epigenetic regulation of phosphatidylinositol 3,4,5-triphosphate-dependent Rac exchanger 1 gene expression in prostate cancer cells.” J Biol Chem **286**(29): 25813-22.

Wu, X., S. Suetsugu, et al. (2004). “Focal adhesion kinase regulation of N-WASP subcellular localization and function.” J Biol Chem **279**(10): 9565-76.

Wyman, K., M.B. Atkins, et al. (2006). “Multicenter Phase II trial of high-dose imatinib mesylate in metastatic melanoma: significant toxicity with no clinical efficacy.” Cancer **106**(9): 2005-11.

Xie, Z., K. Sanada, et al. (2003). “Serine 732 phosphorylation of FAK by Cdk5 is important for microtubule organization, nuclear movement, and neuronal migration.” Cell **114**(4): 469-82.

Xu, L.H., X. Yang, et al. (2000). “The focal adhesion kinase suppresses transformation-associated, anchorage-independent apoptosis in human breast cancer cells. Involvement of death receptor-related signaling pathways.” J Biol Chem **275**(39): 30597-604.

Yachida, S., S. Jones, et al. (2010). “Distant metastasis occurs late during the genetic evolution of pancreatic cancer.” Nature **467**(7319): 1114-7.

Yajima, I., E. Belloir, et al. (2006). “Spatiotemporal gene control by the Cre-ERT2 system in melanocytes.” Genesis **44**(1): 34-43.

Yamazaki, F., H. Okamoto, et al. (2005). “Development of a new mouse model (xeroderma pigmentosum a-deficient, stem cell factor-transgenic) of ultraviolet B-induced melanoma.” J Invest Dermatol **125**(3): 521-5.

Yang, C., Y. Liu, et al. (2006). “Essential role for Rac in heregulin beta1 mitogenic signaling: a mechanism that involves epidermal growth factor receptor and is independent of ErbB4.” Mol Cell Biol **26**(3): 831-42.

Yang, G., D. Curley, et al. (2007). “Loss of xeroderma pigmentosum C (Xpc) enhances melanoma photocarcinogenesis in Ink4a-Arf-deficient mice.” Cancer Res **67**(12): 5649-57.

Yang, C., E.A. Klein, et al. (2008). “Heregulin beta1 promotes breast cancer cell proliferation through Rac/ERK-dependent induction of cyclin D1 and p21Cip1.” Biochem J **410**(1): 167-75.

Yang, J., R. Splittgerber, et al. (2010). “Conditional ablation of Ikkb inhibits melanoma tumor development in mice.” J Clin Invest **120**(7): 2563-74.

Yoshizawa, M., T. Kawauchi, et al. (2005). “Involvement of a Rac activator,P-Rex1, in neurotrophin-derived signaling and neuronal migration.” J Neurosci **25**(17): 4406-19.

Zachary, I. and E. Rozengurt. (1992). “Focal adhesion kinase (p125FAK): a point of convergence in the action of neuropeptides, integrins, and oncogenes.” Cell **71**(6): 891-4.

Zaidi, M.R., C.P. Day, et al. (2008). “From UVs to metastases: modeling melanoma initiation and progression in the mouse.” J Invest Dermatol **128**(10): 2381-91.

Zhao, T., P. Nalbant, et al. (2007). “Signaling requirements for translocation of P-Rex1, a key Rac2 exchange factor involved in chemoattractant-stimulated human neutrophil function.” J Leukoc Biol **81**(4): 1127-36.

Zhao, J. and J.L. Guan. (2009). “Signal transduction by focal adhesion kinase in cancer.” Cancer Metastasis Rev **28**(1-2): 35-49.

Zhao, X., X. Peng, et al. (2010). “Role of kinase-independent and -dependent functions of FAK in endothelial cell survival and barrier function during embryonic development.” J Cell Biol **189**(6): 955-65.

Zheng, Y., Y. Xia, et al. (2009). “FAK phosphorylation by ERK primes ras-induced tyrosine dephosphorylation of FAK mediated by PIN1 and PTP-PEST.” Mol Cell **35**(1): 11-25.

Zhu, H., K. Reuhl, et al. (1998). “Development of heritable melanoma in transgenic mice.” J Invest Dermatol **110**(3): 247-52.

Zoncu, R., A. Efeyan, et al. (2011). “mTOR: from growth signal integration to cancer, diabetes and ageing.” Nat Rev Mol Cell Biol **12**(1): 21-35.

Zuidervaart, W., F. van Nieuwpoort, et al. (2005). “Activation of the MAPK pathway is a common event in uveal melanomas although it rarely occurs through mutation of BRAF or RAS.” Br J Cancer **92**(11): 2032-8.

Zuo, L., J. Weger, et al. (1996). “Germline mutations in the p16INK4a binding domain of CDK4 in familial melanoma.” Nat Genet **12**(1): 97-9.

www.sanger.ac.uk/genetics/CGP/cosmic/

www.who.int/uv/faq/skincancer/en/index1.html

www.espcr.org/micemut

www.cancerresearchuk.org/type/melanoma/treatment/melanoma-statistics-and-outlook

www.cancerresearchuk.org/cancer-info/cancerstats /types/skin/incidence/

www.cancerhelp.cancerresearchuk.org/type/skin-cancer/about/skin-cancer-risks-and-causes

www.cancer.sanger.ac.uk/cosmic/gene/analysis?ln=PTK2#histo

www.cancerresearchuk.org/cancer-info/cancerstats/types/skin/riskfactors/skin-cancer-risk-factors

http://cancer.sanger.ac.uk/cosmic/gene/overview?ln=RAC1